CONSTRUCTION MATERIALS CONSULTANTS, INC.

Improper Repointing of Masonry Mortars In A Historic Monument – A Case Study From Memorial Belltower At North Carolina State University, Raleigh, NC

North Carolina State University
2011 Hillsborough Street
Raleigh, NC 27607

October 25, 2019
CMC 0919153

TABLE OF CONTENTS

IMPROPER REPOINTING OF MASONRY MORTARS IN A HISTORIC MONUMENT – A CASE STUDY FROM MEMORIAL BELLTOWER AT NORTH CAROLINA STATE UNIVERSITY, RALEIGH, NC

EXECUTIVE SUMMARY

Initiated in the 1920s and constructed through 1940s, the 115-ft. tall historic Memorial Belltower at North Carolina State University is a granite stone masonry tower, which stands as a symbol of inspiration to honor North Carolina State alumni killed in World War I. As part of the renovation process of this historic monument, two sets of masonry mortars were provided, one from the lower level of the tower constructed circa 1920s, and the second set from the upper level of the monument built circa 1940s. The samples were examined to determine the types of mortars present in the monument including types and mineralogical compositions mortar sands, chemical, and mineralogical compositions of binders added, sand-to-binders' mix proportions, evidence of any physical or chemical deterioration of mortars during almost a century of service, evidence of past repointing, and recommendations for appropriate pointing mortars to be used with the existing granite masonry units of the monument.

Mortar samples were analyzed by comprehensive laboratory examinations following various industry standards, e.g., ASTM C 1324 and RILEM methods (Middendorf et al. 2004, 2005) starting with visual examinations, extensive optical microscopy, scanning electron microscopy and energy-dispersive X-ray microanalyses (SEM-EDS), followed by wet chemical analyses, X-ray diffraction (XRD), X-ray fluorescence (XRF), thermal analyses (TGA, DTG, DSC), and ion chromatography.

Visual examinations of mortar fragments from both levels showed the presence of multiple mortar types, which are best evident on freshly fractured or sectioned surfaces of fragments, e.g., (1) a dense, hard, dark gray predominantly non-carbonated mortar, which constituents the most prevalent mortar type at both levels, (2) a beige moderately soft, porous, severely carbonated mortar present in the interior of a few dark gray mortars from the lower level (1920s vintage), (3) a medium gray, moderately hard, variably carbonated mortar present in the inside of a few dark gray mortar fragments from both levels from 1920s and 1940s vintages, and (4) an off-white moderately soft, porous, carbonated mortar present mostly as separate fragments found from the upper level from 1940s vintage. Of all these, the brown mortar from the lower level is subsequently determined to be a *hydraulic lime mortar*, the medium gray mortar behind the dark gray ones from both levels is found to be a *lime-based mortar mixed with fine, angular, shard like glassy particles of ground granulated blast furnace slag*, the off-white mortar from the upper level is found to be a *lime-based mortar having higher proportion of lime than Portland cement*, and finally the ubiquitous dense, hard, dark gray mortar present either at the exterior sides of other mortars in a few fragments, or mostly as separate fragments from both levels are found to be *Portland cement-only mortars*, which were probably installed during later pointing events at both lower and upper levels. Sands used in all these earlier and later pointing mortars are silica-based containing major amount of crushed (manufactured) quartz sand having nominal maximum sizes of 1 mm. All mortars examined are non-air-entrained.

Optical microscopical examinations of mortars showed startling differences in microstructures between the Portland cement-only pointing mortars and lime-based earlier mortars from both lower (1920s vintage) and upper (1940s vintage) levels of the monument. The Portland cement-only pointing mortars are found to be similar in compositions and microstructures from both levels, which is indicative of their probable applications at both levels at a later period after the initial constructions were finished. The Portland cement-only mortars are made using crushed silica sand of 1 mm or less in size where sand particles are quartz-based, angular, dense, hard, well-graded, well-distributed and present in sound conditions without any potentially deleterious alkali-aggregate reactions. Pastes in Portland cement-only mortars are dense, mostly non-carbonated in the interiors except a thin layer of carbonation and occasional leaching of lime at the exposed faces in the fragments and contain abundant residual Portland cement particles where cement is found to be finely ground as opposed to coarsely ground Portland cement, which are more common in the early 20th century cements. Microstructures of dense non-carbonated interior pastes of Portland cement mortars showed many features, e.g., (i) ubiquitous dense calcium silicate hydrate products of cement hydration that are optically semi-isotropic, (ii) fine, lath-shaped birefringent crystals of calcium hydroxide component of cement hydration, (iii) abundant residual Portland cement particles having characteristic microstructures of residual calcium silicate (subhedral alite and anhedral belite) particles of Portland cement with interstitial dark brown ferrite phases, thin hydration rims around residual alite grains

due to restricted spaces during hydration, etc., (iv) fine hairline shrinkage microcracks in paste, and (v) occasional secondary ettringite precipitates in air voids and microcracks due to the presence of moisture in the paste during service where sulfates released from cement hydration products have precipitated as secondary ettringite. Fine grain-size of Portland cement, similar compositions and microstructures of Portland cement-only mortars from both 1920s and 1940s vintages, and its presence at the exposed ends with other lime-based mortars behind in some fragments are all indicative of their application in a later pointing event. The main characteristic microstructure of Portland cement-only pointing mortars is the presence of network of fine hairline shrinkage microcracks that are best revealed in SEM-EDS studies, which are not found in the earlier lime-based mortars from both levels. Fibrous acicular secondary ettringite, secondary calcium carbonate precipitates, and occasional fibrous thaumasite precipitates in microcracks are found in some fragments of Portland cement-only mortars mostly at the exposed edges of the fragments. These secondary precipitates at the exposed edges are testaments of the presence of moisture in the mortars for prolonged periods. None of these secondary deposits, however, have affected the interior dense, hard non-carbonated pastes in these mortars. Extensive shrinkage microcracking in pastes, however, have affected the long-term performance and durability of these Portland cement-only mortars, which are found to be due to two reasons – (i) use of Portland cement only without any lime, which has facilitated development of shrinkage microcracks from loss of moisture from the paste, and (ii) use of more cement than sand in Portland cement-only pointing mortars, which are calculated from mix proportions to have 1-part cement to less than1-part sand by volume, which is not only unusual (common cement-to-sand proportions are 1 to $2^1/_4$ to 3) but are also prone to extensive shrinkage microcracking, high stiffness, unworkability, and unaccommodative to masonry movements, etc.

Therefore, lack of lime and grossly undersanded natures of Portland cement-only pointing mortars from both 1920s and 1940s vintages demonstrated highly unusual nature of pointing mortars, both of which have affected the performance and long-term durability of pointing mortar. For a granite masonry, common industry-recommended masonry mortars are ASTM C 270 Type S or M cement-lime or masonry cement mortars in severe-weather environments in load-bearing applications, or, Type N cement-lime or masonry cement mortars in moderate weather environments in non-load bearing applications (e.g., ASTM C 270, Mack and Speweik 1998). Presence of lime is important for workability, water retention, and accommodative natures of mortars without creating undue stresses on mortars or adjacent masonry units.

SEM-EDS studies of Portland cement-only pointing mortars showed typical calcium silicate hydrate compositions of pastes having cementation indices (CI) of paste (after Eckel 1922) ranging between 1 and 2 due to variable degrees of atmospheric carbonation and lime leaching mostly at the exposed edges. Other than extensive microcracking in pastes no other distress is found in these pointing mortars. XRF analyses showed similar silica and lime contents in pointing mortars from both levels, e.g., 47.3% SiO_2 from lower and 47.8% from upper level, and 32.9% CaO from lower and 28.9% from upper level. Sand contents are determined from acid-insoluble residue contents (since sand is quartz-based, which is insoluble in acid), which are also similar 31.7% from lower and 36.7% from upper level. Quartz content in pointing mortar is 27.7% from XRD and 24.8% from DSC for lower level, and 27.8% from XRD and 21.6% from DSC for upper level. Such compositional similarities of Portland cement-only pointing mortars from both levels indicate use of same mortar mix for applications at both levels of monument.

Since Portland cement is the sole binder in the Portland cement-only pointing mortars, Portland cement contents are determined: (a) either from lime contents of mortars from XRF (around 30%) and assuming 63.5% lime in Portland cement, or (b) from subtracting free and combined water contents from losses on ignitions at 110°C and 550°C, respectively and sand contents from acid-insoluble residue contents from 100. Cement contents from both methods are similar between two pointing mortars from lower and upper levels, which are around 50 percent. Cement contents thus calculated are found to be noticeably higher than the sand contents (31.7 to 36.7%). Assuming a bulk density of a Portland cement as 94 lbs./ft^3, and sand as 80 lbs./ft^3, cement and sand volumes are thus determined to be 1-part cement to less than 1-part sand, which shows grossly undersanded pointing mortars contrary to common 1-part cementitious components to $2^1/_4$ to 3-part sand found in masonry mortars.

Contrary to the Portland cement-only pointing mortars, earlier lime-based mortars detected from both levels of monument are judged more appropriate for such applications. Earlier mortars detected in the fragments received are *hydraulic lime mortar* and *slag-lime mortar* from the lower level from 1920s vintage, and, *slag-lime mortar* and *high-lime Portland cement-lime mortar* from the upper level from 1940s applications. All these lime-based mortars were prepared by mixing lime putty, ground slag or Portland cement, and crushed quartz-based silica sand. Sand in these lime-based mortars are similar to the quartz-based crushed sand found in the pointing mortars indicating similar sand source used for all applications. Due to the presence of lime in these earlier mortars along with atmospheric carbon dioxide and

moisture during service, extensive carbonation and occasional leaching of lime is found in optical microscopical and SEM-EDS studies of these early mortars, which are not unusual. Leaching of lime from the edges of these mortars have enriched the altered zones in silica, usually occurring as silica and alumina gel and appear dark (optically isotropic) in crossed polarized light modes in a petrographic microscope, leached zones are situated outside the carbonated zones.

Of all the earlier mortars, probably the slag-lime mortar is most appropriate, which showed best choice to be used with granite masonry as opposed to hydraulic lime or high-lime cement-lime mortars. Fine, angular, shard-like glassy particles of ground granulated blast furnace slag in the fine-grained, variably porous and severely carbonated pastes of slag-lime mortars created a microstructure and microchemistry similar to a modern-day Portland cement-lime mortar where hydration of slag particles has formed calcium silicate hydrate (similar to cement hydration) and subsequent atmospheric carbonation of slag hydration products along with carbonation of lime has provided the long-term durability of this mortar. Hydraulic lime mortar from the lower level showed variable degrees of carbonation and lime leaching resulting in porous fine-grained severely carbonated to denser carbonated pastes later having a few relict carbonated residues of hydraulic phases of original binder, and crushed silica sand. Off-white high-lime Portland cement-lime mortar from the upper level showed variably carbonated pastes having residual Portland cement particles where cement grains are more finely ground than cements manufactured during early 20th century.

Following optical microscopy and SEM-EDS of all lime-based mortars, a representative slag-lime mortar from the lower level and a high-lime cement-lime mortar from the upper level were selected for wet chemical analyses, XRD, XRF, TGA-DTG-DSC studies. Sand contents (from acid-insoluble residue contents) are 59.1% for slag-lime and 41.4% for high-lime cement-lime mortars, which are noticeably higher than sand contents (31.7 to 36.7%) found for Portland cement-only pointing mortars. Bulk silica and lime contents from XRF are 60.9% silica and 14.9% lime for slag-lime mortar and 46.2% silica and 21.1% lime for high-lime cement-lime mortar. Quartz contents are 42.7% from XRD and 46% from DSC for slag-lime mortar, and 25.7% from XRD and 33.2% from DSC for high-lime cement-lime mortar. Such high quartz contents in lime mortars (as opposed to ~ 21 to 27% quartz in the pointing mortars) are consistent with higher sand contents in these mortars compared to pointing mortars. Degree of carbonation and calcite contents from thermal decomposition of mortars at 700-800°C in DTG studies showed 16.1% calcite in slag-lime and 19.5% calcite in high-lime cement-lime as opposed to only 1.9% calcite in portland cement-only pointing mortar from the lower level and 7.3% calcite in pointing mortar from upper level (which showed more atmospheric carbonation than pointing mortar from the lower level).

Ion chromatography of water-soluble anions (fluoride, chloride, bromide, nitrate, nitrite, phosphate, and sulfate) leached out from pulverized Portland cement-only pointing mortars from both levels, a slag-lime mortar from the lower level, and a high-lime cement-lime mortar from the upper level showed (i) high sulfate in Portland cement-only pointing mortars from lower (0.235%) and upper (0.147%) levels, (ii) highest sulfate (0.729%) in high-lime cement-lime mortar from the upper level; (iii) noticeable chloride from the environment, from 0.019 to 0.038%; (iv) a spike in nitrate level in Portland cement-only mortars from the lower (0.264%) and upper (0.379%) level compared to nitrate levels in older mortars (e.g., 0.01% in slag-lime from lower level, and 0.1% in high-lime cement-lime mortar from upper level), and (v) negligible fluoride, bromide, nitrite, and phosphate in all mortars. High sulfate released from high-lime cement-lime mortar at the upper level (even noticeably higher than sulfate released from cement-only pointing mortar) indicates an external sulfate source in this mortar probably from the environment in which the mortar was exposed at the upper level. No sulfate-salt-related distress, however, was found in the optical microscopical examinations of this mortar.

In conclusion, the lower and upper levels of this historic monument have received Portland cement-only mortar in a pointing event, which is unsuitable for its lack of lime, extensive microcracks, and grossly undersanded nature. A more appropriate mortar to be used with granite masonry units of the monument would be an ASTM C 270 Type M or S cement-lime mortar, which would not only provide more malleability, workability, and long-term durability than the present much harder, stiffer non-accommodative cement-only mortar but would be in conformance to common guidelines for masonry construction. Recommended mix proportions of an appropriate pointing mortar would be 1-part cement to $^1/_4$-part lime (for Type M) or $^1/_4$ to $^1/_2$ part lime (for Type S) to $2^1/_4$ to 3 times the sum of separate volumes of cement and lime. Mock-up mortars should be tried on small test locations after cleaning prior cement-only mortars for the desired properties and appearances before large-scale applications.

INTRODUCTION

Initiated in the 1920s and constructed through 1940s, the Memorial Belltower at North Carolina State University is a granite stone masonry tower, which stands as a symbol of inspiration to honor North Carolina State alumni killed in World War I. As part of the renovation process of this historic monument, two sets of masonry mortars were provided, one marked as 'original' reportedly from the base of the tower constructed circa 1920s, and the second set marked as 'upper' from the upper level of the monument built circa 1940s. The samples were provided to determine the types of mortars present, materials and mix proportions of mortars, evidence of any physical or chemical deterioration of mortars during service, and recommendations for appropriate pointing mortar to be used with granite masonry units of the monument.

MEMORIAL BELLTOWER, NORTH CAROLINA STATE UNIVERSITY

Originally built to pay tribute to those who fell in past conflict, the Belltower has become a symbol of inspiration to the Wolfpack community. The idea for a monument to honor NC State alumni killed in World War I originated with Vance Sykes, a member of the class of 1907.

By 1920, Sykes and other alumni had formed a planning committee and hired architect William Henry Deacy to design a memorial tower at the entrance to the campus on Hillsborough Street. Today, the 115-foot monument, called "a legend in stone," is a symbol of the university and a rallying point for the campus community. Constructed at a cost of more than $150,000, the tower is made of 1,400 tons of granite set on a 700-ton concrete base. Its blending of Romanesque features and Gothic verticality are reminiscent of the towers at West Point.

Figure 1: Memorial Belltower at North Carolina State University.

The history of the Belltower mirrors the turbulence of the 20th century. Work commenced quickly after the cornerstone was laid in 1921 with 10 foot sections added in 1924, 1925 and 1926. But construction was halted for extended periods during the Great Depression and again during World War II.

The stonework was finished in 1937 thanks to the federal Works Progress Administration. Student honor societies and the class of 1938 donated the clock, and the class of 1939 purchased a set of floodlights. Finishing touches, including the chimes, shrine room and memorial plaques were completed in the late 1940s and a formal dedication was held on Nov. 11, 1949.

(*Excerpt from https://www.ncsu.edu/belltower/)*

SAMPLES RECEIVED

Table 1 and Figures 2 and 3 show the mortar samples received from lower level (marked as 'original') from 1920s construction, and, from the upper level (marked as 'upper) of the tower representing 1940s construction. For fragments from each level, all mortar fragments were scanned on a flatbed scanner and are shown in three views in Figures 2 and 3, two are from the opposite bedding faces and the third one from the joint faces when possible.

Sample ID, Location, Masonry Company, Type of Masonry	Weight (grams) and Largest Piece Dimensions (mm)	Appearance, Integrity, Figure	Comments
Original from Lower Level of the Monument adjacent to granite stone masonry (Original)	146.95 g, 52 mm × 12 mm × 8 mm	Gray, Light beige, brown Figures 2 and 4	Received in two separate batches, a total of twenty-four (24) fragments of various sizes (see Figure 2) for a total weight of about 150 grams. Most pieces are hard, variably gray, weathered, some have concave sides with exposed sand representing mortar joints
From upper level of monument adjacent to granite stone masonry (Upper)	98.68 g 62 mm × 15 mm × 6 mm	Gray, Off white Figures 3 and 5	Received in two separate batches, a total of thirty-nine (39) fragments of various sizes (see Figure 3) for a total weight of about 100 grams. Most pieces are hard, variably gray, weathered, some have concave sides with exposed sand representing mortar joints

Table 1: Mortar samples received for laboratory examinations.

A close examination of fragments, especially after breaking down a few by finger pressure or by sectioning in a trim saw, showed a dominant mortar type from both levels that is dense, hard and has medium to dark gray interior, which is later found to be Portland cement-only mortar, which is not a common masonry mortar due to the lack of lime. Also present are some other mortar types from both levels that are present in minor amounts either as separate pieces or behind the Portland cement-only types, which are possiblly representative of earlier mortars on which Portland cement-only mortars were applied.

METHODOLOGIES

The mortar samples were tested by following the methods of ASTM C 1324 "Standard Test Method for Examination and Analysis of Hardened Masonry Mortar," which includes detailed petrographic examinations (optical and scanning electron microscopy and microanalysis), followed by chemical analyses, along with various other analytical methods to test masonry mortars from X-ray diffraction to X-ray fluorescence, thermal analysis, etc. as described in various literatures, e.g., Erlin and Hime 1987, Doebley and Spitzer 1996, Chiari et al. 1996, Middendorf et al. 2005 a and b (the RILEM methods), Elsen 2006, Bartos et al. 2000, Valek et al. 2012, Jana 2005, 2006, Goins 2001 and 2004. Details of various analytical techniques followed in CMC laboratories are provided in Appendix 1. Also, visit www.cmc-concrete.com for details on analytical facilities for laboratory examinations of masonry mortars.

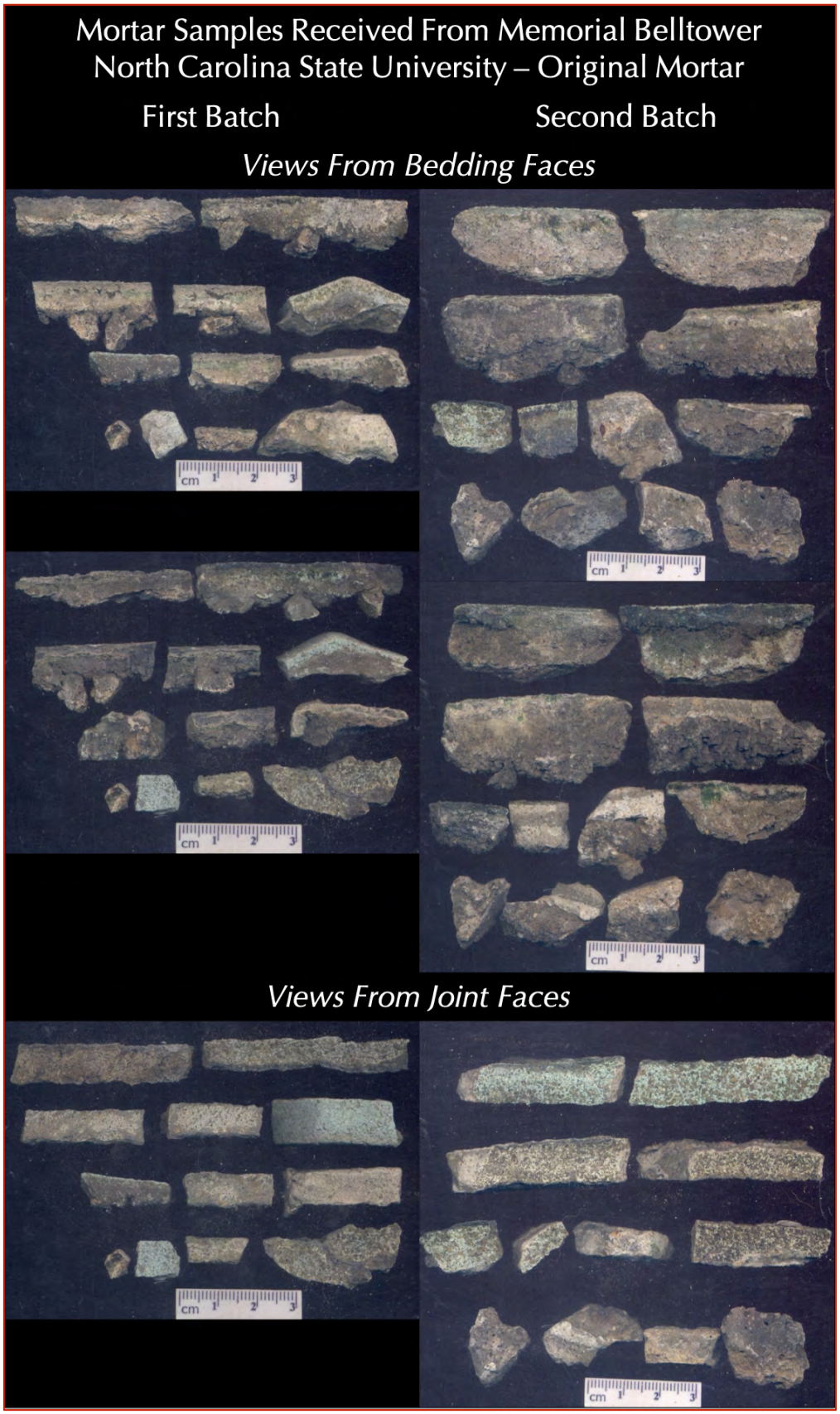

Figure 2: Mortar fragments collected from the lower level of the tower, which are marked as "original," reportedly constructed circa 1920s. The second batch of sample in the right column was provided as per request due to the lower amount of samples received in the first batch.

Most mortar pieces are dense, hard, weathered on the surfaces but when fractured or sectioned show darker gray interiors with a weathering rim. Relatively larger pieces of at least 25 mm length and of visually different appearances were selected for preparation of thin sections for optical and electron microscopical examinations and detection of various mortar types.

Figure 3: Mortar fragments collected from the upper level of the tower, which are marked as "upper," reportedly constructed circa 1940s. The second batch of sample in the right column was provided as per request due to the lower amount of samples received in the first batch.

Most mortar pieces are dense, hard, weathered on the surfaces but when fractured or sectioned show darker gray interiors with a weathering rim. Relatively larger pieces of at least 25 mm length and of visually different appearances were selected for preparation of thin sections for optical and electron microscopical examinations and detection of various mortar types.

RESULTS

Multiple Mortar Types in Cross Sections

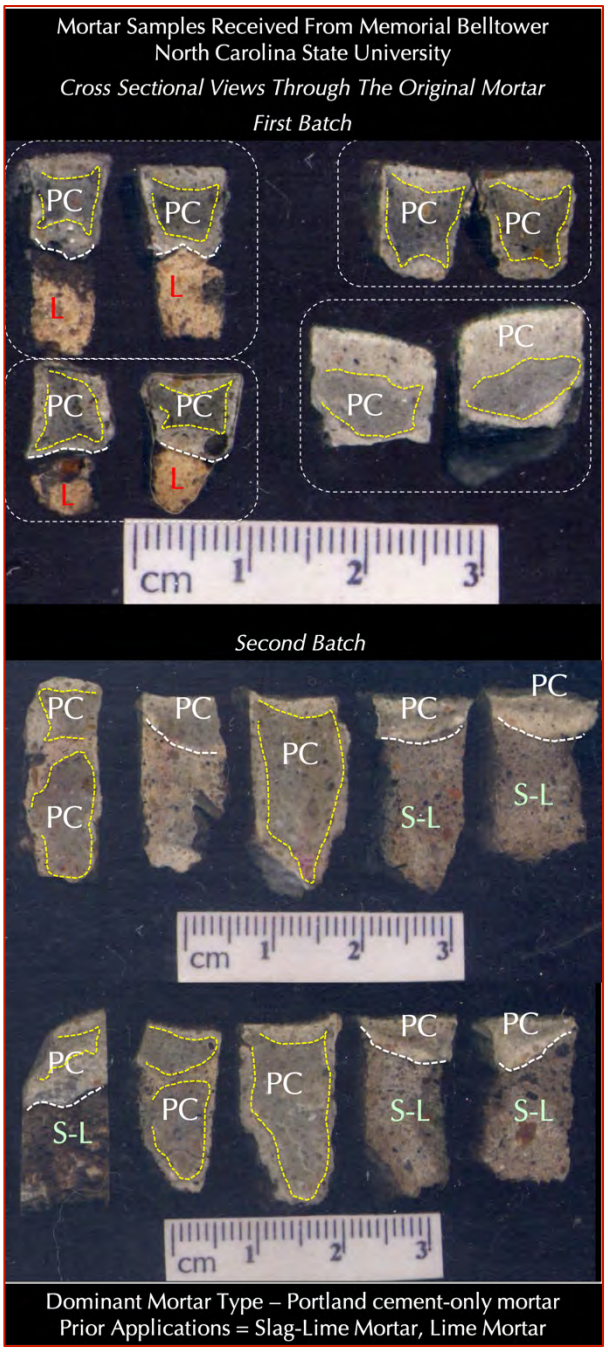

Figure 4: Lapped cross sections of a few representative mortar fragments from the original mortar batch collected from the lower lever of the bellower constructed circa 1920s.

Fragmented pieces show various mortar types that are distinguished based on differences in color tones of the paste as well as other properties, e.g., density, paste porosity, hardness, etc.

White dashed lines separate various mortar types whereas yellow dashed lines within a single mortar type shows depth of alteration of mortar from atmospheric carbonation to leaching of paste, etc.

The dominant mortar type found is the dense, moderate to dark gray mortar type, which was subsequently determined to be a Portland cement mortar, marked as PC containing crushed silica sand and Portland cement as the only cementitious component. In many pieces, this PC mortar shows darker gray interior body and lighter gray surface regions due to alterations of surface that has lightened the color tone of the original PC mortar.

This PC mortar is found to be a pointing mortar applied over various other prior mortar types, which are found to be slag-lime mortar containing angular shard-like glassy particles of ground granulated blast furnace slag, lime, and crushed silica sand, marked as S-L mortar. Sand particles in S-L mortar are somewhat coarser than the sand in PC mortar.

Also found was a brown to beige color mortar, identified as hydraulic lime mortar, marked as L. Paste in this lime mortar is severely carbonated and has variable porosities. Sand is compositionally similar to other types.

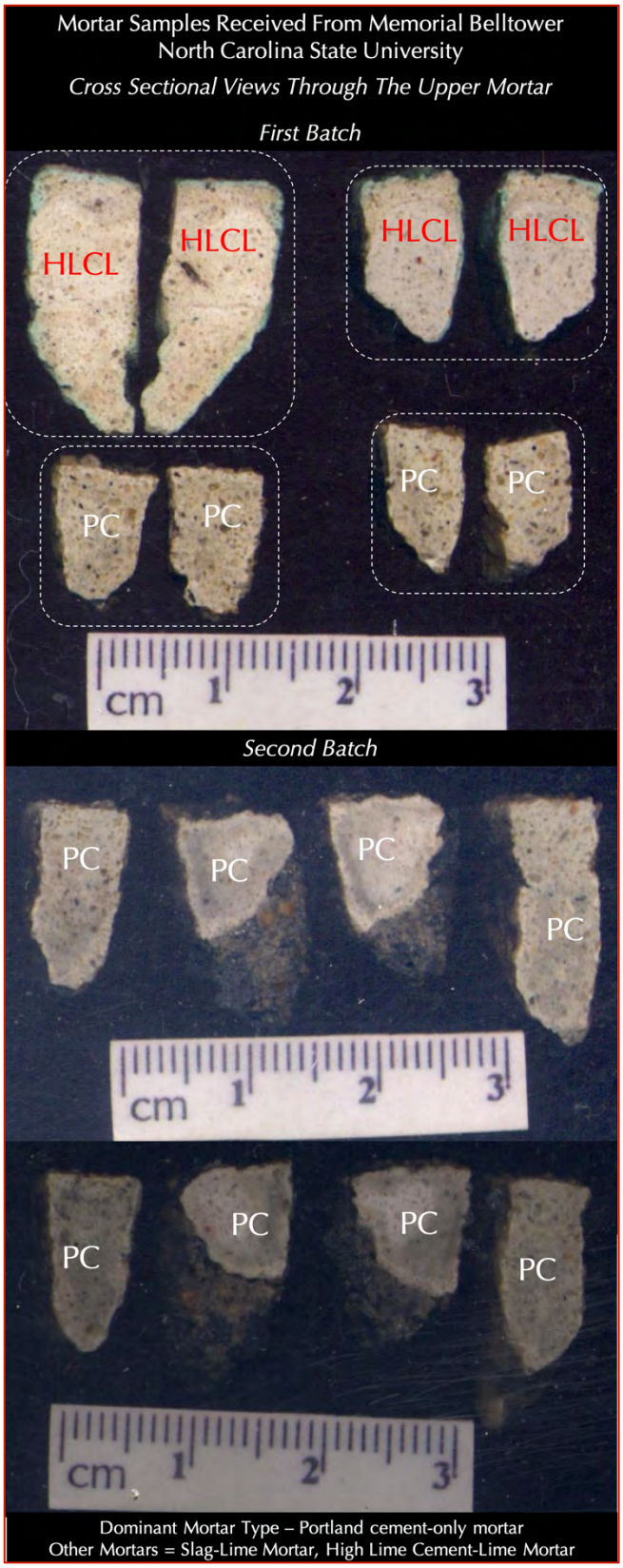

Figure 5: Lapped cross sections of a few representative mortar fragments from the upper-level mortar batch collected from the upper lever of the bellower constructed circa 1940s.

Similar to the mortars from the lower level of the tower constructed circa 1920s, these 1940s mortars also contained Portland cement mortar as the dominant mortar type having similar dense, moderate to dark gray appearance, marked as PC containing crushed silica sand and Portland cement as the only cementitious component. In many pieces, this PC mortar shows darker gray interior body and lighter gray surface regions due to alterations of surface that has lightened the color tone of the PC mortar.

As opposed to PC mortar applied as a later pointing event over slag-lime or hydraulic lime mortar found in the 1920s samples, the present 1940s samples from upper level show most of the fragments as the Portland cement mortar without any underling different prior mortar types. This indicates either PC mortar was applied as the original mortar in the upper level, or it represents mortar from a later pointing event where original mortar behind this PC mortar is not present.

A few fragments are noticeably lighter colored, mostly light gray to off-white in color tones and found to be high-lime cement-lime mortars containing major amount of lime putty and subordinate amount of Portland cement as two binder components along with crushed silica sand. These fragments are marked as HLCL.

Multiple Mortar Types in Thin Sections

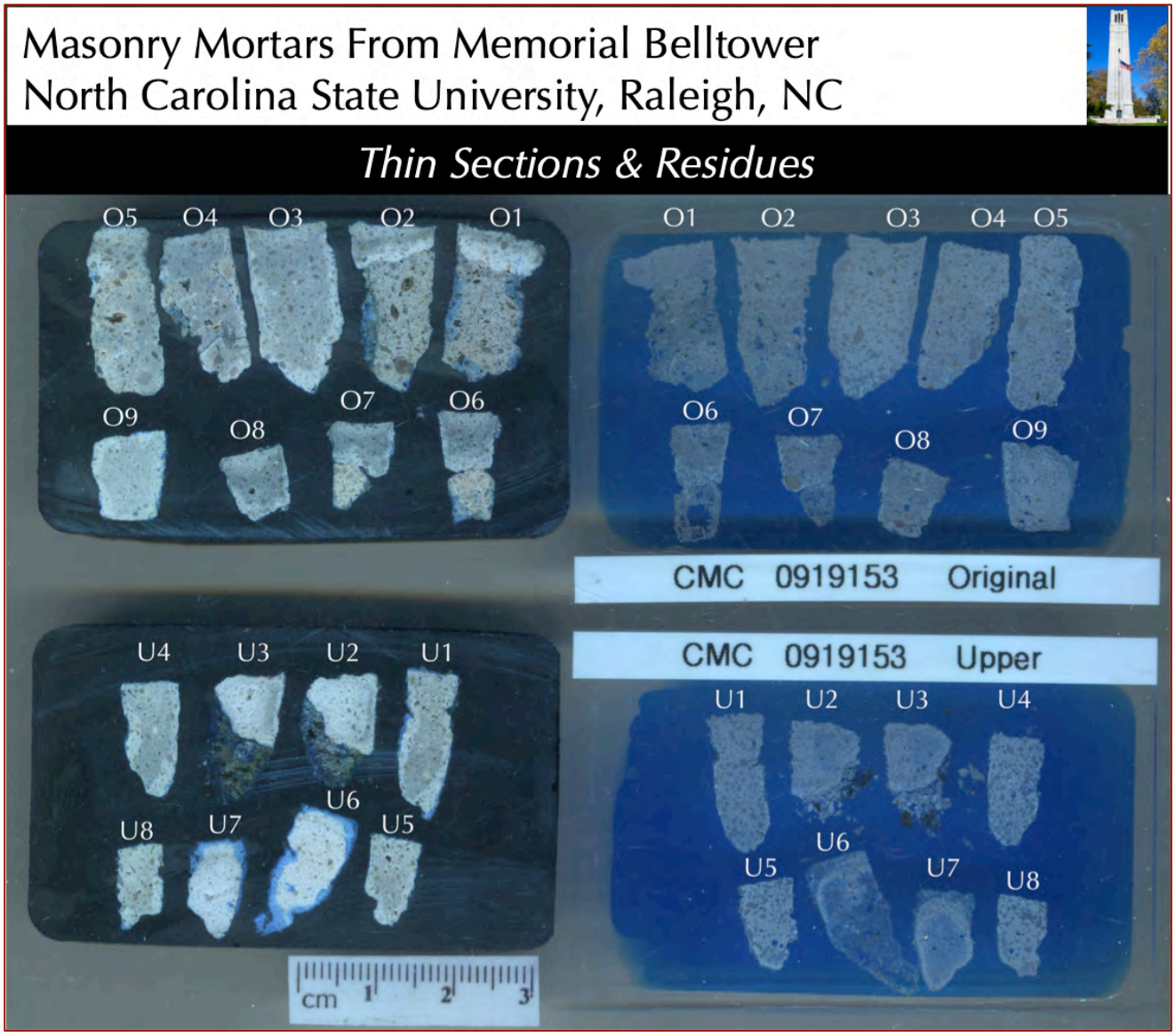

Figure 6: Blue dye-mixed epoxy-impregnated thin sections (right) and residues left after preparation of thin sections (left) of representative pieces of the original mortar from the lower level of belltower from 1920s construction (top row) and from upper level of belltower from 1940s construction (bottom row). Nine representative pieces from 1920s construction (marked as O1 through O9) and eight pieces from 1940s construction (marked as U1 throgh U8) were selected for thin section preparations for detailed petrographic examinations in a stereozoom microscope, a high-power petrographic microscope, and eventually in a scanning electron microscope.

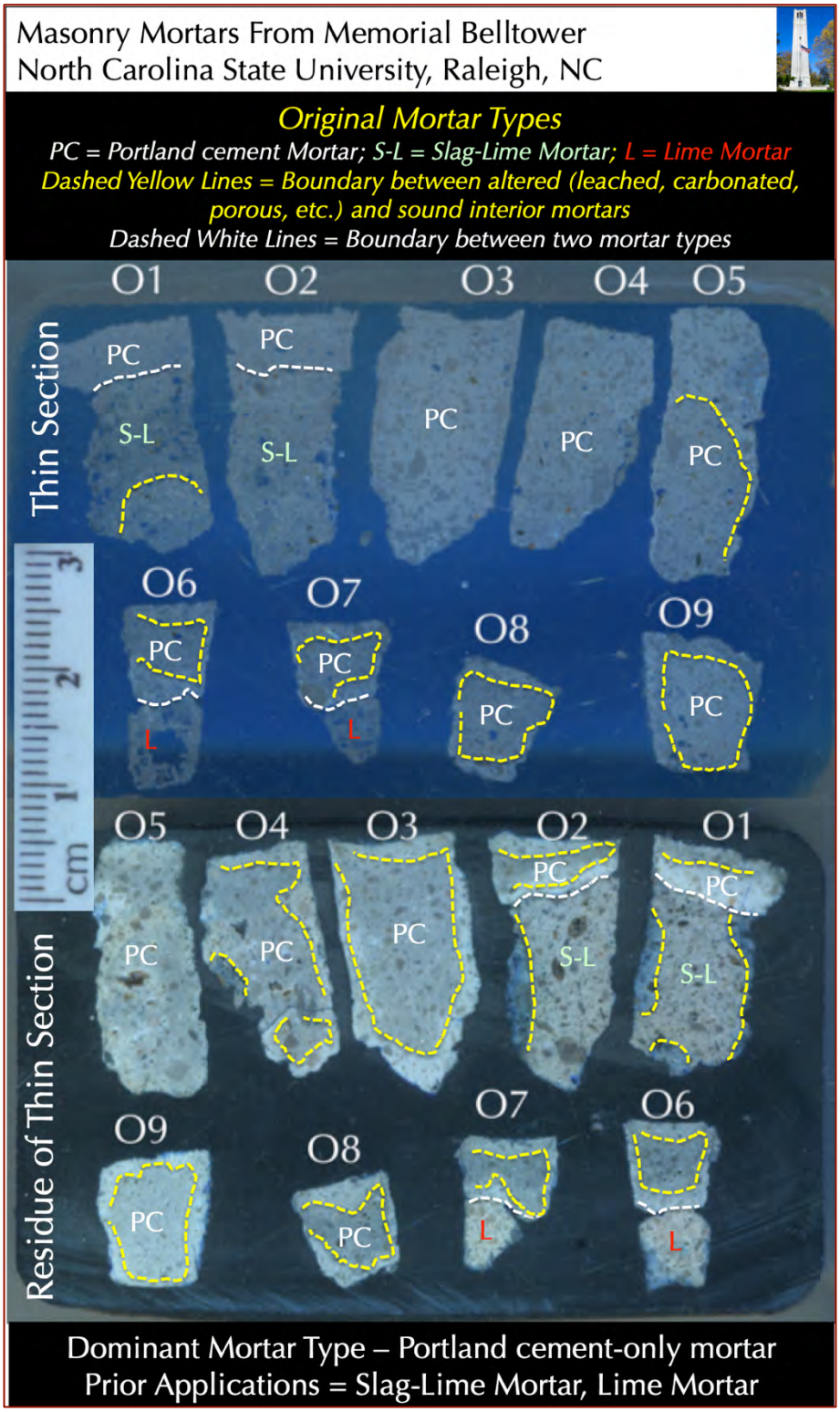

Figure 7: Nine (9) pieces of 1920s' mortars, O1 through O9 showing:

(a) Dominant PC mortar, containing Portland cement as the only binder and crushed silica sand;

(b) Underlying slag-lime mortar (S-L) in pieces O1, and O2, and,

(c) Underlying hydraulic lime mortar (L) in pieces O6 and O7.

White dashed lines separate different mortar types, whereas yellow dashed lines separate altered zone from interior unaltered mortar within single mortar type.

Notice slag-lime (S-L) mortar has a slightly different color tone of paste than the Portland cement mortar; and lime mortar (L) shows the lightest color tone.

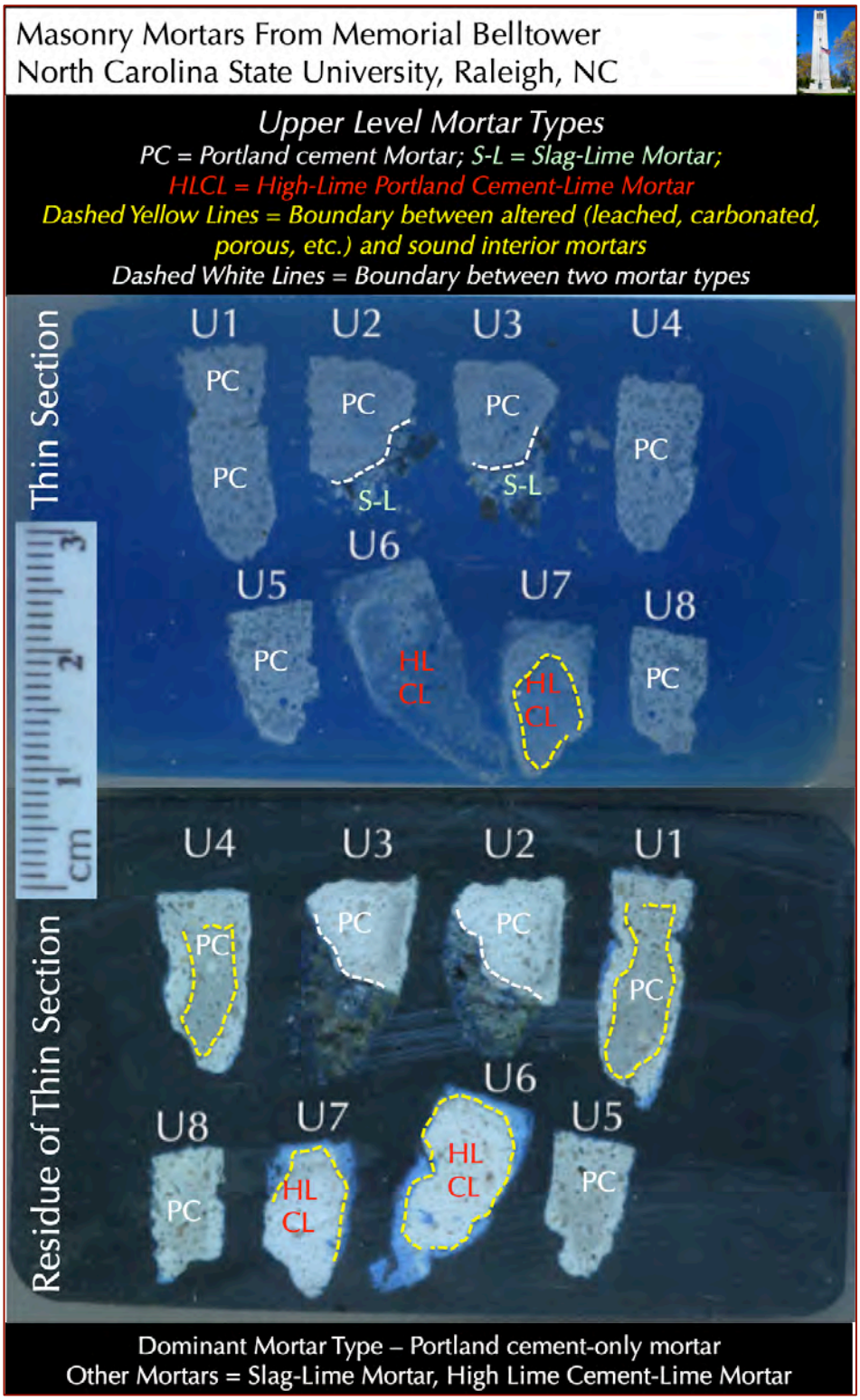

Figure 8: Eight (8) pieces of 1940s' mortars from the upper level, U1 through U8 showing:

(a) Dominant PC-only mortar, containing Portland cement as the only binder and crushed silica sand;

(b) Underlying slag-lime mortar (S-L) in pieces U2, and U3; and,

(c) High-lime cement-lime mortar (HLCL) in two pieces U6 and U7 that contains major amount of lime, subordinate amount of Portland cement and crushed silica sand.

White dashed lines separate different mortar types, whereas yellow dashed lines separate altered zone from interior unaltered mortar within single mortar type.

Notice high-lime cement-lime mortar (HLCL) has a noticeably lighter color tone than the Portland cement mortar. Slag-lime (S-L) mortar in pieces U2 and U3 are noticeably more porous and carbonated than the dominant PC mortars in those pieces.

Optical Microscopy & SEM-EDS of Original Mortars From the Lower Level of Belltower From 1920s Construction

Figures 9 through 32 show optical and scanning electron microscopy of mortars from the lower level of Belltower from 1920s construction, which were taken from the polished thin sections and residues of the mortars shown in Figure 7 by examining the mortar pieces in a low-power Stereozoom microscope (for the thin section residue), high-power petrographic microscope (of the thin sections), and in a scanning electron microscope equipped with energy-dispersive X-ray fluorescence spectrometer for microanalyses of pastes. Figures are arranged as follows:

Figures	Mortars	Microscopy	Features Found
9	PC-only mortar	Stereozoom Microscope	Non-air-entrained dense PC mortar, secondary ettringite in air voids
10	PC-only mortar	Petrographic Microscope	Shrinkage microcracks and secondary ettringite in microcracks, dense paste having residual cement particles
11	Slag-Lime Mortar	Stereozoom Microscope	Non-air-entrained slag-lime mortar, different paste color tone and sand colors from PC-only mortar, location beneath the PC-only mortar
12	Slag-Lime Mortar	Petrographic Microscope	Severely carbonated paste, angular slag particles in paste, secondary carbonates in microcracks
13	Hydraulic Lime Mortar	Stereozoom Microscope	Moderately soft, beige-toned, non-air-entrained nature of the mortar having crushed silica sand, location beneath PC-only mortar
14	Hydraulic Lime Mortar	Petrographic Microscope	Severe carbonation of paste, variable degrees of carbonation and paste densities, relict hydraulic phases
15	PC-only and slag-lime Mortars	Petrographic Microscope	Optical microcopy of Piece #O1 in Figure 7 showing dense PC paste, crushed silica sand, leaching and carbonation at the surface, shrinkage microcracking, secondary carbonates in microcracks
16	PC-only mortar portion	SEM-EDS	SEM-EDS of Piece #O1 showing phosphate enrichment at the surface, typical Ca-silicate paste in the interior of PC-only mortar
17	PC-only and slag-lime Mortars	Petrographic Microscope	Optical microcopy of Piece #O2 in Figure 7 showing microstructures of PC-only and slag-lime mortars
18, 19	PC-only and slag-lime Mortars	SEM-EDS	SEM-EDS of Piece #O2 showing microstructure and microchemistry of PC-only and slag-lime mortars
20, 21	PC-only mortar	Petrographic Microscope	Optical microcopy of Piece #O3 in Figure 7 showing dense PC paste, crushed silica sand, leaching and carbonation at the surface
22	PC-only mortar	SEM-EDS	SEM-EDS of Piece #O3 showing microstructure and microchemistry of PC-only mortar, including secondary ettringite in a crack
23, 24	PC-only mortar	Petrographic Microscope	Optical microcopy of Piece #O4 in Figure 7 showing dense PC paste, crushed silica sand, leaching and carbonation at the surface
25	PC-only mortar	Petrographic Microscope	Optical microcopy of Piece #O5 in Figure 7 showing dense PC paste, crushed silica sand, leaching and carbonation at the surface
26	PC-only and hydraulic lime	Petrographic Microscope	Optical microcopy of Piece #O6 in Figure 7 showing contrasting microstructures of PC-only and underlying hydraulic lime mortars
27	PC-only and hydraulic lime	SEM-EDS	SEM-EDS of Piece #O6 showing contrasting microstructure and microchemistry of PC-only and underlying hydraulic lime mortars
28	PC-only and hydraulic lime	Petrographic Microscope	Optical microcopy of Piece #O7 in Figure 7 showing contrasting microstructures of PC-only and underlying hydraulic lime mortars
29	PC-only and hydraulic lime	SEM-EDS	SEM-EDS of Piece #O7 showing contrasting microstructure and microchemistry of PC-only and underlying hydraulic lime mortars
30	Hydraulic Lime	SEM-EDS	SEM-EDS of Piece #O7 showing microstructure and microchemistry of hydraulic lime mortar portion

Figures	Mortars	Microscopy	Features Found
31	PC-only mortar	Petrographic Microscope	Optical microcopy of Piece #O8 in Figure 7 showing dense PC paste, crushed silica sand, leaching and carbonation at the surface
32	PC-only mortar	Petrographic Microscope	Optical microcopy of Piece #O9 in Figure 7 showing dense PC paste, crushed silica sand, leaching and carbonation at the surface

Table 2: List of figures for mortars from the lower level from 1920s construction.

Conclusions drawn from all these figures regarding microstructures and microchemistries of mortars from the 1920s construction are as follows:

a. The original mortars applied at the lower level of Belltower during 1920s construction appeared to be lime-based (Figures 4, 7, 11, 12, 13, 14), having varieties ranging from hydraulic lime mortar to slag-lime mortar, both of which are present in minor amounts amongst the mortar pieces received and located at the inside ends of noticeably denser, harder, and darker Portland cement-only mortars.

b. Portland cement-only mortars are found to be applied over lime-based mortars as later pointing events (Figures 4 and 7), which are present either at the exposed ends of lime-based mortars in some pieces, or, most commonly received as entire pieces, indicating potential full-depth repointing of the original lime-based mortars, which were replaced with Portland cement-only mortars. Figures 10, 15, 17, 20, 23, 24, 25, 28, 31, and 32 show numerous thin section photomicrographs of Portland cement-only mortars from 1920s construction that were collected during observations in a petrographic microscope.

c. Portland cement-only mortars lack any lime component; hence are not representative of a common masonry mortar, where lime is commonly added for numerous benefits in masonry construction from improvement of properties of freshly placed mortars (water retention, workability) to properties of hardened mortars (reduction in brittleness, improved malleability to accommodate movements of monument without forming cracks).

d. Overall grain size of residual Portland cement particles in the dense pastes of Portland cement-only mortars are more similar to modern-day Portland cements than the cement from 1920s construction, where early cements were more coarsely ground than the modern Portland cements due to inferior grinding technologies during early 20th century. This also indicates a pointing event much later than the reported 1920s construction.

e. The dominant Portland cement-only mortars in most of the pieces received represent a more or less thorough repointing event where most of the original lime-based mortars were replaced with the Portland cement-only mortars.

f. Crushed silica sand is used in all mortars encountered, from the original lime-based mortars to later Portland cement-only mortars. This indicates a silica source, which was used both during the original construction and later pointing event. Sand is angular (crushed, manufactured) containing major amount of quartz and subordinate amount of feldspar and quartzite that are all well-graded, well-distributed, and present in sound conditions in all mortars without any potentially deleterious alkali-aggregate reactions.

g. The change in binder compositions are from the original lime-based binders, which were either hydraulic lime binder (Figures 13, 14, 26, and 28), or lime mixed with ground granulated blast furnace slag (Figures 11, 12, 15, and 17, especially Figure 12) all of which resulted in variably carbonated often leached pastes of variable porosities to much denser, harder Portland cement-only binders where later caused formation of network of fine hairline shrinkage microcracks that are absent in the lime-based mortars.

h. Both the original lime-based mortars and the later Portland cement-only mortars are non-air entrained. Air contents in the Portland cement only mortars applied during later repointing events are estimated to be 4 to 6 percent by volume (Figure 9). Air content in slag-lime mortar is estimated to be 3 to 4 percent (Figure 11). Air content in hydraulic lime mortar is estimated to be 2 to 3 percent (Figure 13).

i. The main microstructural difference between the earlier slag or cement-lime mortars and later pointing Portland cement-only mortars are in paste density and hence carbonation where earlier mortars are less dense, more carbonated, often leached resulting in higher paste porosities, whereas later Portland cement-only pointing mortars are noticeably denser, harder, contain abundant residual Portland cement particles and show only thin surface carbonation and leaching (usually leached zone occurs above carbonated zone) where such altered zones are within 0.2 to 0.5 mm in thickness after which denser, non-carbonated, sound interior paste occurs.

j. Another microstructural difference between the earlier lime-based and later Portland cement-only mortar is best detected in secondary electron images in SEM-EDS studies (Figures 16, 19, 22, 27, 29) where Portland cement-only mortars showed network of closed polygonal-shaped shrinkage microcracks that are not present in the lime-based mortars. Figures 10 and 15 show extensive microcracking only in the thin section photomicrographs of Portland cement-only pointing mortar, but not in the underlying slag-lime mortar where microcracks are filled with secondary calcium carbonate precipitates.

k. Secondary ettringite and secondary calcium carbonate are two common secondary deposits found in many original and pointing mortars that are testaments of the presence of moisture in the mortars for prolonged periods. Such deposits, however, did not cause any deleterious reactions to affect the overall conditions of original or pointing mortars. Leaching of paste, when occurred (mostly at the exposed surface regions) caused loss of lime at the expense of silica. Silica at severely leached regions occurred as gelatinous masses in optically isotropic conditions.

l. Secondary carbonate precipitations at the edges of a few Portland cement-only pointing mortars showed thaumasite formation (Figures 21 and 24) due to the availability of moisture, sulfate, carbonate and silicate in cold weather condition during service.

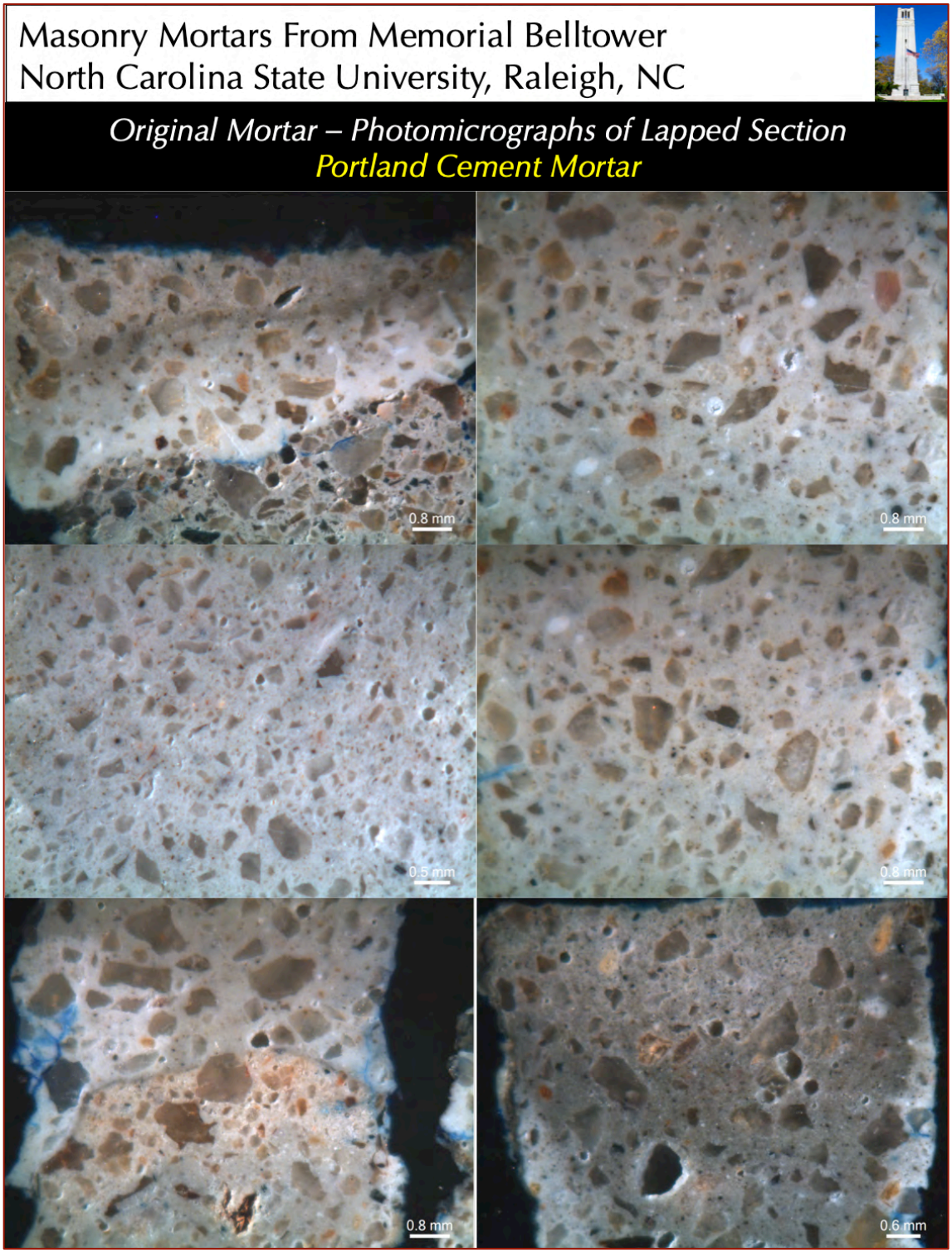

Figure 9: Photomicrographs of lapped section of various Portland cement mortar pieces from 1920s construction from the lower level of the tower (collected from the thin section residue shown in Figure 7) showing the dense, non-air-entrained nature of the mortar having crushed silica sand aggregate of nominal 1 mm size, a few coarse irregularly-shaped entrapped voids, and beige to light to dark gray paste color tones due to various degrees of alterations (from carbonation, leaching, etc.) of original mortar. The top left photo shows interface between PC mortar and underlying slag-lime mortar. Many air voids in top right photo are filled with white secondary ettringite deposits indicating presence of moisture in the mortar during service.

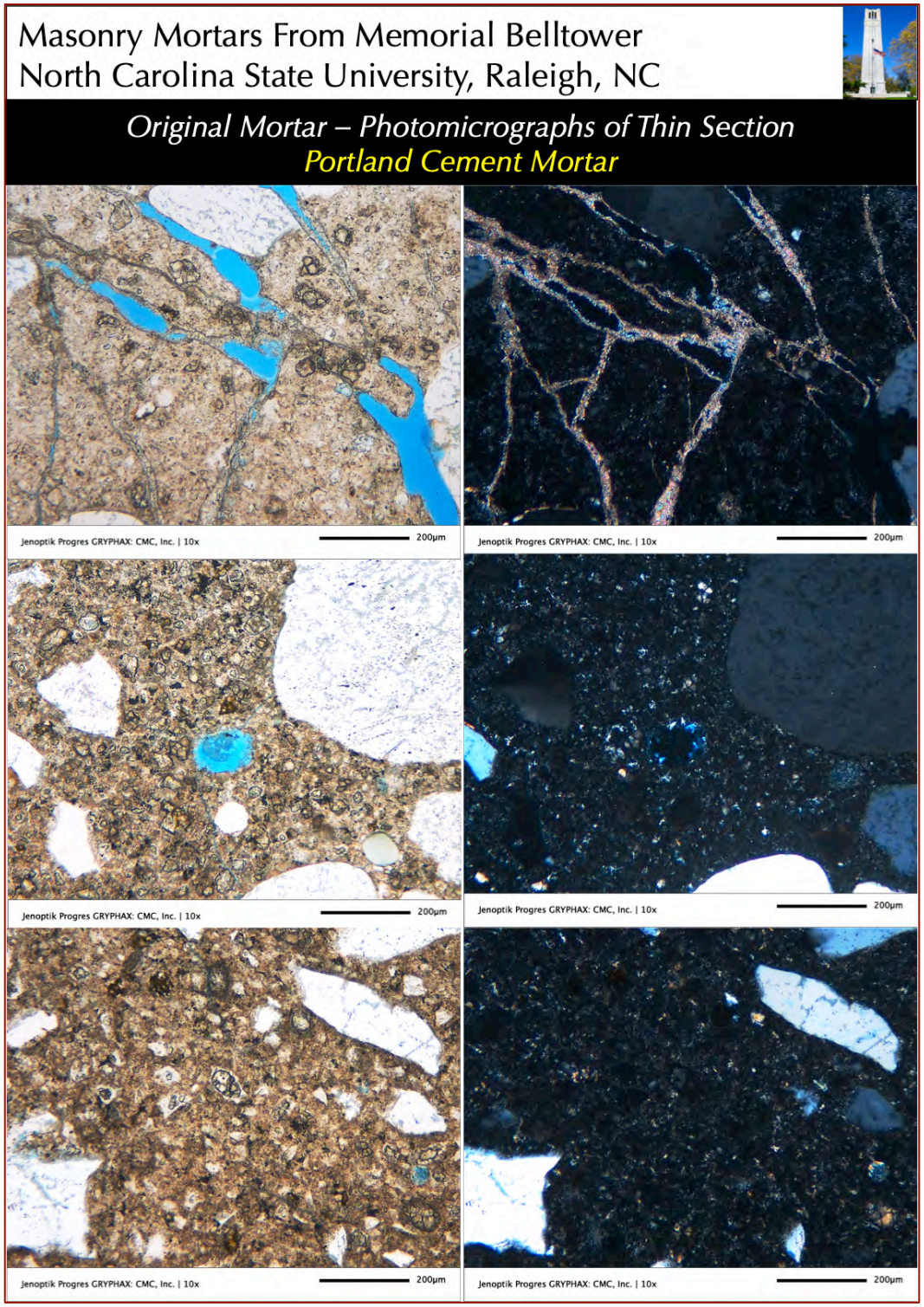

Figure 10: Photomicrographs of thin section of various Portland cement mortar pieces from 1920s construction from the lower level of the tower (collected from the thin section shown in Figure 7) showing: (a) severe shrinkage microcracking in paste many of which are filled with secondary calcium carbonate deposites (top row); (b) dense, overall non-carbonated nature of paste having many residual Portland cement particles (middle and bottom rows) which do not represent coarsely ground cement typically found in 1920s vintage; (c) thin hydration rims around many calcium silicate paritcles of Portland cement; (d) crushed quartz sand particles; and (e) lack of any intentionally introduced entrained air, except a few entrapped ones highlighted by blue epoxy.

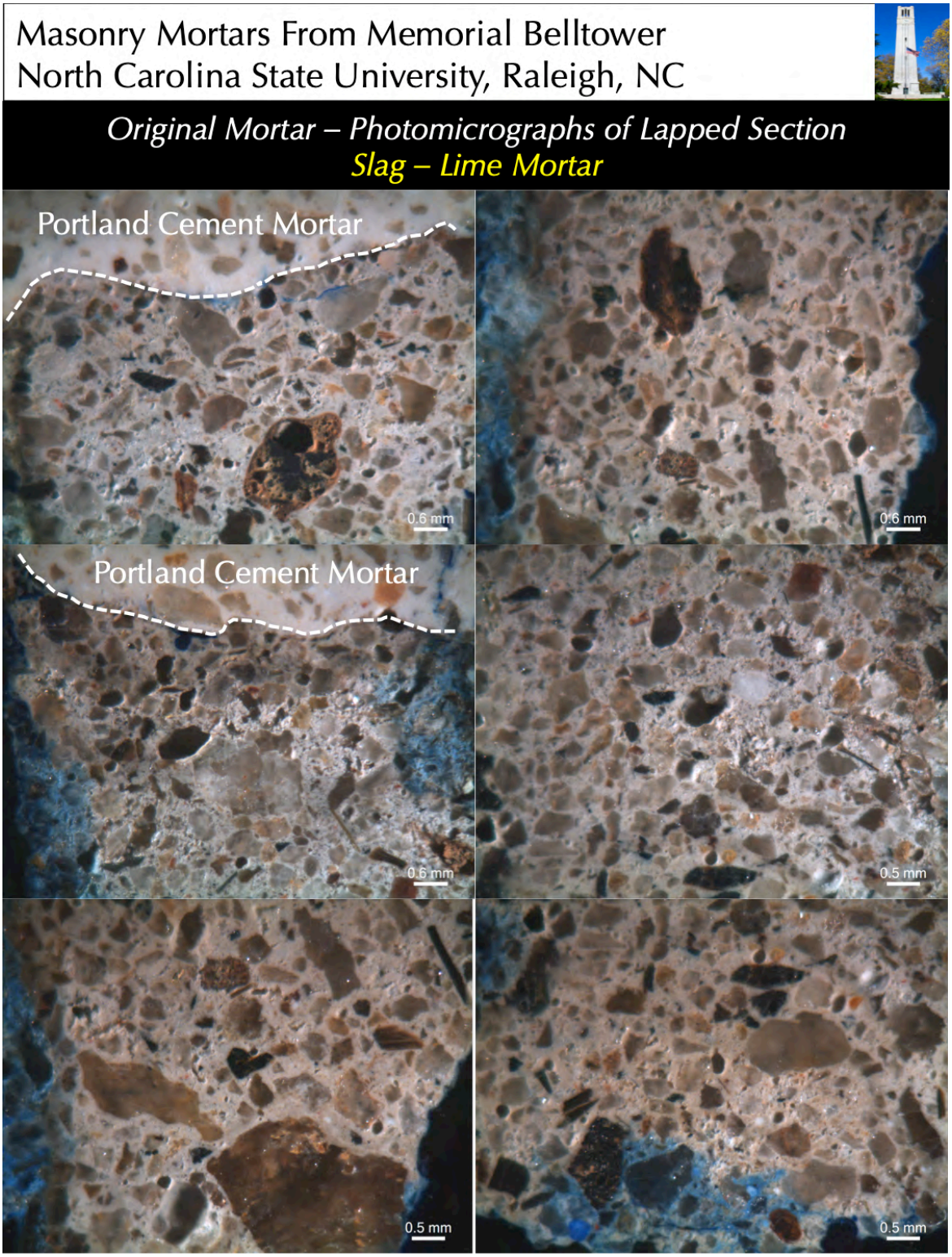

Figure 11: Photomicrographs of lapped section of various slag-lime mortar pieces from 1920s construction from the lower level of the tower (collected from the thin section residue shown in Figure 7) showing the moderately dense, non-air-entrained nature of the mortar having crushed silica sand aggegate of nominal 2 mm size, a few coarse irregularly-shaped entrapped voids, and beige to light gray paste color tones due to various degrees of alterations (from carbonation, leaching, etc.) of original mortar. The top left photo shows interface between PC mortar and underlying slag-lime mortar. Sand particles in slag-lime mortar are coarser than sand in PC mortar.

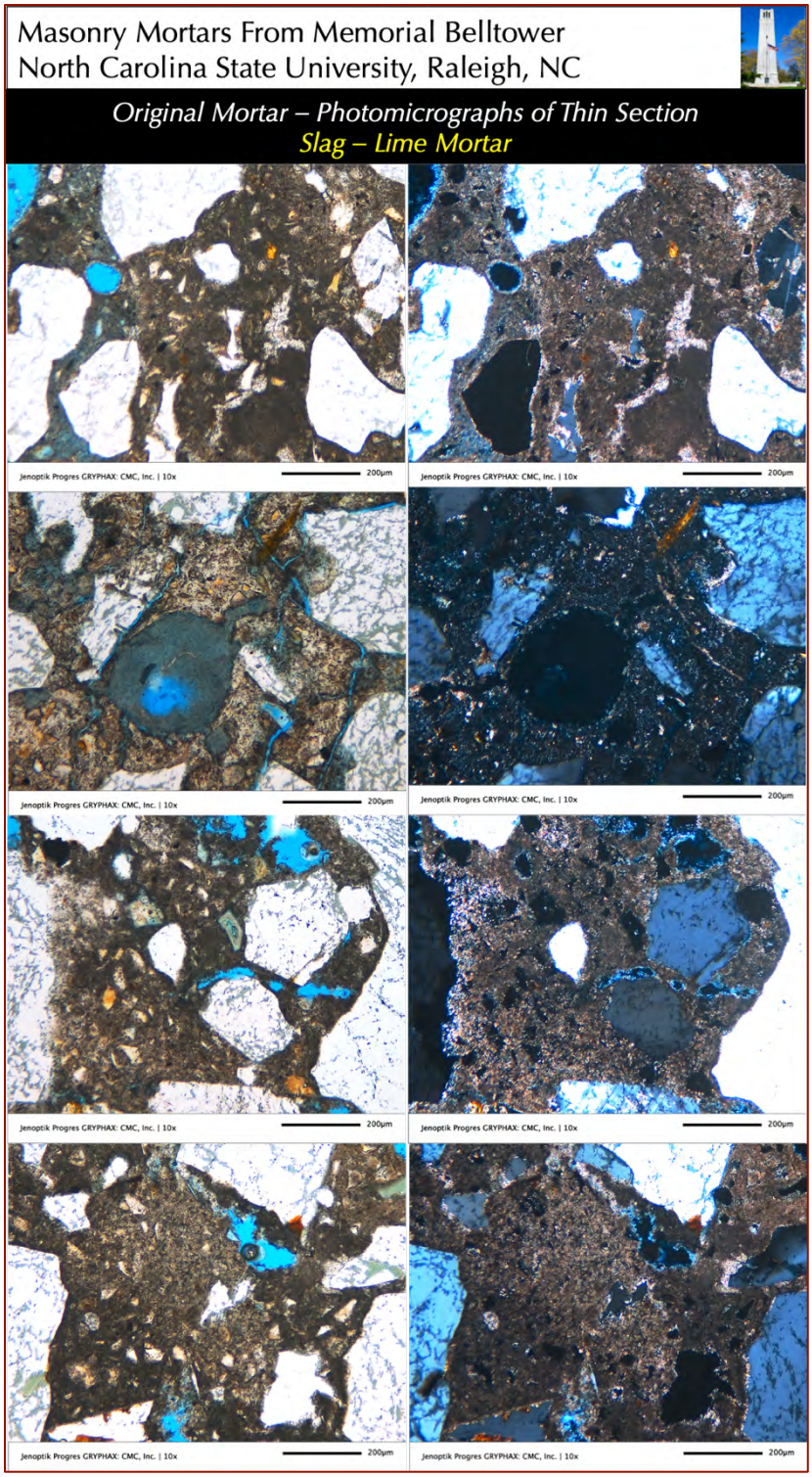

Figure 12: Photomicrographs of thin section of various slag-lime mortar pieces from 1920s construction from the lower level of the tower (collected from the thin section shown in Figure 7) showing: (a) moderately dense, overall carbonated paste having shrinkage microcracks many of which are filled with secondary calcium carbonate deposites (top row); (b) angular, shard-like glassy particles of ground granulated blast furnace slag having the fineness of Portland cement; (c) crushed quartz sand particles; (d) lack of any intentionally introduced entrained air, except a few entrapped ones highlighted by blue epoxy; and (e) secondary ettringite deposits in an air void in the 2nd row from top.

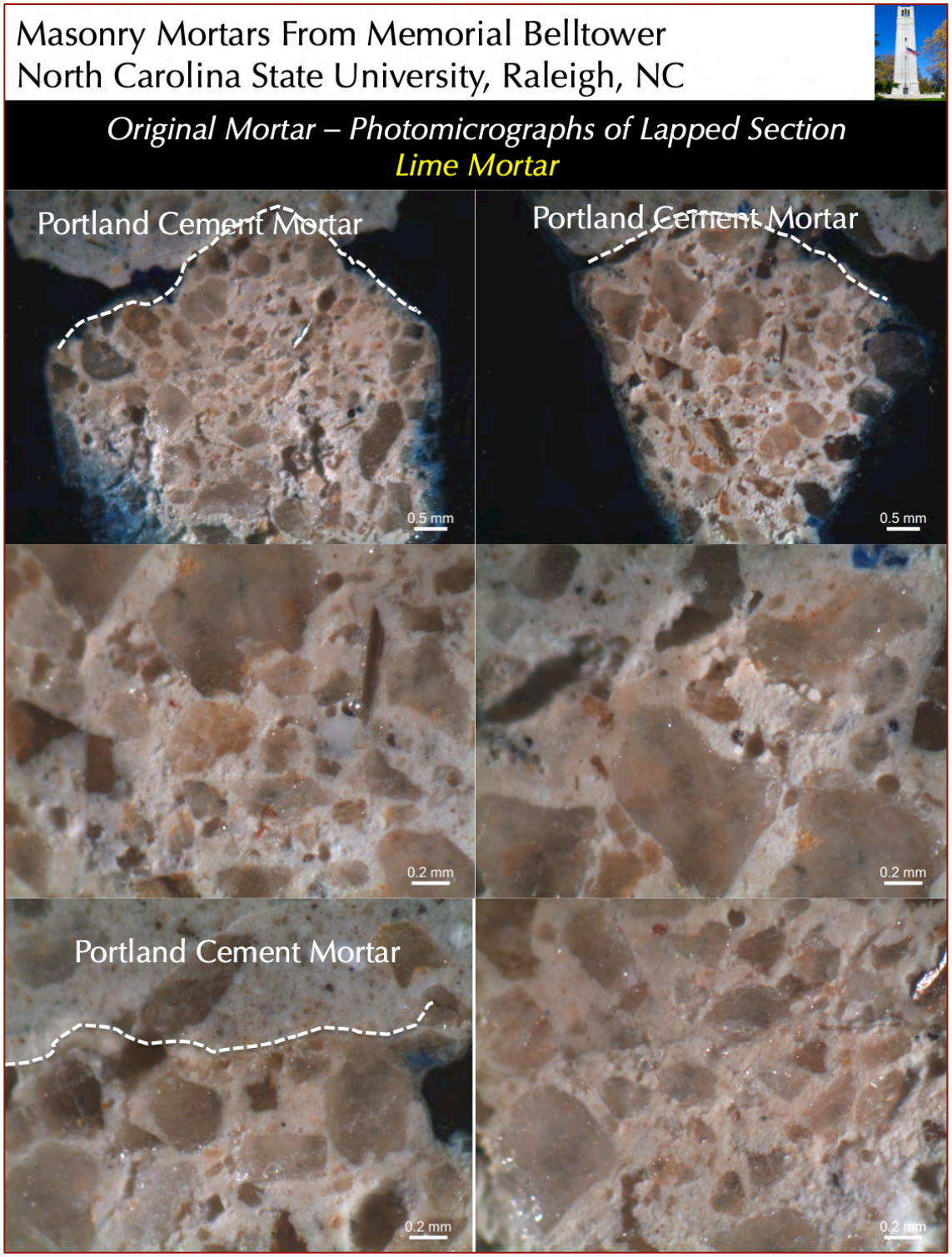

Figure 13: Photomicrographs of lapped section of two hydraulic lime mortar pieces beneath PC mortars in O6 and O7 from 1920s construction from the lower level of the tower (collected from the thin section residue shown in Figure 7) showing the moderately soft, beige-toned, non-air-entrained nature of the mortar having crushed silica sand aggegate of nominal 1 mm size, a few coarse irregularly-shaped entrapped voids, and beige paste color tone due to carbonation and leaching of original lime mortar. The top left photo shows interface between PC mortar and underlying lime mortar in pieces O6 (top right) and O7 (top left).

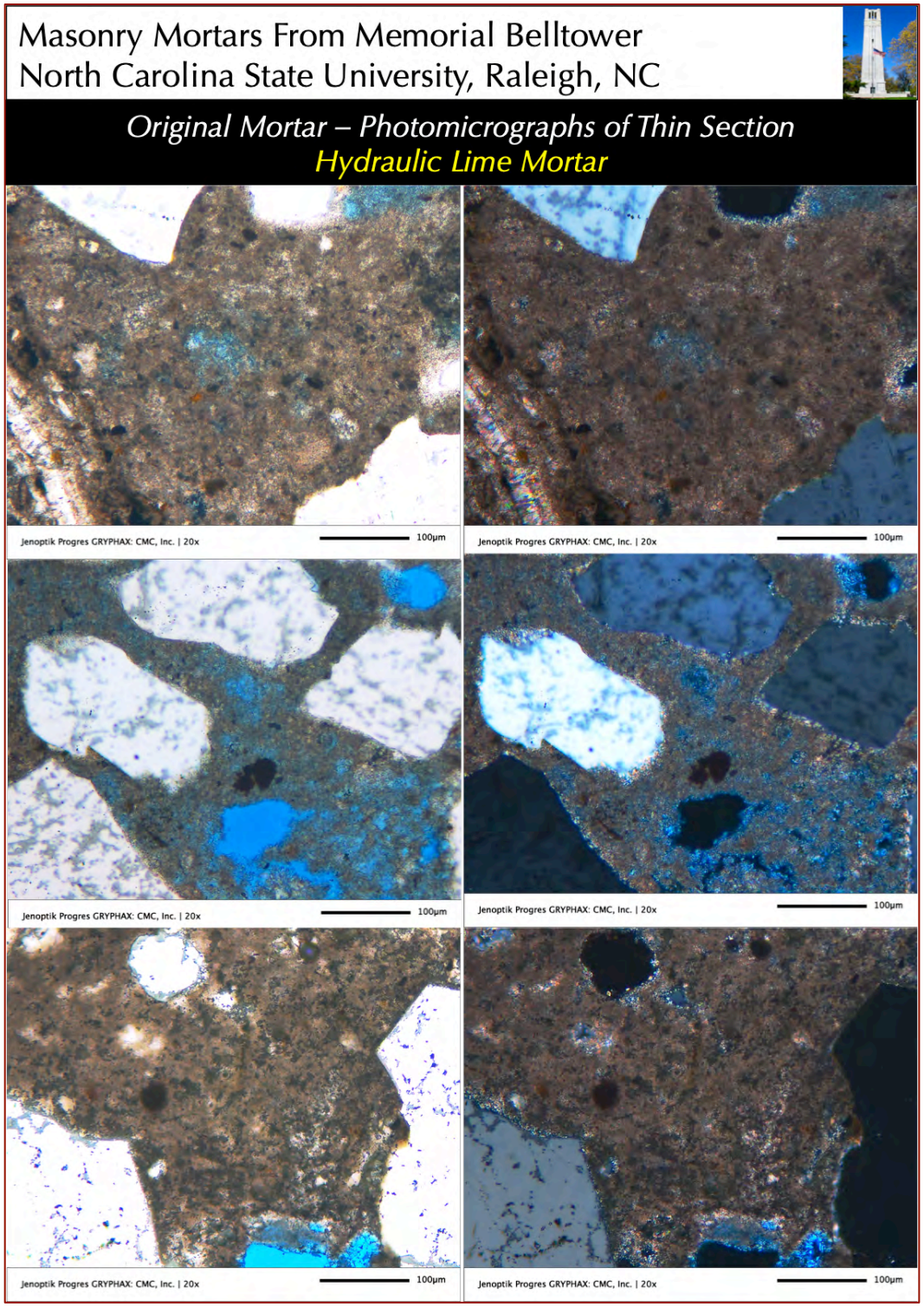

Figure 14: Photomicrographs of thin section of two hydraulic lime mortar (L) pieces beneath PC mortars in O6 and O7 from 1920s construction from the lower level of the tower (collected from the thin section shown in Figure 7) showing the moderately soft, fine-grained, severely carbonated, non-air-entrained nature of the mortar having crushed silica sand aggegate of nominal 1 mm size, a few coarse irregularly-shaped entrapped voids highlighted in blue epoxy, variable paste porosities due to variable carbonation and leaching, and a few relict carbonated residual hydraulic particles (e.g., belite) of original hydraulic lime binder.

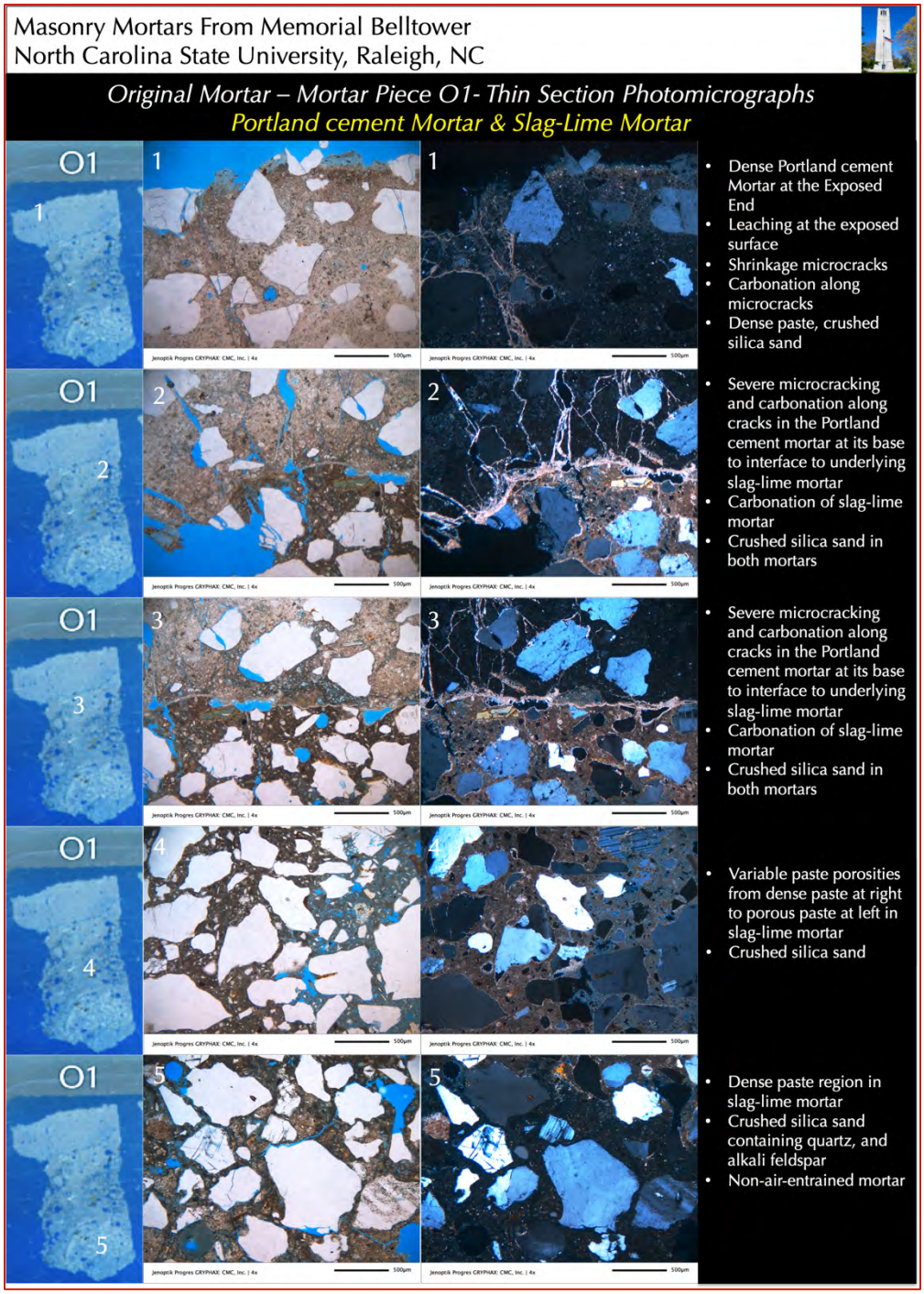

Figure 15: Photomicrographs of thin section of Piece O1 from 1920s construction (see Figure 7) showing: (a) leaching and carbonation at the top 0.5 mm of exposed surface of Portland cement-only (PC) mortar (1st row); (b) shrinkage microcracks in PC mortar many of which are filled with secondary calcium carbonate deposits (2nd row from top); (c) interface between non-carbonated PC mortar at the top and carbonated slag-lime mortar beneath (3rd row from top); (d) variable paste porosities in slag-lime mortar in 4th and 5th rows from top where paste shows severe carbonation, in sharp contrast to dense non-carbonated paste in the PC mortar applied over the slag-lime mortar; and (e) crushed silica sand particles in both mortar types that are well-graded, and well-distributed. Five rows of photos were taken from five different locations shown in the leftmost column on thin section view of Piece O1. Photos were taken in plane (left) and corresponding crossed (right) polarized light modes with a petrographic microscope. Notice lack of air entrainment in the mortars.

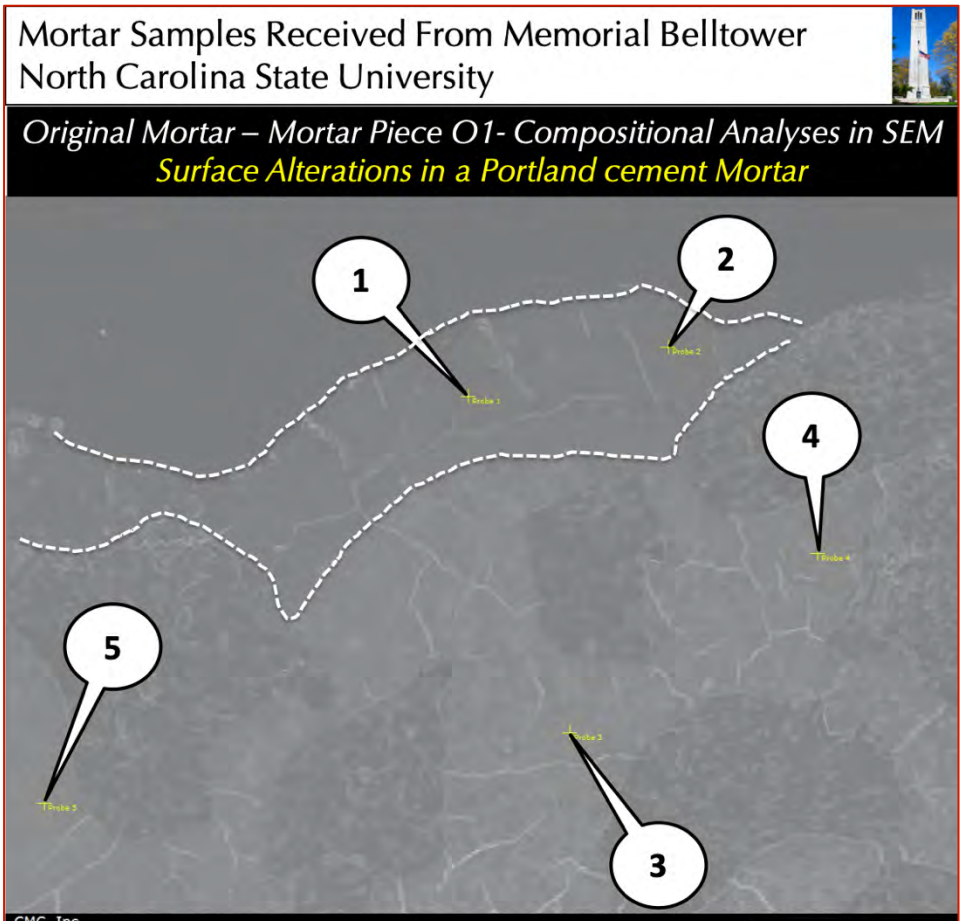

#	CaO	SiO2	Al2O3	Na2O	MgO	SO3	K2O	TiO2	FeO	P2O5	CO2	Total	Phase	Paste CI
1	21.39	40.52	4.42	0.20	0.00	1.22	0.43	0.58	0.81	11.64	18.78	99.18	Surface	-
2	23.18	28.94	4.97	0.32	0.07	0.15	0.18	0.78	3.82	19.29	18.30	96.18	Alterations	-
3	75.35	18.29	0.36	0.00	0.01	0.00	0.00	0.22	1.00	-	4.77	99.00	Paste	0.69
4	46.85	28.19	1.99	0.82	0.82	0.20	0.01	0.40	0.62	-	20.08	99.36	Paste	1.70
5	69.28	23.44	0.41	0.00	0.00	0.00	0.14	0.08	0.23	-	6.42	99.77	Paste	0.96

Figure 16: Secondary electron image (SED) in a scanning electron microscope (top), X-ray elemental maps of calcium (Ca), silicon (Si), aluminum (Al), and phosphorus (P) in the SED (middle), and X-ray compositional analyses at the tips of callouts placed across various areas of paste (avoiding potential interference from nearby grains) in the bottom Table for the Portland cement-only mortar collected from the lower level of tower from 1920s construction. A thin surface layer rich in calcium phosphate alteration is seen in the SED from where Probe #1 and 2 show high phosphorus along with lime and high silica (Ca<Si in Probe #1 and 2 due to leaching of lime that has enriched the silica compared to interior sound paste where Ca is >> Si). Probe #3 to 5 were taken from three different locations of PC mortar's paste showing characteristic calcium-silicate-hydrate composition of paste having Ca>>Si.

Paste-CI (after Eckel 1922) is calculated as CI = $[(2.8*SiO_2)+(1.1*Al_2O_3)+(0.7*Fe_2O_3)]/[(CaO)+(1.4*MgO)]$ from sound unaltered paste, which shows values from 0.7 to 1.7 indicating variable hydraulicities of paste. Carbon, represented as CO_2 is from carbonated paste and epoxy used in thin section preparation.

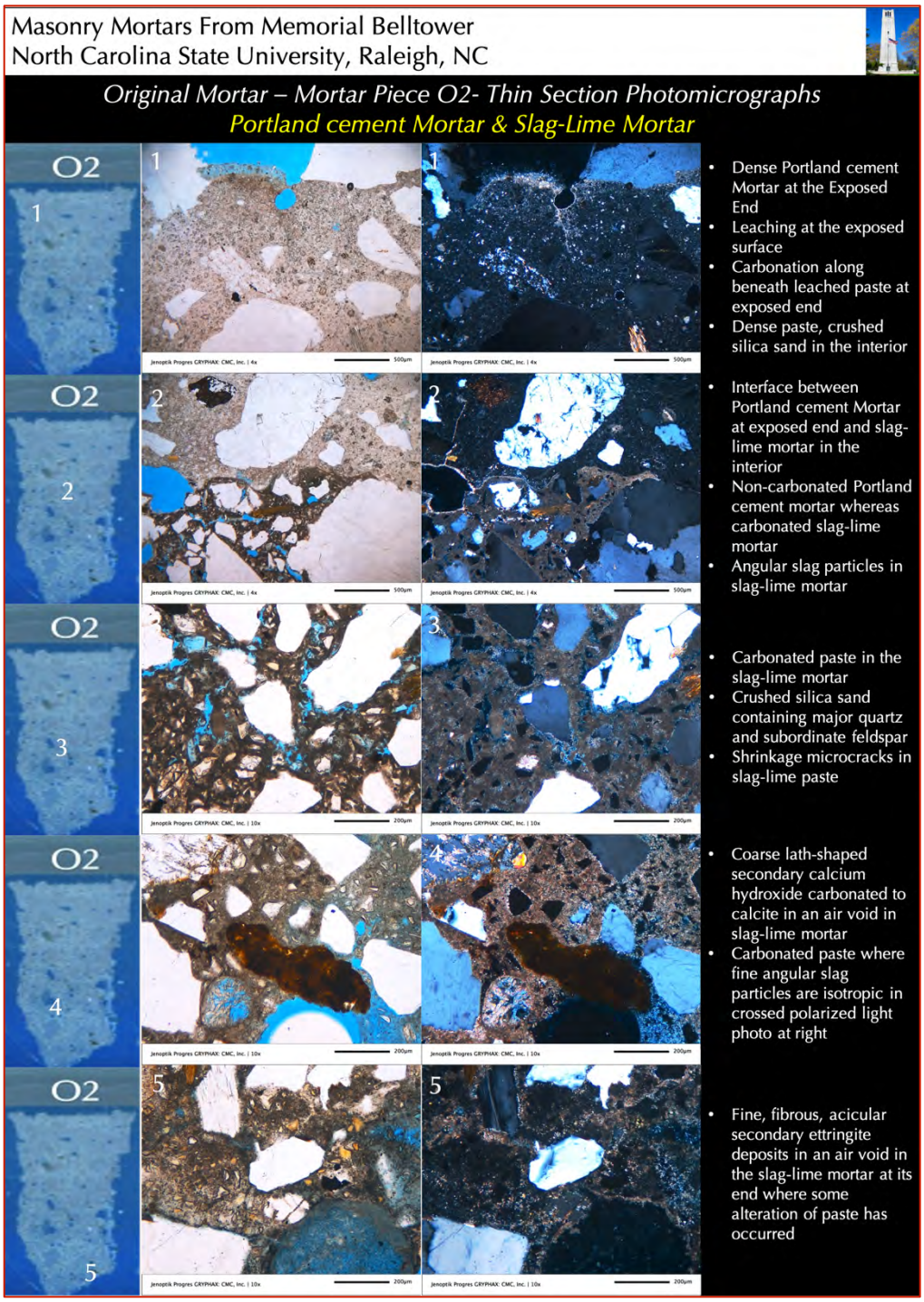

Figure 17: Photomicrographs of thin section of Piece O2 from 1920s construction (see Figure 7) showing: (a) leaching and carbonation at the top 0.2 mm of exposed surface of Portland cement-only (PC) mortar (1st row); (b) interface between non-carbonated PC mortar at the top and carbonated slag-lime mortar beneath (2nd row from top); (c) variable paste porosities in slag-lime mortar in 2nd to 5th rows from top where paste shows severe carbonation, which is in sharp contrast to dense non-carbonated paste in the PC mortar; (d) shrinkage microcracks in slag-lime mortar (3rd row from top); and (d) crushed silica sand particles in both mortar types that are well-graded, and well-distributed. Five rows of photos were taken from five different locations shown in the leftmost column on thin section view of Piece O2. Notice lack of air entrainment in the mortars.

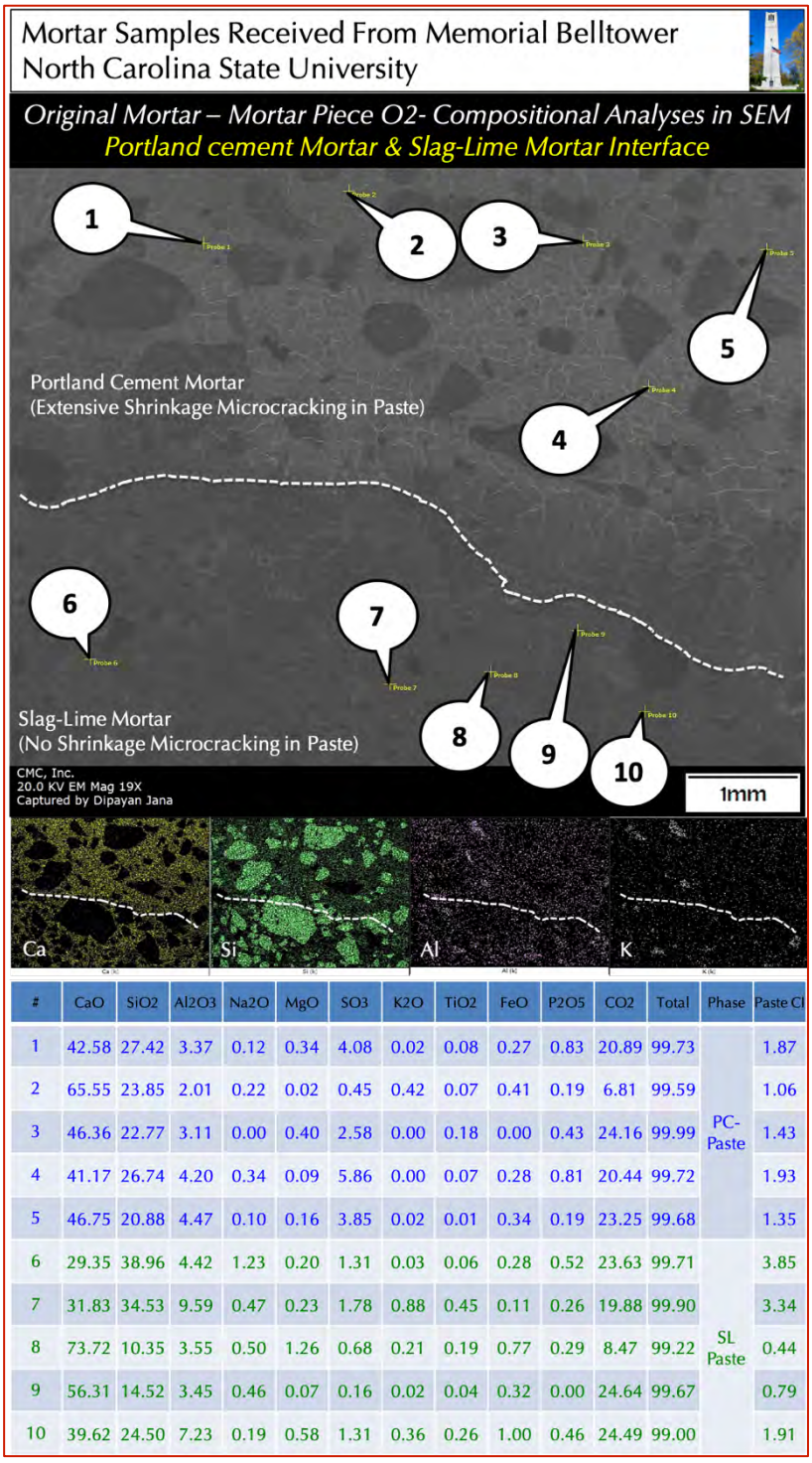

#	CaO	SiO2	Al2O3	Na2O	MgO	SO3	K2O	TiO2	FeO	P2O5	CO2	Total	Phase	Paste CI
1	42.58	27.42	3.37	0.12	0.34	4.08	0.02	0.08	0.27	0.83	20.89	99.73	PC-Paste	1.87
2	65.55	23.85	2.01	0.22	0.02	0.45	0.42	0.07	0.41	0.19	6.81	99.59		1.06
3	46.36	22.77	3.11	0.00	0.40	2.58	0.00	0.18	0.00	0.43	24.16	99.99		1.43
4	41.17	26.74	4.20	0.34	0.09	5.86	0.00	0.07	0.28	0.81	20.44	99.72		1.93
5	46.75	20.88	4.47	0.10	0.16	3.85	0.02	0.01	0.34	0.19	23.25	99.68		1.35
6	29.35	38.96	4.42	1.23	0.20	1.31	0.03	0.06	0.28	0.52	23.63	99.71	SL Paste	3.85
7	31.83	34.53	9.59	0.47	0.23	1.78	0.88	0.45	0.11	0.26	19.88	99.90		3.34
8	73.72	10.35	3.55	0.50	1.26	0.68	0.21	0.19	0.77	0.29	8.47	99.22		0.44
9	56.31	14.52	3.45	0.46	0.07	0.16	0.02	0.04	0.32	0.00	24.64	99.67		0.79
10	39.62	24.50	7.23	0.19	0.58	1.31	0.36	0.26	1.00	0.46	24.49	99.00		1.91

Figure 18: Secondary electron image (SED) in a scanning electron microscope (top), X-ray elemental maps of calcium (Ca), silicon (Si), aluminum (Al), and potassium (K) in the SED (middle), and X-ray compositional analyses at the tips of callouts placed across various areas of paste (avoiding potential interference from nearby grains) in the bottom Table for the interfacial region between the Portland cement-only mortar at the top and slag-lime mortar beneath. Probe #1 through 5 were taken from paste across PC only mortar, whereas Probe #6 through 10 were taken from paste in slag-lime mortar. X-ray elemental maps show relatively higher overall calcium and aluminum in the PC-only mortar than that in the slag-lime mortar, which could be due to leaching of lime and alumina from the latter (which is also the mortar applied prior to the PC mortar).

The clear difference between the two mortar types is in the lime-silica compositions of paste, along with variations in some other oxides, which are shown in different colored rows in the compositional Table.

Paste-CI (after Eckel 1922) is calculated as CI = $[(2.8*SiO_2)+(1.1*Al_2O_3)+(0.7*Fe_2O_3)]/[(CaO)+(1.4*MgO)]$.

Notice severe microcracking as network of closed polygonal-shaped fine shrinkage microcracks in the PC mortar, but no such network of microcracks in the underlying slag-lime mortar. Carbon, represented as CO_2 is from carbonated paste and epoxy used in thin section preparation.

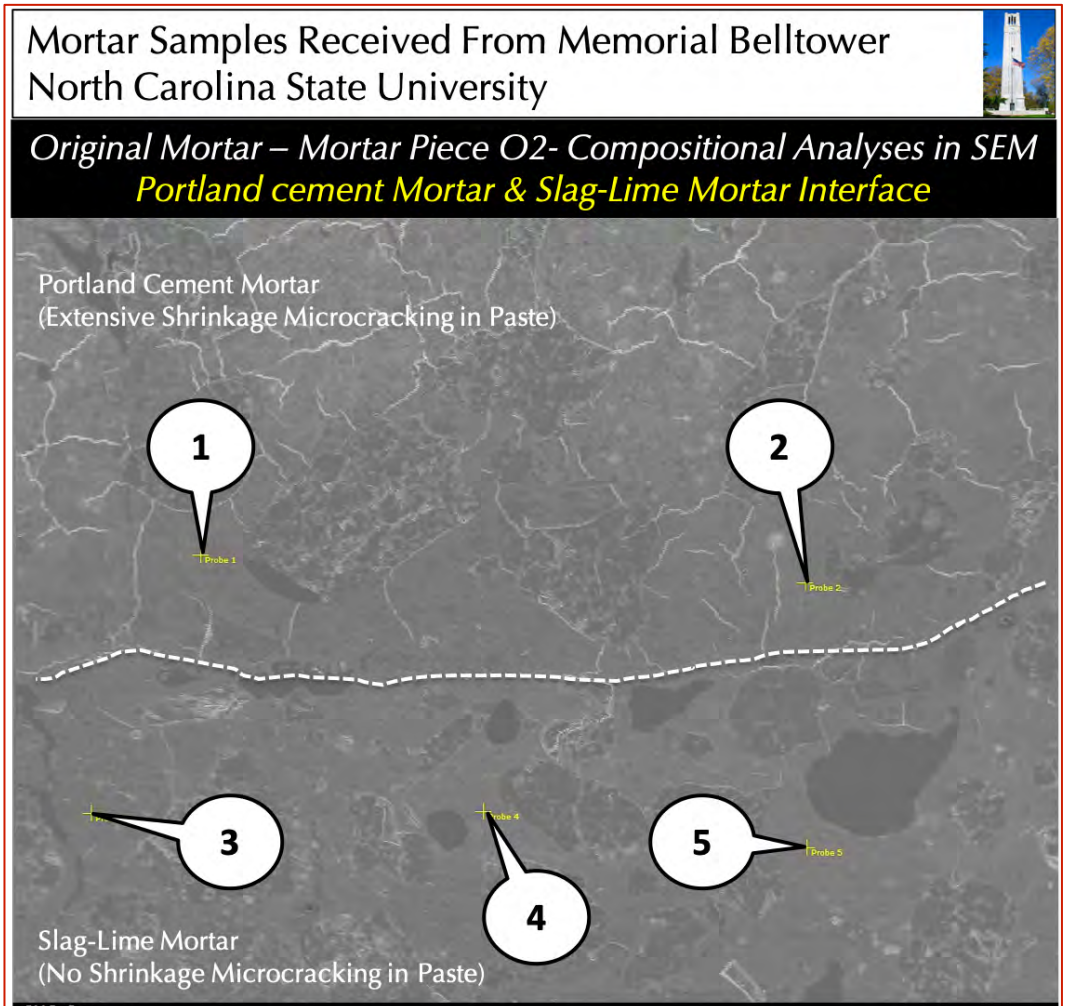

#	CaO	SiO2	Al2O3	Na2O	MgO	SO3	K2O	TiO2	FeO	P2O5	CO2	Total	Phase	Paste CI
1	36.76	37.93	5.06	0.63	0.60	1.26	0.00	0.03	2.11	0.20	15.41	97.88	PC Paste	3.01
2	32.62	36.76	4.05	0.70	0.27	1.65	0.08	0.11	0.29	0.19	23.28	99.71		3.26
3	41.53	19.60	5.15	0.00	0.29	0.40	0.47	0.08	0.24	2.76	29.49	99.77	SL Paste	1.45
4	34.24	33.03	9.80	0.46	1.11	1.15	0.51	0.45	0.32	0.34	18.59	99.68		2.89
5	91.43	2.60	0.18	0.00	0.00	0.07	0.00	0.00	0.03	0.40	5.29	99.97		0.08

Figure 19: Secondary electron image (SED) in a scanning electron microscope (top), and X-ray compositional analyses at the tips of callouts placed across various areas of paste (avoiding potential interference from nearby grains) in the bottom Table for the interfacial region between the Portland cement-only mortar at the top and slag-lime mortar beneath.

Probe #1 and 2 were taken from paste across interfacial region between PC only mortar and slag-lime, whereas Probe #3 through 5 were taken from paste more into the slag-lime mortar.

The clear difference between the two mortar types is in the lime-silica compositions of paste, along with variations in some other oxides, which are shown in different colored rows in the compositional Table.

Paste-CI (after Eckel 1922) is calculated as CI = $[(2.8*SiO_2)+(1.1*Al_2O_3)+(0.7*Fe_2O_3)]/[(CaO)+(1.4*MgO)]$. Notice severe microcracking as network of closed polygonal-shaped fine shrinkage microcracks in the PC mortar, but no such network of microcracks in the underlying slag-lime mortar. Carbon, represented as CO_2 is from carbonated paste and epoxy used in thin section preparation.

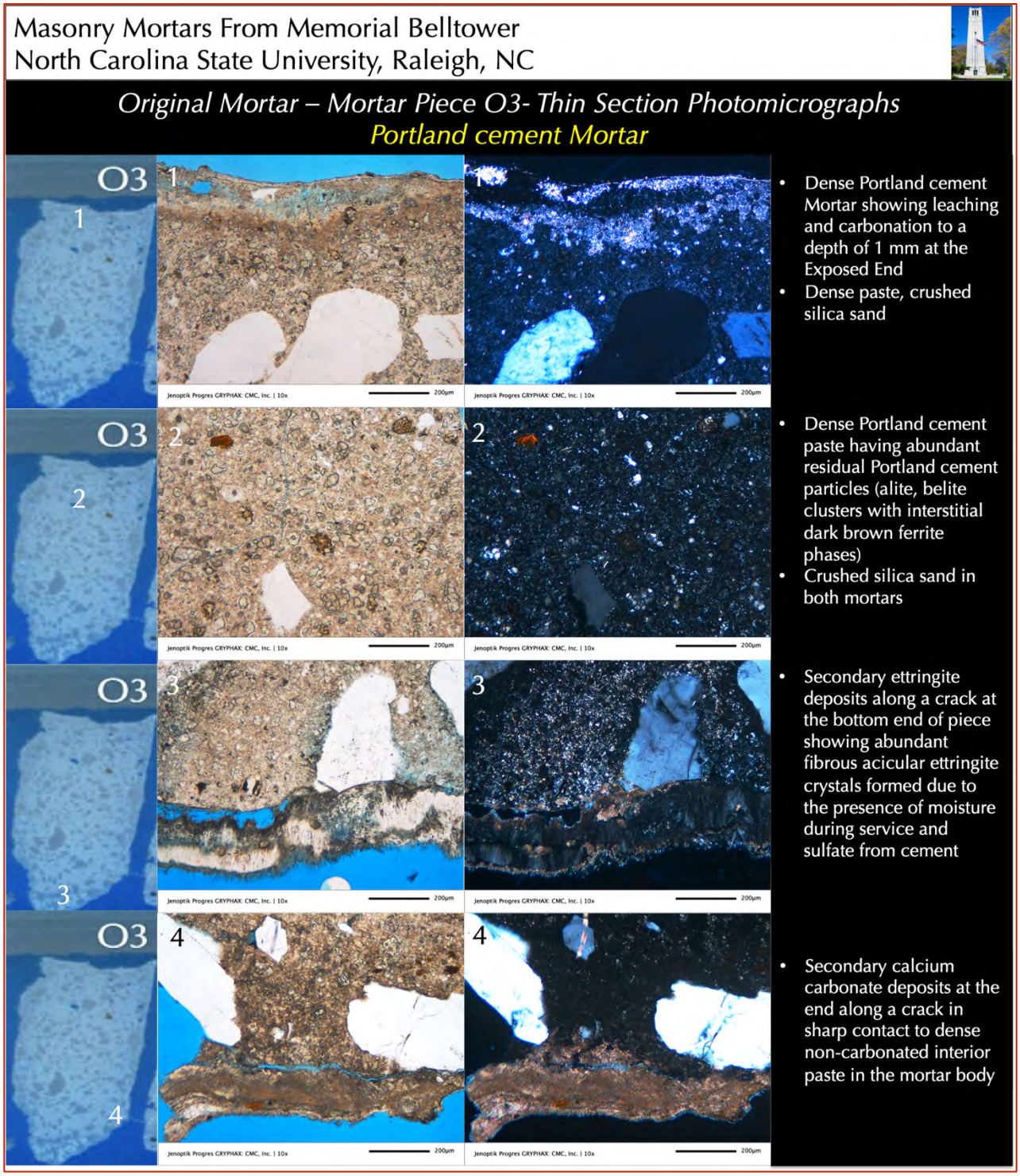

Figure 20: Photomicrographs of thin section of Piece O3 from 1920s construction (see Figure 7) showing: (a) leaching and carbonation at the top 0.5 to 1 mm of exposed surface of Portland cement-only (PC) mortar (1st row); (b) dense PC paste having many residual PC particles and overall non-carbonated nature of interior paste (2nd and 3rd row from top); (c) fibrous secondary ettringite precipitation in a crack at an edge of mortar (3rd row from top); (d) secondary calcium carbonate deposition at another edge of mortar (4th row from top); and (e) crushed silica sand particles that are well-graded, and well-distributed. Four rows of photos were taken from four different locations shown in the leftmost column on thin section view of Piece O3.

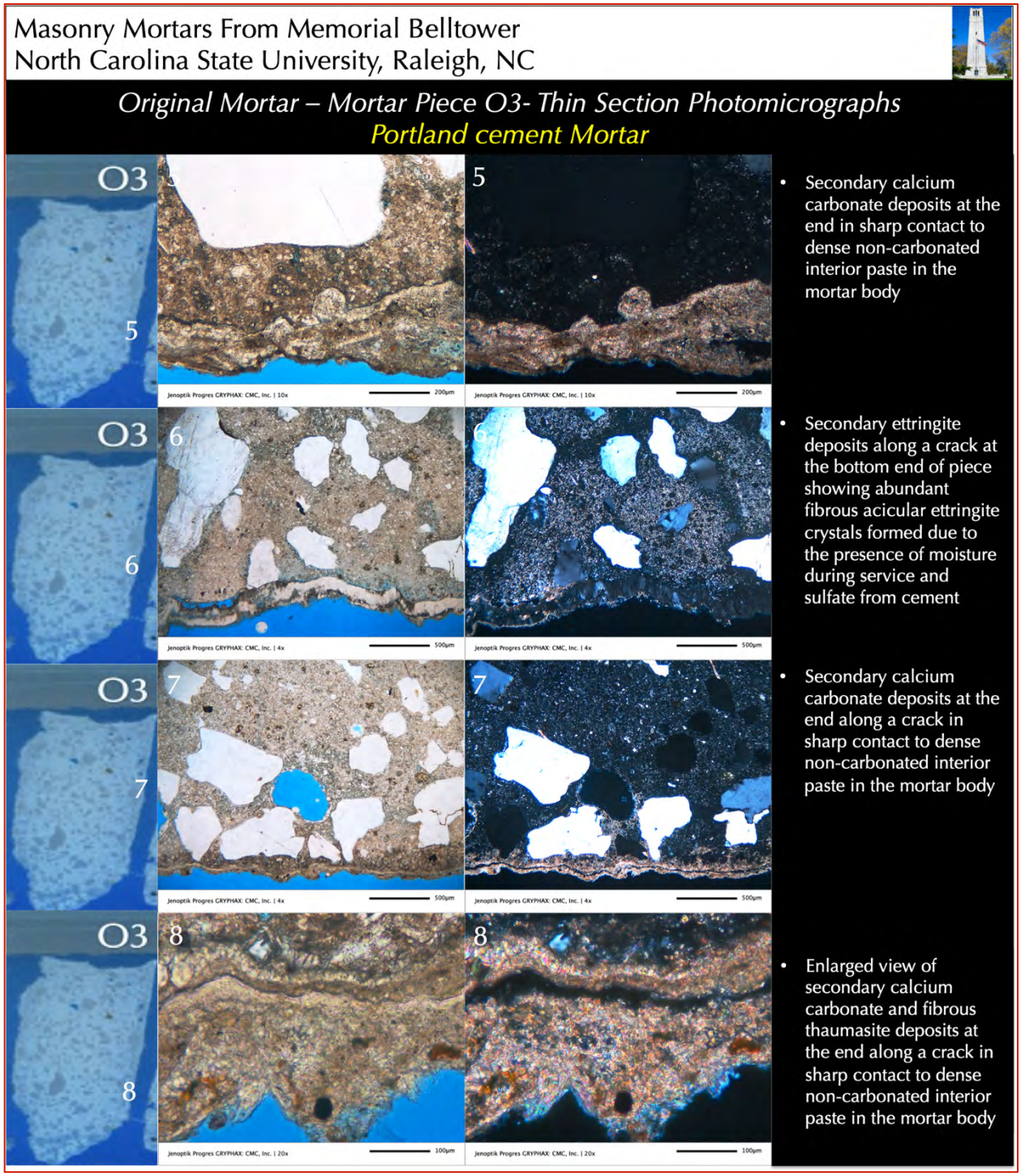

Figure 21: Photomicrographs of thin section of Piece O3 from 1920s construction (see Figure 7) showing secondary ettringite and secondary calcium carbonate precipitates along the edges of the mortar piece that are marked as 5 through 8 (continuation from previous Figure) and shown in four rows. The bottom row shows enlarged view of carbonate precipitate at edge of the mortar (location 8) where some fibrous carbonates indicate possible presence of thaumasite (calcium carbonate-silicate sulfate hydrate analogue of ettringite), which could form in the cold weather condition in the presence of sulfate, silicate, and carbonate ions.

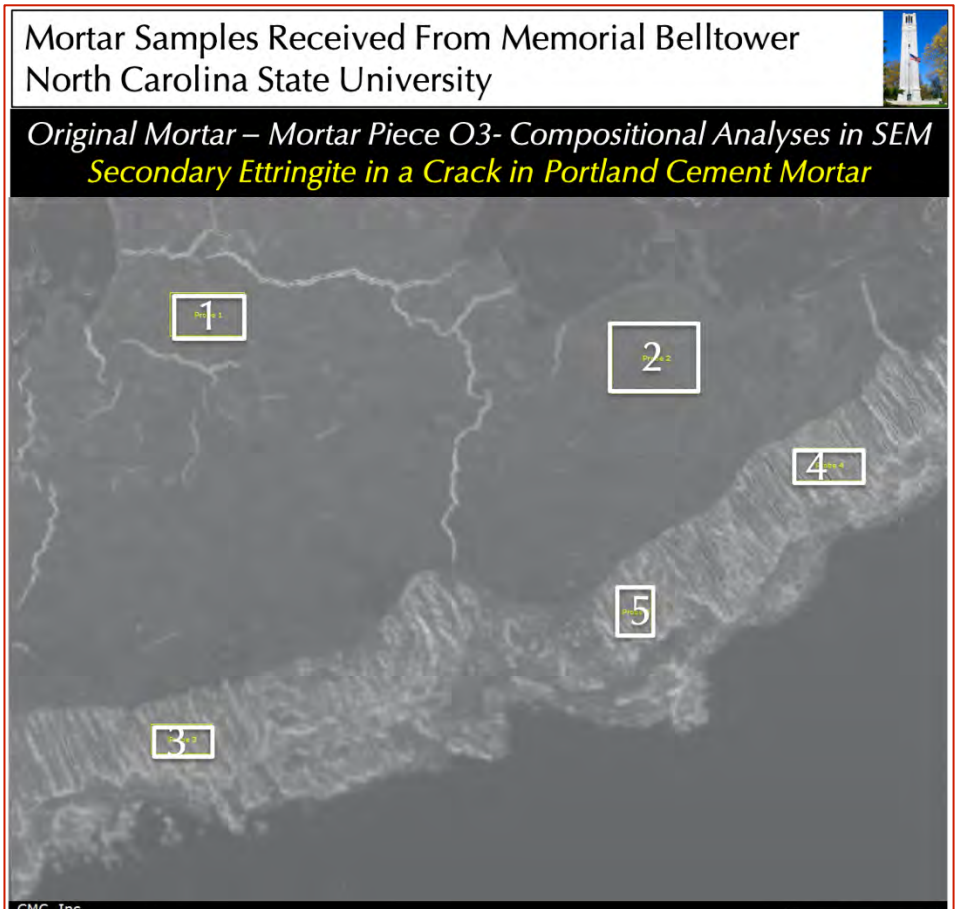

#	CaO	SiO2	Al2O3	Na2O	MgO	SO3	K2O	TiO2	FeO	P2O5	CO2	Total	Phase	Paste CI
1	40.49	34.25	2.00	1.08	0.61	0.61	0.03	0.01	0.96	1.72	18.23	99.03	PC Paste	3.01
2	38.40	31.74	1.58	0.95	0.35	1.11	0.00	0.18	0.57	1.55	23.55	99.41		3.26
3	41.07	8.93	9.63	0.00	0.00	19.63	0.04	0.00	0.06	0.85	19.78	99.93	Secondary Ettringite	1.45
4	42.06	8.83	9.61	0.00	0.00	21.49	0.00	0.04	0.04	0.81	17.12	99.96		2.89
5	40.66	7.94	10.27	0.04	0.00	21.52	0.00	0.03	0.08	0.61	18.85	99.92		0.08

Figure 22: Secondary electron image (SED) in a scanning electron microscope (top), X-ray elemental maps of calcium (Ca), silicon (Si), aluminum (Al), and sulfur (S) in the SED (middle), and X-ray compositional analyses at the boxed areas (raster) placed across various areas of paste (avoiding potential interference from nearby grains) in the bottom Table for the Portland cement only mortar having a crack filled with secondary ettringite deposits. Probe #1 and 2 were taken from paste across PC only mortar whereas Probe #3 to 5 were taken from over ettringite-filled crack.

X-ray elemental maps show characteristic enrichment of calcium, sulfur, and alumina within the ettringite-filled crack, which is consistent with composition of ettringite. This ettringite compositional 'band' is followed by a thin silica-rich lime-poor layer outside the ettringite-filled crack where leaching of lime has enriched the paste in silica (shown by Si enrichment right beside the dark Si-poor region of ettringite-filled crack).

The clear difference between the PC mortar's paste and secondary ettringite deposit in crack are in the Ca-Al-S compositions, which are shown in different color-coded rows in the compositional Table.

Paste-CI (after Eckel 1922) is calculated as CI = $[(2.8*SiO_2)+(1.1*Al_2O_3)+(0.7*Fe_2O_3)]/[(CaO)+(1.4*MgO)]$. Carbon, represented as CO_2 is from carbonated paste and epoxy. Notice severe microcracking as network of closed polygonal-shaped fine shrinkage microcracks in the PC mortar.

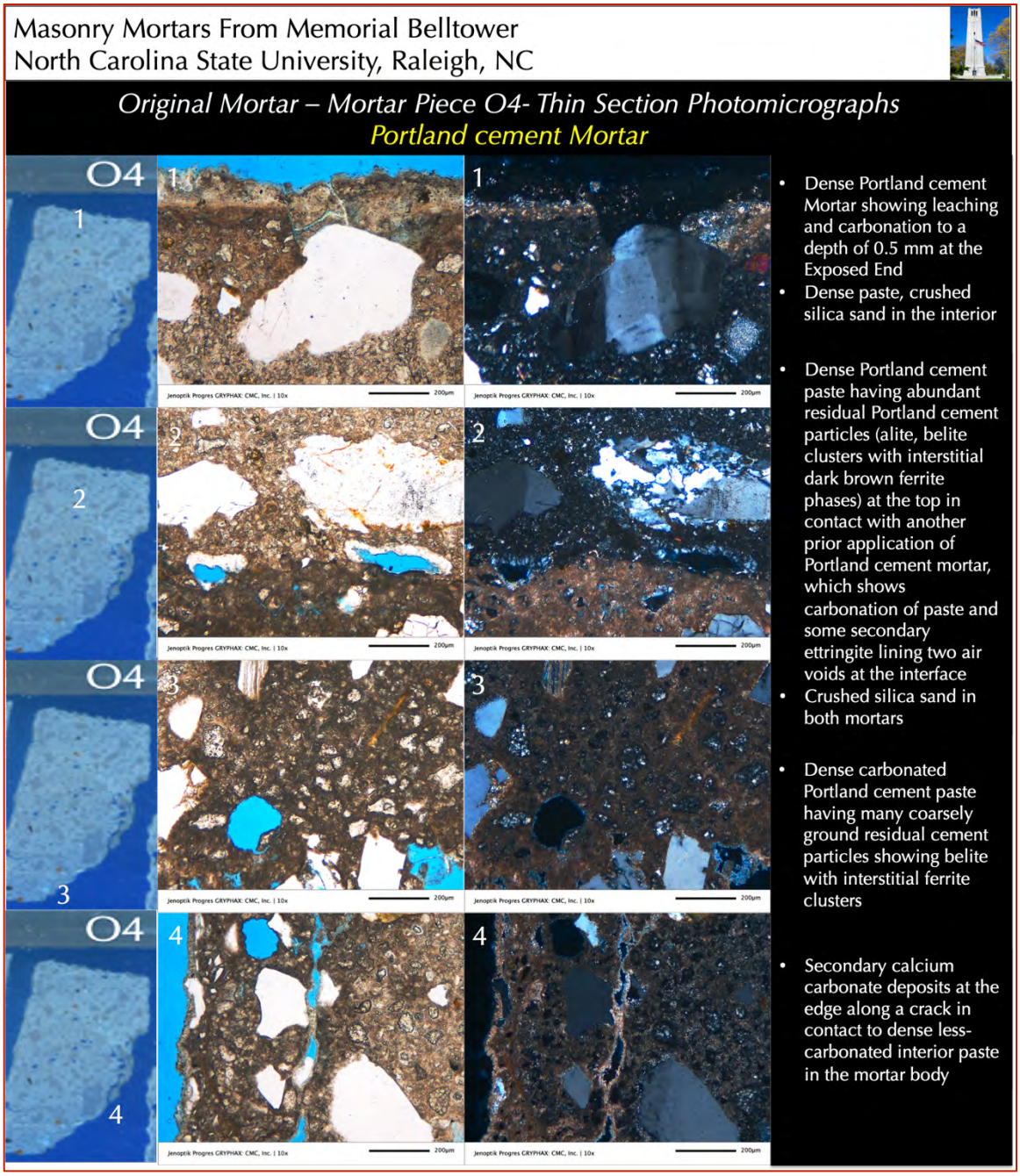

Figure 23: Photomicrographs of thin section of Piece O4 from 1920s construction (see Figure 7) showing: (a) leaching and carbonation at the top 0.5 mm of exposed surface of Portland cement-only (PC) mortar (1st row); (b) interface between two applications of PC mortar – a top one having dense PC paste with many residual PC particles, which is overall non-carbonated (2nd row from top), which was placed over a PC mortar having carbonated paste (notice the interface between two mortars in the 2nd row); (c) dense paste with many residual Portland cement particles in a carbonated matrix in the 3rd row; and (d) typical carbonation, leaching, occasional microcracks, secondary carbonate deposits in microcracks, etc. observed at one edge (location 4) of the piece that are shown in the 4th row from top. Crushed silica sand particles are well-graded, and well-distributed. Four rows of photos were taken from four different locations shown in the leftmost column on thin section view of Piece O4. Notice lack of air entrainment in the mortar. Scale bars are 0.2 mm.

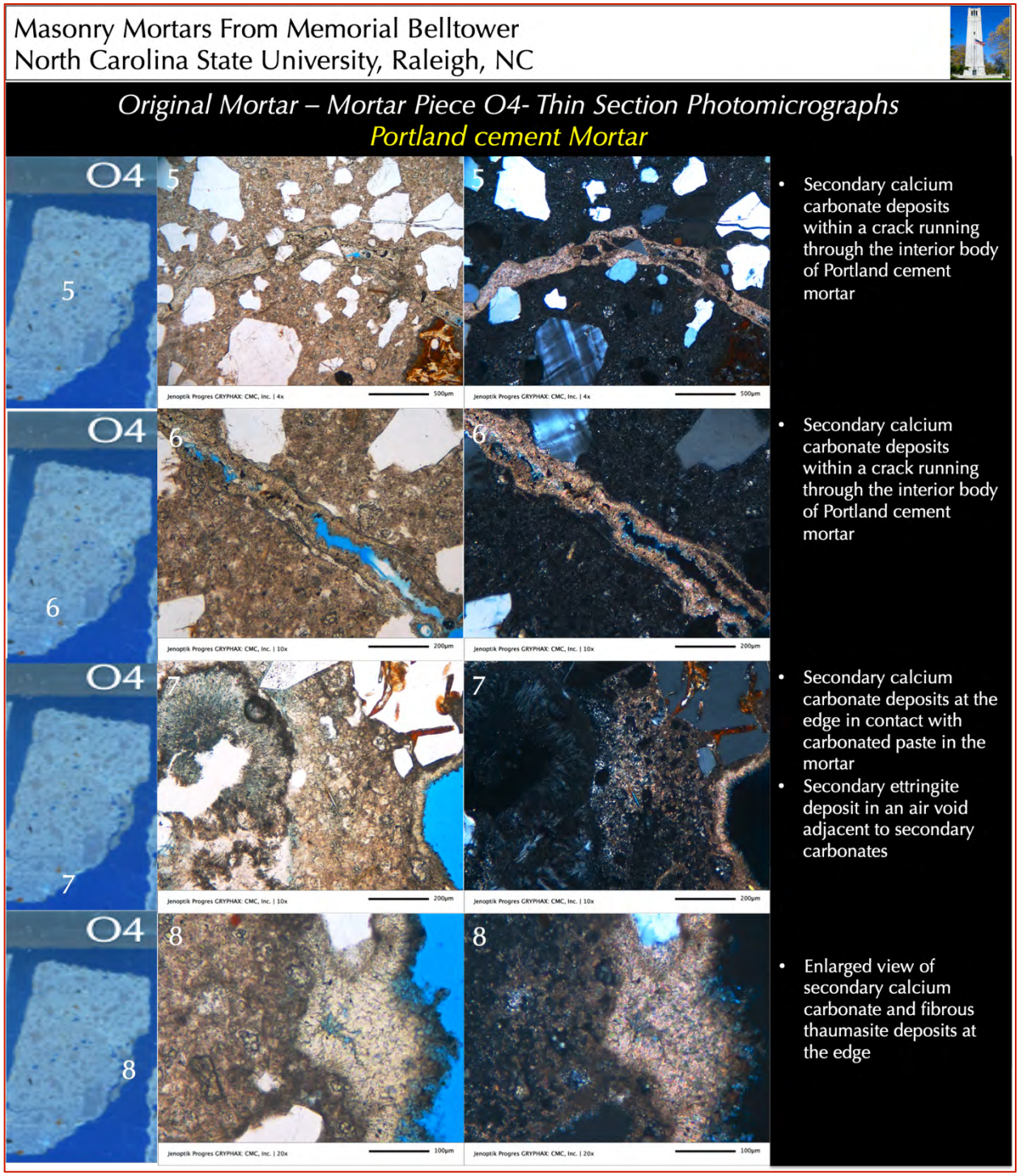

Figure 24: Photomicrographs of thin section of Piece O4 from 1920s construction (see Figure 7) showing secondary calcium carbonate precipitates along cracks and edges of the mortar piece that are marked as 5 through 8 (continuation from previous Figure) and shown in four rows. The bottom row shows enlarged view of carbonate precipitate at edge of the mortar (location 8) where some fibrous carbonates indicate possible presence of thaumasite (calcium carbonate-silicate sulfate hydrate analogue of ettringite), which could form in the cold weather condition in the presence of sulfate, silicate, and carbonate ions. Scale bars are 0.2 mm for first three rows and 0.1 mm for the 4th row.

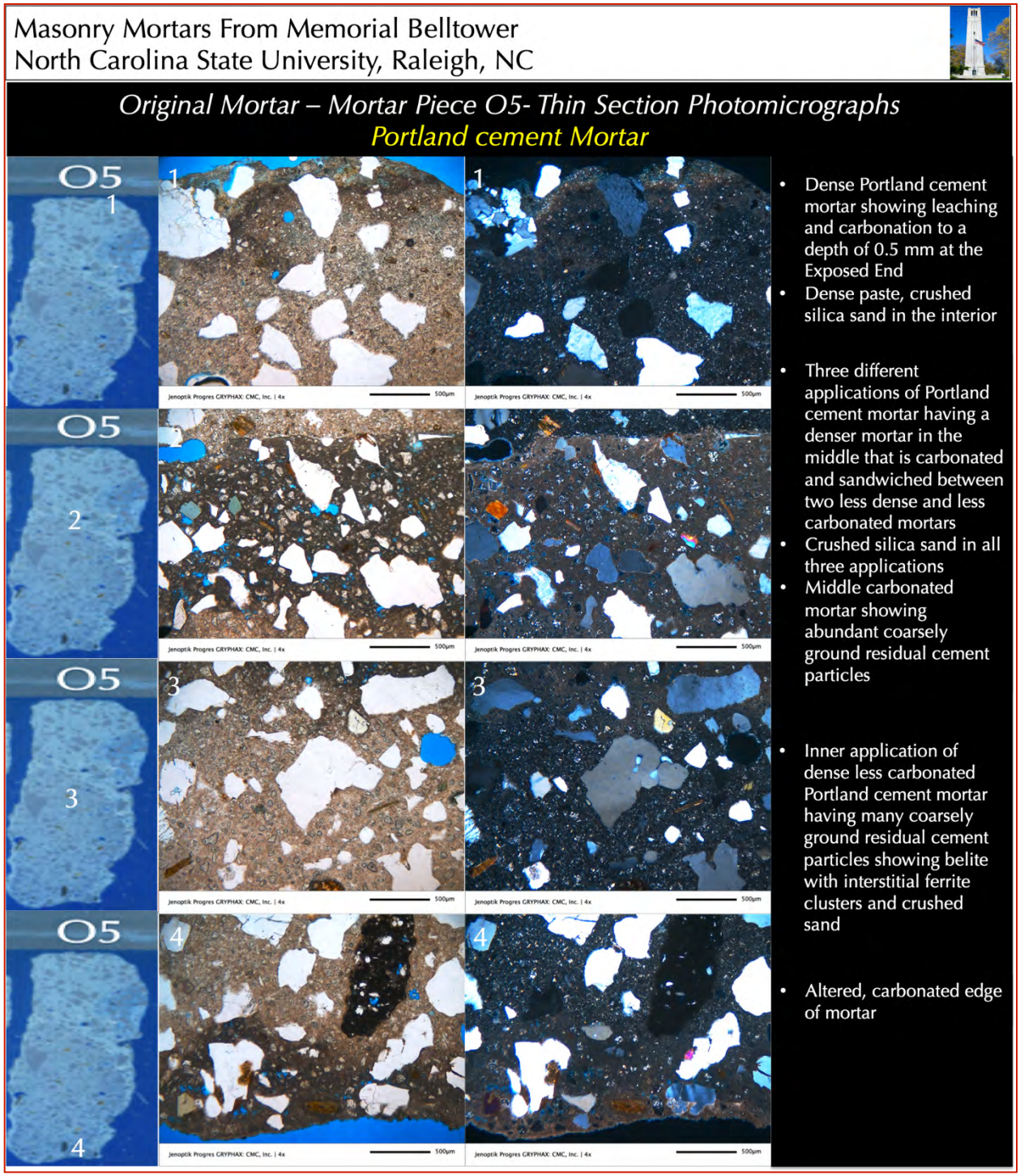

Figure 25: Photomicrographs of thin section of Piece O5 from 1920s construction (see Figure 7) showing: (a) thin carbonation at the top 0.5 mm of exposed surface of Portland cement-only (PC) mortar (1st row); (b) interface between multiple applications of PC mortars that are differentiated by variable degrees of carbonation and paste densities between the mortars (2nd row from top); (c) dense paste with many residual Portland cement particles in a non-carbonated matrix in the 3rd row; and (d) typical carbonation at one edge (location 4) of the piece that is shown in the 4th row from top. Crushed silica sand particles are well-graded, and well-distributed. Four rows of photos were taken from four different locations shown in the leftmost column on thin section view of Piece O5. Scale bars are 0.5 mm.

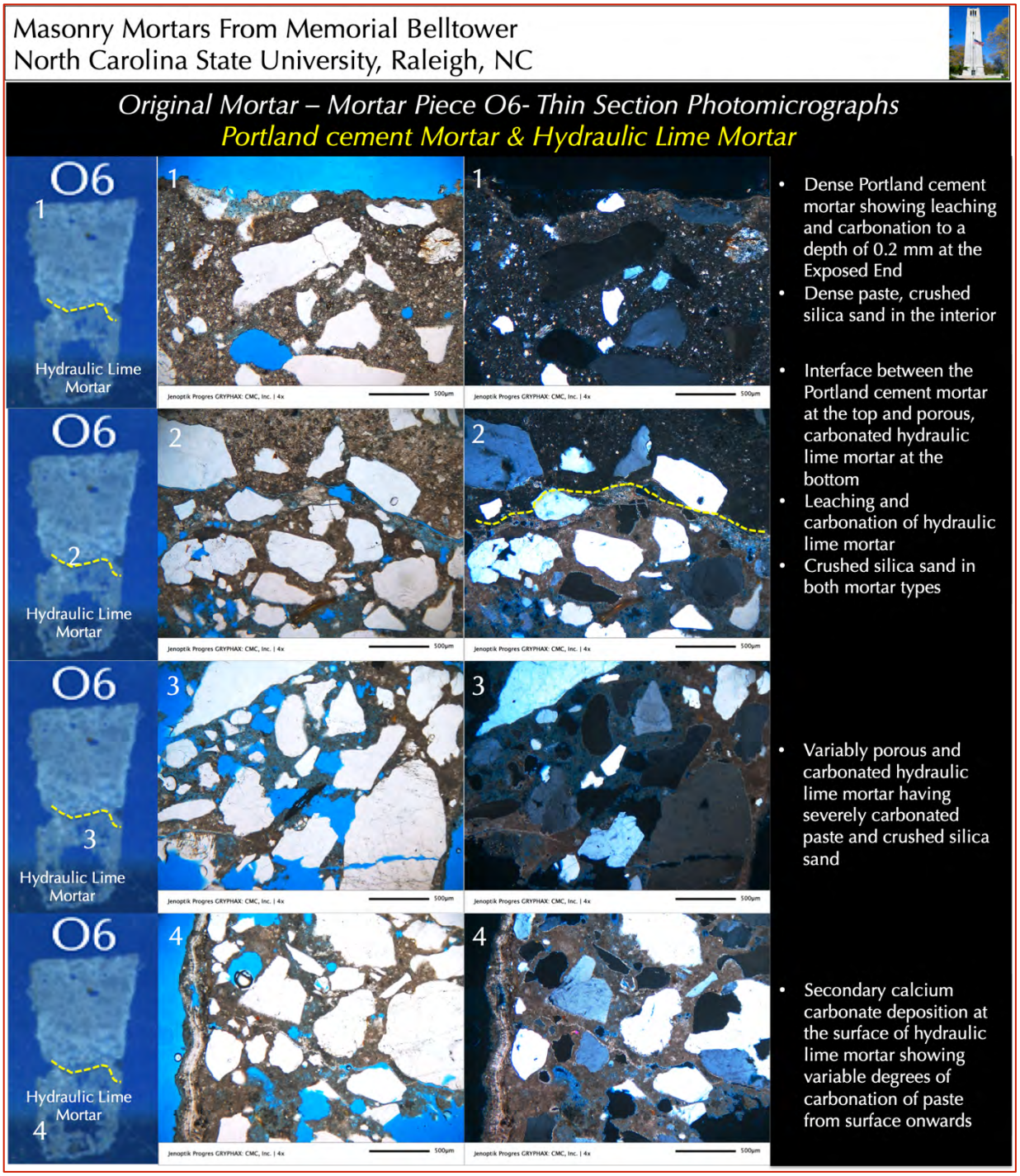

Figure 26: Photomicrographs of thin section of Piece O6 from 1920s construction (see Figure 7) showing: (a) leaching and carbonation at the top 0.2 mm of exposed surface of Portland cement-only (PC) mortar (1st row); (b) interface between PC mortar at the top, which is non-carbonated, and, hydraulic lime mortar beneath, which is characteristically carbonated (2nd row from top); (c) porous, fine-grained, severely and variably carbonated nature of hydraulic lime paste in the 3rd row from top; (d) similar crushed silica sand particles in both mortars that are well-graded, and well-distributed; (e) a thin band of secondary carbonate precipitates over carbonated paste at the edge of hydraulic lime mortar at location 4 shown in the 4th row from top. Four rows of photos were taken from four different locations shown in the leftmost column on thin section view of Piece O6. Dashed yellow line in left column separates PC-only mortar at the top from hydraulic lime mortar beneath. Scale bars are 0.5 mm.

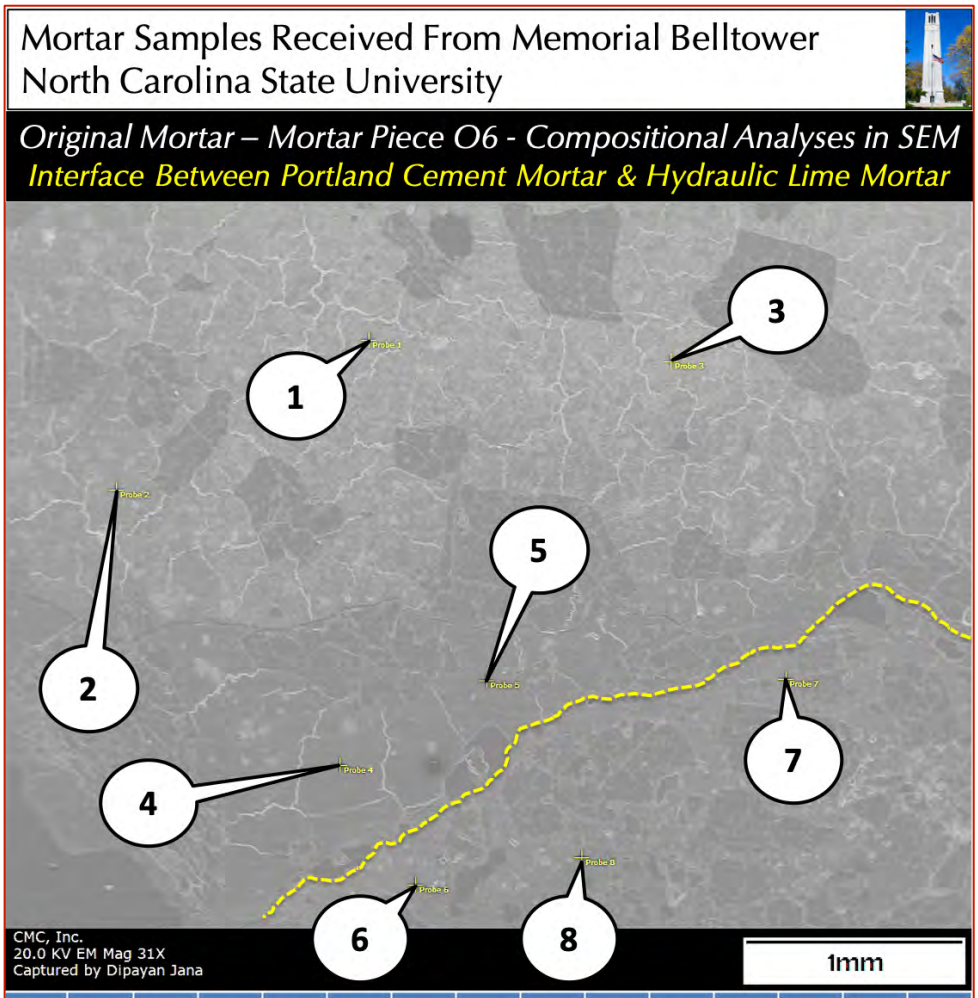

#	CaO	SiO2	Al2O3	Na2O	MgO	SO3	K2O	TiO2	FeO	P2O5	CO2	Total	Phase	Paste CI
1	32.72	19.53	7.57	0.12	0.34	9.30	0.03	0.16	0.27	0.38	29.40	99.75	PC Paste	1.93
2	31.44	33.27	4.12	0.22	0.02	3.15	0.03	0.25	0.44	0.87	25.13	99.57		3.02
3	39.52	29.44	8.98	0.00	0.40	4.37	0.01	0.01	0.09	0.46	15.44	99.90		2.22
4	31.87	41.10	7.01	0.34	0.09	3.33	0.02	0.00	0.19	0.52	14.25	99.81		3.74
5	25.23	31.00	8.70	0.10	0.16	1.14	0.01	0.75	0.73	0.17	26.98	99.27		2.99
6	49.25	14.93	1.40	1.23	0.20	0.59	0.00	0.01	0.25	0.92	28.43	99.75	Hydraulic Lime Mortar	0.79
7	51.63	26.25	1.55	0.47	0.23	0.28	0.06	0.06	0.34	0.64	17.52	99.66		1.42
8	35.90	18.73	1.88	0.50	1.26	0.11	0.06	0.07	0.41	0.63	41.59	99.60		1.51

Figure 27: Secondary electron image (SED) in a scanning electron microscope (top), and X-ray compositional analyses at the tips of callouts placed across various areas of paste (avoiding potential interference from nearby grains) in the bottom Table for the interfacial region between the Portland cement-only mortar at the top and hydraulic lime mortar beneath.

Probe #1 to 5 were taken from paste in PC-only mortar whereas Probe #6 to 8 from interfacial region between PC-only and hydraulic lime mortar. Dashed yellow line separates the two mortar types.

The compositional difference between the two mortar types is in the lime-silica compositions of paste, along with variations in some other oxides, which are shown in different color-coded rows in the compositional Table.

Notice characteristic shrinkage microcracks in the paste of PC-only mortar at the top but its absence in the hydraulic lime mortar beneath.

Paste-CI (after Eckel 1922) is calculated as CI = $[(2.8*SiO_2)+(1.1*Al_2O_3)+(0.7*Fe_2O_3)]/[(CaO)+(1.4*MgO)]$. Carbon, represented as CO_2 is from carbonated paste and epoxy used in thin section preparation.

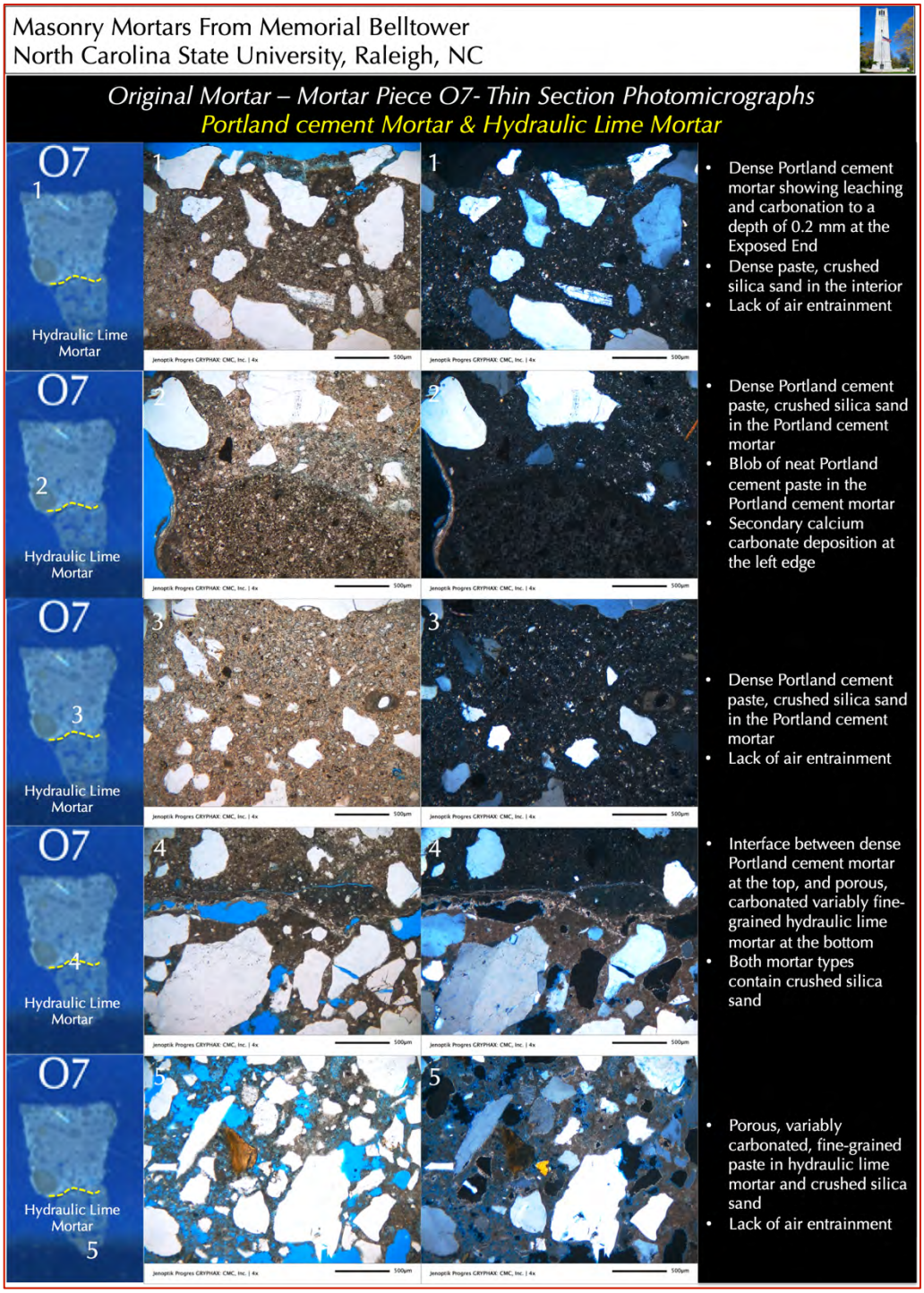

Figure 28: Photomicrographs of thin section of Piece O7 from 1920s construction (see Figure 7) showing: (a) leaching and carbonation at the top 0.2 mm of exposed surface of Portland cement-only (PC) mortar (1st row); (b) interface between PC mortar at the top, which is non-carbonated, and, hydraulic lime mortar beneath, which is characteristically carbonated (4th row from top); (c) porous, fine-grained, severely and variably carbonated nature of hydraulic lime paste in the 4th and 5th rows from top; and (d) similar crushed silica sand particles in both mortars that are well-graded, and well-distributed. Four rows of photos were taken from four different locations shown in the leftmost column on thin section view of Piece O7. Dashed yellow line in left column separates PC-only mortar at the top from hydraulic lime mortar beneath. Notice lack of air entrainment in the mortars. Scale bars are 0.5 mm.

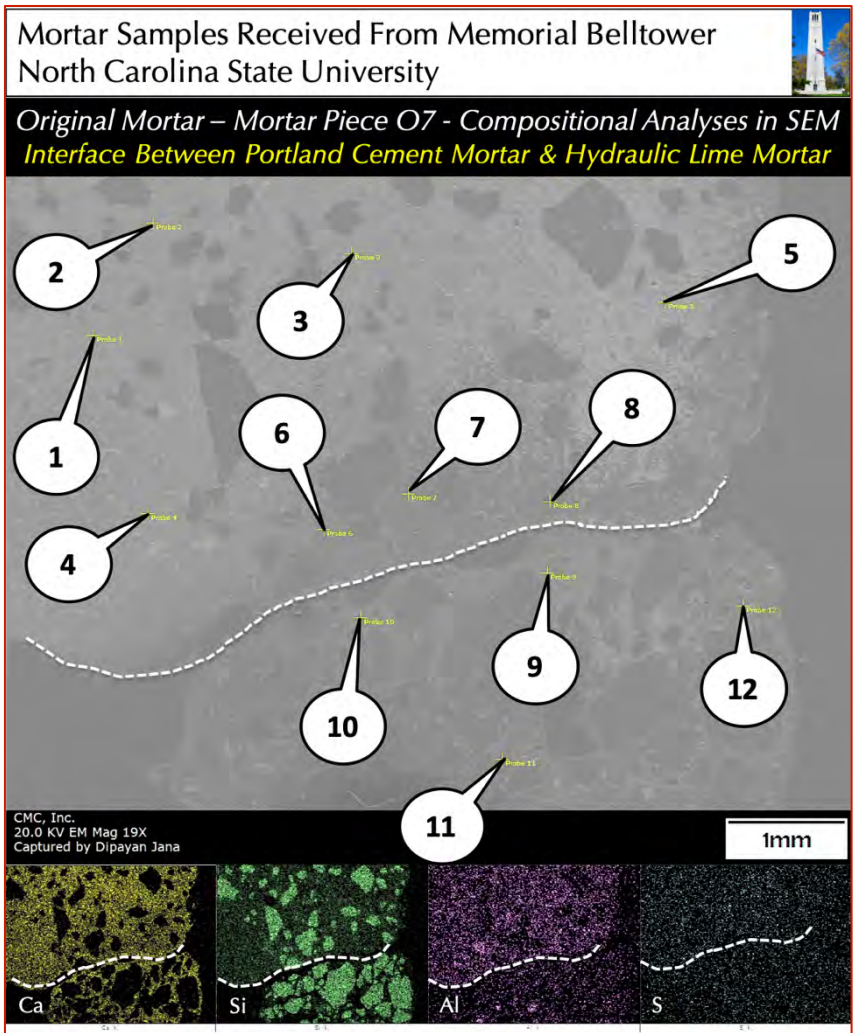

#	CaO	SiO2	Al2O3	Na2O	MgO	SO3	K2O	TiO2	FeO	P2O5	CO2	Total	Phase	Paste CI
1	32.99	27.78	3.21	0.66	1.17	3.92	0.01	0.01	0.00	1.28	28.96	99.99		2.35
2	39.76	27.52	6.69	0.21	0.66	2.22	1.12	0.07	1.33	1.26	19.15	98.66		2.10
3	45.60	22.42	7.07	0.54	0.52	3.47	0.04	0.09	0.49	1.49	18.27	99.51		1.53
4	39.15	37.19	3.02	0.79	0.20	1.84	0.04	0.27	2.08	0.91	14.50	97.91	PC Paste	2.76
5	42.04	35.64	4.92	0.14	0.89	1.40	0.00	0.75	0.88	0.97	12.37	99.12		2.44
6	37.86	22.79	19.44	0.48	3.69	1.31	0.09	0.18	1.66	1.53	10.97	98.34		2.01
7	39.22	38.27	5.15	0.08	2.07	1.53	0.00	0.07	2.89	1.47	9.25	97.11		2.73
8	30.35	32.67	6.89	0.26	2.22	3.07	0.07	0.18	0.31	1.36	22.61	99.68		2.97
9	86.68	4.81	0.12	0.64	1.29	0.06	0.00	0.12	0.05	0.70	5.54	99.96	HL	0.15
10	82.19	7.35	0.71	0.02	0.82	0.15	0.00	0.00	0.88	0.79	7.09	99.12	HL	0.26
11	0.00	0.00	0.00	0.03	0.00	0.08	0.00	0.00	0.06	0.23	99.59	99.93	Epoxy	-
12	30.25	42.96	0.82	0.00	0.23	0.39	0.08	0.00	0.77	2.16	22.33	99.22	Leached PC	3.98

Figure 29: Secondary electron image (SED) in a scanning electron microscope (top), X-ray elemental maps of calcium (Ca), silicon (Si), aluminum (Al), and sulfur (S) on the SED, and X-ray compositional analyses at the tips of callouts placed across various areas of paste (avoiding potential interference from nearby grains) in the bottom Table for the interfacial region between the Portland cement-only mortar at the top and hydraulic lime mortar beneath.

Probe #1 to 8 were taken from paste in PC-only mortar whereas Probe #9 and 10 were from the hydraulic lime mortar side of the interface. Dashed white line separates the two mortar types.

The compositional difference between the two mortar types is in the lime-silica compositions of paste, along with variations in some other oxides, which are shown in different color-coded rows in the compositional Table.

Notice characteristic shrinkage microcracks in the paste of PC-only mortar at the top but its absence in the hydraulic lime mortar beneath.

Paste-CI (after Eckel 1922) is calculated as CI = $[(2.8*SiO_2)+(1.1*Al_2O_3)+(0.7*Fe_2O_3)]/[(CaO)+(1.4*MgO)]$. Carbon, represented as CO_2 is from carbonated paste and epoxy used in thin section preparation.

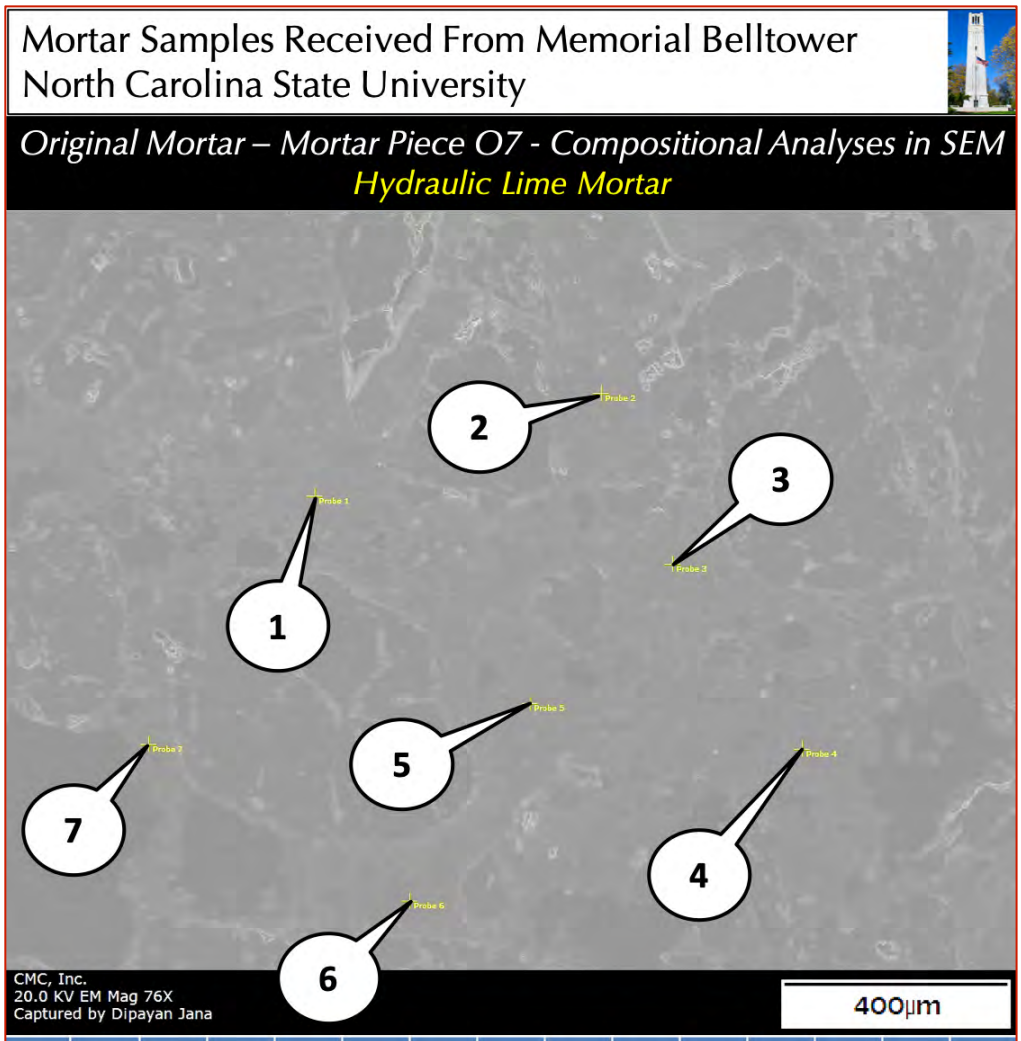

#	CaO	SiO2	Al2O3	Na2O	MgO	SO3	K2O	TiO2	FeO	P2O5	CO2	Total	Phase	Paste CI
1	16.09	20.63	3.27	0.42	2.94	0.10	0.08	0.00	0.28	1.40	54.78	99.71	Hydraulic Lime Mortar	3.05
2	73.97	7.29	0.54	0.00	1.00	0.45	0.00	0.00	0.02	1.95	14.78	99.98		0.28
3	3.21	28.13	4.56	0.77	3.99	0.06	0.47	0.06	0.19	1.24	57.32	99.81		9.54
4	58.91	11.31	1.01	0.20	1.65	0.46	0.01	0.04	0.28	2.47	23.67	99.73		0.54
5	8.55	38.67	4.04	0.13	9.32	1.18	0.09	0.05	0.57	1.73	35.68	99.44		5.24
6	14.87	19.72	4.85	0.19	1.95	0.19	0.36	0.37	4.17	1.52	51.80	95.82		3.61
7	78.24	5.31	0.33	0.00	1.09	0.01	0.01	0.37	0.27	1.62	12.75	99.73		0.19

Figure 30: Secondary electron image (top), and compositional analyses at the tips of callouts placed across various areas of paste in the hydraulic lime mortar portion in O7 (see Figure 7) where paste shows characteristic variations in compositions from leaching and carbonation of paste. The large variation in lime-silica compositions of paste are due to severe leaching and carbonation where former enriched the paste in silica compared to lime (e.g., Probe #1, 3, and 5), whereas latter enriched the paste in lime (e.g., Probe #2, 4, and 7). Paste CI = $[(2.8*SiO_2)+(1.1*Al_2O_3)+(0.7*\ Fe_2O_3)]/[(CaO)+(1.4*MgO)]$. Carbon, represented as CO_2 is from carbonated paste and epoxy used in thin section preparation.

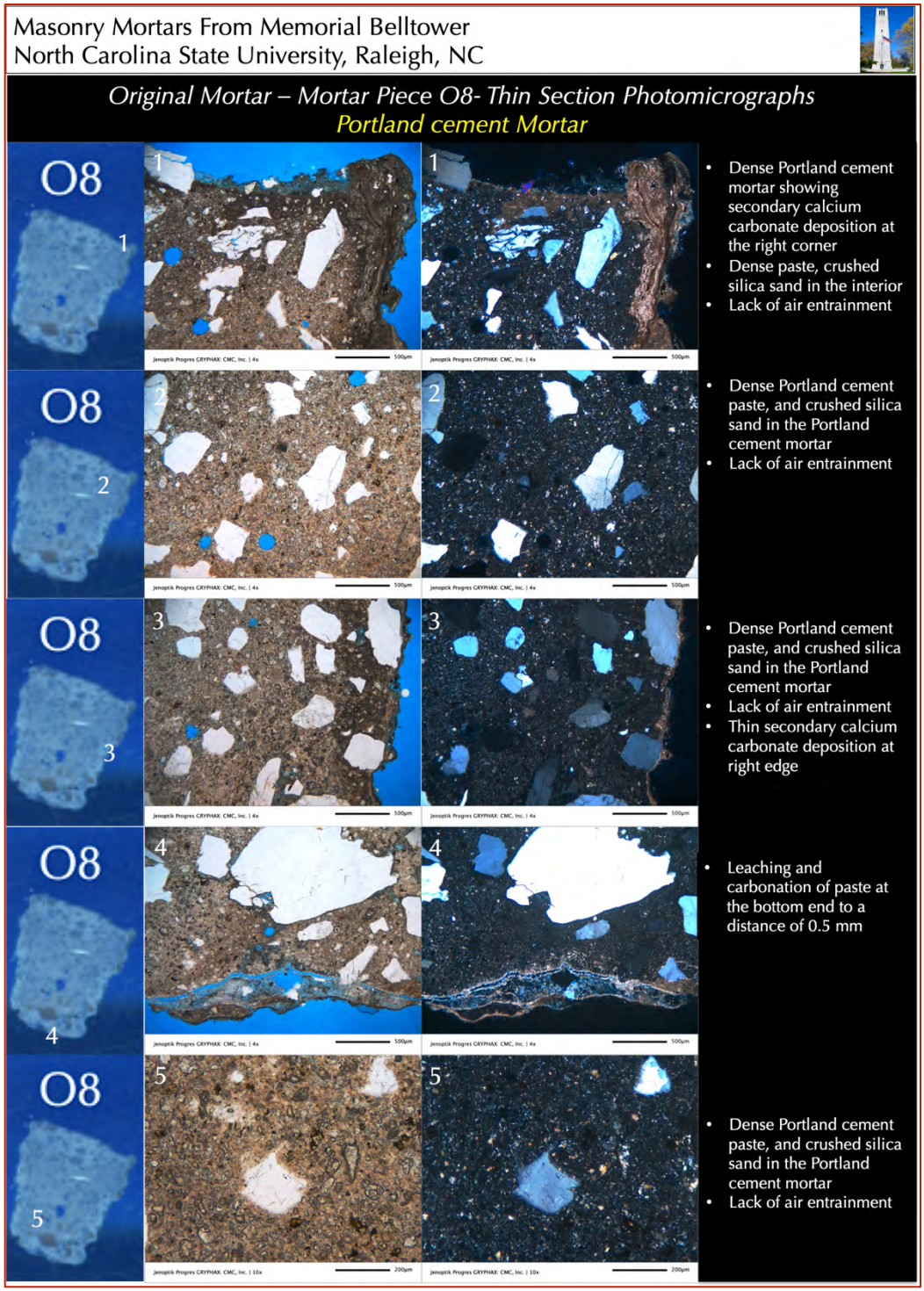

Figure 31: Photomicrographs of thin section of Piece O8 from 1920s construction (see Figure 7) showing: (a) leaching and carbonation at the right corner of exposed surface of Portland cement-only (PC) mortar (1st row); (b) dense Portland cement paste having many fine residual cement particles in the non-carbonated interior of mortar shown in all four rows; (c) secondary calcium carbonate deposition along a near-surface microcrack at the edge of mortar at location 4 shown in 4th row from top; and (d) crushed silica sand particles that are well-graded, and well-distributed. Five rows of photos were taken from five different locations shown in the leftmost column on thin section view of Piece O8. Notice lack of air entrainment in the mortar. Scale bars are 0.5 mm.

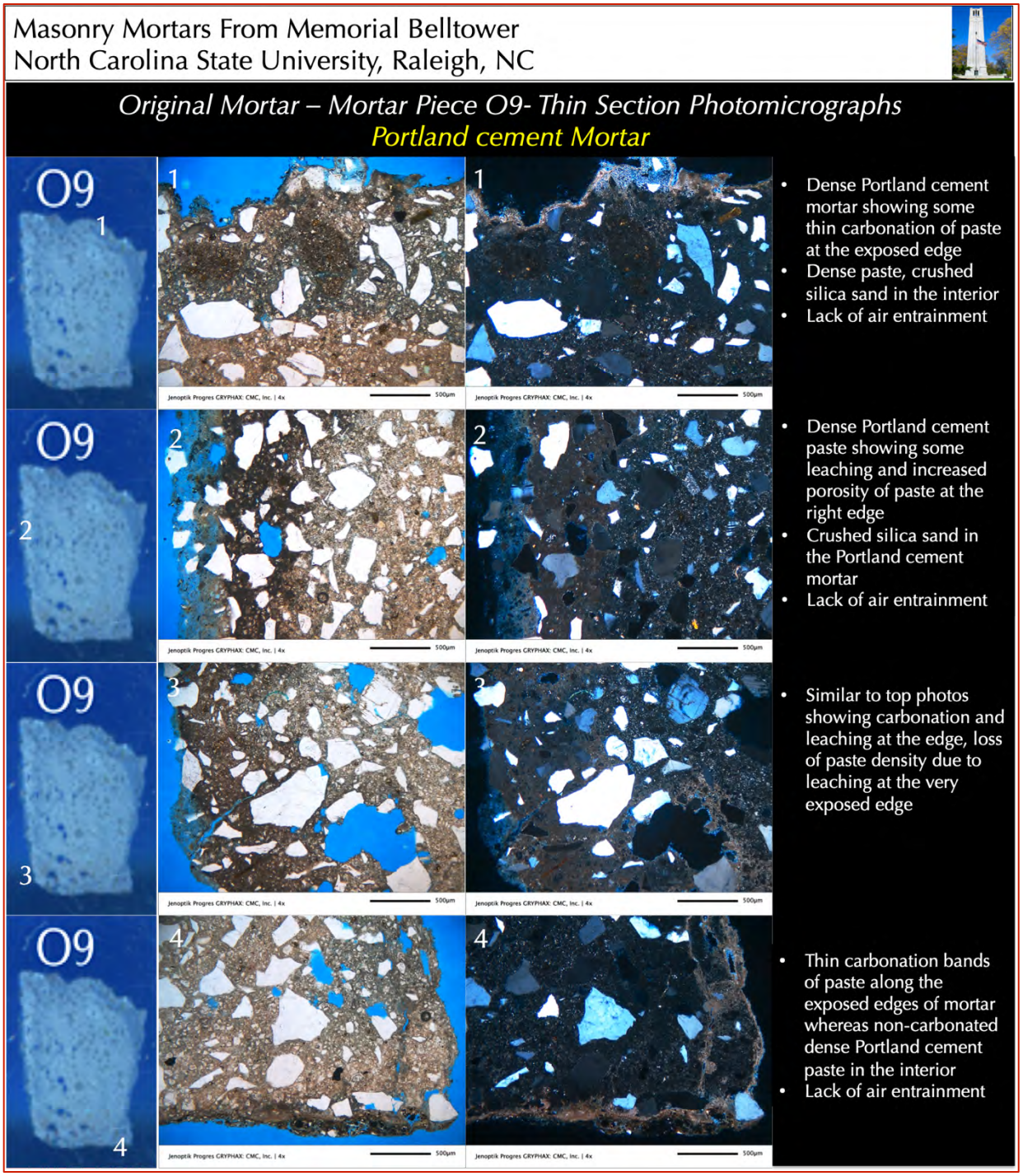

Figure 32: Photomicrographs of thin section of Piece O9 from 1920s construction (see Figure 7) showing: (a) a thin carbonated surface above interior non-carbonated Portland cement paste in the top row; (b) typical surface alterations at location 2 of the mortar in the 2nd row showing leaching at the surface resulting in porous paste, followed by carbonation inside leached zone where paste is relatively denser, which, in turn, is followed by interior less carbonated (further dense) to eventually non-carbonated (densest) interior paste (shown in the 3rd row from top); (c) some thin zone carbonation at the corner region in location 4 shown in the 4th row, such thin carbonation indicates dense interior paste; and (d) crushed silica sand particles that are well-graded, and well-distributed. Four rows of photos were taken from four different locations shown in the leftmost column on thin section view of Piece O9. Notice lack of air entrainment in the mortar. Scale bars are 0.5 mm.

Optical Microscopy & SEM-EDS of Mortars From the Upper Level of Belltower From 1940s Construction

Figures 33 through 55 show optical and scanning electron microscopy of mortars from the upper level of Belltower from 1940s construction, which were taken from the polished thin section and residue of the mortars shown in Figure 8 by examining the mortar pieces in a low-power Stereozoom microscope (for the thin section residue), high-power petrographic microscope (of the thin sections), and in a scanning electron microscope equipped with energy-dispersive X-ray fluorescence spectrometer for microanalyses of pastes. Figures are arranged as follows:

Figures	Mortars	Microscopy	Features Found
33	PC-only mortar	Stereozoom Microscope	Non-air-entrained dense PC mortar
34	PC-only mortar	Petrographic Microscope	Dense Portland cement paste having residual cement particles
35	High-Lime Cement-Lime	Stereozoom Microscope	Non-air-entrained, different paste color tone from PC-only mortar, off-white color
36	High-Lime Cement-Lime	Petrographic Microscope	Variable carbonation, residual cement particles in denser carbonated regions
37	Slag-Lime	Petrographic Microscope	Variable carbonation, residual angular ground slag particles, shrinkage microcracks
38	PC-only mortar	Petrographic Microscope	Optical microcopy of Piece #U1 in Figure 8 showing dense PC paste, crushed silica sand, leaching and carbonation at the surface
39	PC-only mortar	SEM-EDS	SEM-EDS of Piece #U1 showing microstructure and microchemistry of paste
40	PC-only and slag-lime Mortars	Petrographic Microscope	Optical microcopy of Piece #U2 in Figure 8 showing Portland cement mortar portion having surface carbonation and dense non-carbonated interior Portland cement paste having many residual cement particles
41	PC-only and slag-lime Mortars	SEM-EDS	SEM-EDS of Piece #U2 showing X-ray elemental maps of various elements across the interface from PC-only to slag-lime mortar
42	PC-only and slag-lime Mortars	SEM-EDS	SEM-EDS of Piece #U2 showing microstructure and microchemistry of PC-only portion
43	PC-only and slag-lime Mortars	Petrographic Microscope	Optical microcopy of Piece #U3 in Figure 8 showing contrasting microstructures from PC-only to slag-lime mortar
44	PC-only and slag-lime Mortars	SEM-EDS	SEM-EDS of Piece #U3 showing microstructure and microchemistry of PC-only portion
45	PC-only and slag-lime Mortars	SEM-EDS	SEM-EDS of Piece #U3 showing microstructure and microchemistry of slag-lime portion
46	PC-only mortar	Petrographic Microscope	Optical microcopy of Piece #U4 in Figure 8 showing dense PC paste, crushed silica sand, leaching and carbonation at the surface, non-carbonated interior paste having many residual cement particles
47	PC-only mortar	SEM-EDS	SEM-EDS of Piece #U4 showing microstructure and microchemistry of PC-only mortar
48	PC-only mortar	Petrographic Microscope	Optical microcopy of Piece #U5 in Figure 8 showing dense PC paste, crushed silica sand, leaching and carbonation at the surface, non-carbonated interior paste having many residual cement particles
49	PC-only mortar	SEM-EDS	SEM-EDS of Piece #U5 showing microstructure and microchemistry of carbonated and interior non-carbonated PC-only mortar
50	High-Lime Cement-Lime	Petrographic Microscope	Optical microcopy of Piece #U6 in Figure 8 showing leaching, variable degrees of carbonation, residual cement in denser carbonated regions

Figures	Mortars	Microscopy	Features Found
51	High-Lime Cement-Lime	SEM-EDS	SEM-EDS of Piece #U6 showing microstructure and microchemistry of variably carbonated paste
52	High-Lime Cement-Lime	Petrographic Microscope	Optical microcopy of Piece #U7 in Figure 8 showing leaching, variable degrees of carbonation, residual cement in denser carbonated regions
53	High-Lime Cement-Lime	SEM-EDS	SEM-EDS of Piece #U7 showing microstructure and microchemistry of leached and PC rich portions of paste
54	High-Lime Cement-Lime	SEM-EDS	SEM-EDS of Piece #U7 showing microstructure and microchemistry of PC rich portions of paste
55	PC-only mortar	Petrographic Microscope	Optical microcopy of Piece #U8 in Figure 8 showing dense PC paste, crushed silica sand, leaching and carbonation at the surface, non-carbonated interior paste having many residual cement particles

Table 3: List of figures for mortars from the upper level from 1940s construction.

Conclusions drawn from all these figures regarding microstructures and microchemistries of mortars from the 1940s construction are as follows:

a. Similar to the 1920s construction at the lower level, original mortars applied at the upper level of Belltower during 1940s construction also appeared to be slag-lime or cement-lime based (Figures 5 and 8), having varieties ranging from cement-lime mortar having higher proportion of lime than Portland cement (Figures 35, 36) to slag-lime mortar (Figures 37, 40, 43, 45) both of which are present in minor amounts amongst the mortar pieces received and located at the inside ends of noticeably dominant, denser, harder, and darker Portland cement-only mortars (Figures 33, 34).
b. Similar to the 1920s construction at the lower level, Portland cement-only mortars are found to be applied over slag or Portland cement and lime-based mortars as later pointing events (Figures 5 and 7), which are present either at the exposed ends of slag/cement-lime-based mortars in some pieces, or, most commonly received as entire pieces, indicating potential full-depth repointing of the original lime-based mortars, which were replaced with Portland cement-only mortars. Some high-lime cement-lime mortar pieces occurring entirely as single pieces indicate a probable prior pointing event where a more appropriate mortar was used than the Portland cement-only mortar used at later pointing events;
c. Similar to the 1920s construction at the lower level, Portland cement-only mortars applied at the upper level of Belltower lack any lime component (Figure 34), and hence are not representative of a common masonry mortar, where lime is added for numerous benefits in masonry construction from improvement of properties of freshly placed mortars (water retention, workability) to properties of hardened mortars (reduction in brittleness, improved malleability to accommodate movements of monument without forming cracks).
d. Overall grain size of residual Portland cement particles in the dense pastes of Portland cement-only mortars are more similar to 1940s or later cement than coarsely ground cements manufactured during 1920s construction.

e. The dominant Portland cement-only mortars in most of the pieces received represent a more or less thorough repointing event where most of the original slag/cement-lime-based mortars were replaced with the Portland cement-only mortars.

f. Crushed silica sand is used in all mortars encountered, from the original slag/cement-lime-based mortars to later Portland cement-only mortars. This indicates a silica source, which was used both during the original construction and later pointing event. Sand is angular (crushed, manufactured) containing major amount of quartz and subordinate amounts of feldspar and quartzite that are all well-graded, well-distributed, and present in sound conditions in all mortars without any potentially deleterious alkali-aggregate reactions.

g. The change in binder compositions are from the original slag or cement and lime-based binary binders, to much denser, harder Portland cement-only binders where later caused formation of network of fine hairline shrinkage microcracks that are absent in the lime-based mortars.

h. All mortars encountered at the upper level from 1940s construction are also non-air-entrained. Air contents in the Portland cement only mortars applied during later repointing events are estimated to be 4 to 6 percent by volume (Figure 33). Air content in high-lime cement-lime mortar is estimated to be 3 to 4 percent (Figure 35).

i. The main microstructural difference between the earlier slag or cement-lime mortars and later pointing Portland cement-only mortars are in paste density and hence carbonation where earlier mortars are less dense, more carbonated, often leached resulting in higher paste porosities, whereas later Portland cement-only pointing mortars are noticeably denser, harder, contain abundant residual Portland cement particles and show only thin surface carbonation and leaching (usually leached zone occurs above carbonated zone) where such altered zones are within 0.2 to 0.5 mm in thickness after which denser, non-carbonated sound interior paste occurs.

j. Secondary ettringite and secondary calcium carbonate are two common secondary deposits found in many original and pointing mortars that are testaments of the presence of moisture in the mortars for prolonged periods. Such deposits, however, did not cause any deleterious reactions to affect the overall conditions of original or pointing mortars. Leaching of paste, when occurred (mostly at the exposed surface regions) caused loss of lime at the expense of silica. Silica at severely leached regions occurred as gelatinous masses in optically isotropic conditions.

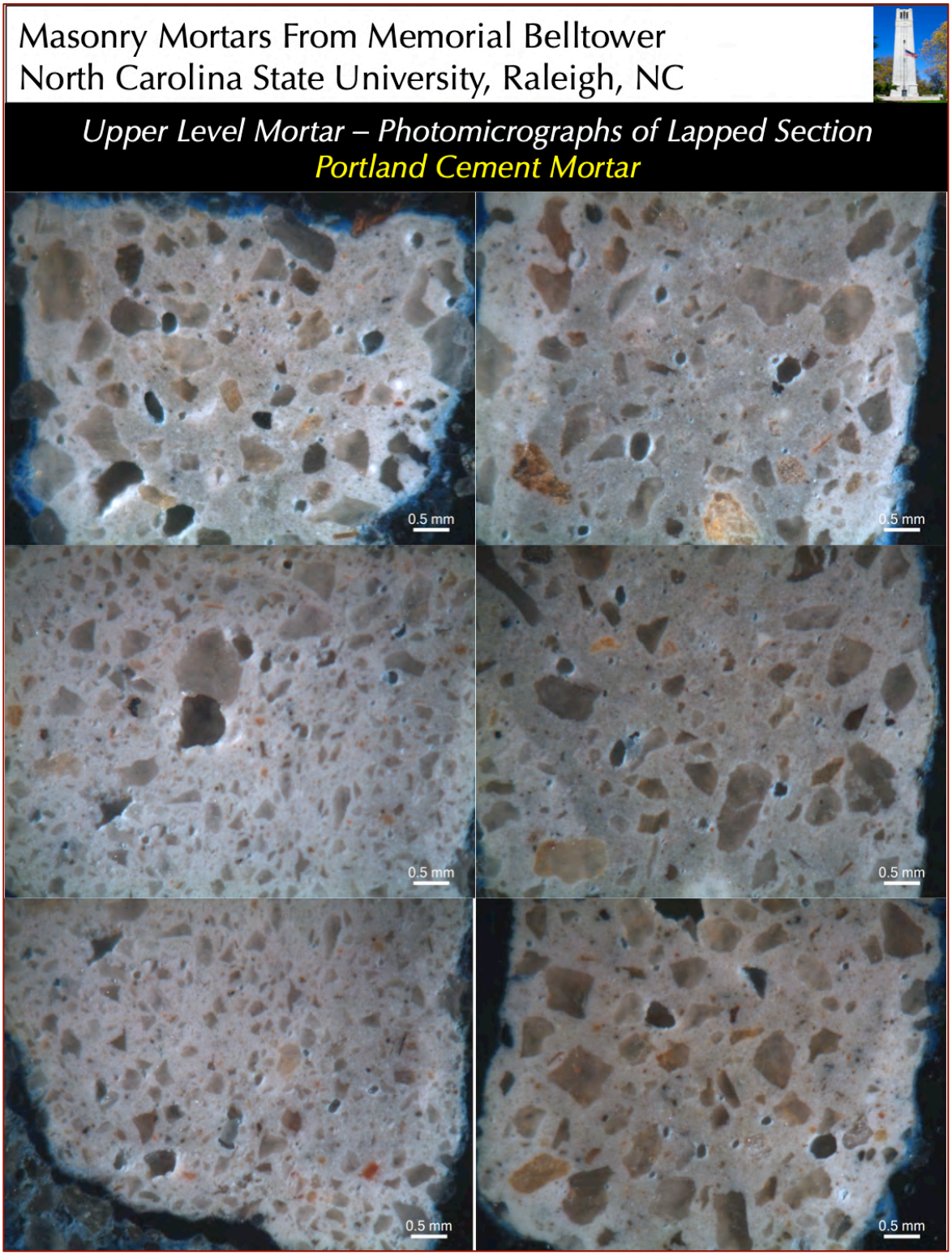

Figure 33: Photomicrographs of lapped section of various Portland cement mortar pieces from 1940s construction from the upper level of the tower (collected from the thin section residue shown in Figure 8) showing the dense, non-air-entrained nature of the mortar having crushed silica sand aggregate of nominal 1 mm size, a few coarse irregularly-shaped entrapped voids, and beige to light to dark gray paste color tones due to various degrees of alterations (from carbonation, leaching, etc.) of PC mortar.

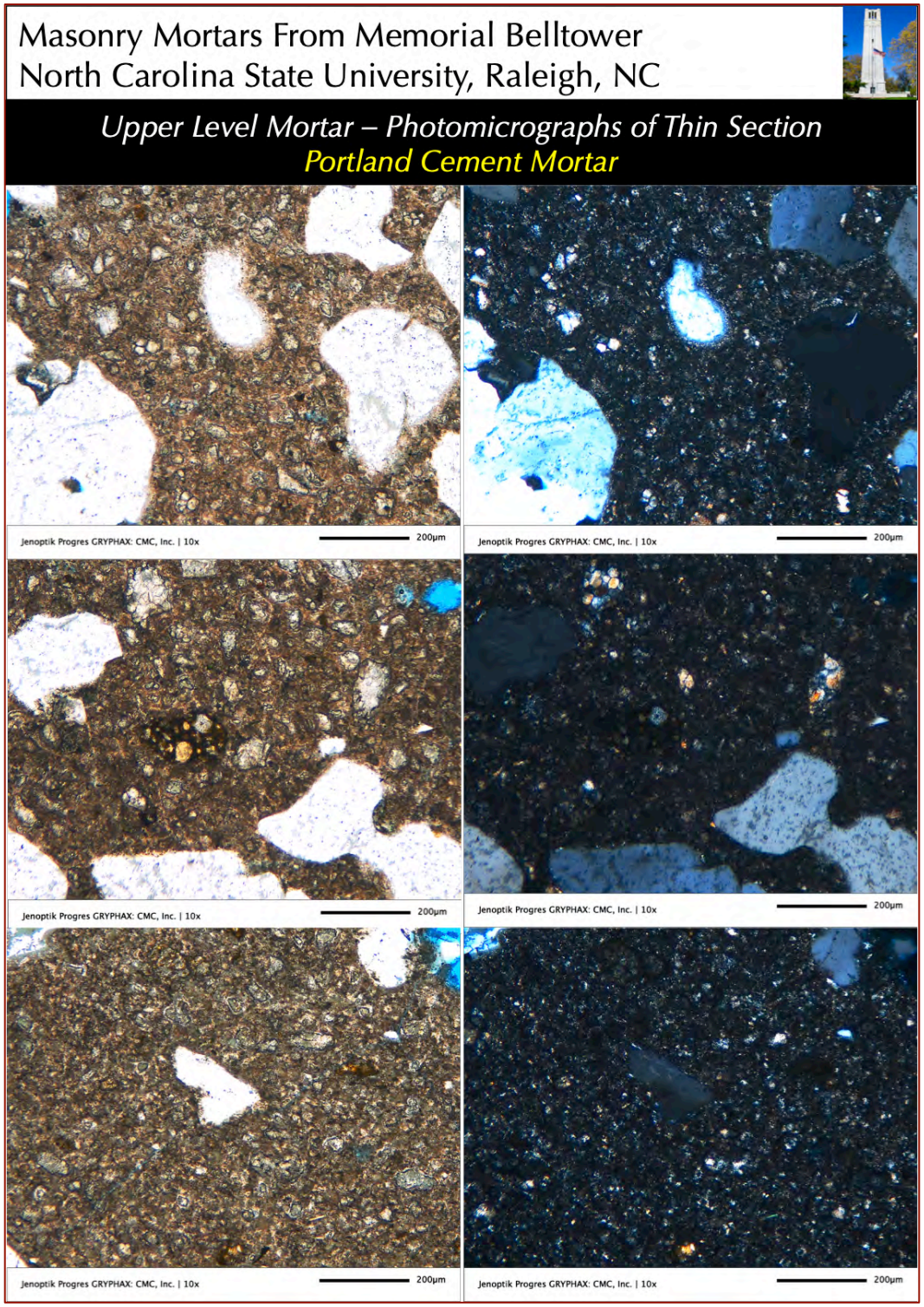

Figure 34: Photomicrographs of thin section of various Portland cement mortar pieces from 1940s construction from the upper level of the tower (collected from the thin section shown in Figure 8) showing: (a) dense, overall non-carbonated nature of paste having many residual Portland cement particles which do not represent coarsely ground cement; (c) thin hydration rims around many calcium silicate particles of Portland cement; (d) spherical belite and interstitial dark brown ferrite phases in a coarse residual cement particle at the center of middle row photos; (e) crushed quartz sand particles; and (f) lack of any intentionally introduced entrained air, except a few entrapped ones highlighted by blue epoxy. Scale bars are 0.2 mm.

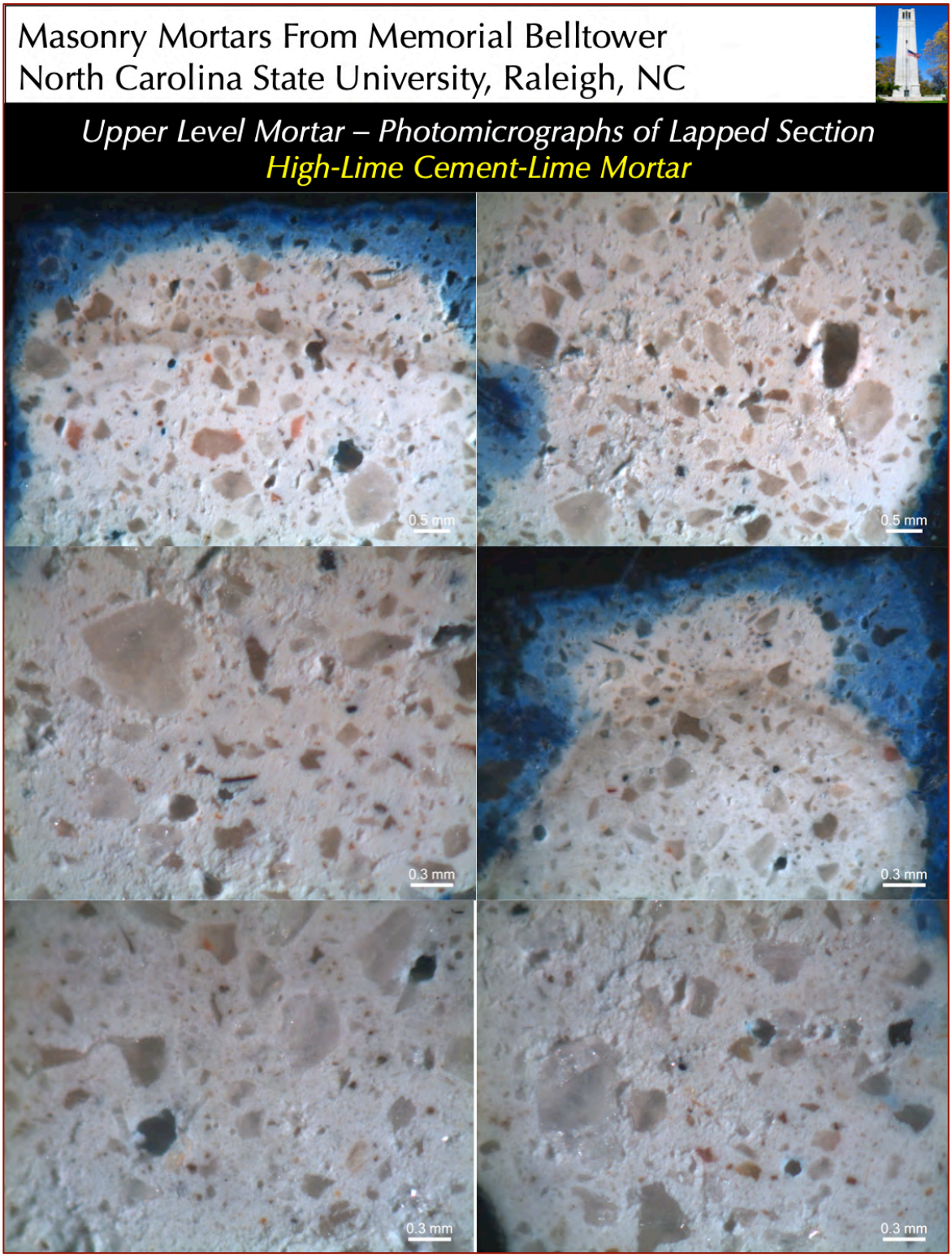

Figure 35: Photomicrographs of lapped section of two off-white colored high-lime cement-lime mortar pieces (U6 and U7 in Figure 8) from 1940s construction from the upper level of the tower (collected from the thin section residue shown in Figure 8) showing the moderately soft, non-air-entrained nature of the mortar having crushed silica sand aggregate of nominal 1 mm size, a few coarse irregularly-shaped entrapped voids, and off-white paste due to various degrees of alterations (from carbonation, leaching, etc.) of high-lime cement-lime (HLCL) mortar.

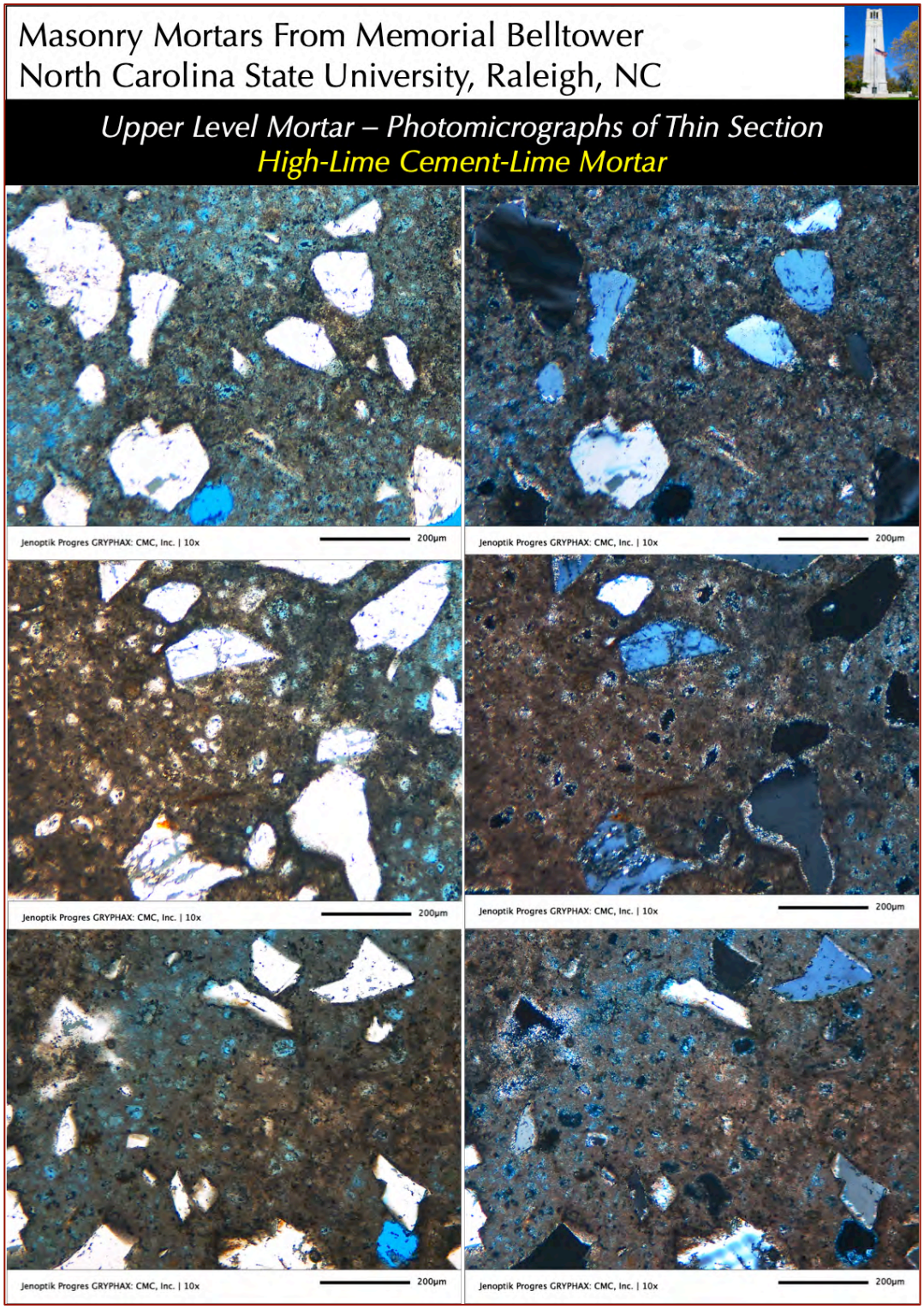

Figure 36: Photomicrographs of thin section of two off-white colored high-lime cement-lime mortar pieces (U6 and U7 in Figure 8) from 1940s construction from the upper level of the tower (collected from the thin section shown in Figure 8) showing the fine-grained, non-air-entrained, severely carbonated nature of the mortar having crushed silica sand aggregate of nominal 1 mm size, and various degrees of alterations (from carbonation, leaching, etc.) resulting in variable porosities of paste in the high-lime cement-lime (HLCL) mortar. Scale bars are 0.2 mm.

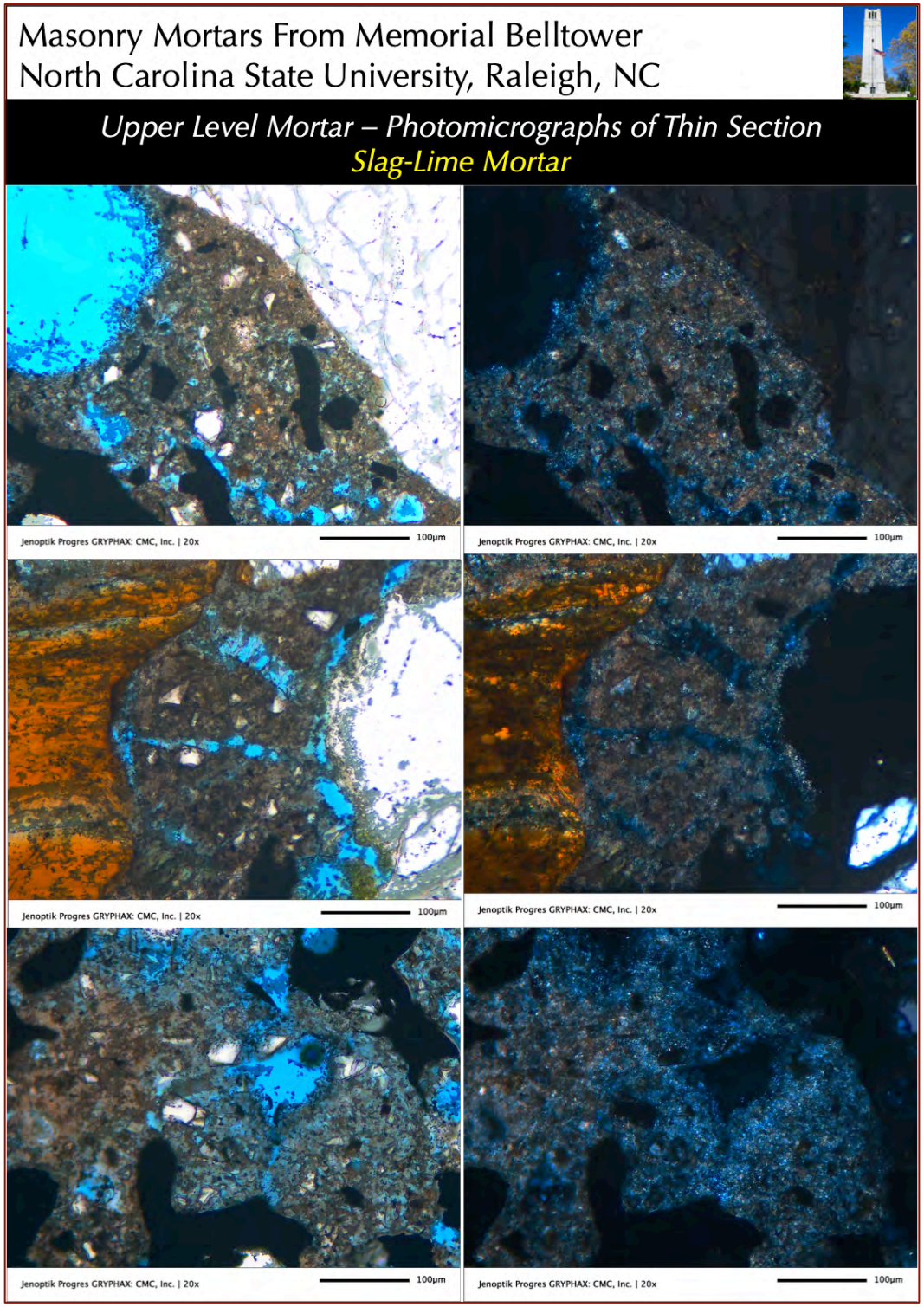

Figure 37: Photomicrographs of thin section of two highly fragmented slag-lime mortar pieces beneath PC mortars in U2 and U3 in Figure 8 from 1940s construction from the upper level of the tower (collected from the thin section shown in Figure 8) showing the fine-grained, non-air-entrained, severely carbonated nature of the mortar having angular, shard-like glassy particles of ground granulated slag, crushed silica sand aggregate of nominal 1 mm size, and various degrees of alterations (from carbonation, leaching, etc.) resulting in variable porosities of paste. Notice optically isotropic nature of angular slag particles in crossed polarized-light photos in right column. Shrinkage microcracks in paste are seen in the middle row photos. Scale bars are 0.1 mm.

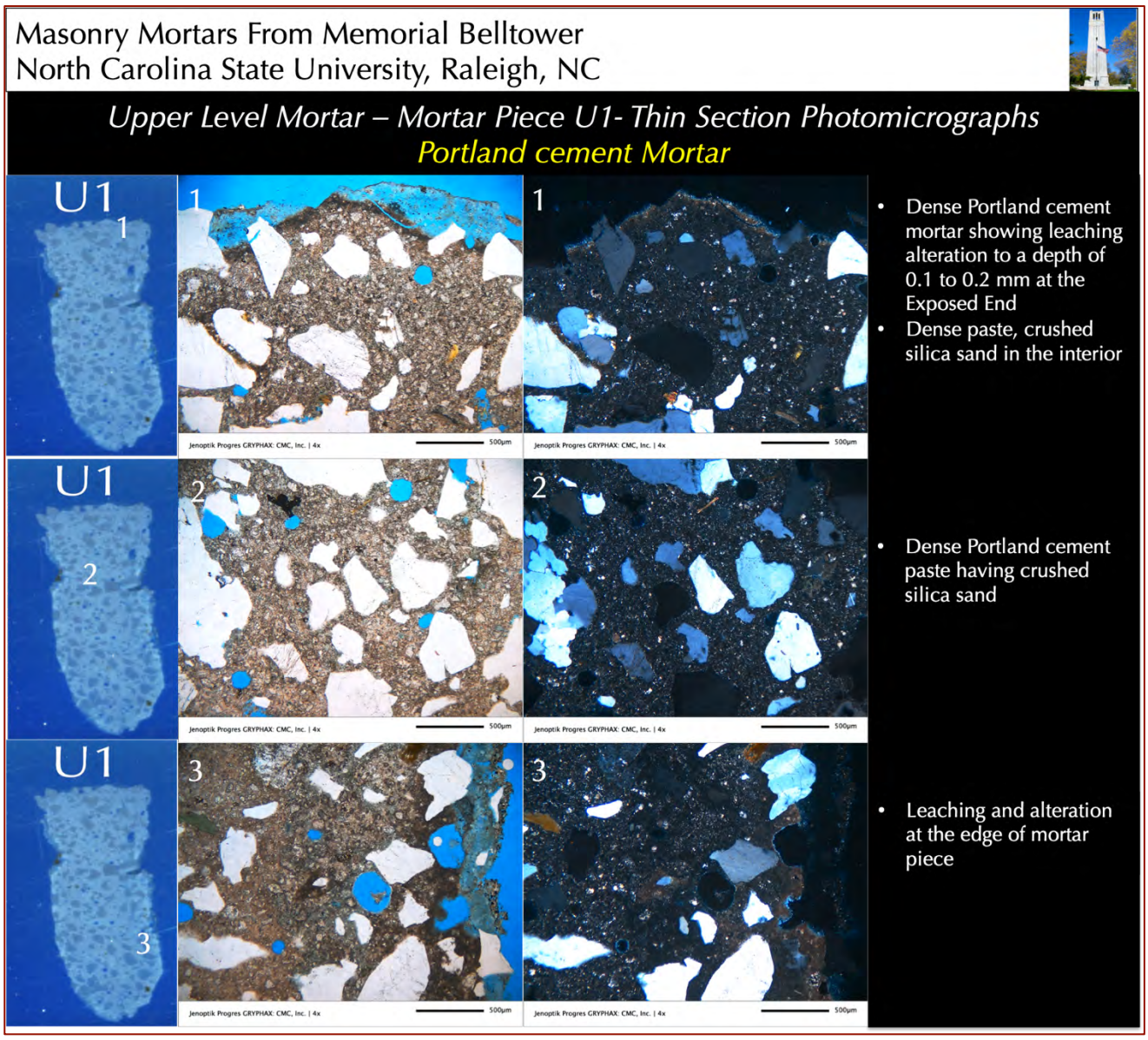

Figure 38: Photomicrographs of thin section of Piece U1 from 1940s construction from the Upper level of Belltower (see Figure 8) showing: (a) leaching and carbonation of paste at the exposed surface of Portland cement-only (PC) mortar (1st row); (b) dense Portland cement paste having many fine residual cement particles in the non-carbonated interior of mortar shown in all rows; (c) leaching and carbonation of paste at one edge of the mortar shown in the bottom row; and (d) crushed silica sand particles that are well-graded, and well-distributed. Three rows of photos were taken from three different locations shown in the leftmost column on thin section view of Piece U1. Notice lack of air entrainment in the mortar. Scale bars are 0.5 mm.

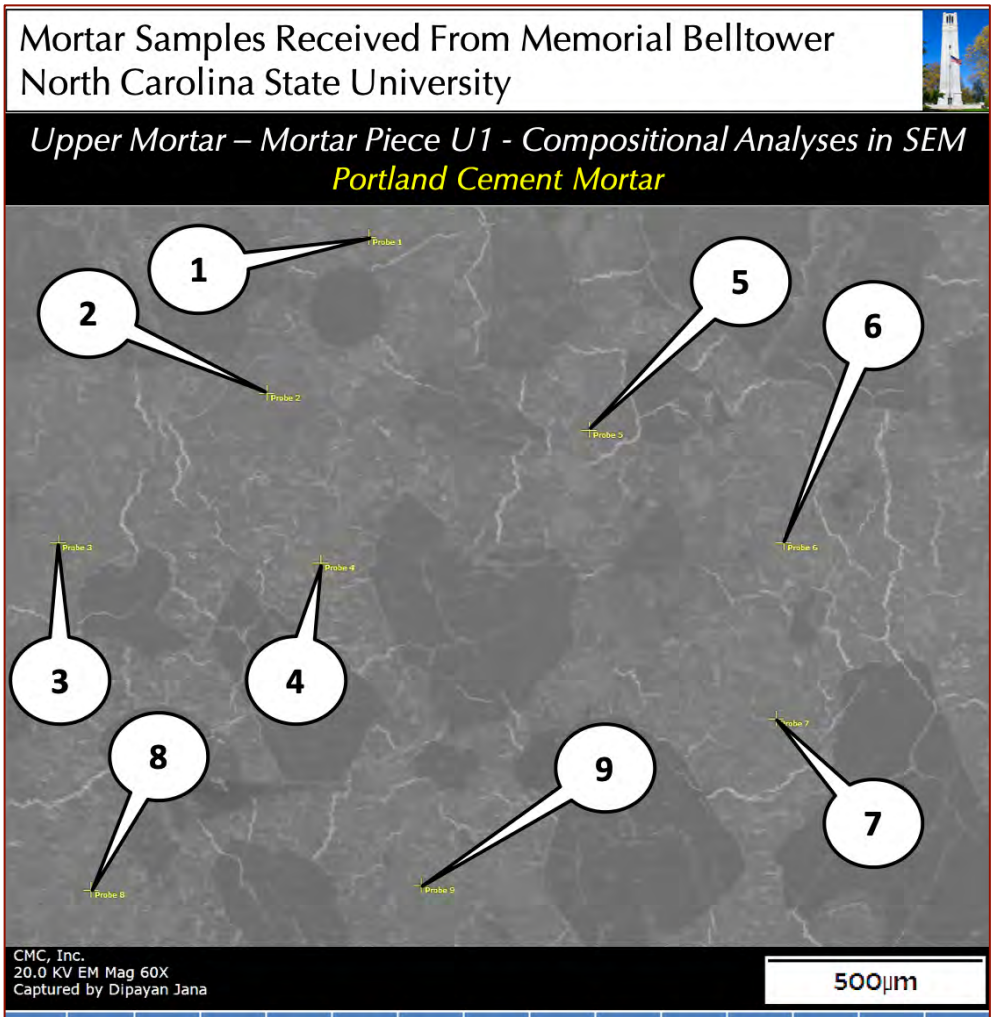

Figure 39: Secondary electron image (top), and compositional analyses at the tips of callouts placed across various areas of paste in the PC mortar portion in U1 (see Figure 8) where paste shows characteristic calcium silicate hydrate compositions from cement hydration.

#	CaO	SiO2	Al2O3	Na2O	MgO	SO3	K2O	TiO2	FeO	P2O5	CO2	Total	Phase	Paste CI
1	40.20	18.63	14.11	0.06	2.76	2.62	0.00	0.41	0.38	0.42	20.41	99.62	PC Paste	1.54
2	66.00	16.03	3.72	1.23	0.36	0.88	0.14	0.00	0.00	0.13	11.51	100.0		0.74
3	42.92	21.36	4.28	0.27	1.15	0.95	0.00	0.02	0.81	0.31	27.93	99.19		1.46
4	39.27	23.16	13.56	0.12	2.33	3.39	0.00	0.28	0.78	0.47	16.64	99.22		1.89
5	38.54	29.50	5.86	0.22	2.22	1.75	0.02	0.22	0.33	0.70	20.63	99.66		2.14
6	68.92	25.55	0.82	0.00	0.08	0.03	0.00	0.19	0.24	0.04	4.12	99.75		1.05
7	44.00	36.32	3.30	0.06	1.25	1.12	0.05	0.05	0.85	0.96	12.04	99.15		2.32
8	50.89	21.36	7.08	0.06	1.38	0.41	0.03	0.40	0.22	0.91	17.26	99.78		1.28
9	44.31	31.57	4.16	0.23	0.24	1.54	0.00	0.09	0.22	0.09	17.56	99.79		2.09

Paste CI = $[(2.8*SiO_2)+(1.1*Al_2O_3)+(0.7*Fe_2O_3)]/[(CaO)+(1.4*MgO)]$. Carbon, represented as CO_2 is from carbonated paste and epoxy used in thin section preparation.

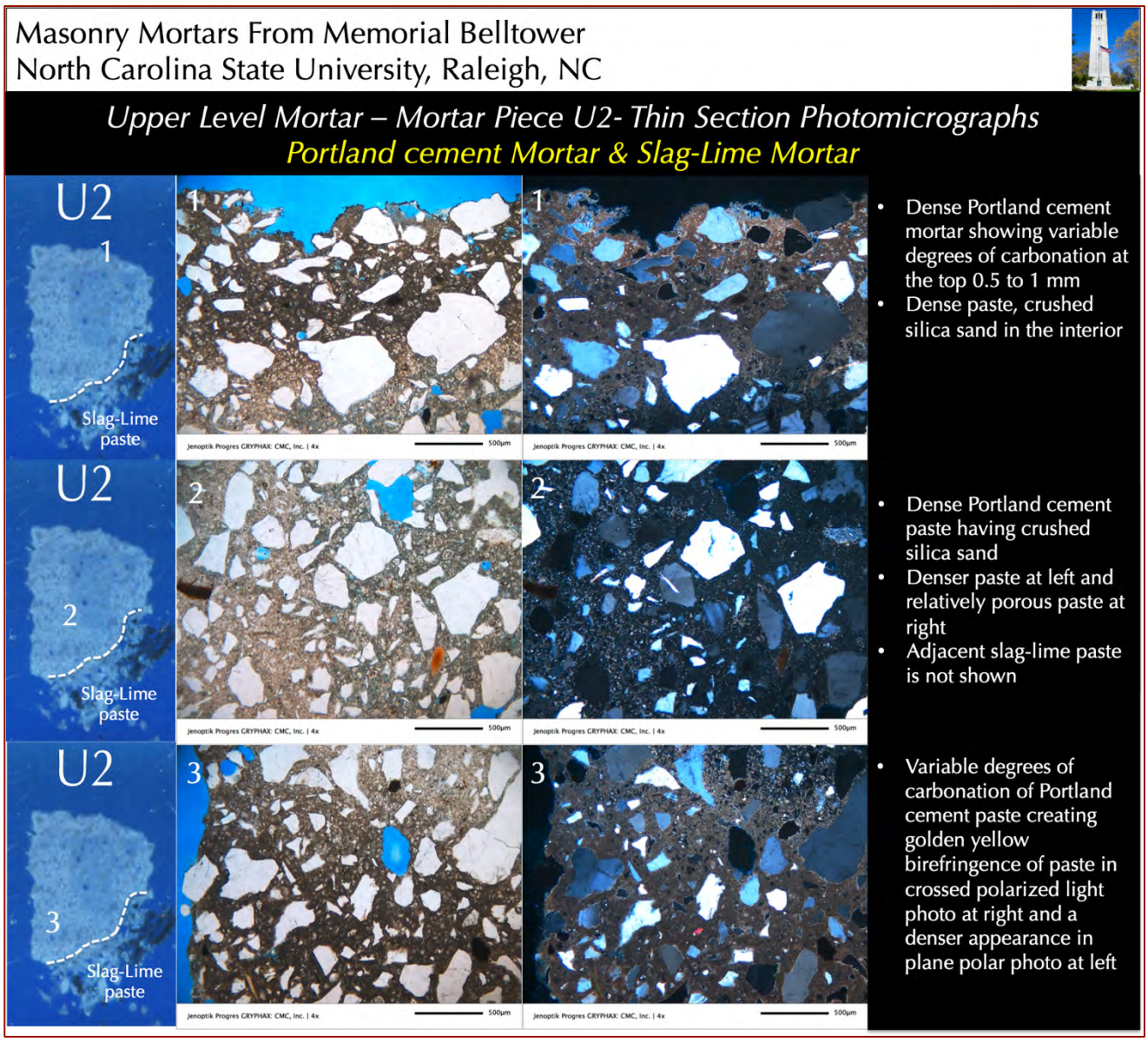

Figure 40: Photomicrographs of thin section of Piece U2 from 1940s construction from the Upper level of Belltower (see Figure 8) showing: (a) leaching and carbonation of paste at the exposed surface of Portland cement-only (PC) mortar (1st row); (b) dense Portland cement paste having many fine residual cement particles in the non-carbonated interior of mortar shown in all rows; (c) leaching and carbonation of paste at one edge of the mortar shown in the bottom row; and (d) crushed silica sand particles that are well-graded, and well-distributed. Three rows of photos were taken from three different locations shown in the leftmost column on thin section view of Piece U2. Notice lack of air entrainment in the mortar. White dashed line in the left column shows interface between the PC mortar at the top and a slag-lime mortar at the bottom where the slag-lime mortar (not shown in the thin section photos) is much softer, more porous and more carbonated than the PC mortar. Scale bars are 0.5 mm.

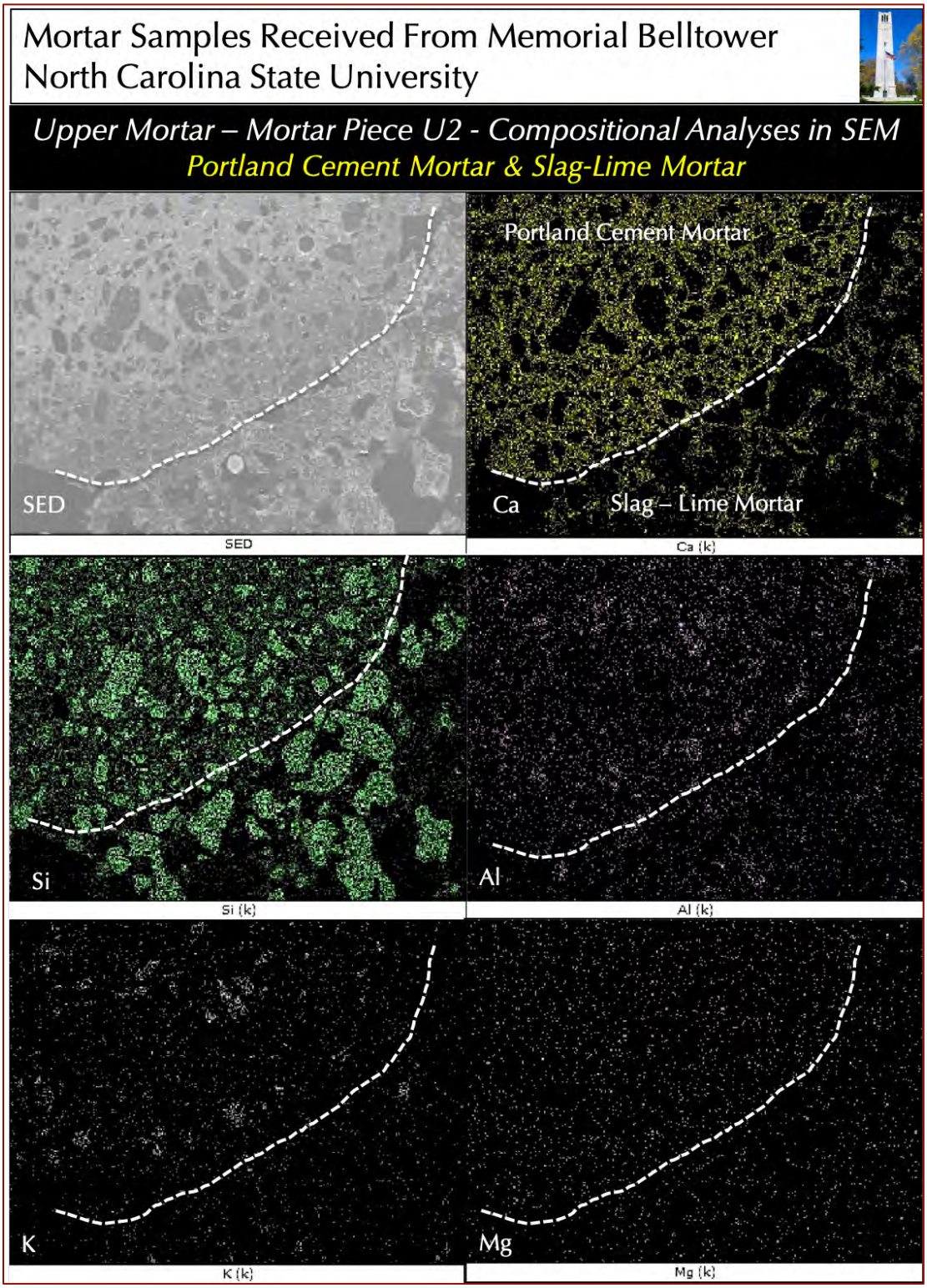

Figure 41: X-ray elemental maps of Ca, Si, Al, K, and Mg of the SED image (shown in top left) showing the interface between the PC mortar and slag-lime mortar in U2 from the Upper level of Belltower from 1940s construction showing overall compositional similarities and differences of both mortars and lack of adequate lime in the slag-lime mortar compared to PC mortar due to lime leaching in slag-lime mortar.

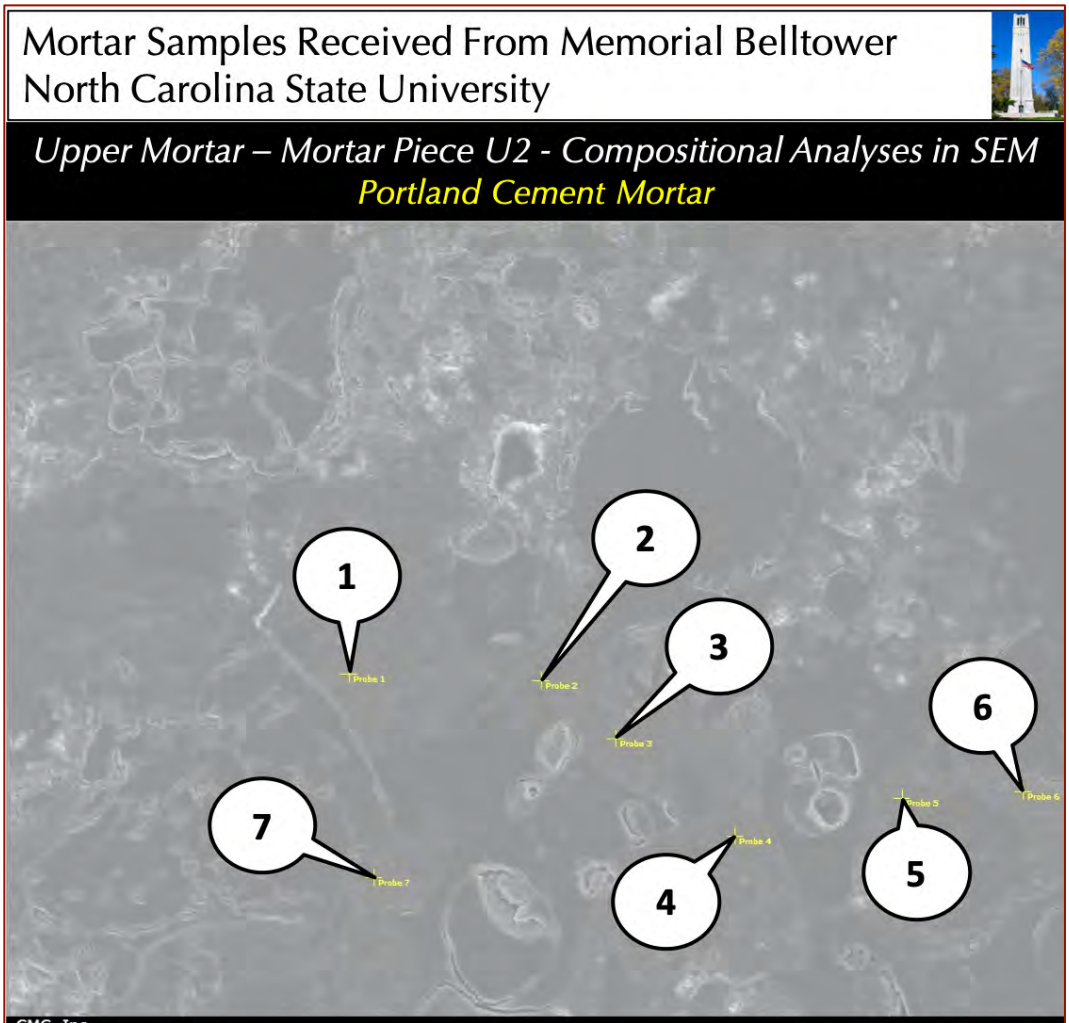

#	CaO	SiO2	Al2O3	Na2O	MgO	SO3	K2O	TiO2	FeO	P2O5	CO2	Total	Phase	Paste CI
1	65.80	7.37	2.48	0.42	0.36	0.76	0.04	0.46	0.26	1.12	20.92	99.73	PC Paste	0.36
2	53.23	19.19	7.49	0.00	0.04	1.68	0.87	0.35	1.06	0.62	15.46	98.93		1.18
3	61.94	14.10	1.88	0.31	0.00	0.47	0.00	0.03	0.66	0.89	19.73	99.35		0.68
4	48.66	31.45	10.45	0.07	0.90	2.60	1.00	0.00	0.29	0.93	3.65	99.71		2.00
5	56.63	18.83	6.23	0.00	0.08	1.29	0.48	0.17	0.07	0.94	15.28	99.93		1.05
6	46.44	6.22	1.40	0.00	0.00	0.17	0.03	0.05	0.00	1.33	44.35	99.99		0.41
7	58.57	15.87	6.08	0.34	0.48	0.81	0.13	0.16	0.83	1.32	15.41	99.17		0.87

Figure 42: Secondary electron image (top), and compositional analyses at the tips of callouts placed across various areas of paste in the slag-lime mortar portion in U2 (see Figure 8) where paste shows large compositional variations due to lime leaching and carbonation. Paste CI = $[(2.8*SiO_2)+(1.1*Al_2O_3)+(0.7*Fe_2O_3)]/[(CaO)+(1.4*MgO)]$. Carbon, represented as CO_2 is from carbonated paste and epoxy used in thin section preparation.

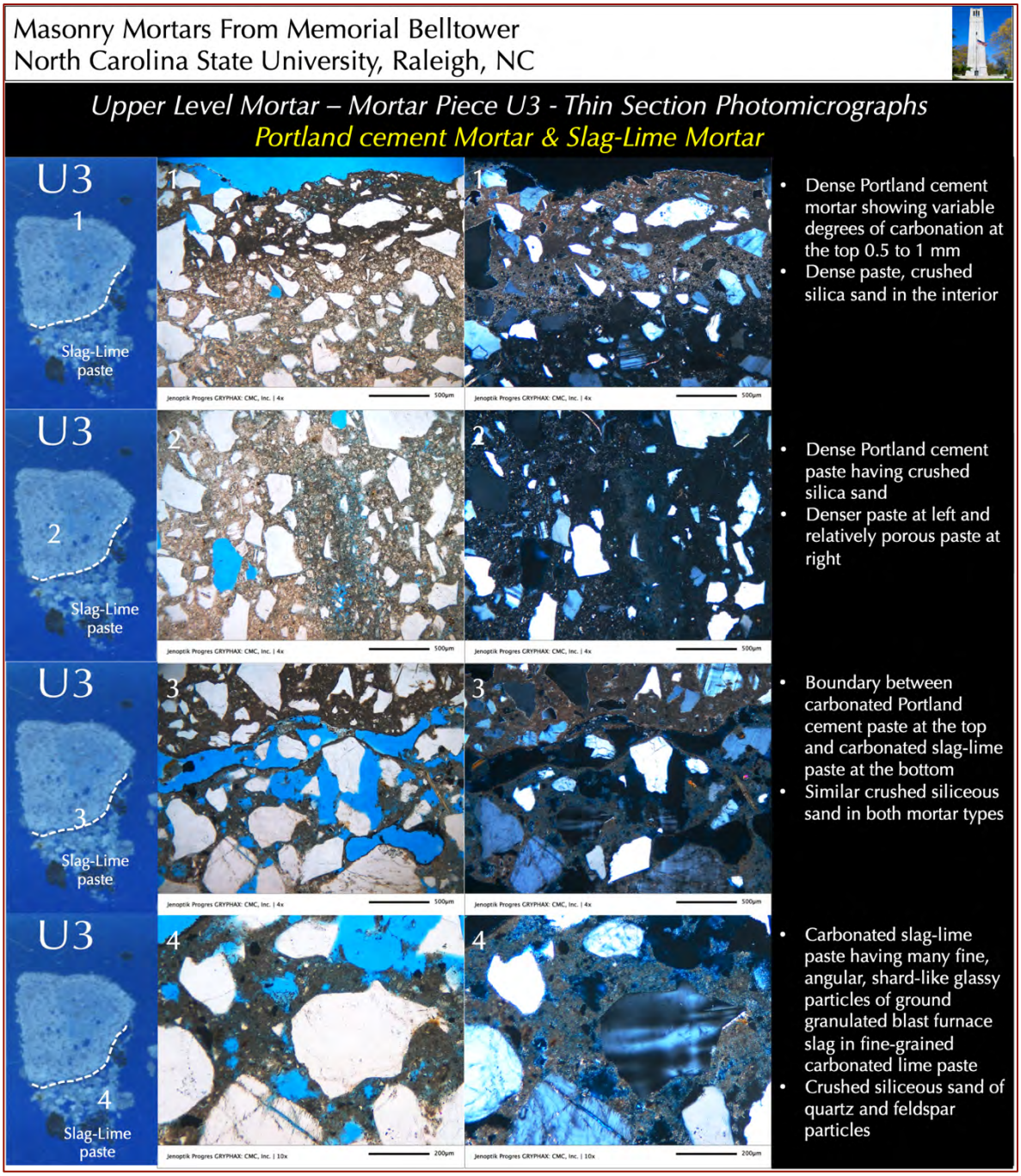

Figure 43: Photomicrographs of thin section of Piece U3 from 1940s construction from the Upper level of Belltower (see Figure 8) showing: (a) carbonation of paste at the exposed surface of Portland cement-only (PC) mortar (1st row); (b) dense Portland cement paste having many fine residual cement particles in the non-carbonated interior of mortar shown in all rows; (c) interface between PC-only mortar at the top and slag-lime mortar at the bottom in the 3rd row from top where former shows denser paste and latter shows porous severely carbonated and leached paste; and (d) crushed silica sand particles in both mortars that are well-graded, and well-distributed. Four rows of photos were taken from four different locations shown in the leftmost column on thin section view of Piece U3. Notice lack of air entrainment in the mortars. White dashed line in the left column shows interface between the PC mortar at the top and a slag-lime mortar at the bottom where the slag-lime mortar is much softer, more porous and more carbonated than the PC mortar. Scale bars are 0.5 mm.

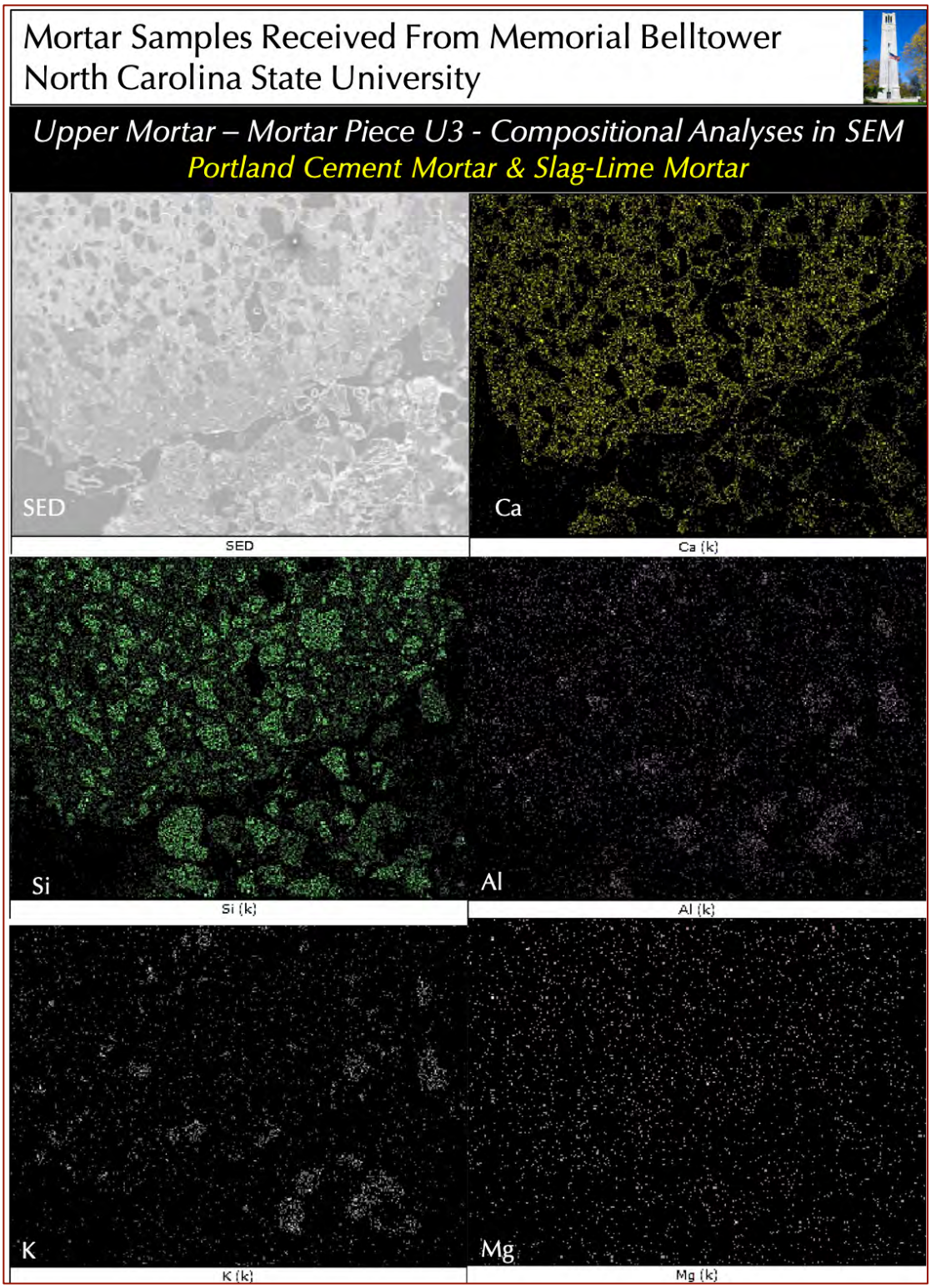

Figure 44: X-ray elemental maps of Ca, Si, Al, K, and Mg of the SED image (shown in top left) showing the interface between the PC mortar at the top and slag-lime mortar at the bottom in U3 from the Upper level of Belltower from 1940s construction showing overall compositional similarities and variations of PC-only and slag-lime mortar, lack of adequate lime in the slag-lime mortar compared to PC mortar due to lime leaching in slag-lime mortar.

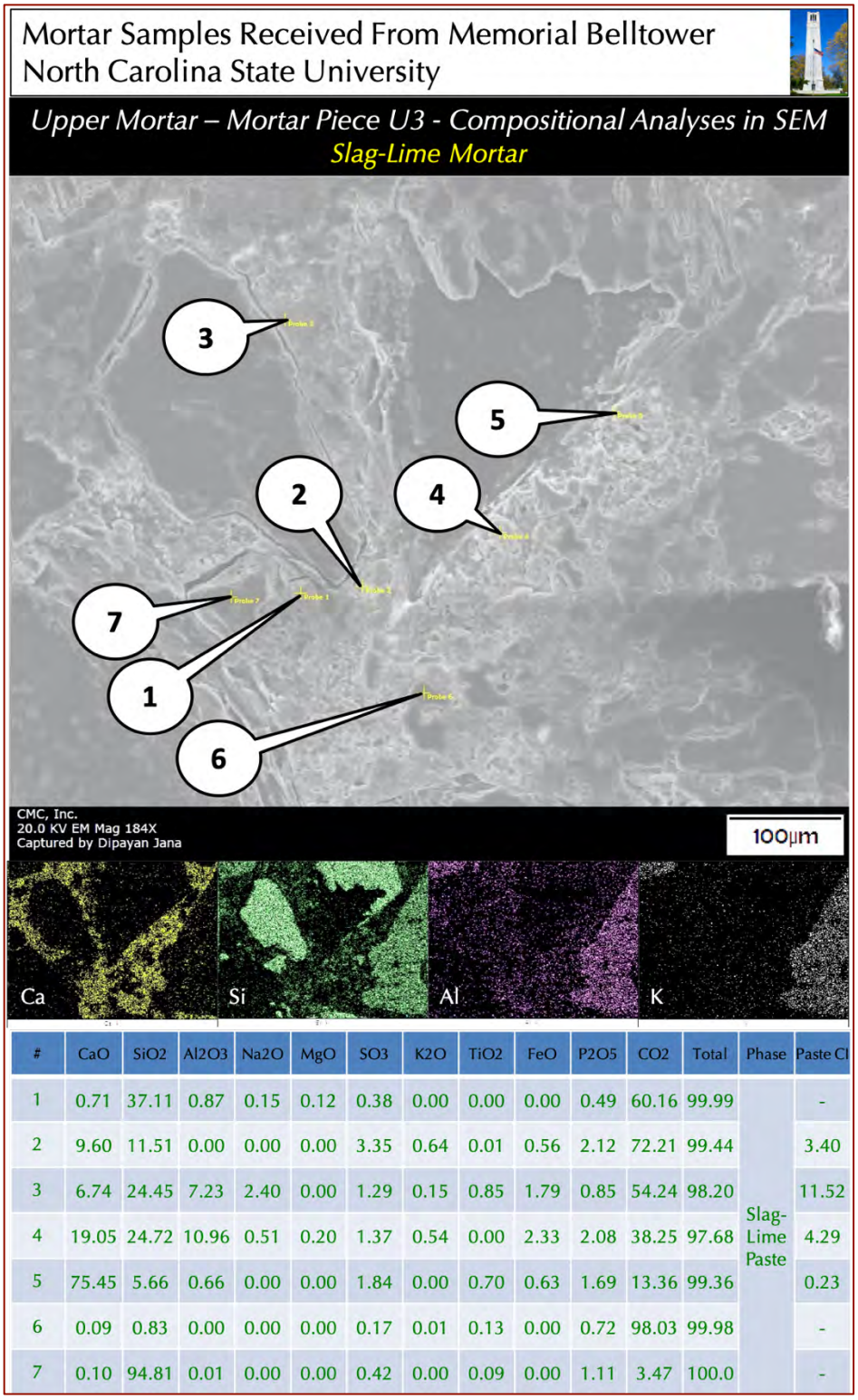

#	CaO	SiO2	Al2O3	Na2O	MgO	SO3	K2O	TiO2	FeO	P2O5	CO2	Total	Phase	Paste CI
1	0.71	37.11	0.87	0.15	0.12	0.38	0.00	0.00	0.00	0.49	60.16	99.99	Slag-Lime Paste	-
2	9.60	11.51	0.00	0.00	0.00	3.35	0.64	0.01	0.56	2.12	72.21	99.44		3.40
3	6.74	24.45	7.23	2.40	0.00	1.29	0.15	0.85	1.79	0.85	54.24	98.20		11.52
4	19.05	24.72	10.96	0.51	0.20	1.37	0.54	0.00	2.33	2.08	38.25	97.68		4.29
5	75.45	5.66	0.66	0.00	0.00	1.84	0.00	0.70	0.63	1.69	13.36	99.36		0.23
6	0.09	0.83	0.00	0.00	0.00	0.17	0.01	0.13	0.00	0.72	98.03	99.98		-
7	0.10	94.81	0.01	0.00	0.00	0.42	0.00	0.09	0.00	1.11	3.47	100.0		-

Figure 45: Secondary electron image (top), X-ray elemental maps of Ca, Si, Al, and K in the middle row, and compositional analyses at the tips of callouts placed across various areas of paste in the slag-lime mortar portion in U3 (see Figure 8) where paste shows large compositional variations due to lime leaching and carbonation. Paste CI = $[(2.8*SiO_2)+(1.1*Al_2O_3)+(0.7*Fe_2O_3)]/[(CaO)+(1.4*MgO)]$. Carbon, represented as CO_2 is from carbonated paste and epoxy used in thin section preparation.

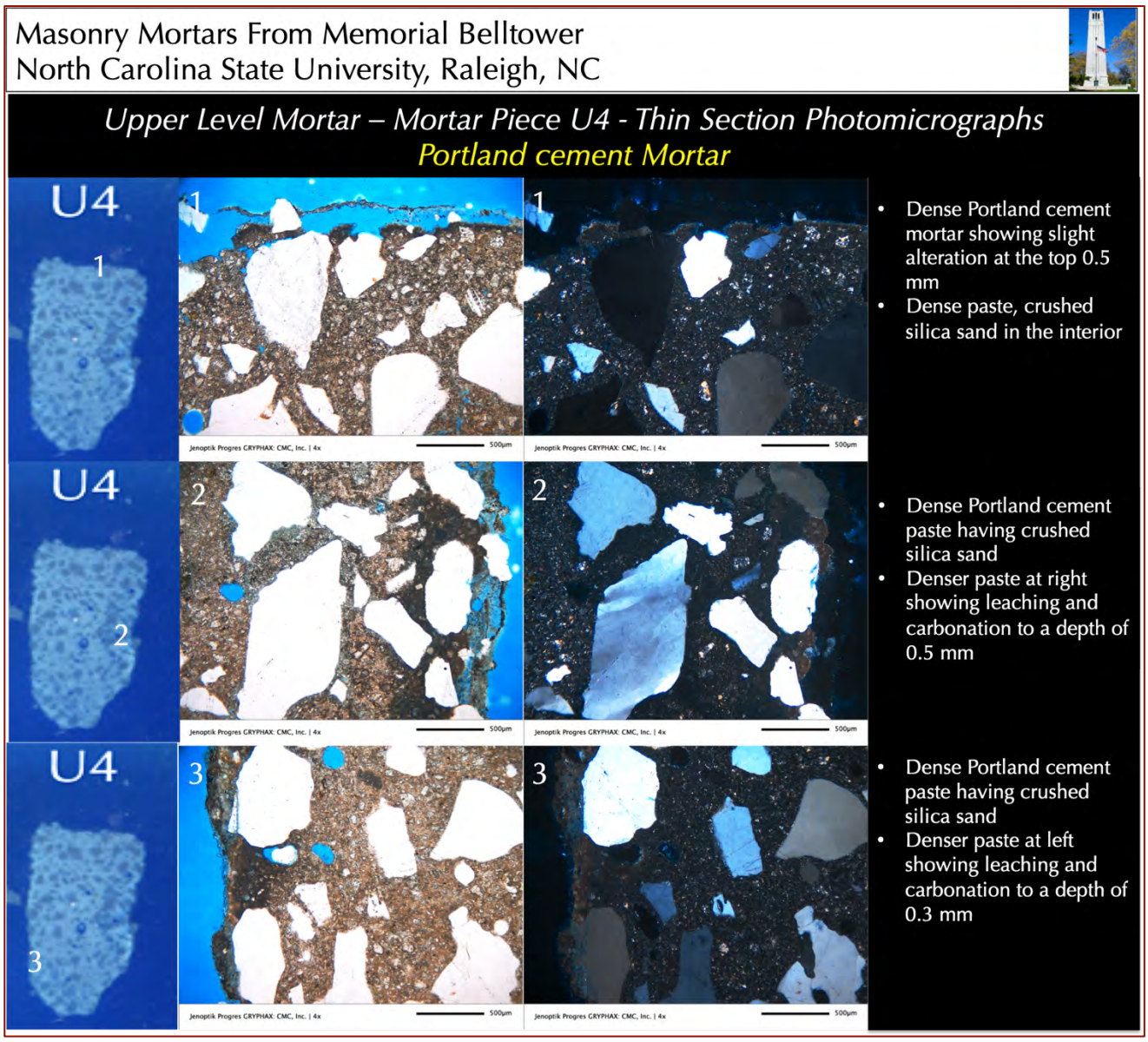

Figure 46: Photomicrographs of thin section of Piece U4 from 1940s construction from the Upper level of Belltower (see Figure 8) showing: (a) leaching and carbonation of paste at the exposed surface of Portland cement-only (PC) mortar (1st row); (b) dense Portland cement paste having many fine residual cement particles in the non-carbonated interior of mortar shown in all rows; (c) carbonation at one edge of mortar shown in the bottom row; and (d) crushed silica sand particles that are well-graded, and well-distributed. Three rows of photos were taken from three different locations shown in the leftmost column on thin section view of Piece U4. Notice lack of air entrainment in the mortar. Scale bars are 0.5 mm.

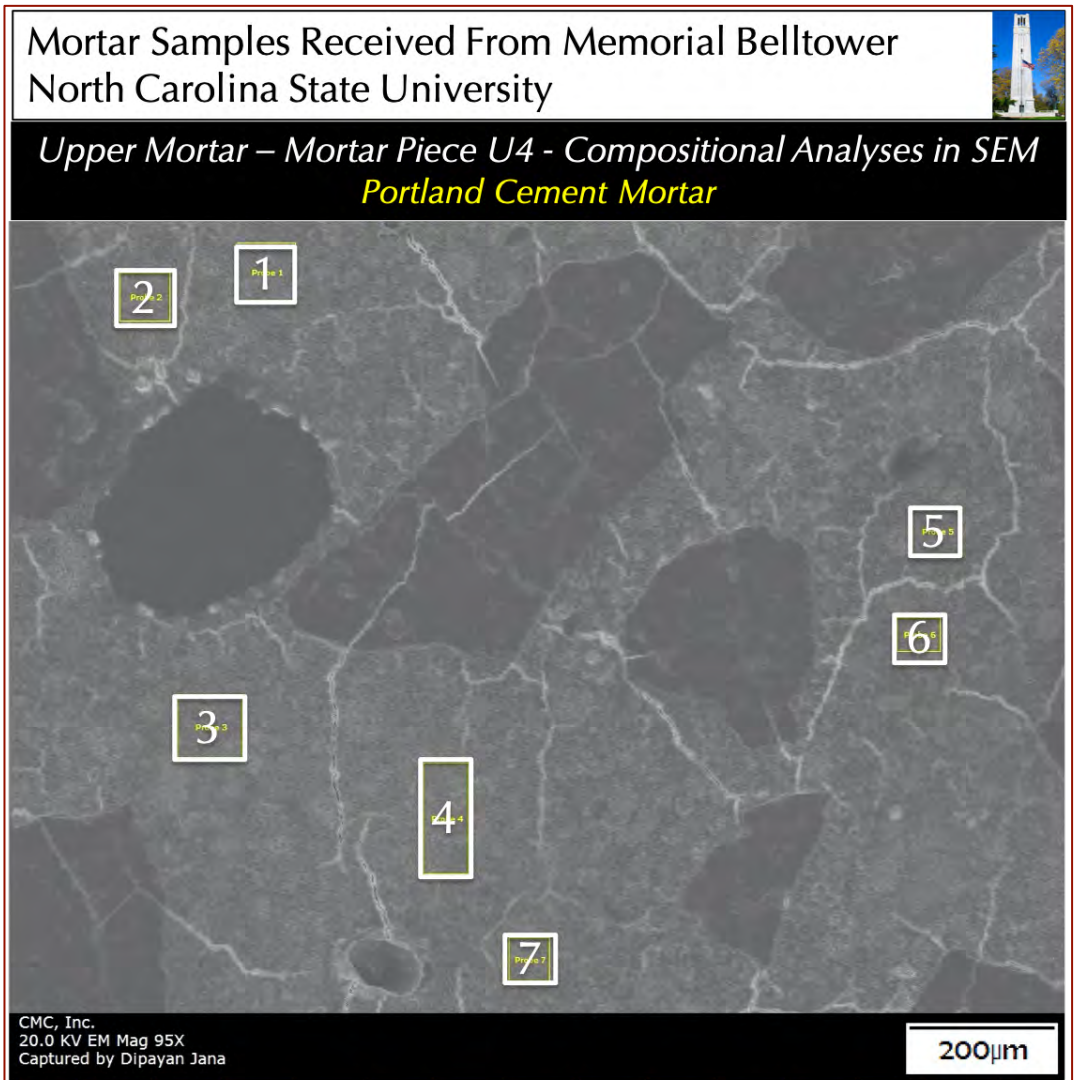

#	CaO	SiO2	Al2O3	Na2O	MgO	SO3	K2O	TiO2	FeO	P2O5	CO2	Total	Phase	Paste Cl
1	41.33	29.70	5.27	0.42	1.29	1.50	0.01	0.20	0.37	0.15	19.75	99.62	PC Paste	2.07
2	44.39	27.41	4.91	0.49	1.07	1.21	0.00	0.00	0.74	0.98	18.79	99.25		1.80
3	44.36	25.47	5.80	0.43	1.89	2.06	0.01	0.12	0.26	0.39	19.20	99.73		1.66
4	44.57	23.85	7.10	0.32	1.83	1.82	0.04	0.22	0.21	0.29	19.75	99.79		1.59
5	40.87	27.46	6.43	0.50	1.23	2.11	0.04	0.26	0.60	1.31	19.18	99.39		1.98
6	43.92	25.51	7.20	0.45	1.94	1.56	0.22	0.13	0.19	0.96	17.92	99.81		1.70
7	43.72	27.25	5.08	0.77	1.06	1.74	0.00	0.41	0.64	0.54	18.79	99.36		1.82

Figure 47: Secondary electron image (top), and compositional analyses at the boxed areas (rasters) placed across various areas of paste in the PC mortar portion in U4 (see Figure 8) where paste shows characteristic calcium silicate hydrate compositions from cement hydration. Carbon, represented as CO_2 is from carbonated paste and epoxy used in thin section preparation.

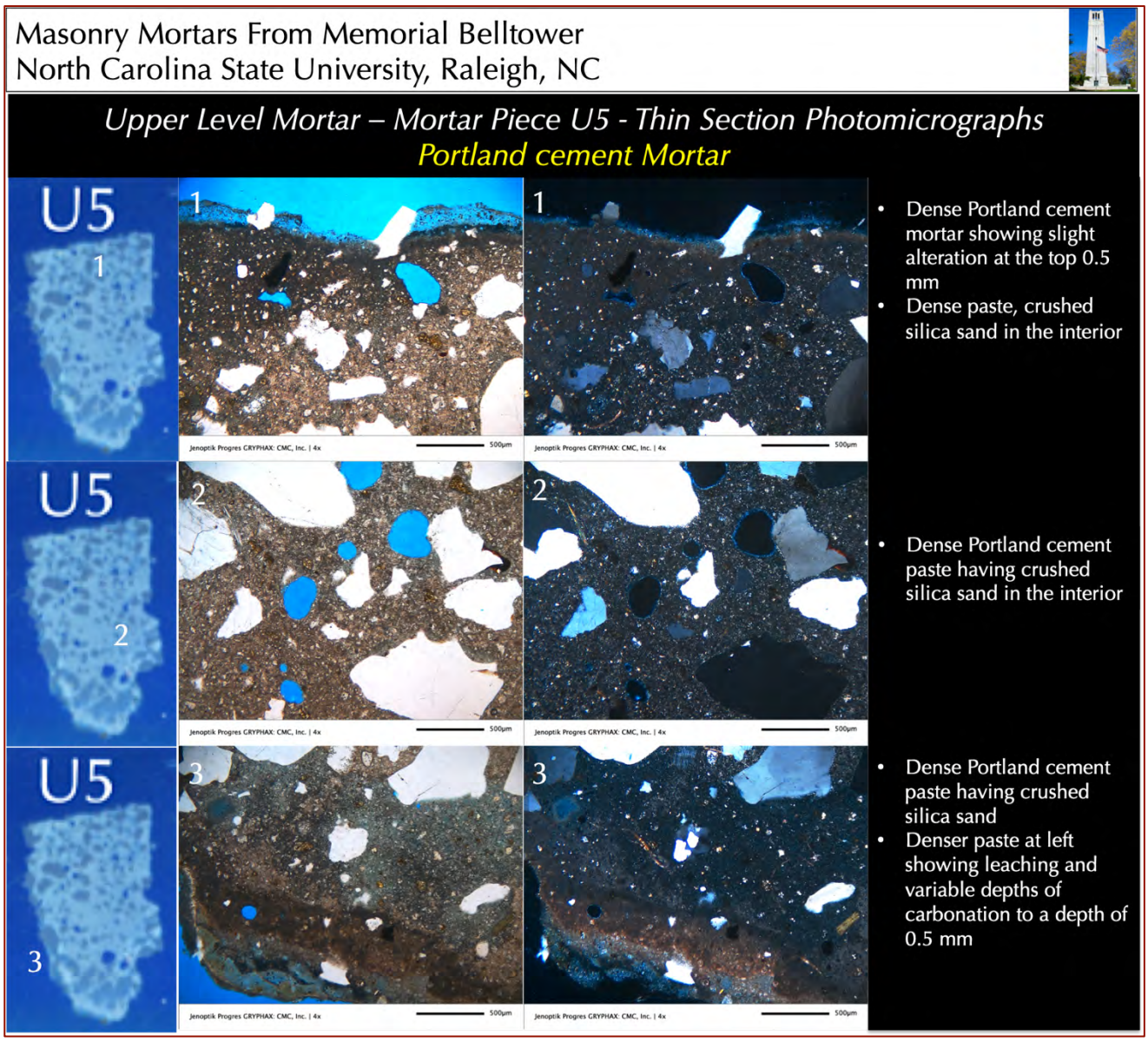

Figure 48: Photomicrographs of thin section of Piece U5 from 1940s construction from the Upper level of Belltower (see Figure 8) showing: (a) leaching and carbonation of paste at the exposed surface of Portland cement-only (PC) mortar (1st row); (b) dense Portland cement paste having many fine residual cement particles in the non-carbonated interior of mortar shown in all rows; (c) leaching and carbonation at one edge of mortar shown in the bottom row; and (d) crushed silica sand particles that are well-graded, and well-distributed. Three rows of photos were taken from three different locations shown in the leftmost column on thin section view of Piece U5. Notice lack of air entrainment in the mortar. Scale bars are 0.5 mm.

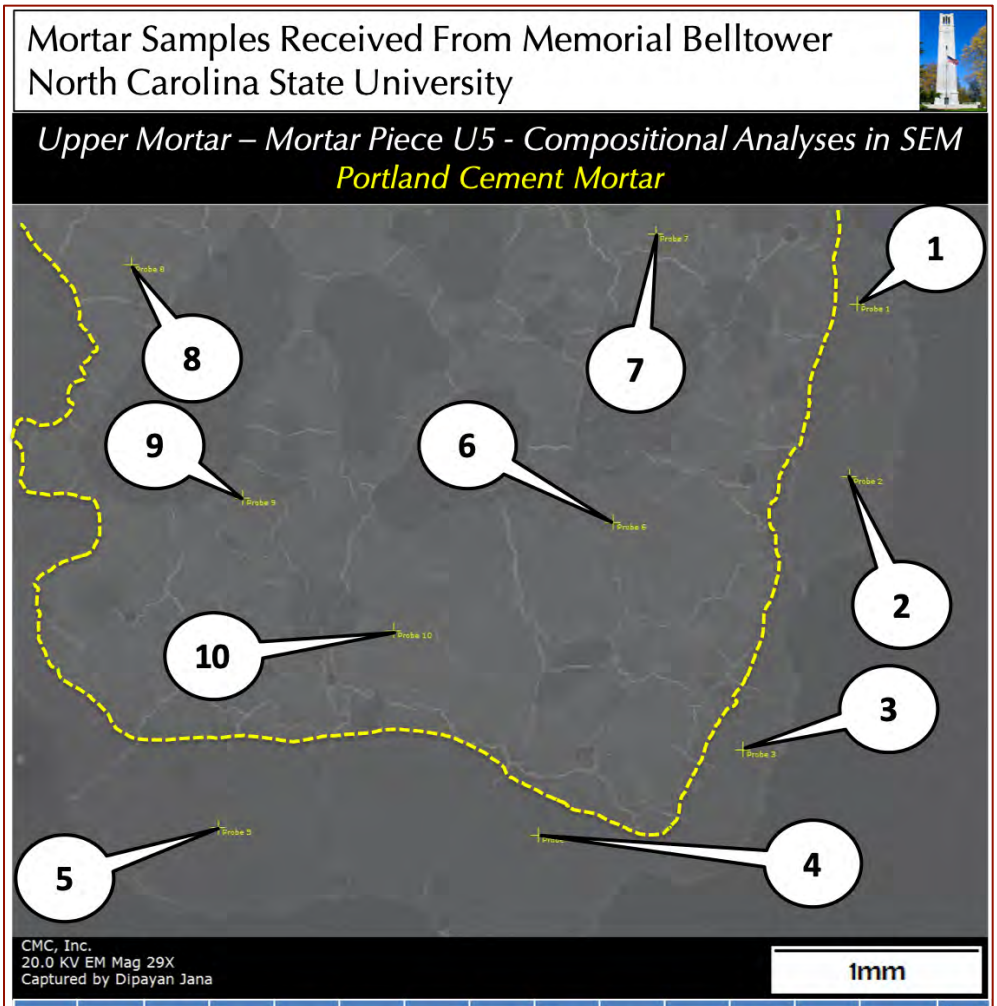

#	CaO	SiO2	Al2O3	Na2O	MgO	SO3	K2O	TiO2	FeO	P2O5	CO2	Total	Phase	Paste Cl
1	42.10	24.99	8.37	0.14	2.75	1.51	0.14	0.22	1.53	1.11	17.15	98.48	PC Paste (#2 and 5 show effects of carbon ation)	1.75
2	66.95	14.32	5.64	0.63	0.70	0.66	0.00	0.09	0.88	1.24	8.89	99.12		0.69
3	39.48	25.38	2.47	0.39	0.29	2.81	0.00	0.12	0.43	1.11	27.51	99.56		1.86
4	40.94	34.46	4.72	0.22	3.11	0.34	0.00	0.48	0.45	1.47	13.82	99.56		2.25
5	68.69	12.98	4.95	0.49	0.05	0.96	0.02	0.00	0.79	1.21	9.86	99.21		0.62
6	37.92	14.44	4.00	0.23	0.58	5.37	0.00	0.01	0.19	0.17	37.09	99.81		1.16
7	44.41	27.20	4.98	0.59	1.62	2.12	0.05	0.00	0.08	1.09	17.86	99.92		1.75
8	43.52	27.37	4.97	0.79	0.42	1.18	0.00	0.03	0.45	0.80	20.48	99.56		1.87
9	30.89	32.06	3.48	0.53	0.53	0.33	0.00	0.21	0.54	1.15	30.27	99.45		2.97
10	34.81	25.80	4.21	0.38	0.59	3.72	0.08	0.14	0.49	1.12	28.68	99.53		2.17

Figure 49: Secondary electron image (top), and compositional analyses at the tips of callouts placed across various areas of paste in the PC mortar portion in U5 (see Figure 8) where paste shows characteristic calcium silicate hydrate compositions from cement hydration. Yellow dashed line separates carbonated edge of mortar from interior non-carbonated paste where carbonated edge (see bottom row in the previous Figure) shows enrichment in lime and lesser silica relative to lime and silica contents in the non-carbonated interior. Carbon, represented as CO_2 is from carbonated paste and epoxy used in thin section preparation.

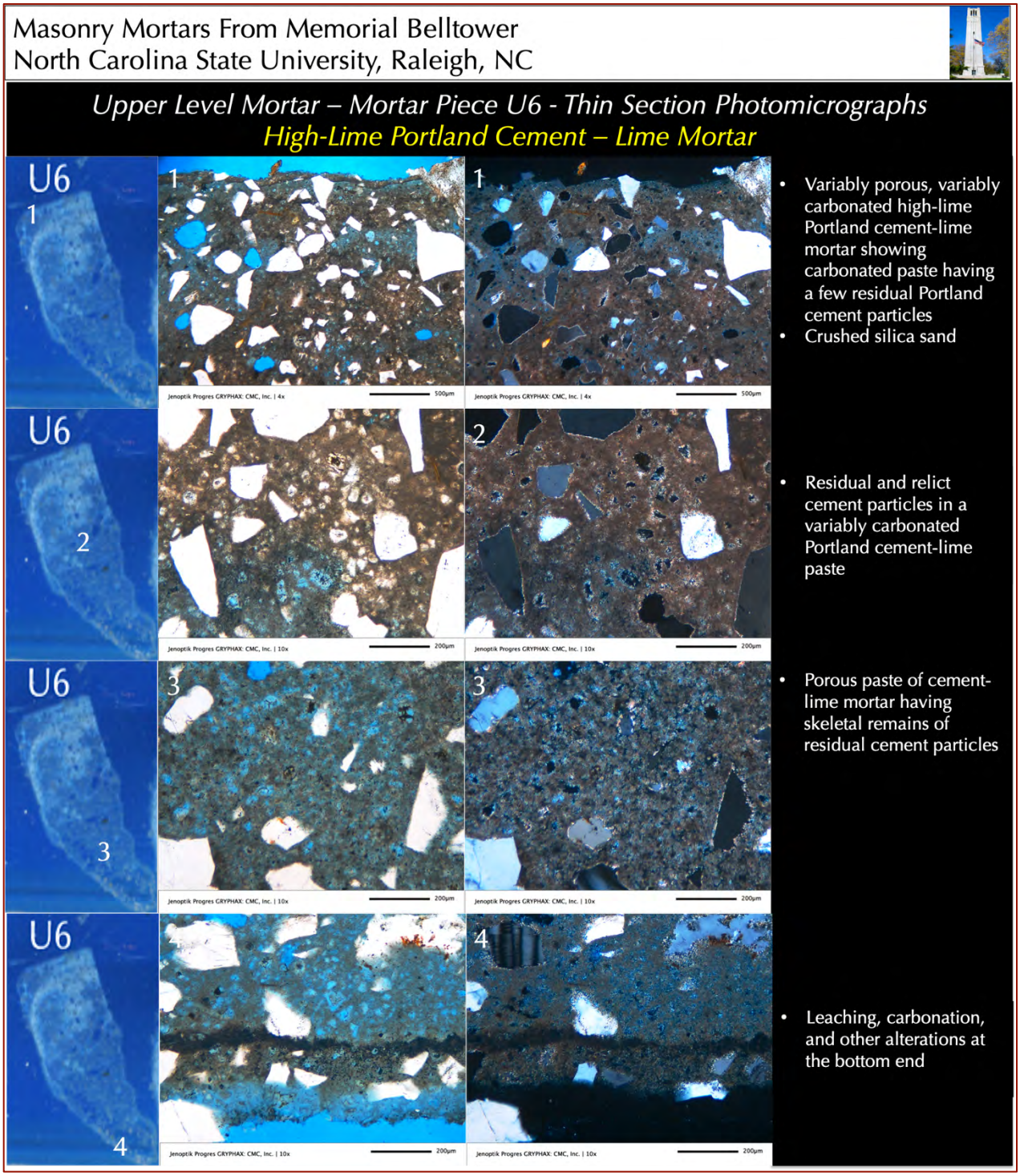

Figure 50: Photomicrographs of thin section of Piece U6 from 1940s construction from the Upper level of Belltower (see Figure 8) showing: (a) severe deep carbonation of paste at the exposed surface of high-lime cement-lime mortar (1st row); (b) variable degrees of carbonation of paste and some relict carbonated residues of Portland cement in the denser regions of paste in the 2nd row from top; (c) leaching and carbonation of paste in the 3rd row resulting in high paste porosity; (d) leaching, carbonation, and dark weathering band at the edge of mortar shown in the bottom row; and (e) crushed silica sand particles that are well-graded, and well-distributed. Four rows of photos were taken from four different locations shown in the leftmost column on thin section view of Piece U6. Notice lack of air entrainment in the mortar. Scale bars are 0.2 to 0.5 mm.

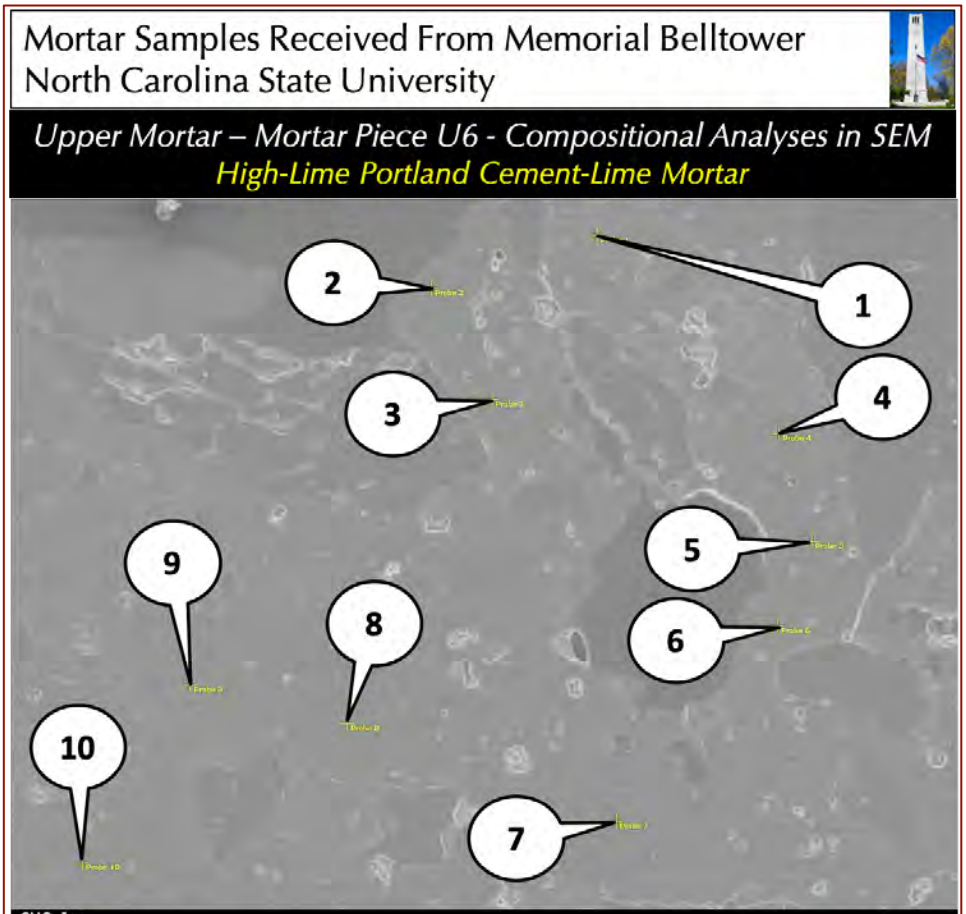

#	CaO	SiO2	Al2O3	Na2O	MgO	SO3	K2O	TiO2	FeO	P2O5	CO2	Total	Phase	Paste Cl
1	50.78	27.10	4.06	0.00	0.04	1.17	0.11	0.43	0.00	1.21	15.09	99.99	PC-rich Paste	1.58
2	71.95	12.32	1.18	0.21	0.00	0.77	0.01	0.00	0.08	1.25	12.23	99.92	Lime-rich	0.50
3	83.17	7.01	0.56	0.74	0.28	0.46	0.00	0.45	0.19	0.89	6.25	99.81		0.24
4	28.44	45.30	5.54	0.75	1.06	1.85	0.19	0.10	0.32	1.77	14.66	99.66	PC-rich Paste	4.45
5	82.79	8.61	0.79	0.13	0.00	0.26	0.00	0.10	0.05	0.98	6.29	99.95	Lime-rich	0.30
6	80.18	8.06	0.58	0.23	0.10	1.35	0.02	0.36	1.36	1.52	6.24	98.64		0.30
7	88.44	4.36	0.02	0.49	0.20	0.54	0.00	0.00	0.04	0.99	4.92	99.96		0.14
8	77.06	12.11	1.38	0.12	0.00	0.88	0.00	0.36	0.62	0.46	7.02	99.39		0.47
9	83.95	8.05	1.08	0.00	0.00	0.18	0.07	0.00	0.23	1.21	5.23	99.77		0.28
10	72.94	14.41	1.42	0.39	0.42	1.15	0.02	0.21	0.10	0.83	8.11	99.90		0.57

Figure 51: Secondary electron image (top), and compositional analyses at the tips of callouts placed across various areas of paste in the high-lime cement-lime mortar portion in U6 (see Figure 8) where paste shows mostly lime-rich regions (Ca>>Si) shown in orange rows from carbonation of cement-lime paste and a few regions shown in blue rows that are denser due to carbonated cement hydration products where Ca is not as high as in severely carbonated regions and Si is higher than the other carbonated regions. The compositional variations of paste are the result of variable degrees of carbonation of cement-lime paste along with the presence of lime and cement components in the binder. Carbon, represented as CO_2 is from carbonated paste and epoxy used in thin section preparation.

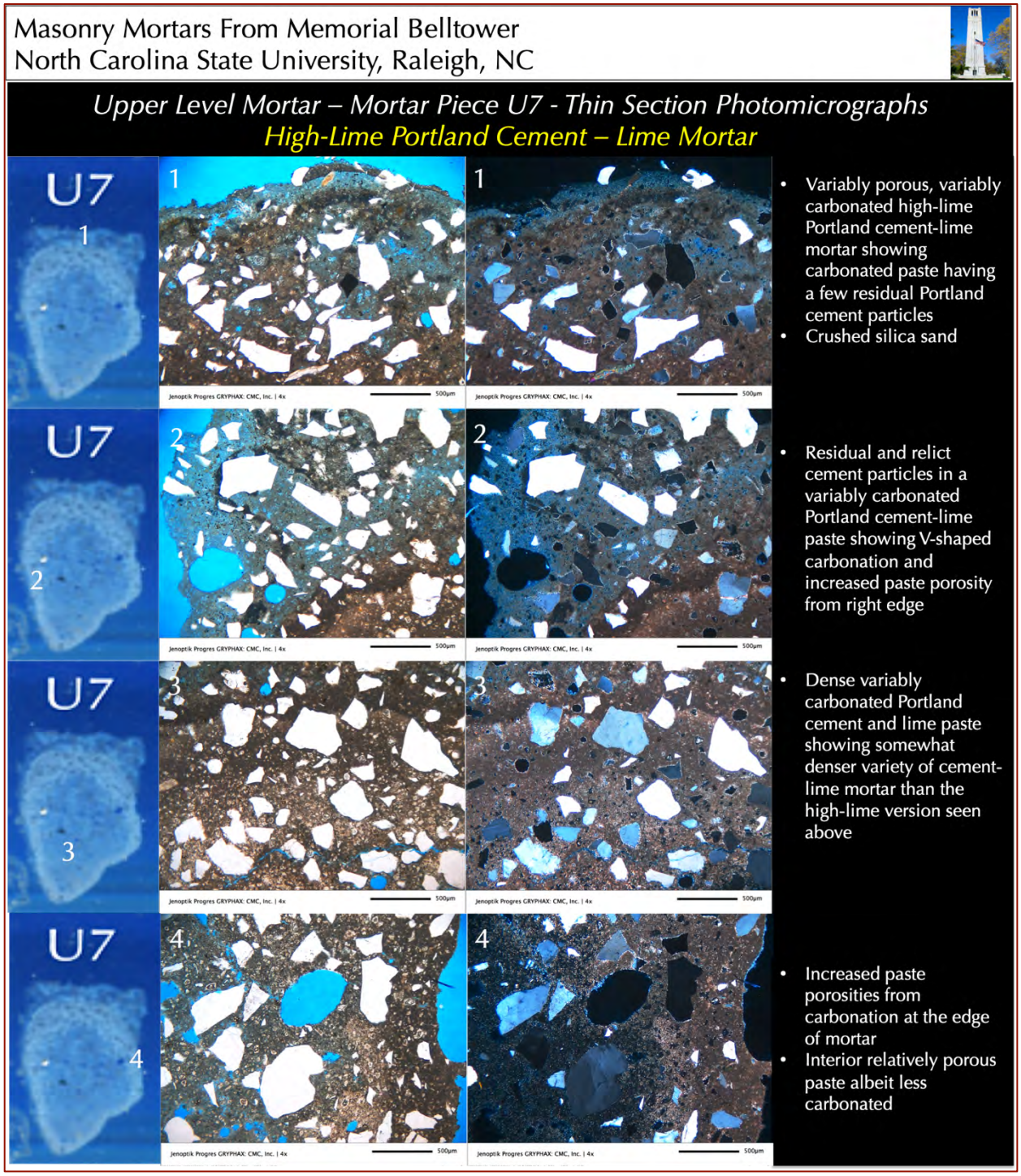

Figure 52: Photomicrographs of thin section of Piece U7 from 1940s construction from the Upper level of Belltower (see Figure 8) showing: (a) leaching and severe deep carbonation of paste at the exposed surface of high-lime cement-lime mortar (1st row); (b) variable degrees of carbonation of paste and some relict carbonated residues of Portland cement in the denser regions of paste in the 2nd and 3rd rows from top; (c) leaching and carbonation of paste in the 4th row where carbonated paste at the surface region is denser than less carbonated paste in the interior where interior paste shows some shrinkage microcracks (4th row); and (d) crushed silica sand particles that are well-graded, and well-distributed. Four rows of photos were taken from four different locations shown in the leftmost column on thin section view of Piece U7. Notice lack of air entrainment in the mortar. Scale bars are 0.5 mm.

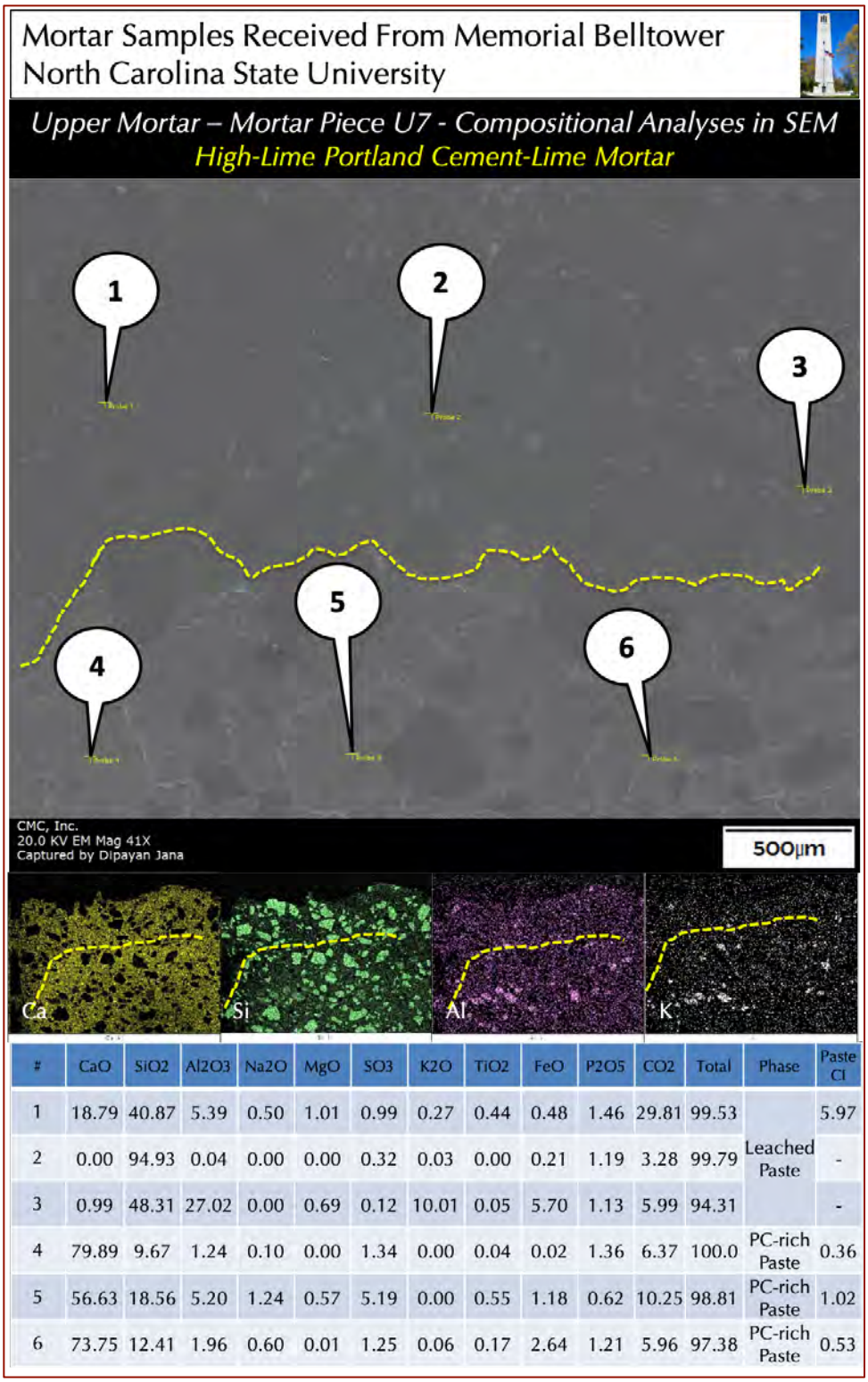

#	CaO	SiO2	Al2O3	Na2O	MgO	SO3	K2O	TiO2	FeO	P2O5	CO2	Total	Phase	Paste Cl
1	18.79	40.87	5.39	0.50	1.01	0.99	0.27	0.44	0.48	1.46	29.81	99.53		5.97
2	0.00	94.93	0.04	0.00	0.00	0.32	0.03	0.00	0.21	1.19	3.28	99.79	Leached Paste	-
3	0.99	48.31	27.02	0.00	0.69	0.12	10.01	0.05	5.70	1.13	5.99	94.31		-
4	79.89	9.67	1.24	0.10	0.00	1.34	0.00	0.04	0.02	1.36	6.37	100.0	PC-rich Paste	0.36
5	56.63	18.56	5.20	1.24	0.57	5.19	0.00	0.55	1.18	0.62	10.25	98.81	PC-rich Paste	1.02
6	73.75	12.41	1.96	0.60	0.01	1.25	0.06	0.17	2.64	1.21	5.96	97.38	PC-rich Paste	0.53

Figure 53: Secondary electron image (top), X-ray elemental maps of Ca, Si, Al, and K (middle row) and compositional analyses at the tips of callouts placed across various areas of paste in the high-lime cement-lime mortar portion in U7 (see Figure 8) where paste shows leached region at the exposed end where Si >> Ca due ro lime leaching at Probes 1 to 3, then interior region rich in cement hydration products in probes 4 to 6 where Si is not as enriched as in the leached region. Yellow dashed lines in the X-ray elemental maps separate leached paste from interior carbonated paste. Carbon, represented as CO_2 is from carbonated paste and epoxy used in thin section preparation.

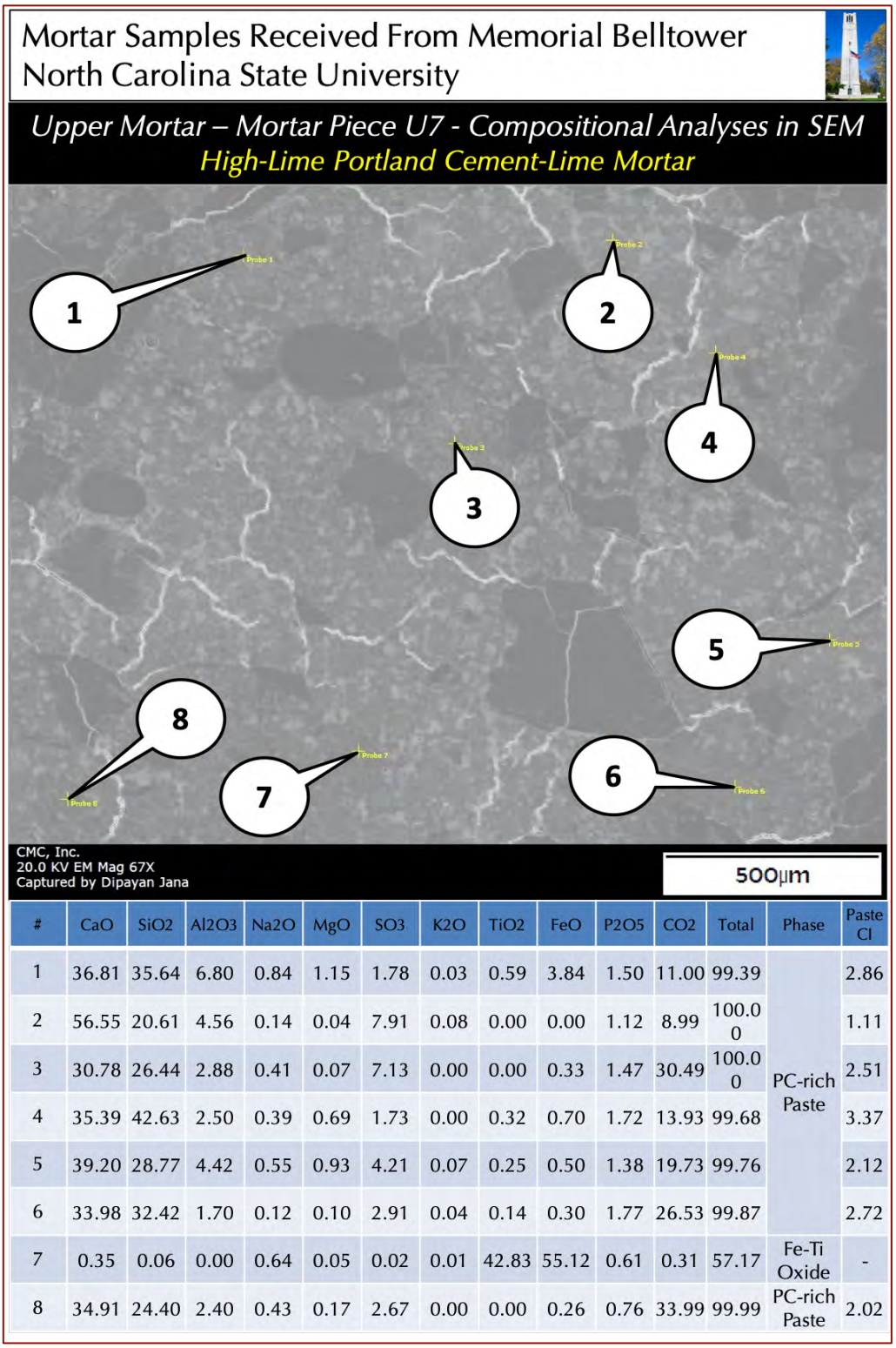

#	CaO	SiO2	Al2O3	Na2O	MgO	SO3	K2O	TiO2	FeO	P2O5	CO2	Total	Phase	Paste Cl
1	36.81	35.64	6.80	0.84	1.15	1.78	0.03	0.59	3.84	1.50	11.00	99.39	PC-rich Paste	2.86
2	56.55	20.61	4.56	0.14	0.04	7.91	0.08	0.00	0.00	1.12	8.99	100.00		1.11
3	30.78	26.44	2.88	0.41	0.07	7.13	0.00	0.00	0.33	1.47	30.49	100.00		2.51
4	35.39	42.63	2.50	0.39	0.69	1.73	0.00	0.32	0.70	1.72	13.93	99.68		3.37
5	39.20	28.77	4.42	0.55	0.93	4.21	0.07	0.25	0.50	1.38	19.73	99.76		2.12
6	33.98	32.42	1.70	0.12	0.10	2.91	0.04	0.14	0.30	1.77	26.53	99.87		2.72
7	0.35	0.06	0.00	0.64	0.05	0.02	0.01	42.83	55.12	0.61	0.31	57.17	Fe-Ti Oxide	-
8	34.91	24.40	2.40	0.43	0.17	2.67	0.00	0.00	0.26	0.76	33.99	99.99	PC-rich Paste	2.02

Figure 54: Secondary electron image (top), and compositional analyses at the tips of callouts placed across various areas of paste in the high-lime cement-lime mortar portion in U7 (see Figure 8) where paste shows interior non-leached region that is rich in cement hydration products. Carbon, represented as CO_2 is from carbonated paste and epoxy used in thin section preparation.

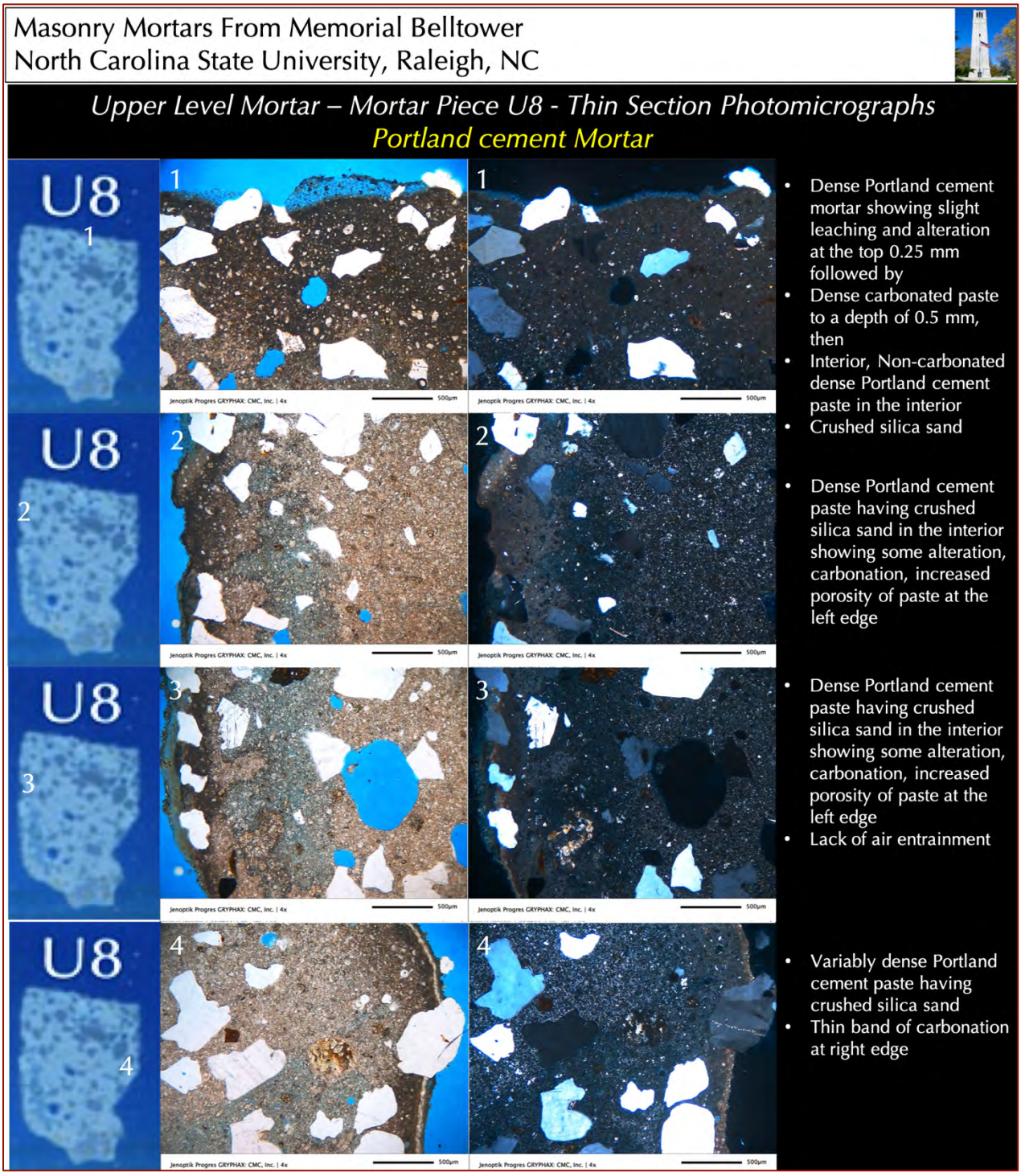

Figure 55: Photomicrographs of thin section of Piece U8 from 1940s construction from the Upper level of Belltower (see Figure 8) showing: (a) leaching and severe deep carbonation of paste at the exposed surface of PC-only mortar (1st row); (b) variable degrees of carbonation of paste at one edge of the mortar shown in the 2nd and 3rd rows from top; (c) thin carbonation of paste at opposite edge shown in the 4th row where carbonated paste at the surface region is denser than less carbonated paste in the interior; and (d) crushed silica sand particles that are well-graded, and well-distributed. Four rows of photos were taken from four different locations shown in the leftmost column on thin section view of Piece U8. Notice lack of air entrainment in the mortar. Scale bars are 0.5 mm.

SEM-EDS Compositional Variations of Pastes in Mortars From 1920s and 1940s Vintages

From the large dataset of SEM-EDS compositional analyses of pastes of various mortars from 1920s and 1940s vintages, a few representative data are selected that are away from leached, carbonated regions, and more from interiors to represent as pristine compositions of pastes as possible. Despite such attempts, compositional variations are still detected beyond different binder types from alterations, e.g., leaching and carbonation of pastes. Table 4 and Figure 56 show results of lime and silica variations with paste-CIs in different 1920s mortars.

Probe	CaO	SiO_2	Al_2O_3	Na_2O	MgO	SO_3	K_2O	TiO_2	FeO	Paste CI	Mortar	Circa
1	42.58	27.42	3.37	0.12	0.34	4.08	0.02	0.08	0.27	1.87	PC only	1920s
2	65.55	23.85	2.01	0.22	0.02	0.45	0.42	0.07	0.41	1.06	PC only	1920s
3	46.36	22.77	3.11	0.00	0.40	2.58	0.00	0.18	0.00	1.43	PC only	1920s
4	41.17	26.74	4.20	0.34	0.09	5.86	0.00	0.07	0.28	1.93	PC only	1920s
5	46.75	20.88	4.47	0.10	0.16	3.85	0.02	0.01	0.34	1.35	PC only	1920s
1	57.97	20.52	10.90	0.26	0.26	0.91	0.00	1.78	1.26	1.21	PC only	1920s
2	41.43	30.16	6.41	0.06	0.58	2.10	0.00	0.09	0.13	2.17	PC only	1920s
1	32.72	19.53	7.57	0.12	0.34	9.30	0.03	0.16	0.27	1.90	PC only	1920s
2	31.44	33.27	4.12	0.22	0.02	3.15	0.03	0.25	0.44	3.11	PC only	1920s
3	39.52	29.44	8.98	0.00	0.40	4.37	0.01	0.01	0.09	2.30	PC only	1920s
1	32.99	27.78	3.21	0.66	1.17	3.92	0.01	0.01	0.00	2.35	PC only	1920s
2	39.76	27.52	6.69	0.21	0.66	2.22	1.12	0.07	1.33	2.10	PC only	1920s
3	45.60	22.42	7.07	0.54	0.52	3.47	0.04	0.09	0.49	1.53	PC only	1920s
4	39.15	37.19	3.02	0.79	0.20	1.84	0.04	0.27	2.08	2.76	PC only	1920s
5	42.04	35.64	4.92	0.14	0.89	1.40	0.00	0.75	0.88	2.44	PC only	1920s
Ave.	**43.00**	**27.01**	**5.34**	**0.25**	**0.40**	**3.30**	**0.12**	**0.26**	**0.55**	**1.97**	PC only	1920s
StDev.	**9.06**	**5.47**	**2.52**	**0.24**	**0.32**	**2.20**	**0.30**	**0.46**	**0.59**	**0.58**	PC only	1920s
6	29.35	38.96	4.42	1.23	0.20	1.31	0.03	0.06	0.28	3.85	Slag-Lime	1920s
7	31.83	34.53	9.59	0.47	0.23	1.78	0.88	0.45	0.11	3.34	Slag-Lime	1920s
8	73.72	10.35	3.55	0.50	1.26	0.68	0.21	0.19	0.77	0.44	Slag-Lime	1920s
9	56.31	14.52	3.45	0.46	0.07	0.16	0.02	0.04	0.32	0.79	Slag-Lime	1920s
10	39.62	24.50	7.23	0.19	0.58	1.31	0.36	0.26	1.00	1.91	Slag-Lime	1920s
3	41.53	19.60	5.15	0.00	0.29	0.40	0.47	0.08	0.24	1.45	Slag-Lime	1920s
4	34.24	33.03	9.80	0.46	1.11	1.15	0.51	0.45	0.32	2.89	Slag-Lime	1920s
Ave.	**46.21**	**22.76**	**6.46**	**0.35**	**0.59**	**0.91**	**0.41**	**0.25**	**0.46**	**1.80**	Slag-Lime	1920s
StDev.	**15.96**	**9.79**	**2.86**	**0.20**	**0.49**	**0.61**	**0.29**	**0.18**	**0.35**	**1.55**	Slag-Lime	1920s
6	49.25	14.93	1.40	1.23	0.20	0.59	0.00	0.01	0.25	0.88	Hydraulic Lime	1920s
7	51.63	26.25	1.55	0.47	0.23	0.28	0.06	0.06	0.34	1.45	Hydraulic Lime	1920s
8	35.90	18.73	1.88	0.50	1.26	0.11	0.06	0.07	0.41	1.45	Hydraulic Lime	1920s
9	86.68	4.81	0.12	0.64	1.29	0.06	0.00	0.12	0.05	0.15	Hydraulic Lime	1920s
10	82.19	7.35	0.71	0.02	0.82	0.15	0.00	0.00	0.88	0.26	Hydraulic Lime	1920s
1	16.09	20.63	3.27	0.42	2.94	0.10	0.08	0.00	0.28	3.05	Hydraulic Lime	1920s
2	73.97	7.29	0.54	0.00	1.00	0.45	0.00	0.00	0.02	0.28	Hydraulic Lime	1920s
3	3.21	28.13	4.56	0.77	3.99	0.06	0.47	0.06	0.19	9.54	Hydraulic Lime	1920s
4	58.91	11.31	1.01	0.20	1.65	0.46	0.01	0.04	0.28	0.54	Hydraulic Lime	1920s
5	8.55	38.67	4.04	0.13	9.32	1.18	0.09	0.05	0.57	5.24	Hydraulic Lime	1920s
6	14.87	19.72	4.85	0.19	1.95	0.19	0.36	0.37	4.17	3.61	Hydraulic Lime	1920s
7	78.24	5.31	0.33	0.00	1.09	0.01	0.01	0.37	0.27	0.19	Hydraulic Lime	1920s
Ave.	**46.62**	**16.93**	**2.02**	**0.38**	**2.15**	**0.30**	**0.10**	**0.10**	**0.64**	**2.22**	Hydraulic Lime	1920s
StDev.	**30.44**	**10.50**	**1.71**	**0.37**	**2.50**	**0.33**	**0.15**	**0.13**	**1.13**	**2.81**	Hydraulic Lime	1920s

Table 4: SEM-EDS oxide compositional variations of pastes from 1920s mortars encompassing original slag-lime and hydraulic lime mortars and later pointing Portland cement-only mortars, from where lime and silica contents are plotted against paste-CIs (after Eckel 1922) to show systematic trends in lime and silica variations in Figure 56.

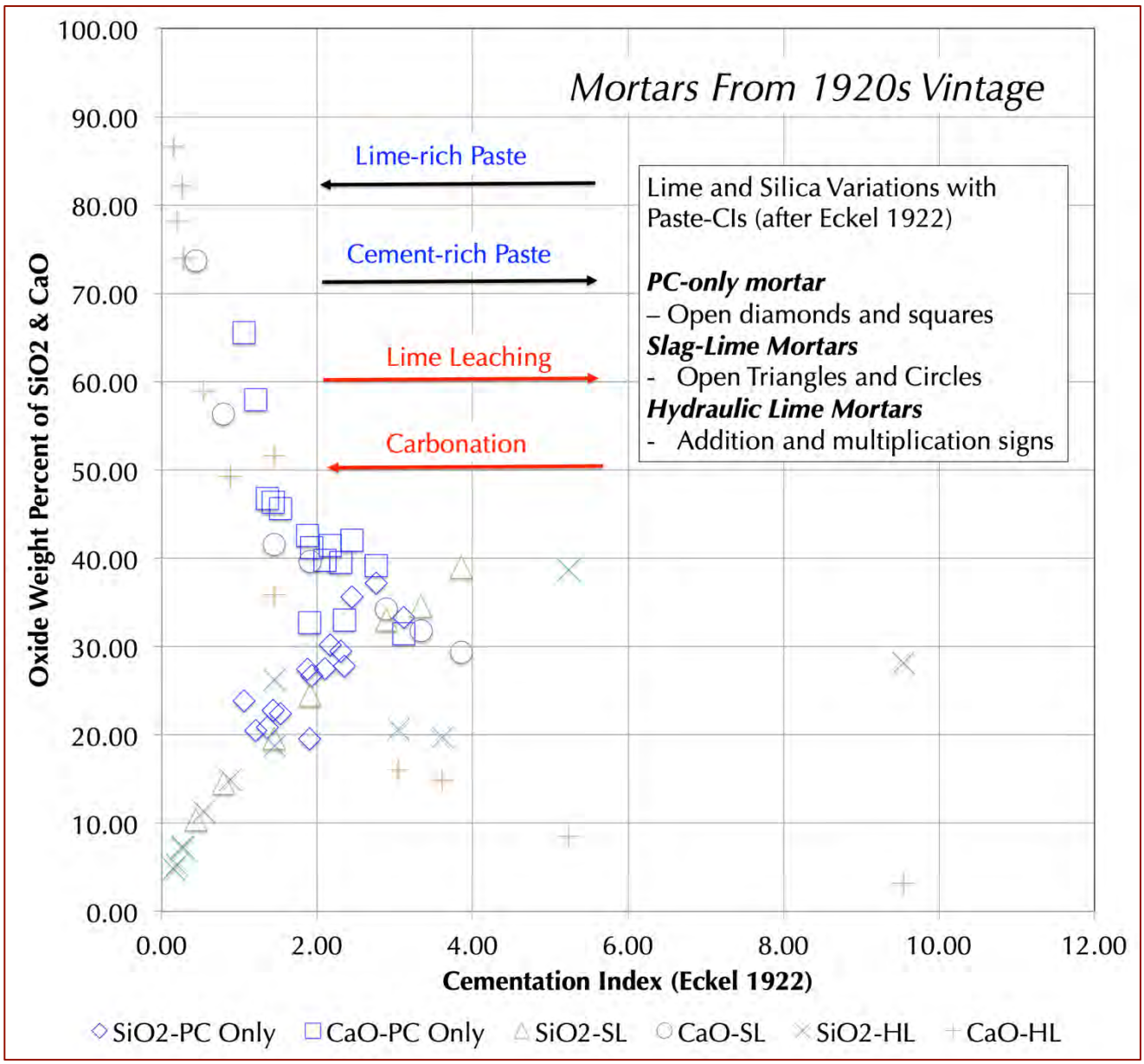

Figure 56: Lime and silica variations in pastes from original slag-lime and hydraulic lime mortars and later pointing Portland cement-only mortars from 1920s vintage showing restricted compositional spread of Portland cement-only mortar due to its consistent composition mostly free of alterations as opposed to large compositional spreads for original slag-lime and hydraulic lime mortars that are attributed to variable degrees of atmospheric carbonation and leaching of lime. Paste-CIs for most plots are results of such alterations, rather than pristine binder compositions (which are usually <1 for lime binders, 1 to 1.5 for cement-lime binders, and 1.5 to 2 for slag-lime binders).

The Portland cement-only pointing mortar showed more restricted composition in the above plot than large compositional spread found for the original slag-lime and hydraulic lime mortars, which is anticipated for alterations of earlier mortars. Table 5 and Figure 57 show results of lime and silica variations with paste-CIs in different 1940s mortars from the upper level of monument.

Probe	CaO	SiO_2	Al_2O_3	Na_2O	MgO	SO_3	K_2O	TiO_2	FeO	Paste CI	Mortar	Circa
1	40.20	18.63	14.11	0.06	2.76	2.62	0.00	0.41	0.38	1.54	PC only	1940s
2	66.00	16.03	3.72	1.23	0.36	0.88	0.14	0.00	0.00	0.74	PC only	1940s
3	42.92	21.36	4.28	0.27	1.15	0.95	0.00	0.02	0.81	1.46	PC only	1940s
4	39.27	23.16	13.56	0.12	2.33	3.39	0.00	0.28	0.78	1.89	PC only	1940s
5	38.54	29.50	5.86	0.22	2.22	1.75	0.02	0.22	0.33	2.14	PC only	1940s
6	68.92	25.55	0.82	0.00	0.08	0.03	0.00	0.19	0.24	1.05	PC only	1940s
7	44.00	36.32	3.30	0.06	1.25	1.12	0.05	0.05	0.85	2.32	PC only	1940s
8	50.89	21.36	7.08	0.06	1.38	0.41	0.03	0.40	0.22	1.28	PC only	1940s
9	44.31	31.57	4.16	0.23	0.24	1.54	0.00	0.09	0.22	2.09	PC only	1940s
1	65.80	7.37	2.48	0.42	0.36	0.76	0.04	0.46	0.26	0.36	PC only	1940s
2	53.23	19.19	7.49	0.00	0.04	1.68	0.87	0.35	1.06	1.18	PC only	1940s
3	61.94	14.10	1.88	0.31	0.00	0.47	0.00	0.03	0.66	0.68	PC only	1940s
4	48.66	31.45	10.45	0.07	0.90	2.60	1.00	0.00	0.29	2.00	PC only	1940s
5	56.63	18.83	6.23	0.00	0.08	1.29	0.48	0.17	0.07	1.05	PC only	1940s
6	46.44	6.22	1.40	0.00	0.00	0.17	0.03	0.05	0.00	0.41	PC only	1940s
7	58.57	15.87	6.08	0.34	0.48	0.81	0.13	0.16	0.83	0.87	PC only	1940s
1	41.33	29.70	5.27	0.42	1.29	1.50	0.01	0.20	0.37	2.07	PC only	1940s
2	44.39	27.41	4.91	0.49	1.07	1.21	0.00	0.00	0.74	1.80	PC only	1940s
3	44.36	25.47	5.80	0.43	1.89	2.06	0.01	0.12	0.26	1.66	PC only	1940s
4	44.57	23.85	7.10	0.32	1.83	1.82	0.04	0.22	0.21	1.59	PC only	1940s
5	40.87	27.46	6.43	0.50	1.23	2.11	0.04	0.26	0.60	1.98	PC only	1940s
6	43.92	25.51	7.20	0.45	1.94	1.56	0.22	0.13	0.19	1.70	PC only	1940s
7	43.72	27.25	5.08	0.77	1.06	1.74	0.00	0.41	0.64	1.82	PC only	1940s
6	37.92	14.44	4.00	0.23	0.58	5.37	0.00	0.01	0.19	1.16	PC only	1940s
7	44.41	27.20	4.98	0.59	1.62	2.12	0.05	0.00	0.08	1.75	PC only	1940s
8	43.52	27.37	4.97	0.79	0.42	1.18	0.00	0.03	0.45	1.87	PC only	1940s
9	30.89	32.06	3.48	0.53	0.53	0.33	0.00	0.21	0.54	2.97	PC only	1940s
10	34.81	25.80	4.21	0.38	0.59	3.72	0.08	0.14	0.49	2.17	PC only	1940s
Ave.	**47.18**	**23.22**	**5.58**	**0.33**	**0.99**	**1.61**	**0.12**	**0.16**	**0.42**	**1.56**	PC only	1940s
StDev.	**9.68**	**7.32**	**3.09**	**0.29**	**0.79**	**1.16**	**0.25**	**0.14**	**0.29**	**0.61**	PC only	1940s
1	50.78	27.10	4.06	0.00	0.04	1.17	0.11	0.43	0.00	1.58	HLCL	1940s
2	71.95	12.32	1.18	0.21	0.00	0.77	0.01	0.00	0.08	0.50	HLCL	1940s
3	83.17	7.01	0.56	0.74	0.28	0.46	0.00	0.45	0.19	0.24	HLCL	1940s
4	28.44	45.30	5.54	0.75	1.06	1.85	0.19	0.10	0.32	4.45	HLCL	1940s
5	82.79	8.61	0.79	0.13	0.00	0.26	0.00	0.10	0.05	0.30	HLCL	1940s
6	80.18	8.06	0.58	0.23	0.10	1.35	0.02	0.36	1.36	0.30	HLCL	1940s
7	88.44	4.36	0.02	0.49	0.20	0.54	0.00	0.00	0.04	0.14	HLCL	1940s
8	77.06	12.11	1.38	0.12	0.00	0.88	0.00	0.36	0.62	0.47	HLCL	1940s
9	83.95	8.05	1.08	0.00	0.00	0.18	0.07	0.00	0.23	0.28	HLCL	1940s
10	72.94	14.41	1.42	0.39	0.42	1.15	0.02	0.21	0.10	0.57	HLCL	1940s
4	79.89	9.67	1.24	0.10	0.00	1.34	0.00	0.04	0.02	0.36	HLCL	1940s
5	56.63	18.56	5.20	1.24	0.57	5.19	0.00	0.55	1.18	1.02	HLCL	1940s
6	73.75	12.41	1.96	0.60	0.01	1.25	0.06	0.17	2.64	0.53	HLCL	1940s
1	36.81	35.64	6.80	0.84	1.15	1.78	0.03	0.59	3.84	2.86	HLCL	1940s
2	56.55	20.61	4.56	0.14	0.04	7.91	0.08	0.00	0.00	1.11	HLCL	1940s
3	30.78	26.44	2.88	0.41	0.07	7.13	0.00	0.00	0.33	2.51	HLCL	1940s
4	35.39	42.63	2.50	0.39	0.69	1.73	0.00	0.32	0.70	3.37	HLCL	1940s
5	39.20	28.77	4.42	0.55	0.93	4.21	0.07	0.25	0.50	2.12	HLCL	1940s
6	33.98	32.42	1.70	0.12	0.10	2.91	0.04	0.14	0.30	2.72	HLCL	1940s
Ave.	**61.19**	**19.71**	**2.52**	**0.39**	**0.30**	**2.21**	**0.04**	**0.21**	**0.66**	**1.34**	HLCL	1940s
StDev.	**21.36**	**12.62**	**1.98**	**0.33**	**0.39**	**2.27**	**0.05**	**0.20**	**1.01**	**1.29**	HLCL	1940s
5	75.45	5.66	0.66	0.00	0.00	1.84	0.00	0.70	0.63	0.23	Slag-Lime	1940s
1	77.41	7.36	1.66	0.18	0.05	0.34	0.17	0.03	4.85	0.33	Slag-Lime	1940s
2	71.14	5.06	2.48	0.57	0.11	0.84	0.02	0.00	0.61	0.24	Slag-Lime	1940s
3	80.85	7.41	1.81	0.26	0.10	0.80	0.16	0.00	0.15	0.28	Slag-Lime	1940s
4	61.52	11.93	2.52	0.61	0.97	0.73	0.13	0.18	0.79	0.58	Slag-Lime	1940s
5	82.26	2.85	0.42	0.11	0.00	1.03	0.06	0.16	0.86	0.11	Slag-Lime	1940s
6	88.63	3.88	0.09	0.03	0.00	0.00	0.02	0.01	0.33	0.13	Slag-Lime	1940s
7	67.00	8.36	2.87	0.71	1.39	0.52	0.09	0.31	1.18	0.40	Slag-Lime	1940s
Ave.	**75.53**	**6.56**	**1.56**	**0.31**	**0.33**	**0.76**	**0.08**	**0.17**	**1.18**	**0.29**	Slag-Lime	1940s
StDev.	**8.76**	**2.86**	**1.06**	**0.28**	**0.54**	**0.54**	**0.07**	**0.24**	**1.52**	**0.15**	Slag-Lime	1940s

Table 5: SEM-EDS oxide compositional variations of pastes from 1940s mortars encompassing original slag-lime and high-lime cement-lime mortars and later Portland cement-only mortars, from where lime and silica contents are plocted against paste-Cis (after Eckel 1922) to show systematic trends in lime and silica variations in Figure 57.

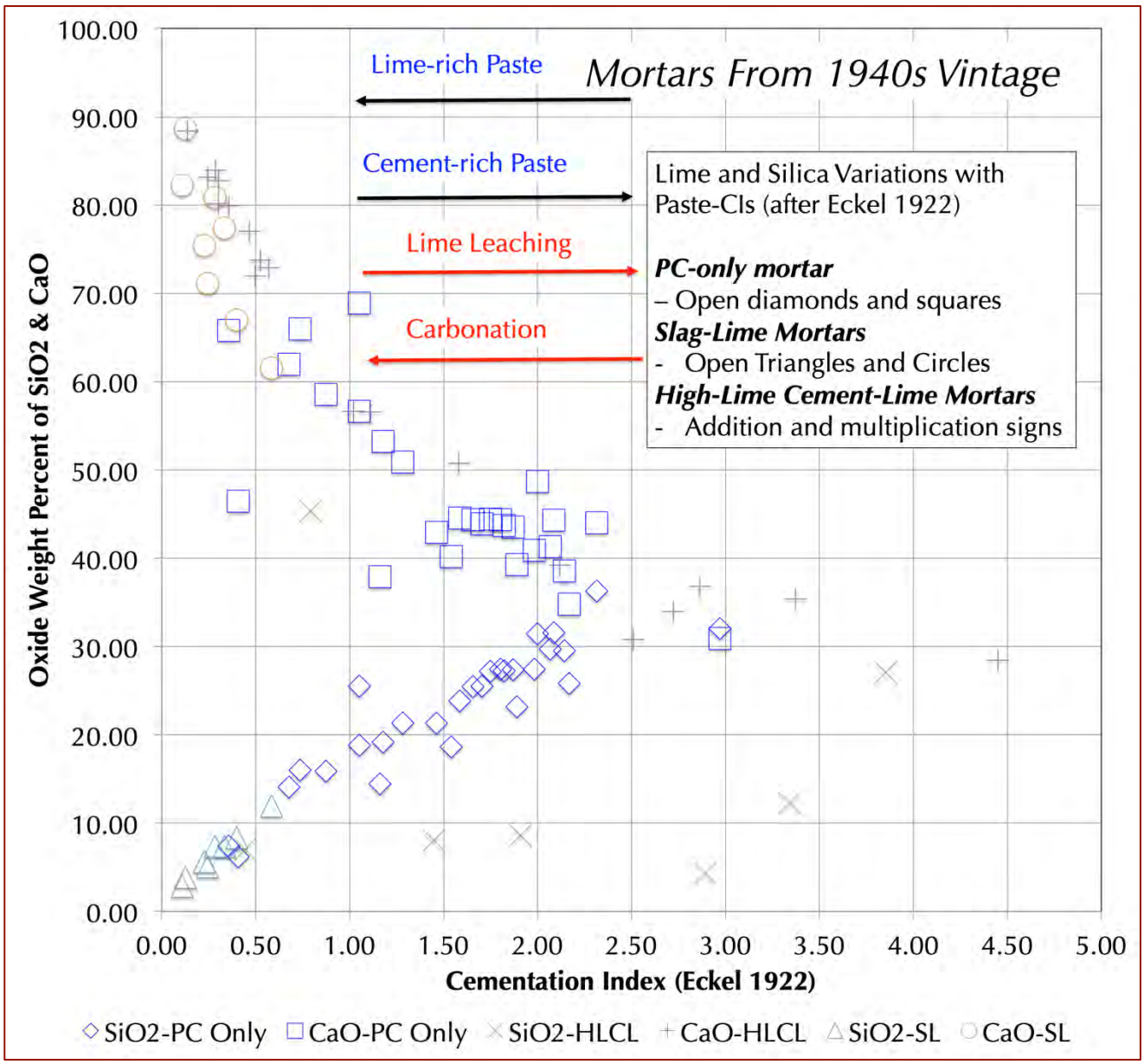

Figure 57: Lime and silica variations in pastes from original slag-lime and high-lime cement-lime mortars and later pointing Portland cement-only mortars from 1940s vintage showing restricted compositional spread of Portland cement-only mortar due to its consistent composition mostly free of alterations as opposed to large compositional spreads for original slag-lime and high-lime cement-lime mortars that are attributed to variable degrees of atmospheric carbonation and leaching of lime. Paste-CIs for most plots are results of such alterations, rather than pristine binder compositions (which are usually <1 for lime binders, 1 to 1.5 for cement-lime binders, and 1.5 to 2 for slag-lime binders).

Lime and Silica versus paste-CI plots from both vintages show a systematic trend of decreasing lime and increasing silica contents in pastes for all mortars with increasing paste-CIs, which is the common consequence of mixing of lime and cement components in modern cement-lime mortars.

Mortar Types From Optical & Electron Microscopy

The following Table summarizes various original mortars that are reveled from optical and scanning electron microscopy and microanalyses, and judged to be present both at the lower and upper levels of the monument as well as the later pointing mortars applied at both levels during a pointing event probably after the reported 1920s and 1940s constructions.

Mortar From Two Different Levels of Monument	Predominant Mortar Type	Additional Mortar Types	Comments
Mortar From Upper Level of Monument (constructed circa 1940s)	• Portland cement mortar containing Portland cement as the only binder and nominal 1-mm size crushed silica sand	• Slag-lime mortar having ground granulated blast furnace slag and lime putty as two separate binder components and nominal 1- mm size crushed silica sand • Hydraulic lime mortar having hydraulic lime (product of calcination of impure limestone) as the sole binder and crushed silica sand	The predominant Portland cement-only mortar appeared to have been applied over slag-lime and hydraulic lime mortars during a later pointing event
Original Mortar From Lower Level (constructed circa 1920s)	• Portland cement mortar containing Portland cement as the only binder and nominal 1-mm size crushed silica sand	• Slag-lime mortar having ground granulated blast furnace slag and lime putty as two separate binder components and nominal 1- mm size crushed silica sand • High-lime cement-lime mortar having lime putty as the sole binder and crushed silica sand	The predominant Portland cement-only mortar appeared to have been applied over slag-lime and high-lime cement-lime mortars during a later pointing event

Table 6: Various mortar types encountered in the 1920s vintage from lower level and 1940s vintage from the upper level of the monument.

Mineralogical Compositions of Mortars From X-Ray Diffraction (XRD)

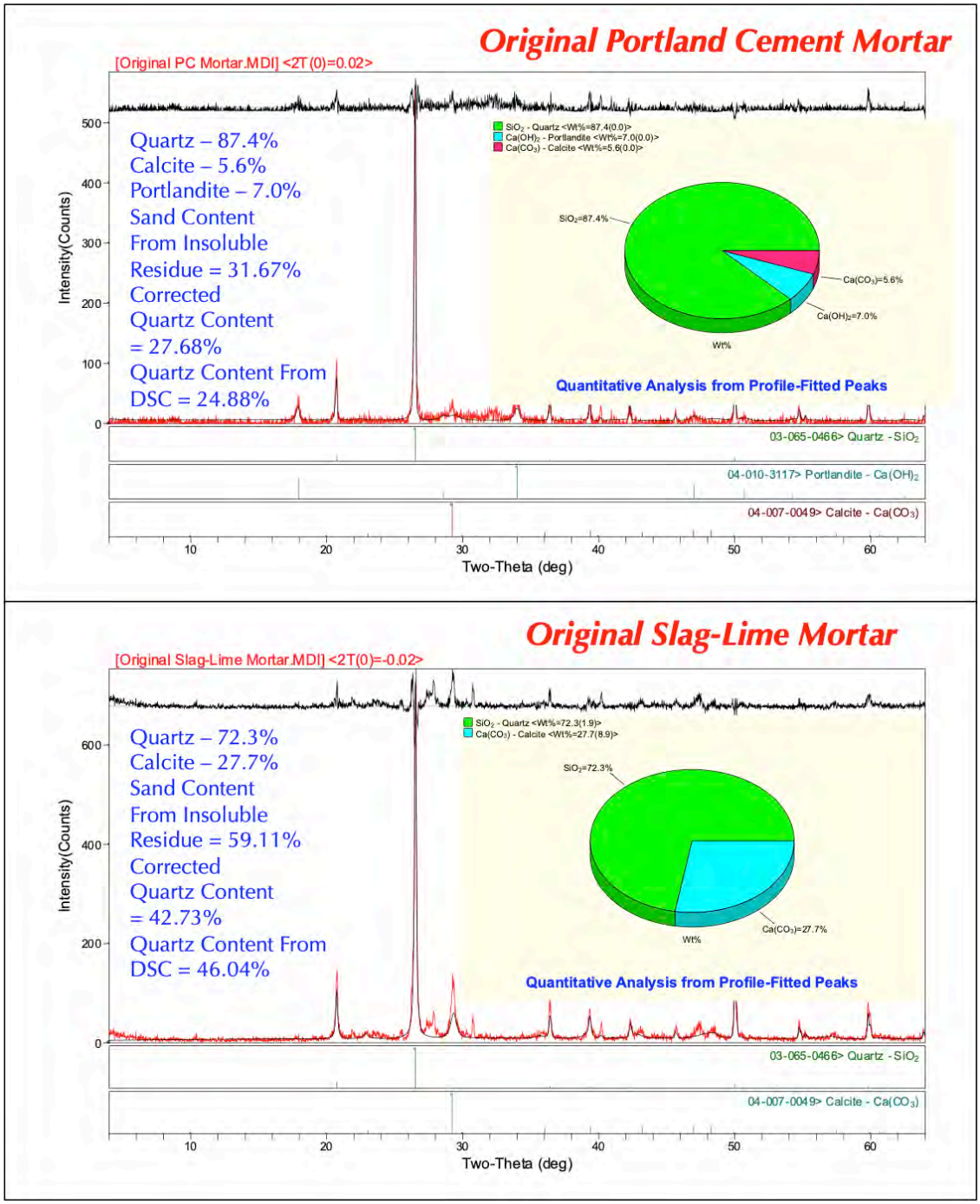

Figure 58: X-ray diffraction patterns of Portland cement-only mortar (top) and slag-lime mortar (bottom) from 1920s construction from the lower level of the belltower showing abundant quartz in both mortar types from use of crushed silica sand in both mortars, portlandite in the PC-only mortar from cement hydration (top), and characteristically different calcite contents from minimum 5.6% calcite in the PC-only mortar (top) to 27.7% calcite in the severely carbonated slag-lime mortar (bottom). Beside quartz, portlandite, and calcite no other phases, especially no potentially deleterious salts were found in the mortars. Quartz contents are corrected from sand contents determined from acid-insoluble residue contents, which show good match to quartz contents determined from DSC (thermal) studies.

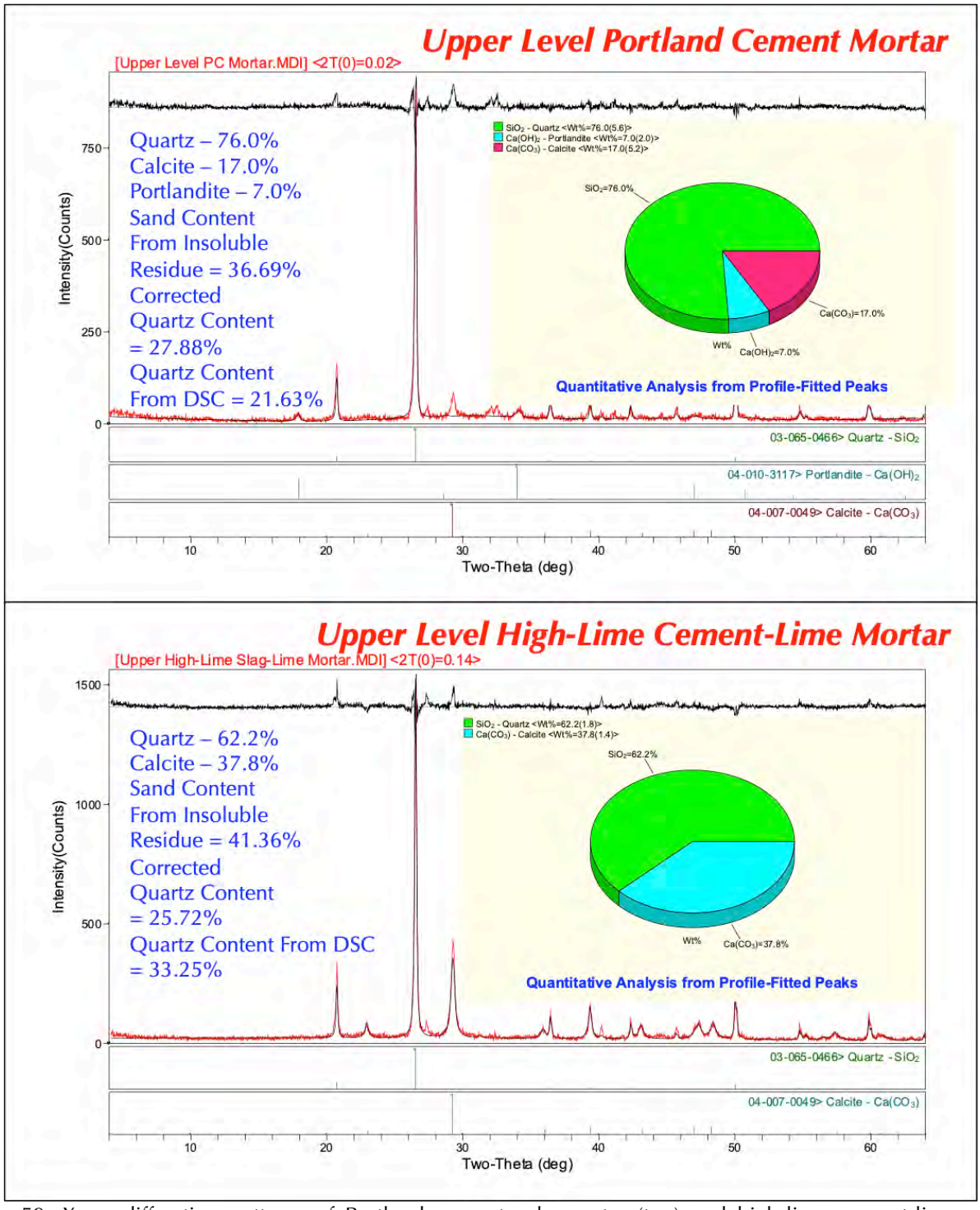

Figure 59: X-ray diffraction patterns of Portland cement-only mortar (top) and high-lime cement-lime mortar (bottom) from 1940s construction from the upper level of the belltower showing abundant quartz in both mortar types from use of crushed silica sand in both mortars, portlandite in the PC-only mortar from cement hydration (top), and characteristically different calcite contents from 17.0% calcite in the PC-only mortar (top) to 37.8% calcite in the severely carbonated high-lime cement-lime mortar (bottom). Beside quartz, portlandite, and calcite no other phases, especially no potentially deleterious salts were found in the mortars. Quartz contents are corrected from sand contents determined from acid-insoluble residue contents, which show good match to quartz contents determined from DSC (thermal) studies.

Chemical Compositions of Mortars From X-Ray Fluorescence (XRF)

Table 7 shows chemical compositions of four representative mortars from original and pointing mortars from 1920s and 19450s construction determined from X-ray fluorescence spectroscopy:

Mortars & Oxides	SiO_2	Al_2O_3	Fe_2O_3	CaO	MgO	Na_2O	K_2O	TiO_2	P_2O_3	SO_3	Balance (LOI)	Total
Original Portland Cement Mortar	47.3	2.6	1.06	32.9	0.936	ND	0.195	0.251	0.154	0.997	13.7	100
Original Slag-Lime Mortar	60.9	5.47	2.08	14.9	1.07	0.706	1.25	0.168	0.185	ND	13.2	100
Upper Level Portland Cement Mortar	47.8	4.07	1.25	28.9	1.2	0.179	0.662	0.237	0.286	0.924	14.5	100
Upper Level High-Lime Cement-Lime Mortar	46.2	3.15	1.6	21.1	0.758	ND	0.784	0.162	0.622	0.791	24.7	100

Table 7: Oxide compositions of mortars determined from X-ray fluorescence spectroscopy. Balance represents loss on ignition parts of mortars.

Chemical Compositions of Mortars From Gravimetry

Table 8 shows loss on ignition and acid-insoluble residue contents of above four mortars:

Mortars	Loss on Ignition (%) at			Acid-Insoluble Residue Content (%)
	110°C	550°C	950°C	
Original Portland Cement Mortar	6.4	11.2	4.5	31.67
Original Slag-Lime Mortar	2.8	4.5	9.1	59.11
Upper Level Portland Cement Mortar	5.8	8.2	6.9	36.69
Upper Level High-Lime Cement-Lime Mortar	8.5	3.2	4.8	41.37

Table 8: Loss on ignition and acid-insoluble residue contents of mortars.

Oxide compositions of Portland cement-only pointing mortars show consistent silica contents from 1920s and 1940s construction (47.3 and 47.8 percent, respectively) which is indicative of use of similar pointing mortar at both upper and lower levels during a later pointing event probably after both upper and lower level constructions were done. Lime contents of both mortars are also similar (32.9 and 28.9 percent, respectively) except a slight variation, which could be from some alterations during service. Silica content of slag-lime mortar from 1920s vintage is highest of four tested, which is consistent with the presence of ground slag, the main source of silica in the mortar after silica sand. Sulfate content in the slag-lime mortar is below the detection limit whereas other three mortars gave detectable sulfates (as SO_3) from 0.79 to 0.99 percent.

The most startling feature came from gravimetry where sand content determined from acid-insoluble residue content (since sand is siliceous, which is insoluble in acid) gave only 31.6 and 36.7 percent sand in the pointing Portland cement-only mortars from both constructions, which are noticeably lower than sand contents found in the original mortars, e.g., 59.1 percent in slag-lime mortar from 1920s construction and 41.3 percent in high-lime cement-lime mortar from 1940s construction. Low sand content in the pointing mortar makes it even more unsuitable to use, especially since the binder fraction lacks lime.

Thermal Analyses

Milligrams of mortars from 1920s and 1940s vintages were subjected to controlled heating experiments in a Mettler-Toledo TGA/DSC simultaneous thermogravimetric and differential scanning calorimetry unit to detect the presence of various hydrous, sulfate, and carbonate phases in these mortars and their relative abundance. Figures 61 and 62 show TGA (in bold black), DSC (in dotted red), and DTG (in dashed blue) curves of mortars showing losses in weight due to decompositions (loss of water and carbon dioxide) of various phases during controlled heating in a Mettler-Toledo's simultaneous TGA/DSC 1 unit from 30ºC to 1000ºC in a ceramic crucible (alumina 70µl, no lid) at a heating rate of 10ºC/min in a nitrogen purge at a rate of 75 mL/min. Dehydration and decarbonation reactions are marked as endothermic peaks in the DTG curve, whereas alpha to beta-form polymorphic transition of quartz is marked at the characteristic temperature of 573 ºC in the DSC curve.

In the DTG curve, successive losses in weights are detected at (i) > 200ºC from loss of free and combined water, (ii) around 450 to 500ºC from dehydroxylation of portlandite phase in Portland cement mortars, and (iii) around 700 to 800ºC from decarbonation of calcite from calcite fines and fine-grained calcite in carbonated pastes. DSC curve shows polymorphic transition from alpha to beta form of quartz around 575ºC from silica (quartz) sand.

Figure 61 shows characteristic differences in TGA-DTG curves of Portland cement only mortar (top) and slag-lime mortar (bottom) from the 1920s construction from the lower level of the tower where loss of hydrate water from dehydration of calcium silicate hydrate phase of cement hydration is noticeably higher in the PC-only mortar as anticipated resulting in large endotherm around 110ºC compared to slag-lime mortar. Quartz content is noticeably higher in the slag-lime mortar than in PC-only mortar. Calcite content from decarbonation endotherm around 750ºC is noticeably higher for the slag-lime mortar. All these results are consistent with the determined compositions of mortars from optical and electron microscopy. PC-mortar shows three major endotherms from loss of combined water at low temperature to dehydroxylation of portlandite at intermediate temperature to calcite decarbonation at high temperature ends. By contrast, slag-lime mortar shows only low and high-T endotherms and lack of endotherm from calcium hydroxide decomposition due to lack of Portland cement.

Figure 62 shows characteristic differences in TGA-DTG curves of Portland cement-only mortar (top) and high-lime cement-lime mortar (bottom) from the 1940s construction where loss of combined water from dehydration of calcium silicate hydrate phase of cement hydration is noticeably higher for the PC-only mortar, as expected, resulting in large endotherm around 110ºC compared to high-lime cement-lime mortar. Quartz content is

noticeably higher in the high-lime cement-lime mortar than in PC-only mortar. Calcite content from decarbonation endotherm around 750ºC is noticeably higher for the high-lime cement-lime mortar. All these results are consistent with the determined compositions of mortars from optical and electron microscopy. PC-mortar shows three major endotherms from loss of combined water at low temperature to dehydroxylation of portlandite at intermediate temperature to calcite decarbonation at high temperature ends (similar to PC mortar from the 1920s construction) whereas high-lime cement-lime mortar shows two major endotherms – a low temperature one from dehydration of combined water and a high-temperature endotherm from decarbonation of carbonated paste (which is also similar to the slag-lime mortar in the 1920s construction).

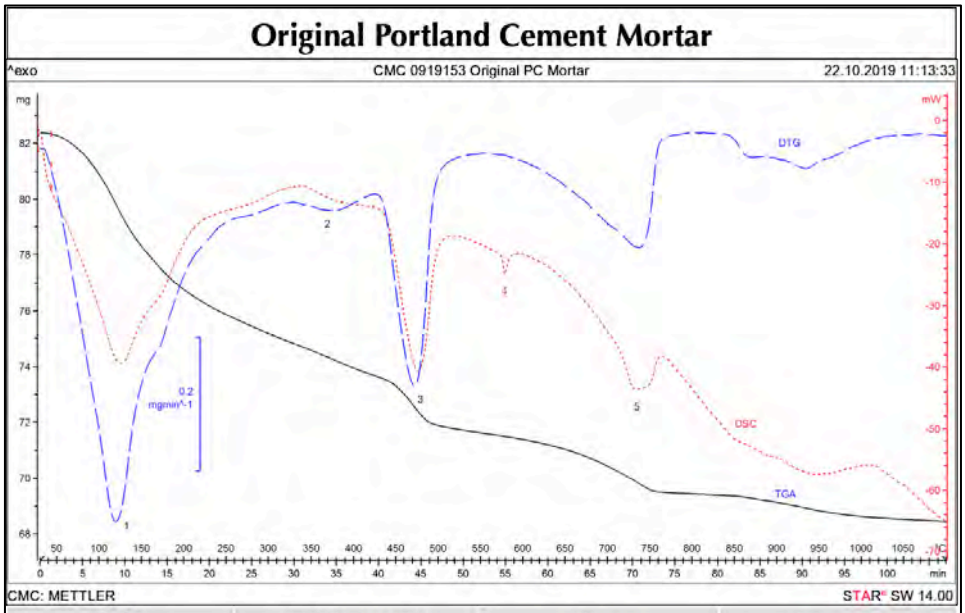

Peak#	Peak Position (°C)	Phase	Amount (%)
1 (DTG)	110.89	Free & Combined Water	5.73
2 (DTG)	378.29	Sulfate	0.96
3 (DTG)	470.12	Portlandite	7.31
4 (DSC)	576.51	Quartz	24.88
5 (DTG)	737.90	Calcite	1.94

Peak#	Peak Position (°C)	Phase	Amount (%)
1 (DTG)	107.15	Free & Combined Water	1.75
2 (DSC)	576.34	Quartz	46.04
3 (DTG)	777.06	Calcite	16.04

Figure 60: TGA (bold black), DSC (dotted red), and DTG (dashed blue) curves of mortars from 1920s construction showing losses in weight due to various decompositions (loss of water and carbon dioxide) during controlled heating in a Mettler-Toledo's simultaneous TGA/DSC 1 unit from 30ºC to 1000ºC in a ceramic crucible (alumina 70µl, no lid) at a heating rate of 10ºC/min in a nitrogen purge at a rate of 75 mL/min.

In the TGA curve, successive losses in

weights occurred from loss of free water, hydrate water, dehydroxylation of portlandite, and decarbonation of finely crystalline calcite in carbonated paste. Dehydration and decarbonation reactions are marked as endothermic peaks in the superposed DSC and DTG curves. DSC curve shows polymorphic transition from alpha to beta form of quartz around 575ºC from silica (quartz) sand.

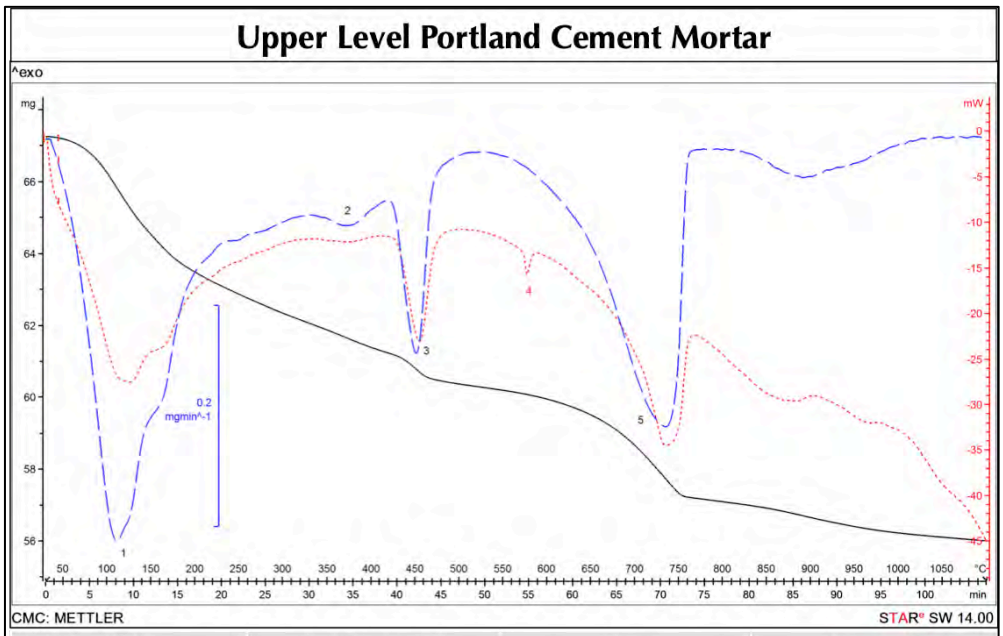

Peak#	Peak Position (°C)	Phase	Amount (%)
1 (DTG)	104.24	Free & Combined Water	5.12
2 (DTG)	375.32	Sulfate	0.85
3 (DTG)	450.53	Portlandite	3.47
4 (DSC)	576.09	Quartz	21.63
5 (DTG)	733.40	Calcite	7.34

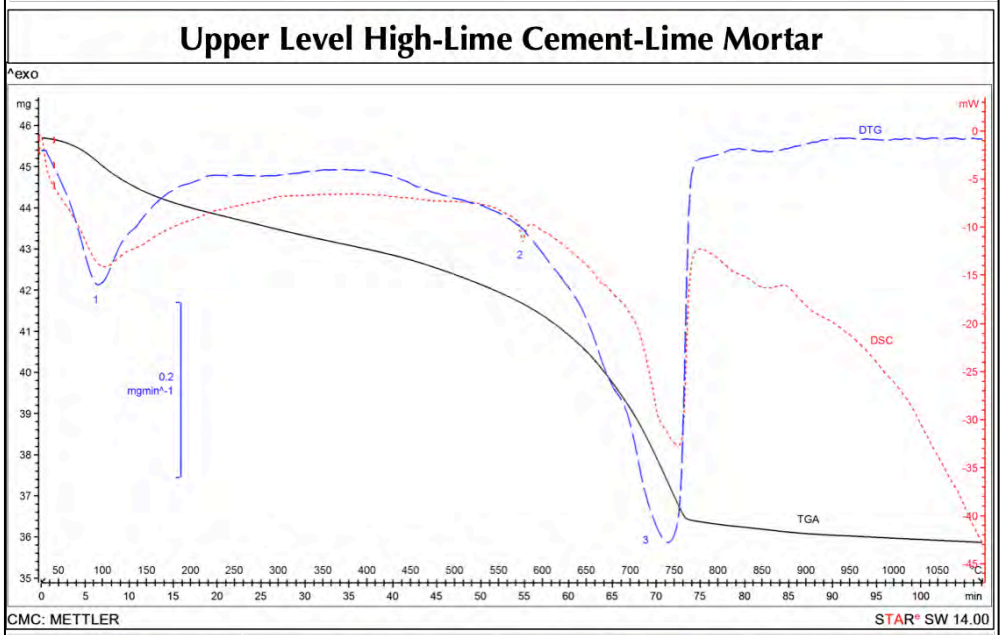

Peak#	Peak Position (°C)	Phase	Amount (%)
1 (DTG)	89.68	Free & Combined Water	2.60
2 (DSC)	576.28	Quartz	33.25
3 (DTG)	741.97	Calcite	19.55

Figure 61: TGA (bold black), DSC (dotted red), and DTG (dashed blue) curves of mortars from 1940s construction showing losses in weight due to various decompositions (loss of water and carbon dioxide) during controlled heating in a Mettler-Toledo's simultaneous TGA/DSC 1 unit from 30ºC to 1000ºC in a ceramic crucible (alumina 70µl, no lid) at a heating rate of 10ºC/min in a nitrogen purge at a rate of 75 mL/min.

In the TGA curve, successive losses in weights occurred from loss of free water, hydrate water, dehydroxylation of portlandite, and decarbonation of finely crystalline calcite in carbonated paste. Dehydration and decarbonation reactions are marked as endothermic peaks in the superposed DSC and DTG curves. DSC curve shows polymorphic transition from alpha to beta form of quartz around 575ºC from silica (quartz) sand.

Ion Chromatography

Original Portland Cement Mortar

Fluoride	0.001 wt%
Chloride	0.019 wt%
Nitrite	0.008 wt%
Bromide	invalid wt%
Nitrate	0.265 wt%
Phosphate	0.001 wt%
Sulphate	0.235 wt%

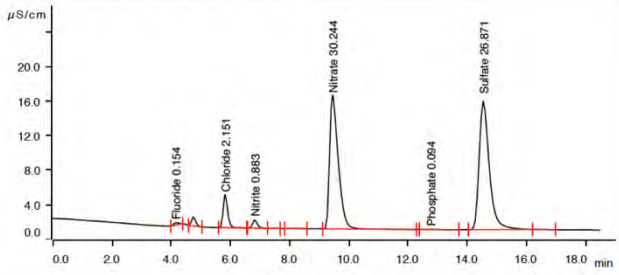

Weight percent concentration of anions in Mortar = [ppm concentration from IC times Dilution factor (1 if entire filtrate is used without further dilution) times Original Filtrate Volume] divided by [Sample Weight] times 10,000 (ppm to weight % conversion)]

Original Slag – Lime Mortar

Fluoride	0.006 wt%
Chloride	0.008 wt%
Nitrite	0.000 wt%
Bromide	0.000 wt%
Nitrate	0.010 wt%
Phosphate	0.001 wt%
Sulphate	0.044 wt%

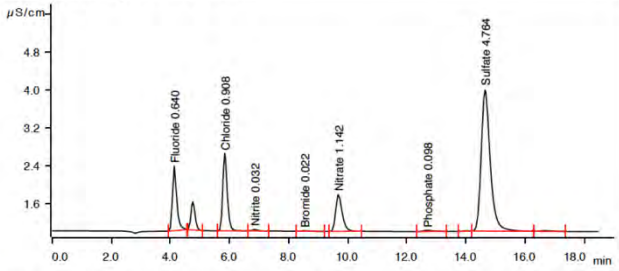

Weight percent concentration of anions in Mortar = [ppm concentration from IC times Dilution factor (1 if entire filtrate is used without further dilution) times Original Filtrate Volume] divided by [Sample Weight] times 10,000 (ppm to weight % conversion)]

Upper Level Portland Cement Mortar

Fluoride	0.002 wt%
Chloride	0.038 wt%
Nitrite	0.032 wt%
Bromide	0.000 wt%
Nitrate	0.379 wt%
Phosphate	0.000 wt%
Sulphate	0.147 wt%

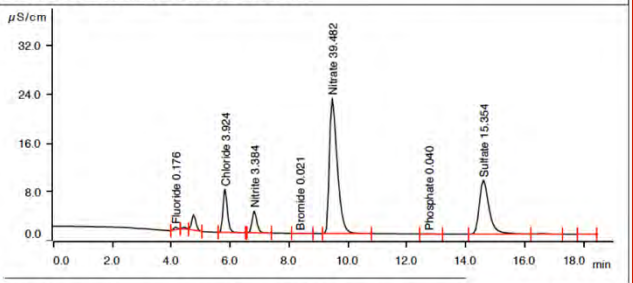

Weight percent concentration of anions in Mortar = [ppm concentration from IC times Dilution factor (1 if entire filtrate is used without further dilution) times Original Filtrate Volume] divided by [Sample Weight] times 10,000 (ppm to weight % conversion)]

Upper Level High-Lime Cement-Lime Mortar

Fluoride	0.073 wt%
Chloride	0.038 wt%
Nitrite	0.001 wt%
Bromide	0.000 wt%
Nitrate	0.107 wt%
Phosphate	0.006 wt%
Sulphate	0.729 wt%

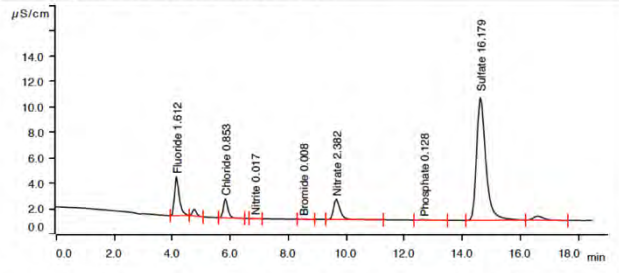

Weight percent concentration of anions in Mortar = [ppm concentration from IC times Dilution factor (1 if entire filtrate is used without further dilution) times Original Filtrate Volume] divided by [Sample Weight] times 10,000 (ppm to weight % conversion)]

Figure 62: Ion chromatograms of water-soluble anions in mortars after digesting representative portions of pulverized mortars (about a gram) in deionized water for 30 minutes at a temperature below boiling, followed by continued digestion in water at the ambient laboratory condition for 24 hours. The digested solution was filtered under vacuum through 2.5-micron followed by 0.2-micron filter papers. The final filtrates diluted to 100 ml were analyzed by ion chromatography.

Results showed:

- High sulfate in PC-only mortars from lower (0.235%) and upper (0.147%) levels, highest sulfate (0.729%) in high-lime cement-lime mortar from the upper level;

- Noticeable chloride from the environment, from 0.019 to 0.038%;

- A spike in nitrate level (in PC-only mortars from the lower (0.264%) and upper (0.379%) level compared to nitrate levels in older mortars, e.g., 0.01% in slag-lime from lower level, and 0.1% in high-lime cement-lime mortar from upper level.

- Negligible fluoride, bromide, nitrite, and phosphate in all mortars.

Mix Proportions

Optical microscopy, SEM-EDS studies, and results of chemical analyses from bulk lime and silica contents of mortars to sand contents from acid-insoluble residue contents and losses on ignition have provided mix proportions of Portland cement-only pointing mortars that were requested. Due to various levels of alterations from leaching to severe carbonation of pastes and unknown composition of slag used in the slag-lime mortars mix proportions of early slag-lime or hydraulic lime mortars are difficult.

Mortars' Compositions & Mix Proportions	PC-only mortar from 1920s Construction	PC-only mortar from 1940s Construction
Acid-Insoluble Residue (%)	31.67	36.69
Sand Content (%) from acid-insoluble residue content, entire sand is siliceous sand)	31.67	36.69
Loss on Ignition: From 0°C to 110°C (Free Water) (%)	6.4	5.8
Loss on Ignition: From 110-550°C (Combined Water)(%)	11.2	8.2
Loss on Ignition: From 550-950°C (Carbonation, CO_2)(%)	4.5	6.9
Bulk silica content of mortar from XRF	47.3	47.8
Bulk lime content of mortar from XRF	32.9	28.9
Portland Cement Content (%) = 100 – [Free water + Combined water + Sand]	50.73	49.31
Portland Cement Content (%) from lime content of mortar from XRF assuming 63.5% lime in cement	51.81	45.52
Bulk Density of Portland Cement, (lbs./ft.^{3})	94	94
Bulk Density of Sand, (lbs./ft.^{3})	80	80
Portland Cement Volume	50.73/94 = 0.539	49.31/94 = 0.524
Sand Volume	31.67/80 = 0.395	36.69/80 = 0.458
Relative Volumes of Masonry Cement: Sand	1 : 0.73	1 : 0.87
Masonry Cement to Sand, by volume	**1-part Portland cement to $^3/_4$ -part sand**	**1-part Portland cement to $^3/_4$ to 1-part sand**

Table 9: Calculations of mix proportions of cement-only pointing mortars from the lower and upper levels.

Since Portland cement is the sole binder in the Portland cement-only pointing mortars and lack any lime, Portland cement contents are determined: (a) either from bulk XRF-lime contents of mortars and assuming 63.5% lime in Portland cement, or (b) from subtracting free and combined water contents from losses on ignitions at 110°C and 550°C, respectively and sand contents from acid-insoluble residue contents from 100. Cement contents from both methods are close within and between two pointing mortars from lower (1920s) and upper (1940s) levels, which are around 50 percent. These values are found to be noticeably higher than the sand contents calculated from acid insoluble residue contents since the sand in all mortar is found to be siliceous (quartz-based), which do not dissolve in acid. Assuming a bulk density of a Portland cement as 94 lbs./ft^3, and sand as 80 lbs./ft^3, cement and sand volumes are then determined, which are found to be around 1-part cement to less than 1-part sand, by volume unlike 1-part cementitious components to 2$^1/_4$ to 3-part sand commonly found in masonry mortars.

DISCUSSIONS

Mortar Types

Visual examinations of mortar fragments from both levels showed the presence of multiple mortar types, which are best evident on freshly fractured or sectioned surfaces of fragments, e.g., (1) a dense, hard, dark gray predominantly non-carbonated mortar, which constituents the most prevalent mortar type at both levels, (2) a beige moderately soft, porous, severely carbonated mortar present in the interior of a few dark gray mortars from the lower level (1920s vintage), (3) a medium gray, moderately hard, variably carbonated mortar present in the inside of a few dark gray mortar fragments from both levels from 1920s and 1940s vintages, and (4) an off-white moderately soft, porous, carbonated mortar present mostly as separate fragments found from the upper level from 1940s vintage. Of all these, the brown mortar from the lower level is subsequently determined to be a *hydraulic lime mortar*, the medium gray mortar behind the dark gray ones from both levels is found to be a *lime-based mortar mixed with fine, angular, shard like glassy particles of ground granulated blast furnace sla*g, the off-white mortar from the upper level is found to be a *lime-based mortar having higher proportion of lime than Portland cemen*t, and finally the ubiquitous dense, hard, dark gray mortar present either at the exterior sides of other mortars in a few fragments, or mostly as separate fragments from both levels are found to be *Portland cement-only mortars*, which were probably installed during later pointing events at both lower and upper levels. Sands used in all these earlier and later pointing mortars are silica-based containing major amount of crushed (manufactured) quartz sand having nominal maximum sizes of 1 mm. All mortars examined are non-air-entrained.

Unusual Pointing Mortars

Optical microscopical examinations of mortars showed startling differences in microstructures between the Portland cement-only pointing mortars and lime-based earlier mortars from both lower (1920s vintage) and upper (1940s vintage) levels of the monument. The Portland cement-only pointing mortars are found to be similar in compositions and microstructures from both levels, which is indicative of their probable applications at both levels at later periods after the initial constructions were finished. The Portland cement-only mortars are made using crushed silica sand of 1 mm or less in size where sand particles are quartz-based, angular, dense, hard, well-graded, well-distributed and present in sound conditions without any potentially deleterious alkali-aggregate reactions. Pastes in Portland cement-only mortars are dense, mostly non-carbonated in the interiors except a thin layer of carbonation and occasional leaching of lime at the exposed faces in the fragments and contain abundant residual Portland cement particles where cement is found to be finely ground as opposed to coarsely ground Portland cement, which are more common in the early 20th century cements. Microstructures of dense non-carbonated interior pastes of Portland cement mortars showed many features, e.g., (i) ubiquitous dense calcium silicate hydrate products of cement hydration that are optically semi-isotropic, (ii) fine, lath-shaped birefringent crystals of calcium hydroxide component of cement hydration, (iii) abundant residual Portland cement particles

having characteristic microstructures of residual calcium silicate (subhedral alite and anhedral belite) particles of Portland cement with interstitial dark brown ferrite phases, thin hydration rims around residual alite grains due to restricted spaces during hydration, etc., (iv) fine hairline shrinkage microcracks in paste, and (v) occasional secondary ettringite precipitates in air voids and microcracks due to the presence of moisture in the paste during service where sulfates released from cement hydration products have precipitated as secondary ettringite. Fine grain-size of Portland cement, similar compositions and microstructures of Portland cement-only mortars from both 1920s and 1940s vintages, and its presence at the exposed ends with other lime-based mortars behind in some fragments are all indicative of their application in later pointing events. The main characteristic microstructure of Portland cement-only pointing mortars is the presence of network of fine hairline shrinkage microcracks that are best revealed in SEM-EDS studies, which are not found in the earlier lime-based mortars from both levels. Fibrous acicular secondary ettringite, secondary calcium carbonate precipitates, and occasional fibrous thaumasite precipitates in microcracks are found in some fragments of Portland cement-only mortars mostly at the exposed edges of the fragments. These secondary precipitates at the exposed edges are testaments of the presence of moisture in the mortars for prolonged periods. None of these secondary deposits, however, have affected the interior dense, hard non-carbonated pastes in these mortars. Extensive shrinkage microcracking in pastes, however, have affected the long-term performance and durability of these Portland cement-only mortars, which are found to be due to two reasons – (i) use of Portland cement only without any lime, which has facilitated development of shrinkage microcracks from loss of moisture from the paste, and (ii) use of more cement than sand in Portland cement-only pointing mortars, which are calculated from mix proportions to have 1-part cement to less than 1-part sand by volume, which is not only unusual (common cement-to-sand proportions are 1 to $2^1/_4$ to 3) but are also prone to extensive shrinkage microcracking, high stiffness, unworkability, and unaccommodative to masonry movements, etc.

SEM-EDS studies of Portland cement-only pointing mortars showed typical calcium silicate hydrate compositions of pastes having cementation indices (CI) of paste (after Eckel 1922) ranging between 1 and 2 due to variable degrees of atmospheric carbonation and lime leaching mostly at the exposed edges. Other than extensive microcracking in pastes no other distress is found in these pointing mortars. XRF analyses showed similar silica and lime contents in pointing mortars from both levels, e.g., 47.3% SiO_2 from lower and 47.8% from upper level, and 32.9% CaO from lower and 28.9% from upper level. Sand contents are determined from acid-insoluble residue contents (since sand is quartz-based, which is insoluble in acid), which are also similar 31.7% from lower and 36.7% from upper level. Quartz content in pointing mortar is 27.7% from XRD and 24.8% from DSC for lower level, and 27.8% from XRD and 21.6% from DSC for upper level. Such compositional similarities of Portland cement-only pointing mortars from both levels indicate use of same mortar mix for applications at both levels of monument.

Original Mortars from 1920s and 1940s Construction

Contrary to the Portland cement-only pointing mortars, earlier lime-based mortars detected from both levels of monument are judged more appropriate for such applications. Earlier mortars detected in the fragments received are *hydraulic lime mortar* and *slag-lime mortar* from the lower level from 1920s vintage, and, *slag-lime mortar* and *high-lime Portland cement-lime mortar* from the upper level from 1940s applications. All these lime-based mortars were prepared by mixing lime putty, ground slag or Portland cement, and crushed quartz-based silica sand. Sand in these lime-based mortars are similar to the quartz-based crushed sand found in the pointing mortars indicating similar sand source used for all applications. Due to the presence of lime in these earlier mortars along with atmospheric carbon dioxide and moisture during service, extensive carbonation and occasional leaching of lime is found in optical microscopical and SEM-EDS studies of these early mortars, which are not unusual. Leaching of lime from the edges of these mortars have enriched the altered zones in silica, usually occurring as silica and alumina gel and appear dark (optically isotropic) in crossed polarized light modes in a petrographic microscope, leached zones are situated outside the carbonated zones.

Of all the earlier mortars, probably the slag-lime mortar is most appropriate, which showed best choice to be used with granite masonry as opposed to hydraulic lime or high-lime cement-lime mortars. Fine, angular, shard-like glassy particles of ground granulated blast furnace slag in the fine-grained, variably porous and severely carbonated pastes of slag-lime mortars created a microstructure and microchemistry similar to a modern-day Portland cement-lime mortar where hydration of slag particles has formed calcium silicate hydrate (similar to cement hydration) and subsequent atmospheric carbonation of slag hydration products along with carbonation of lime has provided the long-term durability of this mortar. Hydraulic lime mortar from the lower level showed variable degrees of carbonation and lime leaching resulting in porous fine-grained severely carbonated to denser carbonated pastes later having a few relict carbonated residues of hydraulic phases of original binder, and crushed silica sand. Off-white high-lime Portland cement-lime mortar from the upper level showed variably carbonated pastes having residual Portland cement particles where cement grains are more finely ground than cements manufactured during early 20th century.

Following optical microscopy and SEM-EDS of all lime-based mortars detected, a representative slag-lime mortar from the lower level and a high-lime cement-lime mortar from the upper level were selected for wet chemical analyses, XRD, XRF, TGA-DTG-DSC studies. Sand contents (from acid-insoluble residue contents) are 59.1% for slag-lime and 41.4% for high-lime cement-lime mortars, which are noticeably higher than sand contents (31.7 to 36.7%) found for Portland cement-only pointing mortars. Bulk silica and lime contents from XRF are 60.9% silica and 14.9% lime for slag-lime mortar and 46.2% silica and 21.1% lime for high-lime cement-lime mortar. Quartz contents are 42.7% from XRD and 46% from DSC for slag-lime mortar, and 25.7% from XRD and 33.2% from DSC for high-lime cement-lime mortar. Such high quartz contents in lime mortars (as opposed to ~ 21 to 27% quartz in the pointing mortars) are consistent with higher sand contents in these mortars compared to pointing mortars. Degree of carbonation and calcite contents from thermal decomposition of mortars at 700-800°C in DTG studies showed 16.1% calcite in slag-lime and 19.5% calcite in high-lime cement-lime as opposed to only 1.9% calcite in Portland cement-only pointing mortar from the lower level and 7.3% calcite in pointing mortar from upper level (which showed more atmospheric carbonation than pointing mortar from lower level).

REFERENCES

ASTM C 10, "Standard Specification for Natural Cement," In Annual Book of ASTM Standards, Section Four Construction, Vol. 04.01 Cement; Lime; Gypsum; ASTM Committee C01 on Cement, 2017.

ASTM C 91, "Standard Specification for Masonry Cement," In Annual Book of ASTM Standards, Section Four Construction, Vol. 04.01 Cement; Lime; Gypsum; ASTM Committee C01 on Cement, 2017.

ASTM C 144, "Standard Specification for Aggregate for Masonry Mortar," In Annual Book of ASTM Standards, Section Four Construction, Vol. 04.05 Chemical-Resistant Nonmetallic Materials; Vitrified Clay Pipe; Concrete Pipe; Fiber-Reinforced Cement Products; Mortars or mortars and Grouts; Masonry; Precast Concrete; ASTM Committee C12 on Mortars or mortars for Unit Masonry, 2017.

ASTM C 1324, "Standard Test Method for Examination and Analysis of Hardened Masonry Mortar," In Annual Book of ASTM Standards, Section Four Construction, Vol. 04.05 Chemical-Resistant Nonmetallic Materials; Vitrified Clay Pipe; Concrete Pipe; Fiber-Reinforced Cement Products; Mortars or mortars and Grouts; Masonry; Precast Concrete; ASTM Committee C12 on Mortars or mortars for Unit Masonry, 2017.

ASTM C 270, "Standard Specification for Mortar for Unit Masonry," In Annual Book of ASTM Standards, Section Four Construction, Vol. 04.05 Chemical-Resistant Nonmetallic Materials; Vitrified Clay Pipe; Concrete Pipe; Fiber-Reinforced Cement Products; Mortars or mortars and Grouts; Masonry; Precast Concrete; ASTM Committee C12 on Mortars or mortars and Grouts for Unit Masonry, 2017.

ASTM C 1713, "Standard Specification for Mortars or mortars for the Repair of Historic Masonry," In Annual Book of ASTM Standards, Section Four Construction, Vol. 04.05 Chemical-Resistant Nonmetallic Materials; Vitrified Clay Pipe; Concrete Pipe; Fiber-Reinforced Cement Products; Mortars or mortars and Grouts; Masonry; Precast Concrete; ASTM Committee C12 on Mortars or mortars and Grouts for Unit Masonry, 2017.

ASTM C 51, "Standard Terminology Relating to Lime and Limestone (as used by the Industry)'" In Annual Book of ASTM Standards, Section Four Construction, Vol. 04.01 Cement; Lime; Gypsum; ASTM Committee C07 on Lime, 2017.

ASTM C 856, "Standard Practice for Petrographic Examination of Hardened Concrete," In Annual Book of ASTM Standards, Section Four Construction, Vol. 04.02; ASTM Subcommittee C 9.65, 2017.

ASTM C 1723, "Standard Guide for Examination of Hardened Concrete Using Scanning Electron Microscopy," In Annual Book of ASTM Standards, Section Four Construction, Vol. 04.02; ASTM Subcommittee C 9.65, 2017.

ASTM C 1329, "Standard Specification for Mortar Cement," In Annual Book of ASTM Standards, Section Four Construction, Vol. 04.01; ASTM Subcommittee C01.11, 2016.

ASTM C 150, "Standard Specification for Portland Cement," In Annual Book of ASTM Standards, Section Four Construction, Vol. 04.01; ASTM Subcommittee C01.10, 2018.

ASTM C 1489, "Standard Specification for Lime Putty for Structural Purposes," In Annual Book of ASTM Standards, Section Four Construction, Vol. 04.01; ASTM Subcommittee C07.02, 2015.

ASTM C 207, "Standard Specification for Hydrated Lime for Masonry Purposes," In Annual Book of ASTM Standards, Section Four Construction, Vol. 04.01; ASTM Subcommittee C07.02, 2011.

ASTM C 979 "Standard Specification for Pigments for Integrally Colored Concrete,' In Annual Book of ASTM Standards, Section Four Construction, Vol. 04.01; ASTM Subcommittee C07.02, 2011.

Bartos, P. Groot, C., and Hughes, J.J. (eds.), "Historic Mortars or mortars: Characteristics and Tests", Proceedings PRO12, RILEM Publications, France, 2000.

Boynton, R., *Chemistry and Technology of Lime and Limestone, 2nd edition*, John Wiley & Sons, Inc. 1980.

Brosnan, Denis, A., Characterization of Rosendale Mortars or mortars For Fort Sumter National Monument and Degradation of Mortars or mortars by Sea Water and Frost Action, Final Report, April 19, 2012.

Callebaut, K., Elsen, J., Van Balen, K., and Viaene, W., "Nineteenth century hydraulic restoration mortars or mortars in the Saint Michael's Church (Leuven, Belgium) Natural hydraulic lime or cement?" Cement and Concrete Research, V 31, pp 397-403, 2001.

Callebaut, K., Elsen, J., Van Balen, K., and Viaene, W., Historical and scientific study of hydraulic mortars or mortars from the 19th century. In International RILEM workshop on historic mortars or mortars: Characterization and Tests; Paisley, Scotland, 12th to 14th May 1999, Edited by Barton, P., Groot, C., and Hughes, J.J., Cachan, France, RILEM Publications, 2000.

Charloa, A.E., "Mortar analysis: A comparison of European procedures." US/ICOMOS Scientific Journal: Historic Mortars or mortars & Acidic Deposition on Stone, 3 (1), pp. 2-5, 2001.

Charola, A.E., and Lazzarin, L., Deterioration of Brick Masonry Caused by Acid Rain, ACS Symposium Series, Vol. 318, pp. 250-258, 2009.

Chiari, G., Torraca, G., and Santarelli, M.L., "Recommendations for Systematic Instrumental Analysis of Ancient Mortars or mortars: The Italian Experience", *Standards for Preservation and Rehabilitation*, ASTM STP 1258, S.J. Kelley, ed., American Society for Testing and Materials, pp. 275-284, 1996.

Doebley, C.E., and Spitzer, D., "Guidelines and Standards for Testing Historic Mortars or mortars", *Standards for Preservation and Rehabilitation*, ASTM STP 1258, S.J. Kelley, ed., American Society for Testing and Materials, pp. 285-293, 1996.

Eckel, Edwin, C., *Cements, Limes, and Plasters*, John Wiley & Sons, Inc. 655pp, 1922.

Edison, M.P. (Editor), *Natural Cement*, ASTM STP 1494, American Society for Testing and Materials, 2008.

Elsen, J., "Microscopy of Historic Mortars or mortars – A Review", *Cement and Concrete Research 36*, 1416-1424, 2006.

Elsen, J., Mertens, G., and Van Balen, K., Raw materials used in ancient mortars or mortars from the Cathedral of Notre-Dame in Tournai (Belgium), Eur. J. Mineral., Vol. 23, pp. 871-882, 2011.

Elsen, J., Van Balen, K., and Mertens, G., Hydraulicity in Historic Lime Mortars or mortars: A Review, In, Valek, J, Hughes, J.J., and Groot, W.P. (Eds.), Historic Mortars or mortars Characterisation, Assessment and Repair, RILEM Book series, Volume 7, pp. 125-139, Springer, 2012.

Erlin, B., and Hime, W.G., "Evaluating Mortar Deterioration", *APT Bulletin*, Vol. 19, No. 4, pp. 8-10+54, 1987.

Goins E.S., "Standard Practice for Determining the Components of Historic Cementitious Materials," National Center for Preservation Technology and Training, Materials Research Series, NCPTT 2004.

Goins, E.S., "A standard method for the characterization of historic cementitious materials." US/ICOMOS Scientific Journal: Historic Mortars or mortars & Acidic Deposition on Stone, # (1), pp. 6-7, 2001.

Groot, C., Ashall, G., and Hughes, J., Characterization of Old Mortars or mortars with Respect to their Repair, State-of-the-art Report of RILEM Technical Committee 167-COM, 2004.

Hughes, D.C., Jaglin, D., Kozlowski, R., Mayr, N., Mucha, D., and Weber, J., "Calcination of Marls to Produce Roman Cement", pp. 84-95, In, Edison, M.P. (Editor), *Natural Cement*, ASTM STP 1494, American Society for Testing and Materials, 2007.

Hughes, J.J., Cuthbert, S., and, Bartos, P., "Alteration Textures in Historic Scottish Lime Mortars or mortars and the Implications for Practical Mortar Analysis", *Proceedings of the 7th Euroseminar on Microscopy Applied to Building Materials*, Delft, pp. 417-426, 1999.

Hughes, R.E., and Bargh, B.L., The weathering of brick: Causes, Assessment and Measurement, A Report of the Joint Agreement between the U.S. Geological Survey and the Illinois State Geological Survey, 1982.

Jana, D., "Application of Petrography In Restoration of Historic Masonry Structures", In: Hughes, J.J., Lesie, A.B. and Walsh, J.A., eds. *Proceedings of 10th Euroseminar on Microscopy Applied to Building Materials*, Paisley, 2005.

Jana, D., "Sample Preparation Techniques in Petrographic Examinations of Construction Materials: A State-of-the-art Review", *Proceedings of the 28th Conference on Cement Microscopy*, International Cement Microcopy Association, Denver, Colorado, pp. 23-70, 2006.

Jedrzejewska, H., Old mortars or mortars in Poland: a new method of investigation, Studies in Conservation 5, pp. 132-138, 1960.

Langley, W.S., Report to CRH Canada on Investigation of Failed Mortar, W.S. Langley Concrete & Materials Technology, Inc. Project No. 191271, June 2019.

Leslie, A.B., and Hughes, J.J., "Binder Microstructure in Lime Mortars or mortars: Implications for the Interpretation of Analysis Results", *Quarterly Journal of Engineering Geology & Hydrogeology*, V. 35, No. 3, pp. 257-263, 2001.

Lubell, B., van Hees, Rob. P.J., and Groot, Casper J.W.P., The role of sea salts in the occurrence of different damage mechanisms and decay on brick masonry, Construction and Building Materials, Vol. 18, pp. 119-124, 2004.

Martinet, G., Quenee, B., Proposal for a useful methodology for the study of ancient mortars or mortars, Proceedings of the International RILEM workshop "Historic Mortars or mortars: Characteristics and tests," Paisley, pp. 81-91, 2000.

Mack, Robert, and Speweik, John P., *Preservation Briefs 2*, U.S. Department of the Interior, National Park Service Cultural Resources, Heritage Preservation Services, pp. 1-16, 1998.

Middendorf, B., Baronio, G., Callebaut, K, and Hughes, J.J., "Chemical-mineralogical and physical-mechanical investigation of old mortars or mortars, Proceedings of the International RILEM workshop "Historic Mortars or mortars: Characteristics and tests," Paisley, pp. 53-61, 2000.

Middendorf, B., Hughes, J.J., Callebaut, K., Baronio, G., and Papayanni, I., Mineralogical characterization of historic mortars or mortars, In. Groot, C., et al. (eds), Characterisation of Old Mortars or mortars with Respect to their Repair, State-of-the-art Report of RILEM Technical Committee 167-COM, pp. 21-36, 2004a.

Middendorf, B., Hughes, J.J., Callebaut, K., Baronio, G., and Papayanni, I., Chemical characterization of historic mortars or mortars, In. Groot, C., et al. (eds), Characterisation of Old Mortars or mortars with Respect to their Repair, State-of-the-art Report of RILEM Technical Committee 167-COM, pp. 37-53, 2004b.

Middendorf, B., Hughes, J.J., Callebaut, K., Baronio, G., and Papayanni, I., "Investigative Methods for the Characterization of Historic Mortars or mortars – Part 1: Mineralogical Characterization," *Materials and Structures*, Vol. 38, 2005a.

Middendorf, B., Hughes, J.J., Callebaut, K., Baronio, G., and Papayanni, I., "Investigative Methods for the Characterization of Historic Mortars or mortars – Part 2: Chemical Characterization," *Materials and Structures*, Vol. 38, pp 771-780, 2005b.

Sarkar, S.L., Aimin, Xu, and Jana, Dipayan, Scanning electron microscopy and X-ray microanalysis of Concretes, pp. 231-274, In, Ramachandran, V.S. and Beaudoin, J.J. Handbook of Analytical Techniques in Concrete Science and Technology, Noyes Publications, Park Ridge, New Jersey, 2000.

Speweik, J.P., *The History of Masonry Mortar in America 1720-1995*, 2010.

Stewart, J., and Moore, J., Chemical techniques of historic mortar analysis, Proceedings of the ICCROM Symposium "Mortars or mortars, Cements, and Grouts used in the Conservation of Historic Buildings," Rome, ICCROM, Rome, pp. 297-310, 1981.

Valek, J., Hughes, J.J., and Groot, C. (eds.), *Historic Mortars or mortars: Characterization, Assessment and Repair*, Springer, RILEM Book series Vol. 7, p. 464, 2012.

Valek, J., Hughes, J.J., and Groot, C. (eds.), Historic Mortars or mortars: Characterization, Assessment and Repair, Springer, RILEM Book series Vol. 7, 2012.

Van Balen, K., Toumbakari, E.E., Blanco, M.T., Aguilera, J., Puertas, F., Sabbioni, C., Zappia, G., Riontino, C., and Gobbi, G., "Procedures for mortar type identification: A proposal." In International RILEM workshop on historic mortars or mortars: Characteristics and Tests; Paisley, Scotland, 13th to 14th May 1999, edited by Barton, P., Groot, C., and Hughes, J.J., Cachan, France: RILEM Publications, 2000.

Vyskocilova, R., W. Schwarz, D. Mucha, D. Hughes, R. Kozlowski, and J. Weber, "Hydration processes in pastes of roman and American natural cements," *ASTM STP*, vol. 4, no. 2, 2007.

Weber, J., Gadermayr, N., Kozlowski, R., Mucha, D., Hughes, D., Jaglin, D., and Schwarz, W., Microstructure and mineral composition of Roman cements produced at defined calcination conditions, Materials Characterization, Vol. 58, pp. 1217-1228, 2007.

END OF TEXT

APPENDIX –
LABORATORY TESTING OF MASONRY MORTARS

Introduction[1]

Until 1970s characterization of masonry mortars were mostly based on traditional wet chemical analyses (Jedrzejewska, 1960, Stewart and Moore, 1981), where interpretation of results were often difficult if not impossible without a good knowledge of the nature of different sand and binder components in mortars. The majority of later mortar characterization proposed optical microscopy (Erlin and Hime 1987, Middendorf et al. 2000, Elsen 2006) as the first step in identification of different components of mortar based on which other analytical techniques including the wet chemistry are performed. Examples include scanning electron microscopy and X-ray microanalysis, X-ray diffraction, X-ray fluorescence, atomic absorption, thermal analysis, infrared spectroscopy, etc. (Bartos et al. 2000, Elsen 2006, Callebaut et al. 2000, Erlin and Hime 1987, Goins 2001, 2004, Groot et al. 2004, Doebley and Spitzer 1996, Chiari et al. 1996, Middendorf et al. 2000, 2004, 2005, Leslie and Hughes 2001, Martinet and Quenee 2000, Valek et al., 2012, Jana 2005, 2006). The choices of appropriate techniques depend mainly on the questions that have to be addressed, and, on the amount of material available.

Purposes of laboratory testing are: (a) to document an in place mortar by examining its sand and binder components, proportions of various ingredients, and their effects on properties and performance of the mortar, (b) evidence of any chemical or physical deterioration of the mortar from unsoundness of its ingredients to effects of potentially deleterious agents from the environment (e.g., salts), (c) records of later repointing events and their beneficial or detrimental effects on the performance of the original mortar and masonry units, and finally, (d) an assessment of an appropriate restoration mortar to ensure compatibility with the existing structure.

Currently there are two standardized procedures available that describe various laboratory techniques for analyses of masonry mortars with special emphasize to historic mortars. One is from the USA, the ASTM C 1324 "Standard Test Method for Examination and Analysis of Hardened Masonry Mortar," which includes detailed petrographic examinations, followed by chemical analyses, along with various other analytical methods to test masonry mortars as described in various literatures, e.g., XRD, thermal analysis, and infrared spectroscopy. The second one is from European studies and described in RILEM (Middendorf et al. 2004 and b, and 2005 a and b).

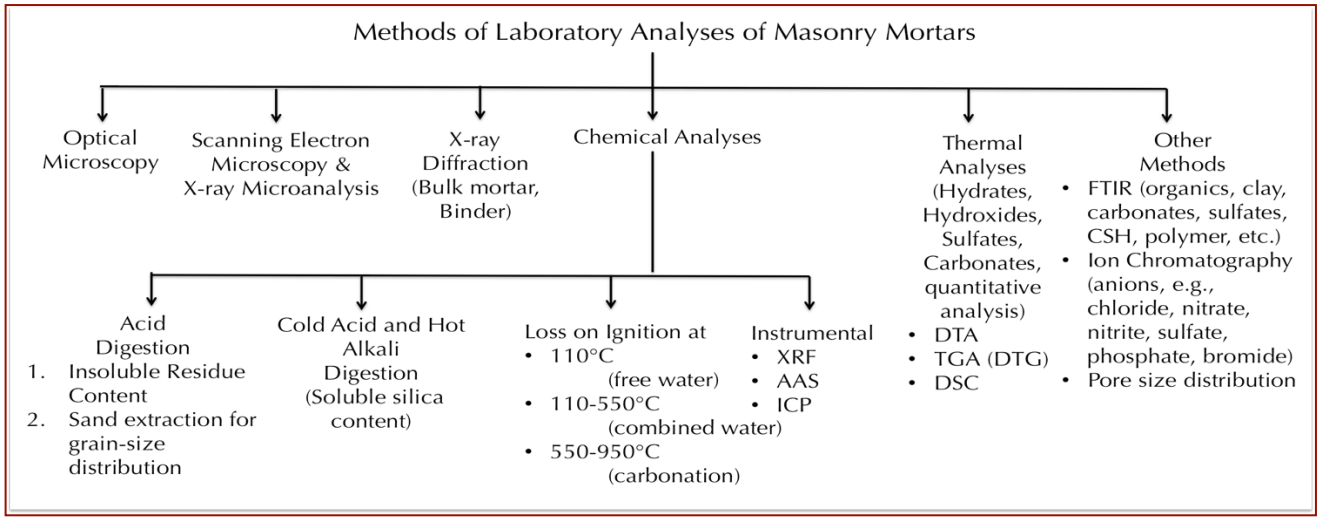

Figure A1: Various methods of laboratory analyses of masonry mortars. Optical microsocpy is the first method that provides many useful information about the mortar and its ingredeints, and dictates the subsequent methods to follow. Electron microscopy, X-ray diffraction, and various chemical analyses are commonly followed after optical microcopy to further determine the composition, microstructure, and mineralogy of sand and binder(s).

[1] For various analytical facilities for laboratory testing of mortars, please visit our website at www.cmc-concrete.com.

Sample Selection and Steps of Laboratory Analyses

Mortar samples are first photographed with a digital camera, scanned on a flatbed scanner, and examined in a low-power stereomicroscope for the preliminary examinations, e.g., to screen any unusual pieces having different appearances, e.g., representing contaminants from prior pointing episodes.

Four (4) subsets of the pieces of interest are then selected from the original amount for: (1) optical microscopy, scanning electron microscopy, and X-ray microanalysis of a representative sizable amount to cover as much of an entire 50 mm × 75 mm thin section per sample with multiple pieces as possible for chemical and mineralogical compositions, and microstructures of sand, paste, and mortar, (2) extraction of masonry sand by acid digestion for grain size distribution of sand (preferably from an un-pulverized or gently pulverized mortar), (3a) loss on ignition for water and carbonate contents, (3b) acid digestion for determination of insoluble residue content, and (3c) cold-acid then hot-alkali digestion for soluble silica content from hydraulic binders – all three after pulverizing the 3rd subset mortar to finer than 0.3 mm size and collecting aliquots of 1 gram, 1 gram, and 5 grams, respectively, and, (4) ultrafine pulverization (finer than 44-micron particle size) of 10 grams of mortar from the 4th subset for XRD, XRF, and thermal analyses. Any additional analyses, if needed, e.g., water digestion for determination of soluble salts by ion chromatography, or, infrared spectroscopy are done from the 4th subset. Organic analysis (e.g., paint or surface coating on masonry) by FTIR is done on the coating of interest from the original mortar pieces.

After preliminary visual examinations, optical microscopy is the first detailed examination that is most crucial in mortar analysis to determine the types of sand and binder used from mineralogical and textural characteristics of mortar, based on which subsequent chemical analyses are done to determine the chemical compositions of binders and proportions of sand, and binder components. Information obtained from petrographic examinations is crucial to devise the appropriate guidelines to follow for chemical methods, and to properly interpret the results of chemical analyses. For example, detection of siliceous versus calcareous versus argillaceous natures of aggregates in mortar, or the presence of any pozzolan in the binder (slag, fly ash, ceramic dusts, etc.) from petrography restricts which chemical method to follow, and how to interpret the results of such analyses, e.g., acid-insoluble residue contents. Therefore, a direct chemical analysis e.g., acid digestion of a mortar without doing a prior petrographic examination to determine the types of aggregates and binder used could lead to highly erroneous results and interpretation. Armed with petrographic and chemical data, and based on assumed compositions and bulk densities of the sand and the binder(s) similar to the ones detected from petrographic examinations volumetric proportions of sand and various binders present in the examined mortar can be calculated. The estimated mix proportions from such calculations can provide at least a rough guideline to use as a starting mix during formulation of a tuck pointing mortar to match with the existing mortar.

Optical Microscopy For Mineralogy & Microstructure of Mortar

After preliminary non-destructive examinations, e.g., from visual examinations, photographing as-received sample with a digital camera, scanning mortar pieces on a flatbed scanner, and examining in a low-power stereomicroscope, subsequent destructive sample preparation steps are followed for examinations of detailed mineralogical and microstructural compositions of mortar sand and binders in thin sections (25 to 30 micron thickness) in (a) a higher power Stereozoom microscope from 5X to 100X, and then in a research-grade petrographic microscope from 40X to 1000X both microscopes are equipped with transmitted, reflected, polarized, and fluorescent light facilities, as well as photo-micrographic capabilities with advanced high-resolution microscope cameras.

The main purposes of optical microscopy of masonry mortar are characterization of: (a) aggregates, e.g., type(s), chemical and mineralogical compositions, nominal maximum size, shape, angularity, grain-size distribution, soundness, alkali-aggregate reactivity, etc. (b) paste, e.g., compositions and microstructures to diagnose various type(s) of binder(s) used, (c) air, e.g., presence or absence of air entrainment, air content, etc., (d) alterations, e.g., lime leaching, carbonation, staining, etc. due to interactions with the environmental agents during service, and effects of such alterations on properties and performance of mortar; and (e) deteriorations, e.g., chemical and/or

physical deteriorations during service, cracking from various mechanisms, salt attacks, possible reasons for the lack of bond if reported from the masonry unit, etc.

Four essential steps followed during optical microscopy are: (1) visual examination of as-received, fresh fractured, and sectioned surfaces of mortar in a stereo-microscope, (2) preparation of a large-area (50 × 75 mm) thin section of homogeneous thickness (25-30 micron), (3) observation of thin section in a transmitted-light stereo-zoom microscope from 5X to 100X preferably with polarized-light facilities to observe large-scale distribution of sand and mortar microstructure, and finally (4) observation of thin section in a petrographic microscope from 40X to 600X equipped with transmitted and reflected polarized and fluorescent-light facilities for examinations of sand and binder compositions and microstructures.

For thin section preparation, representative fragments are oven-dried at 40°C to a constant mass and placed in a flexible (e.g., molded silicone) sample holder, then encapsulated with a colored dye (e.g., blue dye commonly used in sedimentary petrography, or, fluorescent dye, Elsen 2006) mixed low-viscosity epoxy resin under vacuum to impregnate the capillary pore spaces of mortar, improve the overall integrity of sample during sectioning by the cured epoxy, highlight porous areas of mortar, alterations, cracks, voids, reaction products, etc. The epoxy-encapsulated cured solid block of sample is then de-molded and processed through a series of coarse to fine grinding on metal and resin-bonded diamond grinding discs with water or a lubricant, eventually a perfectly flat clean ground surface is glued to a large-area (50 × 75 mm) glass slide. Careful precision sectioning and precision grinding of the sample is then done in a thin-sectioning machine (e.g., Buehler, Logitech, Ingram-Wards, Microtrim, Struers) till the thickness is down to 50-60 micron. Final thinning down to 25-30 micron thickness is done on a glass plate with fine (5-15 micron) alumina abrasive. Thin section is eventually polished with various fine (1 micron to 0.25 micron size) diamond abrasives on polishing wheels for examinations in a petrographic microscope, and eventually in SEM-EDS. Sample preparation steps are described in detail in Jana (2006).

Steps followed during light optical microscopical examinations of a mortar sample include:

a. Visual examinations of mortar fragments, as received, to select fragments for detailed optical microscopy; initial digital and flatbed scanner photography of mortar as received;
b. Low-power stereomicroscopic examinations of saw-cut and freshly fractured sections of mortar for evaluation of variations in color, grain-size and appearances of sand, and the nature of the mortar paste;
c. Examinations of oil immersion mounts for special features and materials from mortar in a petrographic microscope;
d. Examinations of colored (blue or fluorescent) dye-mixed epoxy-impregnated polished thin sections of mortar fragments in a transmitted-light Stereozoom microscope for determination of size, shape, angularity, and distribution of sand, as well as abundance and distribution of void and pore spaces that are highlighted by the colored dye-mixed epoxy;
e. Image analyses of photomicrographs of mortar thin sections for estimations of pores, voids, intergranular open spaces, and shrinkage microcracks by using Image J or other image analysis software where multiple photomicrographs are collected in plane polarized light mode by using a high-resolution Stereozoom microscope equipped with transmitted and polarizing light facilities and stitched to get a representative coverage;
f. Examinations of colored (blue or fluorescent) dye-mixed epoxy-impregnated polished thin sections of mortar fragments in a petrographic microscope for detailed compositional, mineralogical, textural, and microstructural analyses of aggregates and binders in mortars, along with diagnoses of evidence of any deleterious processes and alterations (e.g., lime leaching, precipitation of secondary deposits and alteration products, salts);
g. Examinations of polished thin or solid section in reflected-light (epi-illumination) mode of petrographic microscope after etching the surface with acid to identify various non-hydrated hydraulic phases (e.g., C_2S, C_3S, C_3A, etc. Middendorf et al., 2005);
h. Examinations of any physical or chemical deterioration of mortar or signs of improper construction practices from microstructural evidences;
i. Stereo-microscopical examinations of size, shape, and color variations of sand extracted after hydrochloric acid digestion; and finally,
j. Selection of areas of interest to be examined by scanning electron microscopy.

CMC has a large assortment of optical microscopes from early 20th century to many latest advanced Nikon, Olympus, Leitz, Zeiss stereozoom and petrographic microscopes and several petrographic sample preparation and photomicrography facilities that can be found in our website at www.cmc-concrete.com.

Figure A2: Top - Optical microscopy laboratory in CMC which houses a variety of optical microscopes including low-power stereomicroscopes, high-power transmitted, reflected, fluorescent, and polarized-light stereozoom microcope, metallurgical microcopes, petrographic microcopes with reflected, transmitted, fluoescent, and polarized light facilities, fluoreccent microscopes, inverted microscopes, comparison microscopes, etc. Mortar examinations are done on stereomicroscopes, fluorescent light microscopes, and petrographic microscopes. Bottom – Thin sectioning equipments from Buehler and Microtec that prepare 25 to 30 micron thick thin-sections impregnted in clear, blue, or fluorescent dye-mixed epoxy for observations in petrographic and stereozoom microscopes (left), Nikon Eclipse E600 POL petrographic micorscope (2nd from left), Nikon SMZ-10A stereomicroscope (3rd from left) and Olympus SZX-12 transmitted-light stereozoom microscope (rightmost) all having photomicrographic capabilities with advanced high-resolution microscope cameras (e.g., Jenoptik Progres Gryphax, Luminera Infinity series) for documenting compositional and microstructural features from optical microsocpical examinations of masonry mortar.

Scanning Electron Microscopy & X-Ray Microanalyses For Mineralogy, Microstructure, and Microchemical Compositions of Mortar

Figure A3: CamScan Series 2 scanning electron microscope in CMC that is attached to a backscatter detector, a secondary electron detector and an energy-dispersive X-ray detector.

Methods followed in scanning electron microscopy and energy-dispersive X-ray fluorescence spectroscopy (SEM-EDS) include: (a) secondary electron imaging (SEI) to determine the surface texture, microstructure and morphology of the examined surface, (b) backscatter electron (BSE) imaging to determine compositions of various phases from various shades of darkness/grayness from average atomic numbers of phases from the darkest pore spaces to brightest iron minerals (via minerals e.g., thaumasite, periclase, ettringite, quartz, dolomite, monosulfate, gypsum, calcite, C-S-H, aluminate, calcium hydroxide, belite, alite, free lime, and ferrite having progressively increasing average atomic numbers and brightness in BSE image), (c) X-ray elemental mapping (dot mapping) of an area of interest to differentiate various phases, (d) point-mode or area (raster)-mode analysis of specific area/phase of interest on a polished thin or solid section, and (e) average compositional analysis of a specific phase or an area on a polished thin or solid section or small subset of a sample.

The main purposes of SEM-EDS analyses of mortar are to: (a) observe the morphology and microstructure of various phases of sand and binder, (b) characterize the typical fine-grained microstructure of hydrated hydraulic components that are too fine to be examined by optical microscopy and not well crystallize to be detected by XRD; (c) determine the major element oxide compositions, and compositional variations of paste, and from that determine the type of binder used, especially to differentiate non-hydraulic calcitic and dolomitic lime mortars from hydraulic lime varieties, natural cements, pozzolans, slag cements, Portland cements, etc. all from their characteristic differences in compositions and hydraulicities (e.g., cementation index of Eckel 1922); (d) determine composition of residual hydraulic phases to assess the raw feed and calcination processes used in binder manufacturing; (e) assess hydration, carbonation, and alteration products of binders, (f) investigate effects of various environmental alterations of paste and its role on properties and performance of mortar, (g) detect salts and other potentially deleterious constituents, (h) detect pigments and fillers, (i) examine compositional variations

across multiple coats of binder installed, etc.; and eventually (i) complement and confirm the results of optical microscopy.

Due to characteristic difference in compositions of pastes made using various binders, e.g., non-hydraulic lime (CaO dominants over all other oxides), variably hydraulic lime (CaO with variable SiO_2 contents depending on hydraulicity), dolomitic lime (high CaO and MgO), natural cement (CaO, SiO_2, Al_2O_3, and MgO contents are high, high MgO and FeO contents are characteristic), and Portland cement (CaO and SiO_2 contents are higher than all other oxides), SEM-EDS analysis of paste is a powerful method for detection of the original binder components in the mortar. Effects of chemical alterations and various chemical deteriorations of a mortar (e.g., lime leaching, secondary calcite precipitates, gypsum deposits, etc.) can also be detected effectively by SEM-EDS.

SEM-EDS analysis is done in a CamScan Series 2 scanning electron microscope (Figure A3) equipped with a high-resolution column 40Å tungsten, 40 kV electron optics zoom condenser 75° focusing lens operating at 20 kV, equipped with a variable geometry secondary electron detector, backscatter electron detector, EDS detector for observations of microstructures at high-resolution, compositional analysis, and quantitative determinations of major element oxides from various areas of interest, respectively. Revolution 4Pi software is used for digital storage of secondary election and backscatter electron images, elemental mapping, and analysis along a line, a point, or an area of interest.

Portion(s) of interest on the polished 50 mm × 75 mm size thin section used for optical microscopy are subsequently coated with a thin conductive carbon or gold-palladium film and placed on a custom-made aluminum sample holder to fit inside the large multiported chamber of CamScan SEM equipped with the eucentric 50 × 100 mm motorized stage. Procedures for SEM examinations are described in ASTM C 1723. Sarkar et al. (2000) described various applications of SEM-EDS in concrete and other construction materials.

Acid Digestion for Siliceous Sand Content and Size Distribution of Sand

Acid digestion is perhaps the most commonly used test of masonry mortar, which is done to: (a) extract sand from mortar by dissolving the binder fractions so that grain-size distribution of sand can be done by sieve analysis, and (b) assess sand content in the mortar. Sand content after acid digestion is determined both from: (a) 1.00 gram of pulverized mortar (finer than 0.3 mm size) digested in 50-ml dilute (1+3) HCl (heated rapidly but below boiling), and, (b) from digesting a representative bulk mortar *per se* (for harder mortars perhaps with light pulverization) in multiple fresh batches of (1+3) HCl at ambient temperature. The former usually gives better result due to small amount, pulverization to easily remove the binder fraction for digestion, and use of rapidly heated acid, whereas latter method requires multiple episodes of digestion in fresh acid and is time-consuming. Acid digestion is also done as the first step to determine soluble silica content in a mortar as described below, which is contributed from the hydraulic components in binder.

All these goals of acid digestion depend on the assumptions that: (i) sand is siliceous in composition and does not contain any acid-soluble constituents (e.g., carbonates), and, (ii) binder entirely dissolves in acid and does not contain any acid-insoluble constituents (gypsum, clay, etc.). Applicability of acid digestion to assess these tasks should therefore be first verified by optical microscopy to confirm the siliceous nature of sand without any appreciable acid-soluble constituents, and calcareous nature of binder, and none without any appreciable argillaceous (clay) constituents.

For grain-size distribution of sand (for mortar found from optical microscopy to contain siliceous sand), a few representative fragments of (preferably not pulverized or lightly pulverized in a porcelain mortar and pestle for harder mortars to break down to smaller size fraction without crushing the sand to retain the original sand size) are selected for digestion in multiple fresh batches of (1+3) dilute hydrochloric acid to dissolve away all binder fractions and extract, wash, and oven-dry the acid-insoluble component of aggregate. Usually multiple episodes of acid digestion in fresh batches of acid and filtration of residues are needed to entirely remove the binder fractions without losing the finer fractions of sand. Sand particles thus extracted are washed, oven-dried, and sieved in an automatic mini sieve shaker (e.g., from Gilson) through various U.S. Sieves from No. 4 (4.75 mm) through 8 (2.36 mm), 16 (1.18 mm), 30 (0.6 mm), 50 (0.3 mm), 100 (0.15 mm), and 200 (0.075 mm) for

determination of the size, shape, angularity, and color of sands retained on various sieves. Grain-size distribution of sand is then compared with ASTM C 144 specifications for masonry sand. Photomicrographs of sand retained on each sieve are then taken with a stereomicroscope to record the sand color. For low amount of mortar, or, for mortar having calcareous sand, image analysis (e.g., ImageJ) on stitched photomicrographs of thin sections taken from multiple areas can be done to determine the sand-size distribution (Elsen et al. 2011).

Cold-Acid & Hot-Alkali Digestion For Soluble Silica Content

Digestion of a pulverized sample of mortar in a cold acid followed by further digestion of residue in a hot alkali hydroxide solution are done to determine the soluble silica content contributed from the hydraulic component of binder, where cold acid digestion usually dissolves most of the binder without affecting the sand, followed by hot alkali hydroxide digestion to dissolve remaining soluble silica from calcium silicate hydrate component of paste or in mortars containing hydraulic binders. The soluble silica content corresponds to the silica mostly contributed from the hydraulic binder components (and a minor amount from any soluble silica component in the aggregates).

For determination of soluble silica content (modified from ASTM C 1324), 5.00 grams of pulverized mortar (finer than 0.3 mm size, without excessive fines) is first digested in 100-mL cold (at 3 to 5°C) HCl and filtered through two 2.5-micron filter papers (filtrate#1). The residue with filter papers is then digested again in hot (below boiling) 75-ml NaOH, and filtered through two 2.5-micron filter papers (filtrate# 2). The two filtrates from acid and alkali digestions are then combined, re-filtered twice with 2.5-micron and then through 0.45-micron filter paper to remove any suspended silica fines, brought to 250 mL volume with distilled water, and then used for soluble silica determination by an analytical method, such as atomic absorption spectroscopy (AAS), inductive coupled plasma optical emission spectroscopy (ICP-OES), or X-ray fluorescence spectroscopy (XRF). Multiple steps of filtrations from 2.5-micron to submicron (0.2-micron pore size) filter papers are necessary to remove any suspended silica that can skew the result. Instrument to be used for such determination must be calibrated with several silica standards in matrices similar to the one used in mortar analysis. CMC uses an XRF unit that is calibrated with filtrates from a series of laboratory-prepared standards of Portland cement and silica sand mortars (moist cured at *w/c* of 0.50 for at least 30 days) having various proportions of cements (SiO_2 contents of standards ranging from 1 to 10%) for determining SiO_2 Kα X-ray intensities from known stoichiometric silica (cement) contents of standards (using exact 5.00 grams as samples) prepared by the same procedure of cold HCl-digestion/filtration/hot NaOH-digestion/2nd filtration/combination of two filtrates/re-filtration steps followed for mortars. Hydraulic binder content is then calculated as: [(soluble SiO_2, weight percent in sample as calculated above) divided by assumed soluble SiO_2 content in binder] ×100, where assumed SiO_2 contents of binders varies, e.g., 21% in Portland cement, 20% in natural cement, 27% in slag cement, 7 to 10% in hydraulic lime, etc., or, more preferably, from the average paste-SiO_2 content determined from SEM-EDS for binder content.

Losses on Ignition For Free & Combined Water Contents, and, Carbonate Content

Losses in weight of a mortar on step-wise heating from ambient to 110°C, 550°C, and 950°C temperatures liberate free water from capillary pore spaces by 110°C, combined water from dehydroxylation of various hydrous phases (calcium silicate hydrate, calcium hydroxide, etc.) by 550°C, and liberation of carbon dioxide from decomposition of carbonated paste and carbonate minerals by 950°C. Such losses in weight are measured by following the procedures of ASTM C 1324 by heating 1.00 gram of pulverized mortar (finer than 0.3 mm) in an alumina crucible in a muffle furnace in a controlled step-wise heating at a heating rate of 10ºC/min. Mortars having hydraulic binders and hydration products of such provide measurable combined water contents after calcination to 550°C whereas those having high calcareous components (high-calcium lime, mortar having calcareous sand) produce high weight loss during ignition to 950°C. Usually, a good correlation is found between weight losses at 550°C from dehydration of combined water and soluble silica contents contributed from hydraulic binders amongst series of mortars containing variable amounts of hydraulic phases.

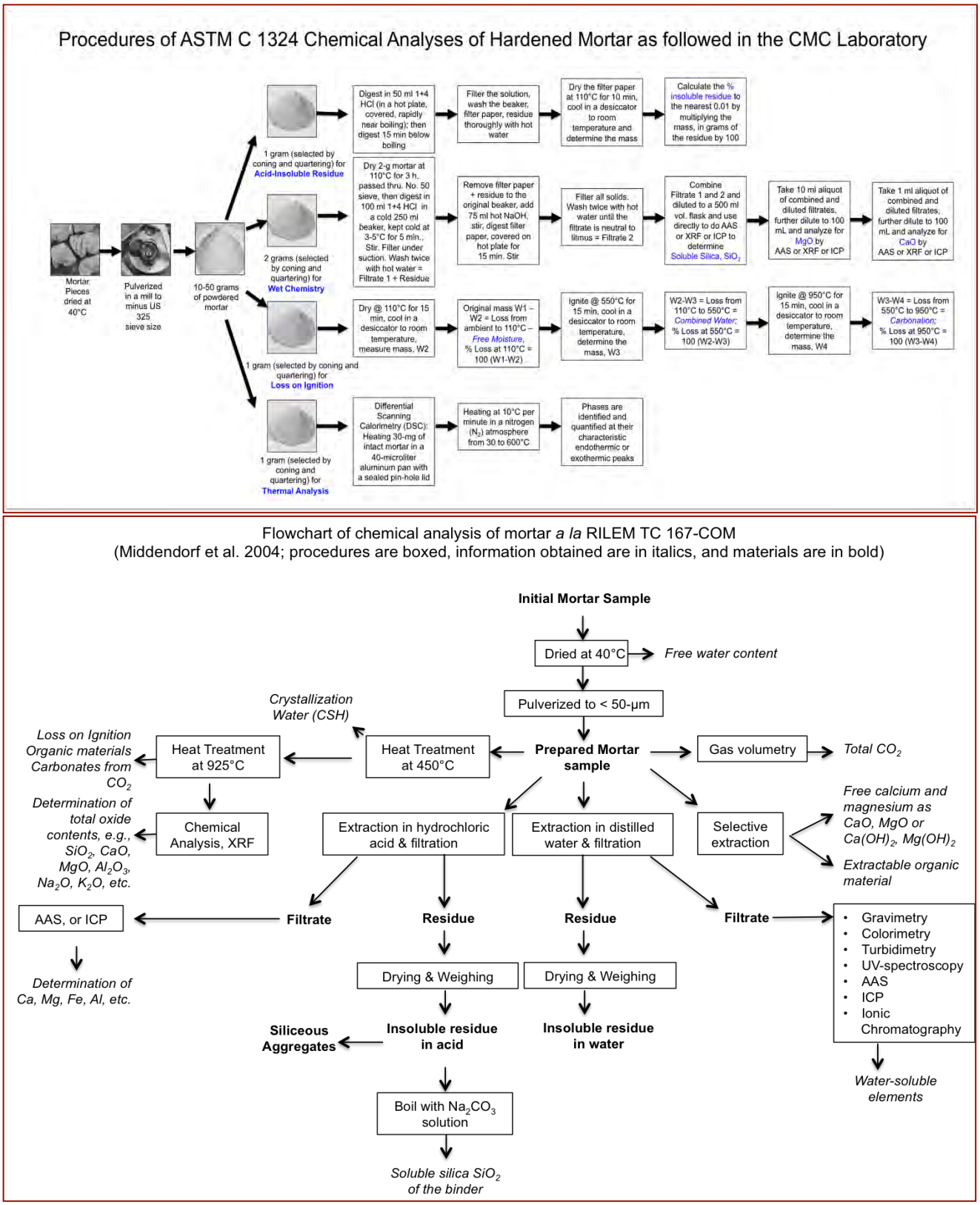

Figure A4: Flow charts for various chemical analyses of masonry mortar according to the US (top, ASTM C 1324) and European (bottom, RILEM) standards.

X-Ray Diffraction For Mineralogy of Mortar

X-ray diffraction (XRD) is a powerful method for: (a) determination of bulk mineralogical composition of mortar, including its aggregate and binder mineralogies (e.g., quartz in sand from major diffraction peaks at 26.65º, 20.85º, 50.14º 2θ, or calcite in sand or carbonated lime binder from major peaks at 29.41º, 39.40º, 43.15º 2θ, or Portlandite in binder from major peaks at 34.09º, 18.09º, 47.12º 2θ); (b) individual primary mineralogy and alteration products of aggregate at various size fractions, and binder phases; (c) detection of dolomitic lime binder from brucite in the mortar from major peaks at 38.02º, 18.59º, 50.86º 2θ; (d) detection of use of lime (portlandite), gypsum (11.59º, 20.72º, 29.11º 2θ), or cement binders from their characteristic mineralogies; (e) detection of any potentially deleterious constituents, e.g., deleterious salts, or efflorescence deposits; (f) detection of a mineral oxide-based pigmenting component in the mortar; and (g) detection of components that are difficult to detect by microscopical methods.

X-ray diffraction can be done on: (i) pulverized (to finer than 45 micron) portion of bulk mortar, or (ii) on the sand extracted from the mortar by acid digestion, if sand has a complex mineralogy, or also (iii) on the binder-fraction by separating the sand from the binder from a carefully ground mortar (in a mortar and pestle) and passing the ground mass through US 200 sieve (75 micron) to collect the fraction rich in binder. Since sands used in mortars are commonly siliceous, XRD pattern of bulk mortar shows quartz as the dominant mineral that surpasses peaks for all other phases (e.g., calcite, dolomite, clay, secondary deposits); hence binder separation is sometimes useful to detect minor minerals of interest (e.g., salts or pigments). For binder mineralogy, mortar is first dried at 40°C to a constant mass, then carefully crushed without pulverizing the sand, and sieved through a 75-micron opening screen to retain sand-rich fraction on the sieve and obtain the passed binder-rich fraction for further pulverization down to finer than 45 micron. Salts and other soft components can also be analyzed from binder fraction. Efflorescence salts on masonry walls are also analyzed routinely in XRD.

For sample preparation, a Rocklab (Sepor Mini-Thor Ring) pulverizer is used to grind mortar sample down to finer than 100 microns. Usually, a few drops of anhydrous alcohol are added to reduce decomposition of hydrous phases from the heat generated from grinding. Approximately 10 grams of sample is ground first in the pulverizer, from which about 8.0 grams of sample is selected, mixed with an appropriate binder (e.g., three Herzog grinding aid pellets from Oxford Instruments having a total binder weight of 0.6 gram for 8 grams of sample for a fixed binder proportion of 7.5 percent); the mixture is then further ground in Rocklab pulverizer and in a McCrone micronizing mill with anhydrous alcohol down to finer than 45-micron size. Approximately 7.0 grams of binder-mixed pulverized sample thus prepared is weighed into an aluminum sample cup and inserted in a stainless steel die press to prepare the sample pellet. A 25-ton Spex X-press is used to prepare 32 mm diameter pellet from the pulverized sample (see Figure A5 for sample preparation). The pressed pellet is then placed in a custom-made circular sample holder for XRD and excited with the copper radiation of 1.54 angstroms. Sample holders made with quartz or silicon are best for working with very small quantities of sample because these holders create no diffraction peaks between 2° and 90° 2θ (Middendorf et al. 2005).

XRD is carried out in a Siemens D5000 Powder diffractometer (θ-2θ goniometer) employing a long line focus Cu X-ray tube, divergent and anti-scatter slits fixed at 1 mm, a receiving slit (0.6 mm), diffracted and incident beam Soller slits (0.04 rad), a curved graphite diffracted beam monochromator, and a sealed proportional counter. Siemens D5000 is equipped with (a) a horizontal stage (fixed), (b) an X-ray generator with CuKα, fine focus sealed tube source, (c) large diameter goniometer (600 mm), low divergence collimator, and Soller slits, (d) fixed detector slits 0.05, 0.2, 0.6, 1.0, 2.0, and 6.0, and (e) Scintillation detector. Generator settings used are 40 kV and 30 mA. Tests are usually run at 2θ from 4° to 64° with a step scan of 0.02° and a dwell time of one second.

The resulting diffraction patterns are collected by DataScan 4 software of Materials Data, Inc. (MDI), analyzed by Jade software of MDI with ICDD PDF-4 (Minerals 2019) diffraction data. Phase identification, and quantitative analyses were carried out with MDI's Search/Match, Easy Quant, and Rietveld modules, respectively.

Figure A5: Siemens D5000 X-ray diffractometer in CMC that is connected to PC through MDI Datascan to collect diffraction data. XRD results are analyzed with MDI Jade software with search-match, easy quant, and Rietveld modules. The bottom row shows sample preparation for XRD where a Sepor Ring pulverizer (2nd from left) followed by McCrone micronizing mill (leftmost one) pulverized the sample to finer than 45-micron size. The pulverized sample is mixed with an appropriate binder and pressed in a 25-ton Spex press to form a 32-mm diameter pellet. Small amount of sample (i.e. not enough to prepare a pellet) is pulverized and spread over a quartz plate coated with a thin film of Vaseline.

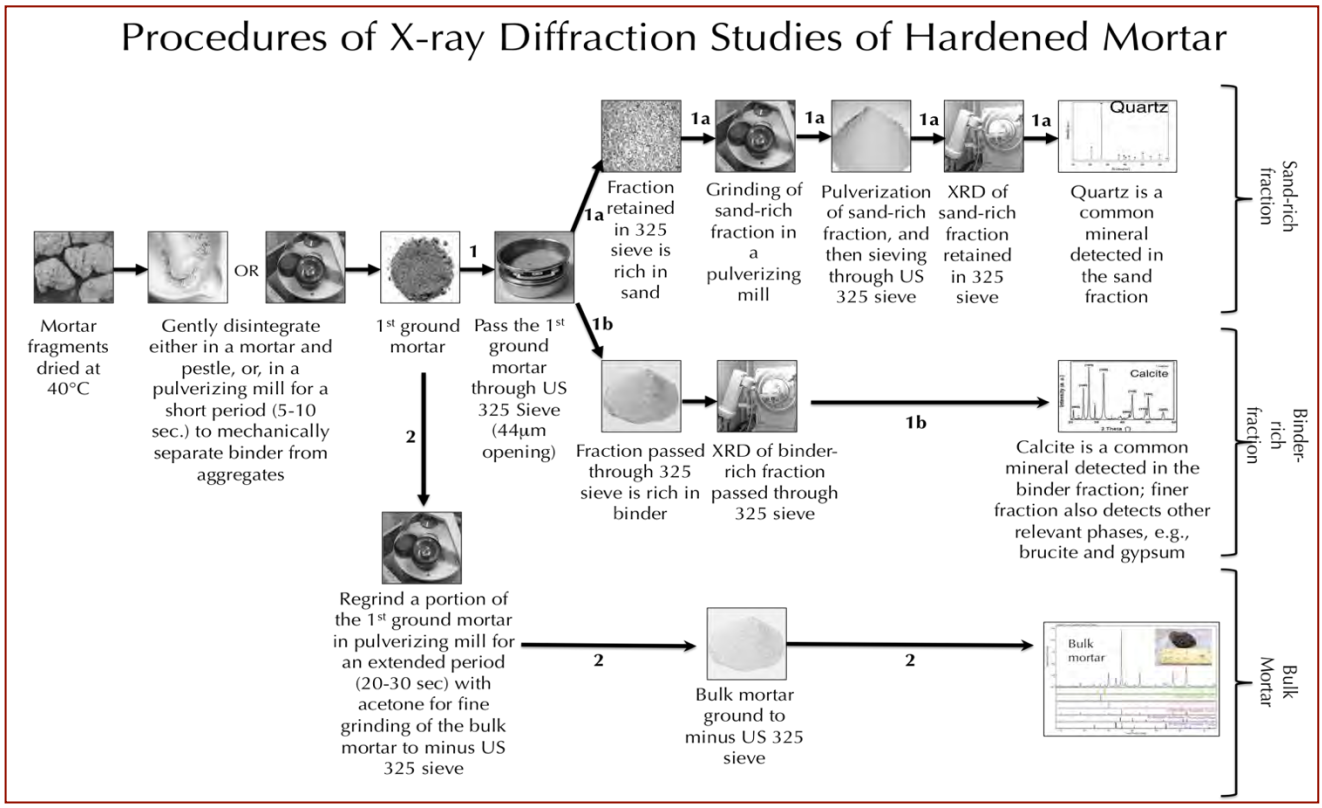

Figure A6: Various procedures for X-ray diffraction analysis of bulk mortar, and sand and/or binder fraction extracted from mortar.

X-Ray Fluorescence Spectroscopy For Chemical Composition of Mortar

X-ray fluorescence (XRF) is used for determining: (a) major element oxide composition of mortar, and (b) soluble silica content of filtrate after digestion of mortar in cold-HCl and hot-NaOH. Major element oxide compositions provide clues about the siliceous sand content of mortar from silica content, type of binder used (e.g., a dolomitic lime or natural cement based binder gives a characteristically higher magnesia than a calcitic lime or Portland cement based binder), calculation of lime content in a cement-lime mortar from bulk CaO content from XRF, effect of alterations and deteriorations (e.g., salt ingress in a mortar from marine environment can be diagnosed from excessive sodium, sulfate, etc.), etc. A series of standards from Portland cements, lime, gypsum, to various rocks, and masonry mortars of certified compositions (e.g., from USGS, GSA, NIST, CCRL, Brammer, or measured by ICP) are used to calibrate the instrument for various oxides and empirical calculations are done from such calibrations to determine oxide compositions of mortars. For mortars with highly unusual compositions (e.g. severely salt-contaminated mortar) a standardless FP calculation is done to determine the best possible composition.

An energy-dispersive bench-top X-ray fluorescence unit from Rigaku Americas Corporation (NEX-CG) is used (Figure A7). Rigaku NEX CG delivers rapid qualitative and quantitative determination of major and minor atomic elements in a wide variety of sample types with minimal standards. Unlike conventional EDXRF analyzers, the NEX CG was engineered with a unique close-coupled Cartesian Geometry (CG) optical kernel that dramatically increases signal-to-noise. By using monochromatic secondary target excitation, instead of conventional direct excitation, sensitivity is further improved. The resulting dramatic reduction in background noise, and simultaneous increase in element peaks, result in a spectrometer capable of routine trace element analysis even in difficult sample types. The instrument is calibrated by using various certified (CCRL, NIST, GSA, and Brammer) reference standards of cements and rocks. The same pellet used for XRD for mineralogical compositions is used for XRF to determine the chemical composition.

Figure A7: Rigaku NEX-CG in CMC, which can perform analyses of 9 pressed pellet or fused bead of mortar. Samples are prepared either as pressed pellet (usually the one already prepared for XRD) or can also accommodate fused bead with proper calibrate of standard beads.

Thermal Analyses For Determination of Hydrous, Carbonate, and Sulfate Phases in Mortar

Thermal analyses encompass: (1) thermogravimetric analysis (TGA), which measures the weight loss in a mortar as it is heated, where weight loss can be related to specific physical decomposition of a phase of interest at a specific temperature that is characteristic of the phase from which both the phase composition and the abundance can be determined; (2) differential thermal analysis (DTA, or first derivative of TGA i.e. DTG) measuring temperature difference between the sample and an inert standard (Al_2O_3) both are heated at the same rate and time where endothermic peaks are recorded when the standard continues to increase in temperature during heating but the sample does not due to decompositions (e.g., dehydration of hydrous or decarbonation of carbonate phases); the endothermic or exothermic transitions are characteristic of particular phase, which can be identified and quantified using DTA (or DTG); and (3) differential scanning calorimetry (DSC), which follows the same basic principle as DTA, whereas temperature differences are measured in DTA, during heating using DSC energy is added to maintain the same and the reference material (Al_2O_3) at the same temperature; this energy use is recorded and used as a measure of the calorific value of the thermal transitions that the sample experiences; this is particularly useful for detection of quartz that undergoes polymorphic (α to β form) transitions and no weight loss.

Thermal analyses are done to determine the presence and quantitative amounts of: (a) hydrates (e.g., combined water liberated from paste dehydration during decomposition of calcium-silicate-hydrate component in paste at 180-190ºC); (b) sulfates (gypsum from decompositions at 125ºC, and 185-200ºC, ettringite at 120-130ºC,

thaumasite at 150ºC); (c) brucite from its dehydroxylation at 300-400ºC to confirm the presence of dolomitic lime; (d) hydrate water from decomposition of Portlandite component of paste at 400-600ºC; (e) quartz from polymorphic transformation (α to β form) at 573ºC; (f) cryptocrystalline calcite in the carbonated lime matrix from decomposition at 620-690ºC, or magnesite at 450-520ºC, or (g) coarsely crystalline calcite e.g., in limestone by decomposition at 680-800ºC or (h) dolomite at 740-800ºC and 925ºC, and (i) phase transition of belite (C_2S) at 693ºC, etc. Phases are determined from their characteristic decomposition temperatures occurring mostly as endothermic peaks or polymorphic transition temperatures as for quartz.

Figure A8: Mettler-Toledo simultaneous TGA/DSC1 unit in CMC that can accommodate 32 samples. The top left photo shows the TGA/DSC1 unit with sample robot for automation as well as the sample holder for pressing aluminum sample holders. Sample is pulverized in a ring pulverizer shown in the bottom left, then a small amount (usually 30-70 mg) is weighed in a precision balance (shown 2nd from left in bottom row) and taken in an alumina sample holder (without lid). For DSC measurements up to 600°C, sometimes sample is taken in an aluminum holder and pressed in sample press (3rd from left in bottom row) and pierced with a needle for release of volatiles from decomposition. A PolyScience chiller (rightmost one in the bottom row) is used to cool the furnace. An ultrapure nitrogen gas is purged through the system during analyses.

Simultaneous TGA and DSC analyses are done in a Mettler Toledo TGA/DSC 1 unit (Figure A8) on 30-70 mg of finely ground (<0.6 mm) mortar in alumina crucible (70 µl, no lid) from 30°C to 1000°C at a heating rate of 10°C/min with high purity nitrogen as purge gas at a flow rate of 75.0 ml/min. By using one of the three removable sensor types the TGA/DSC 1 simultaneously measures heat flow in addition to weight change. The instrument offers high resolution (ultra-microgram resolution over the whole measurement range), efficient automation (with a reliable sample robot for high sample throughput), wide measurement range (measure small

and large sample masses and volumes) broad temperature scale (analyze samples from ambient to 1100°C), superior ultra-micro balance, simultaneous DSC heat flow measurement (for simultaneous detection of thermal events, e.g., polymorphic alpha-to-beta transition of quartz and quartz content), and a gastight cell (ensures a properly defined measurement environment).

Infrared Spectroscopy For Determination of Organic Components in Mortar

Fourier-transform infrared spectroscopy (FT-IR) measures interaction between applied infrared radiation and the molecules in the compounds of interest (Middendorf et al. 2005). Bonds between atoms have distinctive geometrics and natural states of rotation and vibration. Incident infrared radiation will excite these vibrations and rotations when a critical wavelength is reached that can impart energy to the bond. At this point the atomic bond that is being excited will absorb that wavelength of infrared radiation. If the sample is placed between the source of radiation and a detector these times of absorption of infrared radiation can be recorded as reduced intensity and can be related to specific types of atomic bonds characteristic of particular functional groups in compounds (e.g., CO^{3-}group in carbonates). FT-IR is particularly useful for detection of admixture, additives, and polymer resins. FT-IR is used mainly to identify various organic components (functional groups) in mortar (e.g., methyl CH_3, organic acids CO-OH, carbonates CO_3) from their characteristic spectral fingerprints in FT-IR spectrum. FT-IR can also be used for detection of main mineral phases in a hydraulic binder, CSH, carbonates, gypsum, and clays (Middendorf et al. 2005). Organic compounds such as synthetic (e.g., acrylics, polyesters) and natural resins, carbohydrates, colorants, oils and fats, proteins, waxes as well as inorganic compounds, e.g., corrosion products, minerals, pigments, paints, fillers, stone, glass, and ceramics can be detected by this technique.

FT-IR measurements are done in a Perkin Elmer Spectrum 100 FT-IR spectrophotometer (Figure A9) running with Spectrum 10 software. Samples were measured using attenuated total reflection (ATR) on a single bounce diamond/ZnSe ATR crystal. Sample was measured between a frequency range of 4000 to 650 cm^{-1}. Each run was collected at 4 cm^{-1} resolution with Strong Beer-Norton apodization. Data were collected with a temperature-stabilized deuterated triglycine sulfate (DTGS) detector by placing the sample in contact with the ATR crystal and by applying force from the pressure applicator supplied with the ATR accessory. The application of pressure enabled the sample to be in intimate contact with the ATR crystal, ensuring a high-quality spectrum was achieved. Additionally, more conventional KBr pellet is also used for samples on as-needed basis.

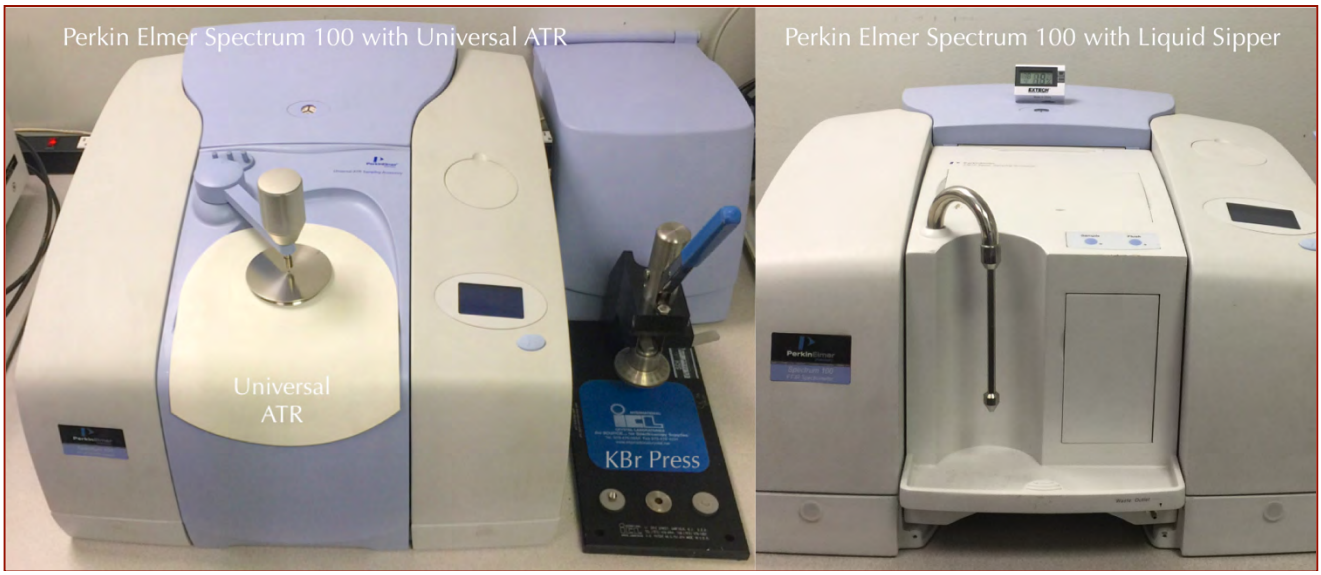

Figure A9: Perkin Elmer Spectrum 100 FT-IR unit in CMC with Universal ATR and Liquid Sipper attachments. The FT-IR unit can analyze a sample as-received in the Universal ATR (left), or as a pressed pellet after mixing with KBr powder in a KBr press (middle), or as a liquid either directly in Universal ATR or in Liquid Sipper unit (right).

Ion Chromatography For Determination of Water-Soluble Cations and Anions in Mortar

Salts can cause various deteriorations in masonry from: (a) mere aesthetic issues of surface efflorescence by precipitation from evaporation of leachates on the masonry wall surfaces followed by atmospheric carbonation of the precipitates where salts deposit as individual crystals or as crust to (b) more serious internal distress in mortar and masonry units from crystallization inside the pores (sub-fluorescence or crypto-fluorescence) from expansive forces associated with crystallization of salt from supersaturated solutions. Some common salts in masonry are calcium carbonates (e.g., calcite, vaterite), magnesium carbonate (magnesite), sodium carbonate hydrate and bicarbonate (thermonatrite, trona, nahcolite), sulphates (gypsum, thenardite, epsomite, melanterite, mirabilite, glauberite, or ettringite and thaumasite from oxidation of sulfides or cement hydrates), and chlorides (halite, sylvite, calcium oxychloride from deicing salts, salt-bearing aggregates, ground water). X-ray diffraction and SEM-EDS can determine many of these salts as long as they are present in detectable amounts.

Ion chromatography is an established technique for analyses of various water-soluble anions and cations in salts (e.g., chloride, sulfate, and nitrate anions, and magnesium, calcium, alkali, ammonium cations) to assess magnitude of environmental impacts on masonry units and mortars, and subsequent effects of such salt ingress. Masonry samples are pulverized, digested in ultrapure deionized water to dissolve all water-soluble salts, then solid residues are filtered out, and finally water-digested filtrates are analyzed by an ion chromatograph.

Procedures followed in Ion chromatography are described in ASTM D 4327 "Standard Test Method for Anions in Water by Chemically Suppressed Ion Chromatography." Briefly, an aliquot of 1 gram of pulverized sample (passing No. 50 sieve) is digested in 50 ml distilled water for 6 to 8 hours on a magnetic stirrer at a temperature below boiling point of water; then the digested sample is filtered through two 2.5-micron filter papers using vacuum, followed by a second filtration through micro-filter (0.2 micron) paper, then the filtrate is either used directly or diluted to 100 to 250 ml with distilled water depending on the concentration of ions, and used for analysis to get ppm-level cations (calcium, magnesium, sodium, potassium, lithium, ammonium), and anions (fluoride, chloride, nitrite, bromide, nitrate, phosphate, and sulfate) in the water-digested sample in Metrohm IC units (Figure A10). The instruments are calibrated against multiple custom-made Metrohm standard solutions having all the ions of interest from 0.1-ppm to 100-ppm levels. To check the accuracy of the instrument, a 50-ppm standard solution was run first prior to the analysis of samples.

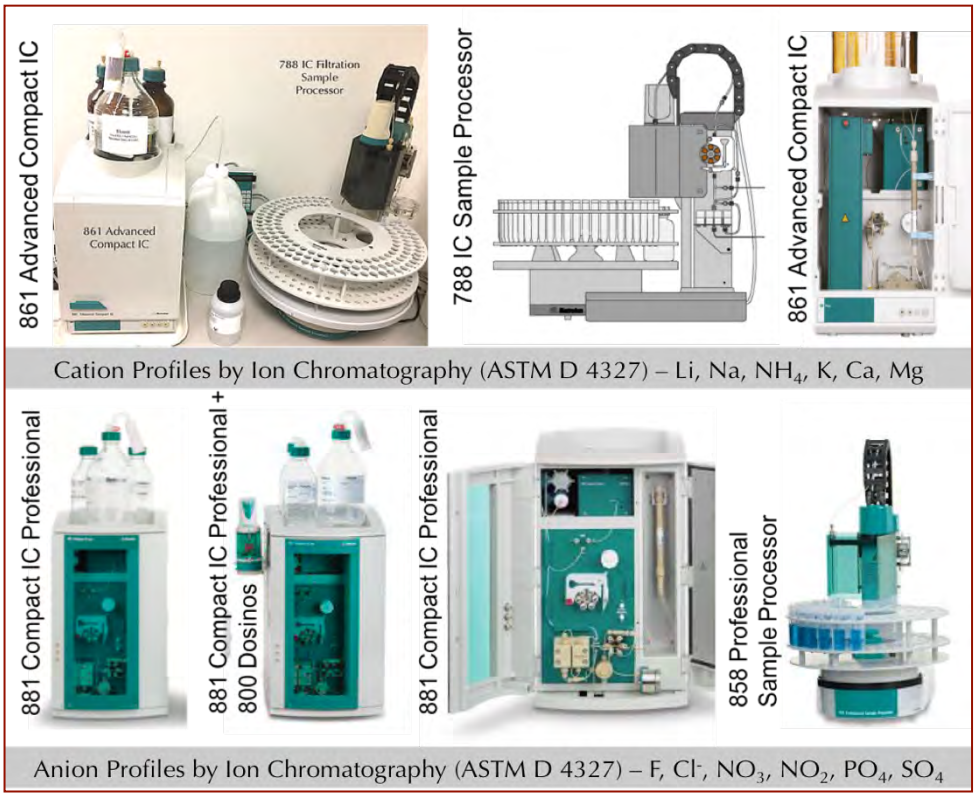

Figure A10: Various ion chromatography units used in CMC for determination of water-soluble ions after digestion of pulverized masonry mortar in deionized water to determine various anions (sulfate, chloride, nitrate, nitrite, phosphate, bromide) extracted from mortar.

Information Obtained From Various Laboratory Methods

Information	Optical Microscopy	SEM-EDS	XRD	XRF	Chemical (Gravimetry)	Chemical (Titration & IC)	Sieve Analyses of Sand	Thermal	FTIR
Mortar Sand Type	X	X	X	X					
Sand Composition	X	X	X	X					
Sand Mineralogy	X	X	X						
Sand Soundness	X	X							
Sand Fineness	X						X		
Sand Grading & Color	X						X		
Mortar Binder Type(s)	X	X	X					X	
Binder Composition	X	X	X					X	
Binder Microstructure	X	X							
Portland Cement	X	X	X	X				X	
Hydrated Calcitic Lime	X	X						X	
Dolomitic Lime	X	X	X					X	
Hydraulic Lime	X	X						X	X
Masonry Cement	X	X							
Natural Cement	X	X							
Carbonation	X	X	X					X	X
Carbonated Paste vs. Carbonate Sand	X							X	
Fillers	X	X						X	
Organic Components		X						X	X
Surface Treatments	X	X				X			X
Clay Contaminants	X		X					X	X
Mortar Type	X	X			X				
Masonry Discoloration	X	X	X	X		X		X	
Masonry Cracking	X	X	X						
Mortar Softening	X	X			X				
Mortar Crumbling	X	X	X		X				
Mortar Cracking	X	X	X	X			X	X	
Mortar Discoloration	X	X	X	X		X			
Mortar Shrinkage, Stiffening	X	X							
Bond to Masonry	X	X							

Information	Optical Microscopy	SEM-EDS	XRD	XRF	Chemical (Gravimetry)	Chemical (Titration & IC)	Sieve Analyses of Sand	Thermal	FTIR
Masonry Efflorescence	X	X	X	X					
Salt Attack	X	X	X			X		X	
Lime Leaching	X	X				X			
Polymer		X						X	X
Mix Proportion	X	X	X	X	X				
Tuckpointing Mortar Suggestions	X	X	X	X	X		X	X	X
Miscellaneous Failure Analysis	X	X	X	X	X			X	X

Table 10: Information obtained from various laboratory methods.

Steps Followed in Laboratory Analyses

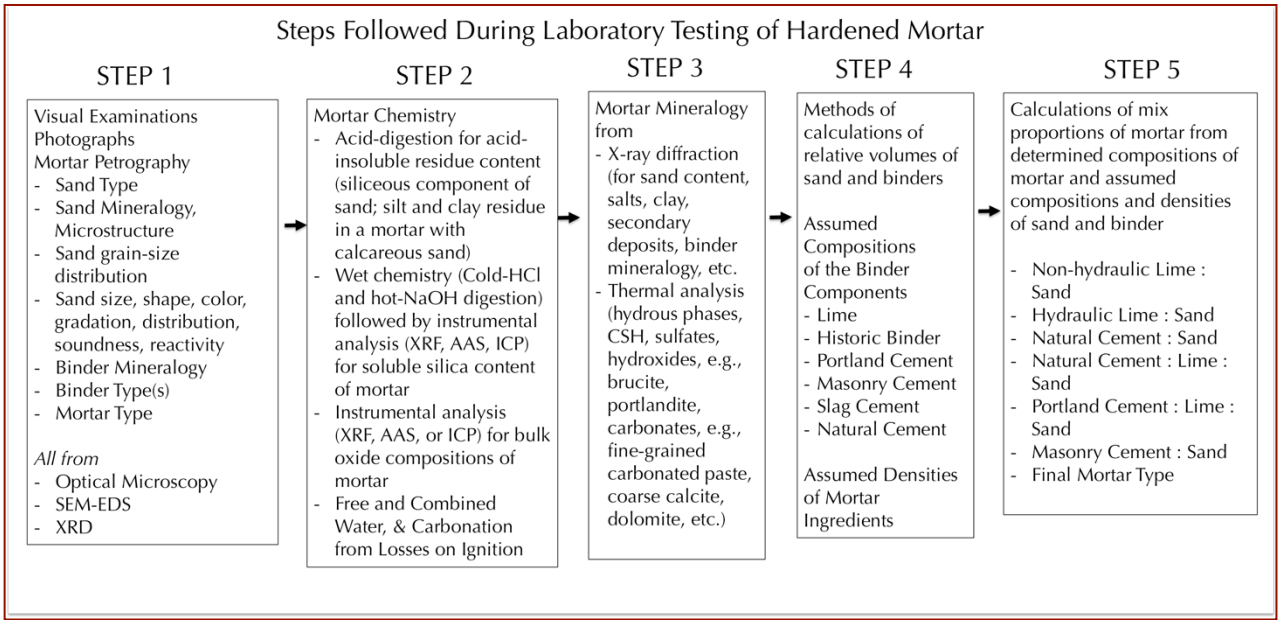

Figure A11: Sequence of steps commonly followed during laboratory analyses of masonry mortars.

Mix Calculations From Petrography & Chemical Analyses of Mortar

ASTM C 1324 provides procedures of calculations of volumetric proportions of Portland cement, lime, and sand in a modern cement-lime mortar containing siliceous or calcareous sand, and proportion of Portland cement in a masonry cement and masonry cement to sand proportion in a masonry cement mortar. Such approaches can be extended for other mortars having other binder types from non-hydraulic lime, to hydraulic lime, to natural cement, slag cement etc. These approaches, however, are based on many underlying assumptions that are important to know and verify against the results of laboratory tests to validate for a particular mortar, especially of historic nature. For example, for mix calculations in a common modern-day Portland cement-lime-silica sand mortar, such approach assumes fixed composition of cement (21% silica and 63.5% lime), fixed composition of magnesian or dolomitic lime (brucite), negligible effect of pozzolanic and other cementitious materials, negligible soluble silica or lime contribution from sand, etc. The following Figure provides examples of various approaches of mix calculations for mortars containing a wide range of sand and binder.

Binders and Sand	Assumed Compositions and Methods of Calculation	Assumed Bulk Density (lbs./ft^3)
High-Calcium Non-hydraulic Lime	[CO_2 data from loss on ignition at 950°C divided by 0.594], where 0.594 is ratio of molecular weights of CO_2 to $Ca(OH)_2$ i.e. 44/74.09	40
Magnesian Non-hydraulic Lime	[100 times (brucite content in mortar from TGA/DSC/5.8)], assuming magnesian lime has 71% CaO and 4% MgO, or 5.8% brucite, since ratio of molecular weights of brucite to MgO (58.32 / 40.32) is 1.447	40
Dolomitic Non-hydraulic Lime	[100 times (brucite content in mortar from TGA or DSC divided by 42)], assuming dolomitic lime has 41% CaO and 29% MgO, or 42% brucite, since ratio of molecular weights of brucite to MgO (58.32 / 40.32) is 1.447	40
Calcitic or Magnesian Hydraulic Lime	[100 times (soluble silica in mortar/0.07] assuming hydraulic lime has 7% SiO_2, or average SiO_2 content calculated from SEM-EDS data of paste	40
Dolomitic Hydraulic Lime	[100 times (soluble silica in mortar/0.07] assuming hydraulic lime has 7% SiO_2, or average SiO_2 content calculated from SEM-EDS data of paste Or [100 times (brucite content in mortar from TGA/DSC/38)], assuming lime has 38% CaO and 26% MgO, or 38% brucite, since ratio of molecular weights of brucite to MgO (58.32 / 40.32) is 1.447	40
Portland Cement in Cement-Lime Mortar	100 × [Soluble silica in mortar / 21.0], assuming 21% silica in Portland cement	94
Calcitic Lime in Portland Cement-Lime Mortar	Lime content = 1.322 × CaO assignable to Lime, which is [CaO content of Mortar – (CaO assignable to portland cement, which is portland cement content × 0.635, assuming 63.5% CaO in portland cement)], where the factor 1.322 comes from ratio of molecular weights of $Ca(OH)_2$ to CaO i.e. 74.09/56.03	40
Dolomitic Lime in Portland Cement-Lime Mortar	100 times (brucite content in mortar from TGA/DSC/42)], assuming dolomitic lime has 41% CaO and 29% MgO, or 42% brucite, since ratio of molecular weights of brucite to MgO (58.32 / 40.32) is 1.447	40
Slag Cement	100 × [Soluble silica in mortar / 27.0], assuming 27% silica in slag cement, or average SiO_2 content determined from SEM-EDS data	90
Natural Cement	100 × [Soluble silica in mortar / 20.0], assuming 20% silica in natural cement, or average SiO_2 content determined from SEM-EDS data	75
Masonry Cement	(i) 100 – [Sand + Total Water], if sand is all siliceous and hence sand content is obtained directly from the acid-insoluble residue content; (ii) PC content (from the soluble silica data) divided by factor 0.50, 0.66, or 0.75 with an assumed masonry cement type of N, S, or M, respectively. MC Type (M, S, N) is determined from PC/MC = 0.75 (for M), 0.66 (for S), or 0.50(for N) – if sand has calcareous component	70 (Type N) 75 (Type S) 80 (Type M)
Gypsum Plaster	Gypsum content from XRD or thermal analysis times 0.843 (ratio of molecular weight of plaster to gypsum)	70
Sand	If sand contains acid-soluble component (carbonates), Sand content = 100 – [Total Binder + Total Water from LOI to 550°C i.e. free plus hydrated water]; If sand has no acid-soluble component (i.e. all siliceous sand) Sand content is directly obtained from the acid-insoluble residue content	80

Figure A12: Various procedures followed for calculations of binder-to-sand volumetric proportions from (a) the determined sand and binder, (b) calculated contents of ingredients, and (c) assumed bulk densities of sand and binders.

Flow Chart of Procedures Followed in Laboratory Analyses of Masonry Mortars

Finally, Figure A13 provides step-by-step procedures followed during laboratory analyses of masonry mortars.

Laboratory Analyses of Masonry Mortars

Initial Mortar (50 to 100 grams) [Photographed with digital camera & flat-bed scanner, As-received condition, total weight, and dimensions of largest piece are documented]

Intact Pieces (20+ g)

1. *Optical Microscopy*

I. Perform visual examination of mortar as received, then saw-cut and fractured surfaces and with a low-power stereomicroscope,
II. Take digital and flat bed scanner photos of intact piece(s),
III. Encapsulate the piece for thin section microscopy in a flexible mold with a low-viscosity colored or fluorescent dye-mixed epoxy to highlight voids, pores, cracks, etc.,
IV. Prepare thin section (< 30 micron thickness) and polish the thin section for optical and SEM-EDS analyses,
V. Scan the thin section on a flat-bed scanner with the thin section residue,
VI. Take transmitted light high-power stereo-zoom photomicrographs of thin sections from different areas to be stitched to determine volumes and size distributions of pore spaces and sand grains by Image J,
VII. Take plane and crossed polarized-light photomicrographs of sand and binder fractions in thin section from a petrographic microscope and determine areas for further studies by SEM-EDS,
VIII. Do detailed petrographic examinations to determine the sand and binder compositions, sand mineralogy and texture, binder phases, residual binders, alterations, and products of any deleterious reactions, immersion mounts of specific areas of interest, etc.

2. *SEM-EDS*

I. Put conductive coating only on the portion of polished thin section intended for SEM-EDS studies from optical microscopy,
II. Take backscatter and/or secondary electron images, and if needed X-ray elemental maps,
III. Select multiple areas on paste to determine oxide compositions and Eckel's cementation indices,
IV. Tabulate the paste composition variations across the backscatter/secondary electron image.
V. Determine chemical compositions of resides left from the original components of the binders, as well as the hydration and carbonation and other alteration products

Lightly hand-ground in a Mortar & Pestle (30+ g)

3. *Acid Digestion - Sand Color & Sand Size Distribution* (10 g)

I. Take 10 g. of mortar lightly ground in mortar & pestle and digest in HCl (1+3) in a 250 ml beaker on a magnetic stirrer until all sand separates and settles at the bottom of beaker,
II. Filter all through two 2.5 micron filter paper, wash the beaker, filter paper, and all sand residue with dist. water,
III. Dry the residue at 110°C in an oven for 10 min., gently brush out from the filter paper and collect, then sieve the entire sand residue through No. 4 through 200 sieves in a mini sieve shaker (e.g., from Gilson),
IV. Determine the mass retained on each sieve, and on the pan (finer than No. 200 sieve),
V. Take photomicrographs of sand particles retained on each sieve for sand color variations in a stereomicroscope.

4. *Acid & Alkali Digestion – Soluble Silica for Hydraulic Binder* (5 g)

I. Grind 10 g of lightly ground fraction from mortar & pestle in a WC pulverizer for 30 sec.
II. Sieve thru. No. 50 sieve, collect the fraction passing the sieve,
III. Re-grind the residue retained on sieve for 15 sec. and mix thoroughly with the previous fraction;
IV. Use 5.00 g of thus prepared powder (passing No. 50 sieve) for digestion in 100 ml cold (3-5°C/38-41°F) HCl (1+4) in a 250 ml beaker for 15 min. on a magnetic stirrer,
V. Filter thru. two 2.5 micron filter paper and keep the filtrate# 1,
VI. Digest the residue with filter paper in 75 ml hot NaOH (below boiling) on hot plate for 15 min. on magnetic stirrer,
VII. Cool down to room temp. and filter thru. two 2.5 micron filter paper and collect filtrate# 2,
VIII. Combine these two filtrates, filter the combined filtrates thru. two 2.5 micron filter paper to remove any suspended silica (especially for sand-rich mortars, or if mortar is grounded too long); then dilute to 250 ml in a volumetric flask with dist. water, an aliquot (about 10 ml) is then used for XRF for soluble silica determination against the calibrations with standard PC mortars of known soluble silica contents prepared in the same way.

5. *Acid Digestion – Acid-Insoluble Residue Content for Siliceous Sand Content* (2 g)

I. Take 1-2 g of prepared mortar powder from Step 4 iii (passing No. 50 sieve) and digest in 50 ml HCl (1+3) in a 250 ml beaker (covered) on a hot pate rapidly near boiling, then 15 min. at a temp. below boiling, then cool down to room temperatures,
II. Filter thru. two pre-weighed 2.5 micron filter papers, washing the beaker, paper, and residue thoroughly with hot water,
III. Dry the filter paper at 110C for 10 min, cool in a desiccator to room temp. and measure the weight.
IV. Subtract from mass of dry filter paper to determine acid-insoluble residue content.

6. *Chemical Analysis – Loss On Ignition for Free and Combined Water Content, and Carbonate plus Carbonation* (2 g)

I. Take 1-2 g (W_1) of prepared mortar powder from Step 3 iii (passing No. 50 sieve) in a tarred porcelain crucible (keep a record of mass of the empty crucible),
II. Dry at 110°C for 15 min in a muffle furnace pre-set to 110°C, cool in a desiccator to room temp. and measure the mass (W_2) by subtracting the empty crucible mass from the total mass,
III. Ignite at 550°C for 15 min. in the muffle furnace pre-set to 550°C, cool in a desiccator to room temp. and measure the mass (W_3) by subtracting the empty crucible mass from the total mass,
IV. Ignite at 950°C for 15 min. in the muffle furnace pre-set to 950°C, cool in a desiccator to room temp. and measure the mass (W_4) by subtracting the empty crucible mass from the total mass,
V. Calculate the losses on ignition at 110°C, 550°C, and 950°C for free water, combined water, and carbonate plus degree of carbonation, respectively.

7. *Mineralogy of Bulk Mortar, Extracted Sand, Extracted Binder, or Salt from XRD* (at least 8 g)

I. Weigh 8.00 g of mortar (or extracted sand or binder as needed) lightly ground in a mortar & pestle, add three grinding/pelletizing aid tablets (e.g., from Oxford Instruments) and pulverize in a suitable mill to minimize contamination (e.g., Rocklab pulverizer with WC bowl or McCrone Micronizing Mill with agate) for 3 min. with anhydrous alcohol to get <45 micron size particles passing U.S. No. 325 sieve,
II. Take 6.8 to 7.0 g. of ground <45 micron prepared mass in an aluminum sample holder inside a stainless steel die to prepare a 32 mm pellet with 25 ton pressure for 1 min,
III. Use the prepared pellet for XRD and then use the same pellet for XRF.
IV. Do XRD on the binder-rich fraction, or salt either on a shallow-depth sample holder or preferably on a zero background quartz plate for small volume of sample.

8. *Bulk Mortar's Composition from X-Ray Fluorescence (XRF)* (same pellet used in XRD)

I. Use the same pellet prepared for XRD in the XRF, or, use a fused bead if sample volume is low to prepare a pellet. In either method, have calibrations of measured oxides with adequate standard.
II. XRF can also be used with proper calibrations for soluble silica determination on the filtrates after acid and alkali digestions, as described in Section 3.

9. *Thermal Analyses* (0.1 g), TGA, DTG, DSC, DTA, for quantitative analysis of various hydrous, sulfate, and carbonate phases in mortar, content of dolomitic lime added from the brucite content in mortar as determined from TGA or DSC, etc.

I. Simultaneous TGA and DSC analyses can be done on 30-70 mg of finely ground (<0.6 mm) mortar in alumina crucible (70 µl, no lid) from 30°C to 1000°C at a heating rate of 10°C/min with high purity nitrogen as purge gas at a flow rate of 75.0 ml/min .

10. *Infrared Spectroscopy,* for determination of various organic additives, and clays in mortar

I. Take an aliquot of powder prepared for thermal analysis and use that in Universal ATR of FTIR.
II. Alternately, digest a pulverized mortar in acetone to extract the organic additive and analyze the liquid in FTIR for characteristic functional groups.

11. *Ion Chromatography of Water-Soluble Salts* (1 g)

I. Take an aliquot of 1 gram powder prepared for chemical analysis (i.e. passing U.S. No. 50 sieve), digest in distilled or deionized water for at least 24 hours in a beaker on a magnetic stirrer, filter the solid residues out to collect the filtrate and analyze the filtrate for soluble salts (chloride, sulfate, nitrate, nitrite, phosphate, etc.) by ion chromatography.

Figure A13: Step-by-step procedures followed for various laboraotry analyses of masonry mortars.

END OF REPORT[2]

[2] The CMC logo is made using a lapped polished section of a 1930's concrete from an underground tunnel in the U.S. Capitol.